1993

Studies of high temperature ternary phases in mixed-metal-rich early transition metal sulfide and phosphide systems

Gregory Allen Marking
Iowa State University

Order Number 9414003

Studies of high temperature ternary phases in mixed-metal-rich early transition metal sulfide and phosphide systems

Marking, Gregory Allen, Ph.D.

Iowa State University, 1993

U·M·I
300 N. Zeeb Rd.
Ann Arbor, MI 48106

Studies of high temperature ternary phases in mixed-metal-rich early transition metal sulfide and phosphide systems

by

Gregory Allen Marking

A Dissertation Submitted to the

Graduate Faculty in Partial Fulfillment of the

Requirements for the Degree of

DOCTOR OF PHILOSOPHY

Department: Chemistry
Major: Inorganic Chemistry

Approved:

Signature was redacted for privacy.

In Charge of Major Work

Signature was redacted for privacy.

For the Major Department

Signature was redacted for privacy.

For the Graduate College

Iowa State University
Ames, Iowa

1993

TABLE OF CONTENTS

1. GENERAL INTRODUCTION

After diffraction of X-rays was observed and described in 1912 [1,2] and the science of crystallography began to develop during the early part of this century it became possible to examine the structure of solid state materials on the atomic scale where the fundamental differences exist. From this structural and basic chemical knowledge the probable bonding can be deduced. This ability to differentiate between crystallographic structures is a major theme of this dissertation in which the application of modern crystallographic techniques to the determination of the metal-rich structures and compounds is discussed.

The compounds of interest can be denoted M_xX_y, normally with $x/y \geq 1$, where M symbolizes an early transition metal (or mixture of such metals) and X symbolizes a nonmetal such as sulfur or phosphorus. A metal-rich compound is classified by the presence of significant metal-metal interactions (as well as significant metal-nonmetal interactions) which are indicated by the short metal-metal distances in the early transition-metal sulfides and phosphides discussed here. The early transition metals have extensive d-orbitals and there are electrons available to fill the lower energy bonding orbitals, but not the higher energy antibonding orbitals, even if the nonmetals localize some of the electrons, so that short metal-metal distances are associated with considerable d-orbital overlap and thus bonding. Na_2O in the anti-fluorite structure can reasonably be considered "ionic" and even though Na/O = 2, there is no significant metal-metal bonding in this structure and Na_2O is not a metal-rich compound by the criteria used here. $Zr_{1-x}S$ [3,4], on the other hand, is found in two different superstructures of the "rocksalt" structure type with the ratio Zr/S < 1. The rhombohedral structure of $Zr_{1-x}S$ is well characterized [3,5] and is a metal-rich compound because it exhibits metallic behavior and important metal-metal interactions.

Many of the early investigations of metal-rich compounds were carried out by Hägg [6] and these compounds were commonly thought of as metals with impurities (hydrogen, boron, carbon, nitrogen, oxygen, etc.) dissolved into them. These were,

in the early literature, called "interstitial" compounds, for they could be described as metal structures with the small, light impurity atoms occupying tetrahedral or octahedral holes within those structures. The impurity atoms were thought to have a minor role (if any) in the bonding of the compound.

In 1947 Rundle reported a simple, but surprising, observation concerning interstitial compounds [7] which had radical implications. While it is true that carbon, nitrogen, and oxygen occupy interstitial sites in MX compounds, where M = early transition and early rare earth metals and X = C, N, and O, the structure of the majority of these compounds is NaCl type irrespective of the M/X radius ratio while that of the majority of the pure metals is *bcc* or *hcp*. The impurity atoms participate so strongly in the overall bonding of the compounds that the structure is changed relative to that of the pure metals! Obviously, these compounds cannot be regarded as merely "interstitials".

The octahedral coordination of these nonmetals was described in Rundle's paper as arising from resonance of bonding electrons between two hybrid s-p orbitals and the remaining two p orbitals on the nonmetal for a total of six partial bonds. The brittleness of these metal-rich compounds is consistent with the directional nature of the M-X bonding and the metallic conductivity is consistent with resonance of the M-X bonding electrons as well as the M-M bonding electrons. In addition, the idea of partial M-X bond character is corroborated nicely by the agreement of observed M-X distances with those calculated for ½ or ⅔ bonds using the Pauling bond order equation [8], $D(n) = D(1) - 0.6 \log n$, where n is the bond order, D(n) is the observed M-X distance, and D(1) is the sum of the relevant Pauling single bond radii.

As alluded to above, metal-rich compounds are similar to their metallic components. They tend to exhibit metallic conductivity and luster, and they generally exhibit Pauli paramagnetism. These compounds tend to be hard, have high melting points (sometimes higher than the metals themselves, e.g. ZrC m.p. = 3540 °C vs. 1855 °C for elemental Zr [9]), and are relatively stable in air. They have potential

uses as refractory materials. Metal-rich compounds are also different from metals, tending to be brittle, not malleable, in contrast to the pure metals.

Binary metal-rich C, N, and O compounds gave some of the earliest insights and were valuable in developing concepts of solid state bonding, but the early transition metal-rich chalcogenides and pnictides added another dimension to these concepts. Whereas the former compounds are commonly found in the well-known NaCl structure type, with the nonmetals located in the octahedral holes of a metallic fcc structure, the chalcogenides and pnictides often form in beautiful and complicated new structures [10] which are far removed from the "interstitial" concept.

Transition-metal-rich sulfides and phosphides can be found with a wide variety of structure types. When the monometal species are considered, simple structure types such as rocksalt, nickel arsenide, and tungsten carbide are common, however there are other more complex monometal sulfide and phosphide structures. When compounds with a metal/nonmetal ratio greater than one are considered, the structures tend to be more complicated. Rather than discuss all the known structure types for metal-rich sulfides and phosphides, only three broad classifications of structure will be described and related to the work covered by this dissertation.

Many of the early transition-metal-rich sulfides and phosphides, e.g. compounds which form in the Ta_2P [11], $Nb_{21}S_8$ [12], $Nb_{14}S_5$ [13], Ti_8S_3 [14], Nb_7P_4 [15], Nb_8P_5 [16], Nb_5P_3 [17], and other structures, can be classified into one structurally related group. During the course of this research, a new structure, $(Zr,Nb)_{11}P_4$ [18], was found which was the simplest known example of this general category. One characteristic of this class of structures is a short axis in the unit cell with mirror planes perpendicular to that axis. Because of size constraints, all atoms lie on the mirror planes. The metal coordinations generally include capped cubes of metal derived from *bcc* where one or two edges may be substituted by nonmetals. Pentagonal prismatic coordination of the metal where two nonadjacent edges of the metal prism are substituted by nonmetals is also observed. The nonmetals are invariably coordinated by trigonal prisms of metal atoms. The trigonal prisms can be

either vertical or horizontal with respect to the mirror planes and may be capped by 0, 1, 2, or 3 metal atoms. The solid solution compounds $(Zr,Nb)_7P_4$ and $(Zr,Ta)_7P_4$ form in the Nb_7P_4 structure and $(Zr,Hf)_2S$ [19] forms in the Ta_2P structure. All three are members of this class and were investigated in this research.

Although the structure-types found for metal-rich sulfides and phosphides are similar, and in a few cases identical, there is a major difference in their chemistries. For $M/X \geq 2$, sulfides have been reported only with early transition group IV and group V metals but phosphides are reported to form with nearly all of the transition metals [20]. If middle and late-transition-metal phosphides are included in this broad structural classification, compounds with MnP [21], Mo_8P_5 [22], Mo_4P_3 [23], Fe_2P [24], and other structure types must be considered. Arsenides, selenides, and tellurides which are members of this structural family [10] can also be found. Additionally, compounds which are not necessarily chalcogenides or pnictides, but fit the above description, such as those forming in the Co_2Si-type [25], Re_3B-type [26] (and its variants) are numerous. When ternary and quaternary compounds are included, the list is further expanded.

During the course of this work, a new compound, ZrNbP in the Co_2Si structure, which only forms in the ternary system and not in the Zr-P or Nb-P binary systems, was found. Approximately 500 compounds, including many phosphides such as ZrP_2 [27] and TT′P (T ≡ Zr, Nb, Ta and T′ ≡ Ru, Rh) [28], have been reported to form with this structure type.

A second class of early transition-metal sulfides and phosphides consists of twenty-two atom doubly-centered polyhedral building blocks. These two-centered polyhedra can be described as two interpenetrating C.N. 14 Kasper polyhedra with the apex of one polyhedron centering the other. Short metal-metal distances are observed between the double centers in the group IV and V early transition metal-rich phosphides with this structure. Four out of the twenty-two polyhedral atoms are nonmetals and the specific structure and stoichiometry depends on the interconnectivity of these polyhedral units. The sulfides found in this class include

only α-V_3S [29], β-V_3S [29], and Zr_9S_2 [30] structure types while some phosphides are found in the Ti_3P [31] structure. Investigations of $(Hf,Nb)_3P$ and $(Ta,Nb)_3P$ [19] solid solutions in the Ti_3P structure are discussed in this research. Many middle and late transition-metal phosphides have been found in the Ni_3P [32] structure which also is a member of this class and Mo_3P [33] is found in the α-V_3S structure.

The last class of compounds to be discussed here includes the binary tantalum metal-rich sulfides Ta_2S [34], α-Ta_6S [35], β-Ta_6S [36], and Ta_3S_2 [37]. The determining structural features of these compounds are the metal chains of face-sharing centered pentagonal antiprisms which can also be described as chains of condensed Ta icosahedra where the apical atom of one icosahedron centers the neighboring icosahedron and vice versa. Strong metal-metal interactions are apparent within these chains since the shortest metal-metal distances between the centering atoms are less than the distances found in *bcc* Ta metal, 2.86 Å. The sulfur atoms are found between these metallic chains linking them together. The packing arrangements of the bridging sulfur atoms and metal chains vary with the different stoichiometries.

The ternary compound $Ta_{6-x}V_xS$ [38] is a member of this family and, in a similar fashion, the new compounds which were found in the κ-phase structure [39,40] and studied in this research exhibit metallic chains (but of distorted face-sharing centered icosahedra) with nonmetals located between them. Another recently discovered structure, $Zr_6Ni_6TiSiO_x$ [41], contains similar chains of distorted face-sharing centered icosahedra and can be included in this general category. The shortest metal-metal distances between the atoms forming the icosahedra and the atoms centering those icosahedra (determined by X-ray single crystal diffraction experiments) in the κ-phases $Zr_{9.7}Ta_{3.3}S_{2.3}$ (2.85 Å), $Zr_{8.1}Nb_{4.9}S_{2.7}$ (2.84 Å), $Hf_{10.0}Nb_{3.0}S_{3.0}$ (2.84 Å), Zr_9V_4S (2.66 Å), and $Hf_9V_4SO_{0.6}$ (2.65 Å) are comparable to the distances found in elemental Ta (2.86 Å), Nb (2.86 Å), Nb, V (2.62 Å), and V respectively which suggests that strong metal-metal bonding is present. The presence of oxygen in these κ-phases

as determined through a combination of X-ray diffraction, neutron scattering, and SEM-EDS techniques will be discussed later.

S and Ni have been found to both partially occupy the same trigonal prismatic site in the κ-phase $Zr_9W_4(S,Ni)O_3$ [42] which suggests that sulfur behaves somewhat similar to nickel, i.e. has metallic character, in this compound. Nickel substitution for sulfur has previously been reported in $Nb_6Ni_xS_{3-x}$ and $Nb_9Ni_{2-x}S_{3+x}$ [43] and the κ-phases Zr_9Mo_4S [42] and Zr_9Mo_4Ni [44] are known with the sulfur and nickel occupying crystallographically identical trigonal prismatic sites.

One other structure found in this research can be included in this category. The "stuffed" γ-brass $Hf_{10}Ta_3S_3$ [45] exhibits twenty-six atom metal cluster units which are centered by Ta tetrahedra. Sulfur atoms are arranged around the cluster units. Although this structure is not easily discussed as chains of centered face-sharing polyhedra, chainlike behavior of these twenty-six atom units is exhibited along the body diagonals of the cubic unit cell where the shortest interatomic distance ($d_{Hf\text{-}Ta}$ = 3.06 Å) between the cluster units is comparable to the shortest corresponding distance within the cluster unit ($d_{Hf\text{-}Ta}$ = 2.96 Å). This distance and the shortest Ta-Ta distances (2.95 Å) found in the clusters are between those found in Ta (2.86 Å) and Hf (3.13 Å) metals indicating that metal-metal bonding is important in this structure.

The work on ternary sulfides and phosphides reported in the dissertation succeeded the graduate research of Xiaoqiang Yao on the Ta-Nb-S metal-rich system at high temperatures [46]. His work answered an interesting question, "Although Ta and Nb are chemically similar due to the lanthanide contraction among other reasons, their binary metal-rich sulfides exhibit mutually exclusive structures. What new structures (if any) will one find when one investigates the ternary Ta-Nb-S metal-rich system?"

Binary tantalum sulfides and niobium sulfides are dramatically different in structure. Ta_2S [34], α-Ta_6S [35], and β-Ta_6S [36] exhibit strongly metal-metal bonded icosahedral tantalum chains with sulfur atoms bridging these chains. $Nb_{21}S_8$ [12] and

$Nb_{14}S_5$ [13], on the other hand, are based on capped trigonal prismatic coordinations of sulfur and fragments derived from bcc metal.

Four new compounds [47-50], three of which are new structure types, were discovered and investigated by Yao. Two of the new structures, $M_{11}S_4$ [47] and $M_{12}S_4$ [48], are based on capped trigonal prisms and *bcc*-like fragments similar to those found in the Nb-S system and are members of the first class of metal-rich sulfides and phosphides previously described in this introduction. The other two compounds, M_5S_2 [49] and M_4S_2 [50], exhibit surprising structures based upon a stacking of *bcc* units along the *c* axis. If one considers the atoms at the bottom of the first cell as one layer, the atom at the center as the next layer, the atoms at the top of the first cell and the bottom of the second as the third layer, and so on, one can count two adjacent sulfur layers separated by four metal layers in M_4S_2 and separated by five metal layers in M_5S_2. These compounds exhibit minimum interlayer S-S distances of 3.26 Å for M_5S_2 and 3.20 Å for M_4S_2 which are consistent with their graphitic character and are indicative of van-der-Waal's interactions. Both are candidates for intercalation and catalytic studies.

The presence of van-der-Waal's sulfur layers in a structure like MoS_2 is not surprising because there is a preponderance of sulfur and there must be S-S contact. These new metal-rich sulfides are surprising in that the van-der-Waal's layers are separated by robustly metallic regions within the same structure. One expects the sulfur-sulfur repulsive forces to be quite strong in a metal-rich sulfide with the result that nonmetallic sulfur is most satisfied in an all metal coordination environment. This is true for the Nb-S system but not for the Ta-S and Ta-Nb-S systems. It is also not true for the related Ta-Se system where diselenide layers are found in Ta_2Se [51], the isotypic structure for the M_4S_2 phase.

One reason that the S-S repulsions are not dominating forces in the formation of structures such as that of Ta_2S and these new layered structures is that sulfur has metallic character and participates in delocalized bonding in early transition-metal-rich sulfide systems. That early transition-metal-rich sulfides are not ionic in character can

clearly be seen through a comparison of facts with theory. Ti_2S [52], in the Ta_2P structure, was synthesized and characterized at about the same time that a paper by Moody and Thomas was published [53] which showed that all the transition metal chalcogenides, M_2X, (including Ti_2S but excluding Cu_2X) would be thermodynamically unstable with respect to the elements and/or competing phases if they were ionic. Since Ti_2S, Hf_2S [54], Zr_2S [55], Ti_2Se [56], Zr_2Se [57], Ta_2S, Ta_2Se, and Nb_2Se [58] are known stable phases, they must be strongly covalent or metallic.

Based on the false assumption that transition metal chalcogenides are "ionic", Moody and Thomas used Kapustinskii's empirical equations [59] to calculate lattice energies for M_2X and MX and then used the Born-Haber cycle to calculate the corresponding heats of formation. With these results they were able to arrive at ΔH_{rxn} = -175 kcal/mol = -732 kJ/mol for the condensed phase reaction $Ti_2S \rightarrow TiS + Ti$. To a first order approximation $\Delta S_{rxn} = 0$ and "ionic" Ti_2S is not thermodynamically stable at any temperature. If $\Delta S \neq 0$, its magnitude is small (on the order of 1 J/mol·K and certainly < 10 J/mol·K). Using the lower limit ΔS_{rxn} = -10 J/mol·K in the formula $\Delta G_{rxn} = \Delta H_{rxn} - T\Delta S_{rxn}$ requires a temperature of ~ 70,000 K for ΔG_{rxn} to become < zero. It is apparent that "ionic" Ti_2S cannot form.

Entropic stabilization and the interplay between M-M and M-S bonding are key ingredients to the successful formation of the M_4S_2 and M_5S_2 layered compounds at high temperatures. These compounds can easily be prepared with the arc-melting technique (indicating that $\Delta G_{rxn} < 0$ at high temperatures), but when they are annealed at 1350° C, they disappear forming instead $M_{11}S_4$ and other unknown phases. These two facts indicate that all of the ΔH's and ΔS's for the possible conproportionation reactions must be positive, and according to the equation $\Delta G = \Delta H - T\Delta S$ these compounds are entropically stabilized at high temperatures.

The idea of entropically stabilized high-temperature phases is not new. However, the interplay between metal-metal and metal-sulfur bonding as found in the Ta-Nb-S system is an exciting new concept. Mixed Ta-Nb behaves as if it is a new

element in this metal rich sulfide system, different from both Ta and Nb, forming new and unusual structures.

Comparison of the ΔH_{atm}'s [60] for Ta, 186,800 ± 600 cal/g·atom, and Nb, 172,400 ± 1,000 cal/g·atom, suggests that Ta is able to form stronger metal-metal bonds than is Nb. Based on the ideas that Ta and Nb are nearly identical in size and that electronegativity decreases going down Group V in the periodic table, Ta-S bonds of a specific length have a larger electronegativity difference and thus are stronger than Nb-S bonds of the same length. Ta is capable of forming both stronger M-M and M-S bonds than is Nb, however participation of Ta in polar M-S bond formation tends to localize Ta electrons thereby lessening the ability of Ta to participate in metal-metal bond formation. In compounds of this type, Ta sacrifices its ability to form M-S bonds in favor of forming strong M-M bonds by preferentially occupying those sites which have largest number of short metal-metal contacts (and the smallest number of short metal-sulfur contacts). This sacrifice of M-S bonding to gain M-M bonding is not surprising because in metal-rich compounds, the M-M bonds are more numerous than M-S bonds and more important taken as a whole.

Extended Hückel band calculations showed that the above interpretation is correct [50]. Ta prefers the metal-metal bonding sites over the metal-sulfur bonding sites because the structure gains more M-M bonding (as measured by the calculated overlap populations) than it loses M-S bonding from this occupancy pattern relative to one where Nb is placed on the metal-metal bonding sites.

The work described in this dissertation began with two initial questions related to the new compounds and structures found in the Ta-Nb-S system: 1) The disulfide layers in stacked *bcc*-like M_4S_2 and M_5S_2 are both similar to and different from the disulfide layers found in hexagonal MoS_2 which are believed to be responsible for its catalytic activity. Can new compounds with useful catalytic properties be synthesized with these stacked *bcc*-like structures in other systems, e.g. Ta-W-S, Ta-Mo-S, Ta-Ru-S, etc.? 2) The fact that new and strikingly different phases are stabilized in the ternary Ta-Nb-S system relative to the binary Ta-S and Nb-S systems is intriguing.

Is this phenomenon specific to the Ta-Nb-S system or is it more general and will it be observed in other systems such as Hf-Zr-S and Ta-Nb-P?

Investigations pertaining to the first question identified M_5S_2 (and M_4S_2 in the Ta-Ti-S case) type compounds (through comparison of X-ray Guinier powder patterns of the synthesized materials with calculated powder patterns of the known Ta-Nb-S phases) as the major phases in the Ta-W-S, Ta-Mo-S, Ta-Ru-S, and Ta-Ti-S tantalum-rich systems (~Ta_4MS_2). Single crystals and pure phases of the layered structure types were not obtained and catalytic studies could not be undertaken because the minor (and catalytically active) MS_2 phase [61] was present in all cases and would have rendered any positive catalytic results for the bulk phases meaningless.

Although the initial goal of preparing new catalytically active Ta-M-S layered compounds was not attained, the synthesis and characterization of other new types of Ta-M-S compounds was realized. The first tantalum containing κ-phase, $Zr_{9.7}Ta_{3.3}S_{2.3}$, was synthesized as well as the novel "stuffed" γ-brass, $Hf_{10}Ta_3S_3$, which has far-reaching theoretical implications in the context of the Hume-Rothery rules [62] and the Brewer-Engel correlation [63]. Investigations based on similarities between the Group IV metals Zr and Hf and between the Group V metals Ta and Nb led to the discovery of the low-temperature superconducting κ-phases $Hf_{10.0}Nb_{3.0}S_{3.0}$ and $Zr_{8.1}Nb_{4.9}S_{2.7}$ [64] and also the oxygen stabilized κ-phase $Hf_8Ta_5S_{3.5}O_x$ ($x \leq 0.5$). $Hf_9V_4SO_{0.6}$ and Zr_9V_4S kappa phases were also synthesized.

The stoichiometry $M_{9+x}M'_{4-x}X_{4-y}$ appeared to have significance in the formation of new mixed early-transition-metal sulfide compounds but investigations of the corresponding phosphide systems showed that the significance of this stoichiometry did not carry over into the phosphides. Investigation of the Zr-Nb-P system did, however, yield interesting results. A new structure, $M_{11}P_4$, and a new compound, ZrNbP in the Co_2Si structure, were characterized and the Mo Kα X-radiation anomalous scattering difference between Zr and Nb was found to be useful in determining the metal site occupancies.

The second goal, as specifically stated, was not attained (no new phases were discovered in the Ta-Nb-P or Zr-Hf-S systems), however new structures and compounds which are ternary (or quaternary) compounds stabilized relative to the phases found in the corresponding binaries were discovered.

2. EXPERIMENTAL

Synthetic Techniques

Introduction

High temperature techniques have proved to be useful in the synthesis of metal-rich chalcogenides and pnictides [65,66]. Most of the early transition metal-rich ($M/X \geq 1$) chalcogenides and pnictides were synthesized at temperatures above 1200 °C with a recent, notable exception, Ta_3S_2 [37]. The synthetic techniques discussed in this dissertation are classified as "high-temperature" methods with a temperature range from 400 °C, the lowest temperature used in this work, up to 3000 °C (or more), above the melting point of Ta metal.

Three synthetic techniques were used in this work on the high temperature chemistry of early transition metal sulfides and phosphides: 1) Initial binary starting materials were prepared using evacuated quartz tubes for sample containment and tube furnaces for low temperature heating. 2) Samples were prepared through arc-melting which provided the opportunity for complete mixing of the reactants in a short period of time at extremely high temperatures. 3) Generally, the arc-melted samples were annealed to promote crystallinity. This was usually performed at intermediate to high temperatures using induction heating techniques. Each of the above techniques will now be described in more detail.

Low temperature tube furnace techniques (< 1100 K)

The binary sulfide and phosphide materials used in this research were prepared using tube furnace techniques. The general procedure for the tube furnace syntheses of binary metal sulfides follows. The metal phosphides were similarly prepared except that phosphorus was handled inside of a glovebox under an inert argon atmosphere.

Fused-silica tubes with ground joints were prepared and heated with an oxygen-natural gas flame on the vacuum line under dynamic vacuum in order to drive off as much residual H_2O as possible. The appropriate quantities of metal (Ta, Nb, V, Hf, or Zr) and sulfur were weighed using a Mettler analytical balance to ± 0.0005

grams and then transferred to the fused-silica tubes. Because sulfur and powdered metals tend to electrostatically cling to the walls of the funnel and the quartz tubes, the actual stoichiometry of a sample prepared in this fashion was not known precisely, but it was known to about ± 1% in S/M or better (e.g. $Ta_{2.98}S$ instead of Ta_3S).

The tubes containing the unreacted metal and sulfur were transferred to a vacuum line and slowly evacuated (taking care not to evacuate any of the sample along with the air) with a rough pump down to a pressure of 10^{-1} torr and then, to remove as much H_2O as possible, evacuated with an oil-based diffusion pump down to a pressure of about 10^{-5} torr. The valves to the fused-silica tubes were closed and the tubes removed from the vacuum line and sealed off using an oxygen-natural gas torch.

The sealed tubes were allowed to cool and then checked with an oxygen-natural gas flame to make sure that they were under vacuum. A properly sealed tube is under vacuum and will begin to collapse in the area where the "glass" becomes fluid because of contact with the flame. Air will leak into an improperly sealed tube and the tube will bulge outward in the heated area because the air expands. The properly sealed tubes were then transferred to a tube furnace. The tube furnaces used in this research were either Marshall model 1016, 110 V, 7.4 A (Varian, Palo Alto, Calif) or Astro model A223, 115 V, 1375 W (Santa Barbara, Calif). The samples were then pre-reacted using one of two techniques: 1) They were heated at 400 °C until no yellow sulfur vapor (or red phosphorus vapor) was detected and then the temperature of the tube furnace was increased to approximately 800 °C and the samples heated for up to a week at this temperature. The phosphides reacted more slowly than did the sulfides, due to kinetic barriers. Iodine could have been used to facilitate reaction of the metal phosphides [67], although iodine contamination of the materials might have occurred. In this work, up to two months of time was taken to react the binary phosphides.

2) The second method involved heating the furnace to 800 °C and extending part of the sample tube out of the furnace so that a cold reservoir was maintained in order to keep the sulfur or phosphorus pressure inside of the tube at a safe level. With the metal at the hot end of the tube, this was a fast method for obtaining binary materials.

The major drawback to preparing samples within evacuated "quartz" tubes is that at temperatures above 800 °C, especially with the use of transport agents, oxygen (ZrOS) and/or silicon ($Zr_6Ni_6TiSiO_x$ [41]) can be incorporated into the samples due to reactivity between the sample and the fused-silica container.

The ternary metal-rich sulfides and phosphides discovered and investigated in this work could not be prepared using transport techniques but crystals of other compounds were obtained through transport methods during this research. The use of I_2 as a transport agent, a temperature gradient of 100 °C from the center to the side of the tube furnace, and a maximum temperature of 1050 °C resulted in the formation of beautifully shaped crystals of two known phases, yellow octahedral crystals of ZrOS [68] and maroon crystals of rhombohedral $Zr_{1-x}S$ [3,5].

Binary starting materials corresponding to the following stoichiometries (not necessarily to actual compounds) were prepared during this research by tube furnace techniques: NbS, Nb_2S, Nb_3S, TaS, Ta_2S, Ta_3S, Zr_2S, Zr_3S, Hf_2S, Hf_3S, VS, V_2S, V_3S, NbP, TaP, ZrP, HfP, and others with nonintegral M/S ratios such as $Hf_{2.25}S$ and $Ta_{2.5}S$. The elemental materials used in this research include: sulfur (Aldrich, -100 mesh, sublimed), phosphorus (Alfa, red amorphous, -100 mesh, 99%), niobium (Alfa, -325 mesh, 99.8%), niobium (Johnson Matthey, -60 mesh, 99.8%), tantalum (Johnson Matthey, -60 mesh, 99.98%), vanadium (Aldrich, -325 mesh, 99.5%), zirconium (Johnson Matthey, -20 +60 mesh, 99.9%), and hafnium (Ames lab, single crystal turnings).

Inhomogeneous, polyphasic materials (particles of metal surrounded by polysulfide or polyphosphide coatings) formed with the tube furnace technique caused problems when used for arcmelting. Samples made with "NbP" were difficult to melt

at 10V, 80A presumably because the polyphosphide coating around the Nb particles would not conduct the electrical current necessary to form an arc. Additionally, polyphasic materials lost substantial amounts of the nonmetal upon arcmelting. The binary Hf and Zr sulfides caused the most problems in this respect because they were prepared from large particles of metal and the sulfur did not diffuse evenly into the particles. In the later stages of this work, Hf and Zr sulfides synthesized by the tube furnace technique were annealed in the induction furnace up to 1300 °C by slowly increasing the temperature while keeping the residual pressure under 1×10^{-5} torr and then arcmelted several times to promote homogeneity in the materials and minimize loss of sulfur in later reactions.

High temperature arcmelting techniques (> 2300 K)

The high-temperature technique of arcmelting [69] is a valuable synthetic tool in the study of early transition metal-rich sulfide and phosphide systems. Historically, this technique has been used by metallurgists to prepare alloys, but it works equally well for solid state chemists in the preparation of refractory materials. The beauty of this technique lies mostly in its short reaction times but also in its simplicity and safety of use. Major drawbacks include incorporation of unwanted contaminants (primarily oxygen) into the bulk sample, loss of volatile components, and/or inhomogeneity of the arcmelted sample. Incorporation of adventitious oxygen into a sample is not always undesirable as evidenced by the new oxygen-stabilized phases that have recently been found in this laboratory [41,42,70].

The arcmelting apparatus used in this research consisted of a Centorr model 5SA single arc furnace (Suncook, NH) with a 300 amp DC power supply which was reported as being capable of reaching temperatures > 3500 °C. A thoriated tungsten (non-consumable) "stinger" electrode mounted in a water-cooled copper tube with a wooden handle was used to strike and manipulate the arc. A water-cooled copper hearth was the other contact of the arc and was used to hold and cool the samples during and after reaction. The arcmelting was performed under inert argon gas to avoid reaction of the sample with atmospheric gases which in an extreme case could

cause an explosion, e.g. arcmelting finely powdered metal in the presence of large amounts of oxygen. The reaction chamber was purged three to five times with argon and then kept at a slight (~ 3 torr) dynamic overpressure to exclude the ambient atmosphere. The arc was struck by pulling the stinger up from its initial contact with the copper hearth when the power was applied and a piece of Zr metal was melted before and after reaction of the samples to getter as much residual oxygen and/or water vapor as possible and minimize contamination of the sample. The arcmelting of one sample was normally from 15 seconds to 1 minute in duration.

Variable power settings were used when arcmelting although the temperature was not determined. When the arc was struck, the potential was constant at 10 V and the current was adjusted within the range of 40 to 80 A. The brightness of the arc was observed to increase with increasing current. The arc was observed through a darkened window, similar to that of welder's glasses but darker, which was a plate of glass coated with a thin gold film. The temperature of the arc, although unknown, depended upon the sample size, shape, and composition. The crimped corners of a Ta tube (m.p. ≈ 3300 °C) were quickly melted at the lowest power settings while a bulk piece of Ta required a much higher power setting.

An arcmelting procedure began with the initial sample preparation and cleaning of the apparatus. The desired proportions of various materials with a usual total weight of 0.5 to 1.0 grams were combined and then pelletized at 10,000 psi. Samples as large as 2 or 3 grams were arcmelted with this equipment although inhomogeneity was a problem because of the temperature gradients between the top and bottom of the sample. The molten sample formed a ball-like pellet which rested on the water-cooled copper hearth and the bottom of the pellet cooled more rapidly than the rest of the sample. Samples were generally allowed to cool, turned over, and arcmelted again to promote homogeneity. This was repeated two or three times.

Sometimes, beautifully shaped single crystals were formed directly from the arcmelt (usually in well-known binary structures) but more commonly, microcrystalline

samples were obtained which had severe twinning and needed to be annealed in the induction furnace.

Copper contamination of samples was observed when large amounts of the nonmetal component were volatilized and reacted with the copper hearth. This copper sulfide or phosphide then reacted with the molten sample. As mentioned above, polyphasic binary materials obtained from tube furnace reactions were annealed at high temperatures in the induction furnace to minimize loss of their nonmetal components upon arcmelting. This procedure solved the problem of copper contamination resulting from the arcmelting synthetic technique.

Intermediate temperature induction heating techniques (1100 - 2400 K)

Induction heating was used to maintain samples at high temperatures (up to 2100 °C) for relatively long periods of time, several hours to several days. Because the solid state reactions were not diffusion limited and the vapor pressures were low (< 10^{-7} torr) for the metal-rich systems at high temperature, thermodynamic equilibrium was approached. High-temperature (endoentropically stabilized) phases were formed through the induction heating technique which could not have been prepared with arcmelting or tube furnace techniques.

The induction furnace consisted of a vacuum line with a Televac gauge and a Lepel (Woodside, NY) high frequency (rf) induction heating unit with a 20 kW power supply. Temperatures were determined with an optical pyrometer (Leeds & Northrup, Philadelphia, PA). Samples were contained in tungsten crucibles held by a tantalum tripod stand on top of a boron nitride holder at the end of a "quartz" cylinder which protruded from the vacuum line. This assembly was covered with a water-cooled fused-silica jacket and evacuated. A water-cooled copper work coil was placed around (but did not touch) the fused-silica jacket so that the sample approximately centered the coil. The vacuum line was first evacuated to a pressure < 10^{-1} torr with a rough pump and then by an oil-based diffusion pump. Dynamic vacuums of 10^{-7} torr were commonly obtained while heating metal-rich samples at high temperatures. Polyphasic samples prepared with tube furnace techniques sometimes had a P_s or

P_p which became large at elevated temperatures. When the pressure inside the vacuum line, near the area of the work coil, reached above 4×10^{-4} torr, arcing occurred within the vacuum line and the current to the work coil had to be temporarily terminated.

After induction heating was finished, the power supply was turned off and the sample and crucible cooled through radiative heat loss (rapidly at first and then more slowly as the temperature diminished) according to the Stefan-Boltzmann law, $I = \epsilon\sigma AT^4$ [71], where I = power radiated, A = area, ϵ = emissivity, and σ = Stefan's constant. Normally, the sample and crucible were cooled enough to be safely handled in the air, i.e. did not oxidize and did not burn fingers, after 2½ hours.

When the arcmelted samples were poorly crystalline, annealing at temperatures close to the melting points of the samples generally improved their crystallinity. Most of the large single crystals (suitable for X-ray intensity data collections) used in this research were obtained from samples which had been partially melted and then annealed in the induction furnace. Many crystals (κ-phase crystals in particular) obtained from samples which had been annealed but not partially melted were too small to be used for X-ray intensity data collections.

Finding the melting point of the sample was done by trial and error. A sample was heated at a maximum temperature for < 3 minutes, cooled, and then examined for signs of melting. When the sample showed no signs of melting, the maximum temperature was increased by 50 °C and the sample was again heated, cooled, and examined. It was possible to determine the temperature at which the sample began to melt without completely melting the whole sample. The turn-around time for one cycle of incremental heating in this fashion was approximately 4 hours, so that this was a time consuming experiment when the initial temperature was too low.

Determination of the melting point for a sample in this way resulted in a temperature (read through an optical pyrometer) which was approximately 100 °C lower than the true temperature but was reproducible to within ± 10°C of the apparent temperature. The errors in absolute temperature were not relevant to these

syntheses because the melting points of the materials were constant (under constant conditions) and independent of the apparent temperatures. The error associated with the statement "Anneal the sample at 50°C below its melting point." was on the order of ± 10 °C. The experiments could be reproduced in different heating devices, e.g. Ta crucibles instead of W crucibles, once the melting point was determined for a particular sample in a specific crucible.

A slightly different technique for annealing a sample at just below its melting point was used almost exclusively in this work. Experience and practice were required to be successful with this technique but it alleviated two major problems caused by melting samples accidentally: 1) ruining expensive tungsten crucibles, and 2) contaminating samples with tungsten.

The tungsten crucibles were Knudsen effusion cells and, as such, had small orifices in their lids. An upside down lid was used as the bottom of the crucible with another lid used for the top. A thin piece of foil was placed in the lower lid and the sample was placed upon this foil. If the sample contained Nb, Nb foil was used and if the sample contained Ta, Ta foil was used, etc. When the sample was heated, the foil was observed to glow, like a black body, through the orifice. When the sample began to melt, the foil bent or tore or became darker or lighter or changed in some other subtle way which experience clarified. When this "change" was observed, the temperature of the sample was slightly decreased before the sample completely melted. When two pieces of sample were placed close together and annealed at a temperature approaching their melting point, single crystals of large size and regular shape sometimes grew between them.

Techniques of Characterization

Introduction

Determination of structure by X-ray crystallographic methods was the most prominent technique of characterization used in this work, however neutron scattering experiments were used as well. Along with structural investigations, elemental

analysis by SEM-EDS (scanning electron microscopy energy dispersive analysis) and measurements of magnetic susceptibility were performed on selected samples.

A distinct order for the different characterization techniques used on each sample was followed, beginning with the Guinier X-ray powder technique. When a new phase was detected through powder techniques, single crystals were selected from the bulk sample and examined by X-ray single crystal techniques, culminating with collection of intensity data for a crystal on a diffractometer. After the structure and composition of the new phase were determined through least-squares refinement of the diffractometer data, a bulk phase sample was prepared and examined with X-ray powder photographic methods. Elemental analysis and neutron scattering experiments were performed in order to answer remaining questions of structure and/or stoichiometry. New phases were routinely checked by the flux exclusion method of magnetic susceptibility measurement for superconductivity at low temperatures. All of the above techniques will be covered in more detail below.

X-ray powder crystallographic techniques

Guinier photography

The initial step in the structural determination of a new phase involved obtaining a Guinier film pattern [72] of the sample and comparing it to calculated powder patterns of known phases. The vacuum Guinier cameras used in this research were Enraf-Nonius, Delft, model FR552 cameras. A piece of bulk sample was finely ground, mixed with NBS silicon standard, mounted on a piece of cellophane tape stuck to a metal sample holder, and this sample holder was placed on a rotating stage inside the shell of the Guinier camera. Rotation minimized the effect of preferred orientation upon the sample and ensured that the maximum number of diffracting planes in the various particles were oriented correctly (at least some of the time) for focusing on that part of the Ewald sphere with which the film was aligned. The camera was evacuated and the film exposed to diffracted 45 kV, 20 mA Cu $K\alpha_1$ monochromated X-rays (λ = 1.54056 Å) for approximately two hours. When the camera was poorly aligned or the quantity of sample was small (or if the

sample was only a weak scatterer of X-rays) the amount of time for exposure was increased. The cameras were evacuated for two reasons, the most important of which, reaction between the sample and the atmosphere, was not relevant to the work covered by this dissertation. None of the phases discussed here were air sensitive. The second reason, that atmospheric gases scatter X-rays, was avoided in principle, even though the effect was negligible.

After a Guinier photograph of a new sample was obtained, it was compared to powder patterns of known phases which might have been present in the sample. The program PWDR [73] was used to calculate 2θ values and intensities for known phases and PLOT [74] was used to plot this information in a format suitable for direct visual comparison with Guinier films. In the search for new materials, it was encouraging when such a comparison yielded no match.

In order to gain further information from Guinier photographic techniques, the Guinier film was read to obtain d-spacings, 2θ values, or other equivalent data for the various diffraction lines. The diffraction lines on a developed film were measured with two different film readers. A manual Guinier Viewer (Enraf-Nonius, Delft) was used to measure lines (in mm) relative to an arbitrary zero point. The spacings of the sample lines were compared to those of the known NBS silicon standard with the program GUIN [75] and the 2θ values were calculated. Intensities were visually estimated. The measurement of the diffraction lines, comparison to those of the Si standard, and calculation of the 2θ values were also done automatically with a KEJ Instruments Line Scanner LS-20 and SCANPI software [76] which additionally determined relative integrated intensities.

After 2θ values for an unidentified phase were obtained, the program TREOR [77] was used to determine the lattice type and lattice parameters for the new phase. This program worked best when the diffraction lines were sharp and belonged to a single phase. It was more likely to give the correct results for high symmetry phases (≥ orthorhombic) than for low symmetry phases.

Sometimes a known phase was identified in a new system through comparison of the experimental Guinier film with a calculated powder pattern. When the match was not "exact", the 2θ and hkl values of the diffraction lines were used to obtain least-squares lattice parameters for the new phase with the program LATT99 [78]. This program was used to study the effects of substitution upon cell parameters in various systems.

Rietveld analysis of powder diffraction data

Rietveld analysis of X-ray powder diffraction data is a powerful tool which was used to characterize bulk samples in contrast to single crystal techniques which are not "bulk" techniques. The Rietveld analyses discussed here were performed using GSAS (Generalized Crystal Structure Analysis System) software [79] which allowed refinement of multi-phase samples. The analyses discussed in this dissertation were based on structural models which had previously been obtained through X-ray single-crystal methods.

A bulk sample was pulverized and loaded into a small cavity (~ 15 × 20 × 0.5 mm^3) on a zero background sample holder (made out of single crystal quartz) and smoothed so that the top of the sample was even with the top of the sample holder. The sample holder was then placed into a spring loaded device in the target area of a Scintag XDS 2000 (45 kV, 30 mA) θ-θ powder diffractometer which held the sample in the properly aligned position. Data were collected for all samples using Cu Kα X-radiation (λ_1 = 1.5405 Å, λ_2 = 1.5443 Å, $\langle\lambda\rangle$ = 1.5418 Å) over a specified range in 2θ, usually 10 to 160°, using a Kevex Peltier detector (8.04 keV, 300 eV window) at a usual scan rate of 6 sec/step with a usual step size of 0.02°.

Initial stages of the Rietveld analyses included refinement of up to twelve background parameters (terms of cosine Fourier series), phase fractions (the number of unit cells of each phase that were present relative to the overall histogram scale factor which was set equal to unity), and the lattice parameters of the different phases. The middle stages of analysis included refinement of the Lorentzian profile coefficient LY (strain broadening) and the positional and isotropic thermal parameters.

The isotropic thermal parameter, U_{iso}, is obtained from the following formula for the thermal correction to the structure factor,

$$T'' = \exp -(8\pi^2 U_{iso} \sin^2\theta/\lambda^2).$$

In the final stages of analysis, refinements of additional profile coefficients, e.g. "shift" or the Lorentzian profile coefficient LX (particle size broadening), anisotropic thermal parameters, and fractional or mixed occupancies were attempted. The anisotropic thermal parameters are the U_{ij}'s in the formula for the thermal correction to the structure factor,

$$T'' = \exp -[2\pi^2(U_{11}h^2a^{*2} + \ldots + 2U_{12}hka^*b^* + \ldots)].$$

Gaussian profile coefficients and extinction and absorption parameters were not refined for any of the X-ray powder data sets discussed here. Correlations between profile, occupancy, and thermal parameters are common in Rietveld analyses of powder data [80] and were observed to some extent in the refinements discussed in this dissertation. The positional parameters were relatively unaffected by these correlations. Various approaches to dealing with the correlation problems were attempted including refinement of the correlated parameters on an individual basis and fixing of thermal and occupancy parameters at values found in X-ray single crystal experiments. Specific details on the Reitveld analyses of various samples will be found in the applicable chapters.

The program GSAS was used to refine the X-ray powder data because it contained Rietveld refinement software for X-ray powder data as well as both CW (constant wavelength) and TOF (time of flight) neutron powder data. The Rietveld method of powder refinement [81] is based on the idea that the observed intensity at every data point can be expressed as the sum of the background intensity and the intensities from each contributing Bragg peak, $I_{calc} \cong I_{obs} = I_{back} + \Sigma Y_h$ where the Y_h's are the Bragg intensities of the various peaks. A function, $M = \Sigma[w(I_o - I_c)^2]$, was minimized by the least-squares program GENLES where w, the weighting for each point, was computed according to the variance between observed and calculated intensities. The quality of the minimizations was inferred from the residuals, Rp =

$\Sigma | I_o - I_c | / \Sigma I_o$ and Rwp = $(M/\Sigma(w I_o^2))^{1/2}$. The reduced χ^2, goodness of fit, was defined, $\chi^2 = M/(N_{obs} - N_{var})$, and should have approached the value of one. The expected Rwp was calculated manually, expRwp = Rwp/$[(\chi^2)^{1/2}]$. Finally, the Durbin-Watson statistic, Dwd, was calculated by GENLES and was close to 2 when no serial correlation in the differences [$I_o - I_c$] was present.

GSAS contains a variety of useful programs, some of which follow: Fourier maps were calculated and plotted with FOURIER and FORPLOT. Sorted lists of reflections suitable for publication were produced through HKLSORT and an interactive version of ORTEP [82] was available for crystal structure plotting. POWPLOT is an interactive program which produced observed and calculated diffraction patterns, difference curves, and reflection markers. Another useful program, RCALC, computed residuals for different parity classes of reflections based on either F_{obs} or F_{obs}^2 and generated plots of the residuals versus various parameters. SXTLDATA was used to process X-ray single crystal data into the GSAS format.

X-ray single crystal techniques

Rotation camera photography

Rotation and Weissenberg [83] X-ray single crystal photographic techniques were used to determine whether a crystal was suitable for data collection and also to gain information about possible space-groups appropriate to a crystal. Model 9000 Weissenberg cameras and model 401 goniometer heads from Charles Supper Company, Natick, Mass., were used for these photographic techniques with nickel filtered Cu Kα X-rays (λ = 1.5418 Å) generated at 45 Kv, 20 Ma. Single crystals of all phases discussed in this dissertation were mounted on thin glass fibers with either Apiezon T-grease or epoxy.

Particles which appeared to be crystalline were photographed with an exposure time of approximately one minute/degree of oscillation (rotation). With practice, examination of developed photographs quickly indicated whether the suspected crystal was suitably "singular". Crystals which gave "good" diffraction spots on a

photograph with the exposure time of one minute/degree were, in general, suitable for an intensity data collection using a diffractometer.

Once a crystal was determined to be "single", the next goal was to align it along a reciprocal axis and take a rotation photo in order to determine the length of that axis in real space. Sometimes, knowledge of the length of one real axis combined with phase information from a powder pattern of the bulk sample was enough to determine (with a fair degree of certainty) that the crystal had a known structure. Crystals were occasionally aligned along secondary axes (body-diagonals, face-diagonals, etc.) so that care was taken in the interpretation of rotation and Weissenberg photographs.

After a crystal was aligned along a reciprocal axis, Weissenberg photos (usually zero, first, and second layers) were taken in order to determine the symmetry of the lattice (in theory, a maximum of six layer photographs could be required to gather all of the information about some hexagonal lattices). The lengths of the other two real axes could usually be determined as well as the unit cell angles. Systematic absences were used to determine centering conditions. In general, photographs obtained from orthogonal cells aligned along primary axes were easy to interpret. Those obtained from monoclinic cells, not aligned along their unique axes, and from hexagonal cells, not aligned along the c* direction, were more difficult to interpret.

Diffractometer intensity data collections

Refinement of intensity data collected on an X-ray single crystal diffractometer is one of the most common and powerful techniques available for the structural characterization of solids. In this work three different X-ray single crystal diffractometers were used to collect single crystal data. The majority of the data sets were collected on the rotating anode Rigaku AFC6R diffractometer using monochromated Mo Kα X-radiation (λ = 0.71069 Å) however data sets were also collected, using Mo Kα X-radiation, on sealed-tube Enraf-Nonius CAD4 (λ = 0.71073 Å) and Siemen's P3 (λ = 0.71028 Å) diffractometers. The AFC6R diffractometer operated at a high level of power, 7 Kw (usually 50 kV, 140 mA),

generating intense X-rays which were useful in collecting data from weakly diffracting crystals. Because it generated high intensity X-rays, data were rapidly collected.

The CAD4 and P3 diffractometers operated at lower power levels, around 1.5 kW (usually 50 kV, 32 mA for the CAD4 and 50 kV, 30 mA for the P3), but were suitable for collecting data from many crystals. These latter two diffractometers operated at slower speeds than the AFC6R so that data collections took more time, but they obtained lattice parameters (and orientation matrices) which were more accurate, or at least corresponded more closely to the lattice parameters of the bulk samples obtained through Guinier methods, than did the lattice parameters obtained with the AFC6R diffractometer.

A single crystal data collection began by manually centering the crystal in the X-ray beam followed by using a search routine to find and center 10 to 25 reflections which were indexed. The use of reflection coordinates obtained from an oscillation photograph to find and center the initial set of reflections was faster than using the search routine when the unit cell was small and this procedure gave more control over the initial reflection list. Once a unit cell had been indexed, it was reduced to the correct lattice and the Laue class was determined. A high-angle cell was commonly refined in order to obtain the best possible orientation matrix for use in the data collection. Data collection parameters were set, including scan speed, scan width, scan type (usually ω or ω-2θ), scan range (commonly from 0° to 60° in 2θ), octants collected (at least one set of redundant data is normal), and others. Selection of the proper data collection parameters enabled the gathering of useful information from "poor" crystals. Once the data collection was complete, psi scans were collected for later use in an empirical absorption correction.

Processing and refinements of all intensity data were performed using TEXSAN [84] software. The data sets from the AFC6R and CAD4 diffractometers were processed directly (as obtained from the instrument) while data from the P3 diffractometer had to first be processed through an "in house" data conversion program [85] before further processing in TEXSAN.

The program PROCESS in TEXSAN processed and analyzed the raw data and produced an hkl.dat file which was used in all further steps of the structural solution. PROCESS produced valuable statistical information which helped to determine the correct space groups for the crystals. Raw data were visually inspected for systematic absences in order to manually determine possible space groups as well. HKL is a program which applied the empirical psi scan absorption correction and averaged the data according to the chosen space group. DIFABS [86] θ-dependant empirical absorption corrections were used in several structure refinements. A direct methods program, SHELXS86 [87], was used to determine the initial model for all structural solutions discussed here.

ATOMED is the program by which the structural models were stored and modified. Refinements of scale factors, isotropic secondary extinction coefficients, atomic positional, isotropic or anisotropic thermal, and occupancy parameters were controlled with this program.

The isotropic thermal parameter, B_{iso} or B(eq), refined in TEXSAN is obtained from the following formula where $\beta_{ij} = 2\pi^2 a_i^* a_j^* U_{ij}$,

$B(eq) = 4/3[a^2\beta_{11} + b^2\beta_{22} + c^2\beta_{33} + (2abcos\gamma)\beta_{12} + (2accos\beta)\beta_{13} + (2bccos\alpha)\beta_{23}]$.

B_{iso} is related to U_{iso} (refined in GSAS) by the formula, $B_{iso} = 8\pi^2 U_{iso}$. The anisotropic thermal parameters, U_{ij}'s, are defined in TEXSAN much like in GSAS from the thermal correction to the structure factors,

$T = exp[-2\pi^2(a^{*2}U_{11}h^2 + b^{*2}U_{22}k^2 + c^{*2}U_{33}\ell^2 + 2a^*b^*U_{12}hk + 2a^*c^*U^{13}h\ell + 2b^*c^*U_{23}k\ell)]$.

LS is the program which controlled the actual least-squares refinement of the structural solution and was used to select the number of cycles, the weighting scheme (usually sigma weights), and the sigma cutoff for the data (when $I > 3\sigma(I)$, the reflection was considered to be observed). Refinements were normally based on *F* but were occasionally based on F^2. Difference Fourier calculations, controlled with the program FOURIER, were used to find missing atoms in structural models. Tables of atomic parameters, interatomic distances and angles, and structure factors were

generated by the program FINISH. Publication quality pictures were produced on the DEClaser 2100 printer using the ORTEP [82].

The single crystal refinements reported in this work were based on *F* and minimized the function $\Sigma w(|F_o| - |F_c|)^2$, where $w = 1/\sigma^2(|F_o|)$, in contrast to the Rietveld minimization function based on *I*. The single crystal residuals were defined as $R = \Sigma | |F_o| - |F_c| | / \Sigma |F_o|$ and $R_w = [\Sigma w(|F_o| - |F_c|)^2 / \Sigma w |F_o|^2]^{1/2}$ and "goodness of fit" was defined $GOF = \Sigma((|F_o| - |F_c|) / \sigma_i) / (N_{obs} - N_{parameters})$. Single crystal refinements based on *F* reached lower residual values than those based on F^2. Since $I \propto F^2$, direct comparison between residuals obtained for single crystal and powder work was misleading as to which was the better result.

TOF neutron powder scattering techniques

Neutron scattering experiments were performed on the HIPD (high intensity powder diffractometer) at the LANSCE (Manual Lujan Jr. Neutron Scattering Center) facility of Los Alamos National Laboratory with the help of instrument scientist Robert Von Dreele. LANSCE has a spallation neutron source which uses accelerated and pulsed (20 ns pulses at 50 Hz) high energy protons striking a tungsten target to produce neutrons with the same pulse characteristics. Spallation produces approximately 20 to 30 high-energy neutrons per each proton which strikes the target because of a chain-reaction type mechanism. These neutrons are moderated with heavy water to the lower energy levels of "thermal" neutrons which are useful for diffraction studies because their wavelengths, 1-2 Å, are similar to the interatomic distances in many solid state materials and the resolution in a diffraction experiment is close to the wavelength used. The physical size of the moderator is small, minimizing the spread in the neutron pulse and maximizing the time resolution. A small amount of cadmium is used in the moderators to absorb the highest energy neutrons and keep the moderator functional with a small size.

When these data were collected, the HIPD instrument had six TOF (time-of-flight) detectors at ± 153.4°, ± 90.0°, and ±39.8° in 2θ. Data were collected from all six available banks of detectors but, in general, the latter five banks did not yield data

of as high a quality as the high resolution +153.4° bank and consequently were not used in the refinements discussed here.

The TOF (time-of-flight) neutron scattering data were continually summed with each pulse until the change in diffraction data relative to the change in time, was nearly constant. This corresponded to "roughly" two hours of beam time when the proton flux was at its maximum of 75 μA, however considerable amounts of "down time" and/or reduced proton flux increased the actual time of data collection up to a maximum of 6 hours for one sample.

TOF neutron scattering can be described in terms of Bragg's law, $\lambda = 2d \sin \theta$, but not exactly like constant wavelength X-ray scattering is described. In X-ray powder diffraction, the d-spacings are determined from differing 2θ values for various reflections at constant λ. In TOF powder neutron scattering, the d-spacings are determined at constant 2θ from differing wavelengths where $\lambda = Th/Lm$ (T = measured time interval, L = total flight path, h = Planck's constant, and m = mass of a neutron). The frequency of the neutron pulses determines, in part, the range of measurable wavelengths but since the total flight paths vary from detector to detector, the accessible λ's also vary.

GSAS was used to refine the collected neutron data which was appropriate since GSAS was developed at Los Alamos where the data were collected. Because the incident intensities were not identical for each data point in the neutron TOF experiments, the observed intensities were normalized. The same function, $M = \Sigma[w(I_o - I_c)^2]$, used in the Rietveld X-ray powder refinements was minimized by GENLES in the neutron powder refinements and w, the weighting, was computed according to the normalization mentioned above. The least-squares refinement procedures for the neutron data were comparable to those for the X-ray data. The profile coefficients were somewhat different, although the coefficient for strain broadening, sig1, was again refined while that for particle size broadening, sig2, was not. The diffractometer zero and absorption parameters were refined for the neutron

data but not for the X-ray data. The thermal parameters used by GSAS in refinement of neutron data are the same as those used by GSAS in refinement of X-ray data.

Two fundamental differences between neutron and X-ray scattering experiments exist. First, neutron scattering experiments have lower resolution than X-ray diffraction experiments and it was easier to model the neutron data than it was to model the X-ray data. Lower residuals were obtained for refinements of neutron data than were obtained for refinements of X-ray data from the same samples. The second fundamental difference [88] concerns the scattering behavior of different elements in the two experiments. X-rays are diffracted in a manner directly proportional to electron densities which vary periodically across the periodic table. Sulfur has twice as many electrons as oxygen and X-rays are diffracted (very nearly) twice as strongly by sulfur as by oxygen. Neutron scattering, on the other hand, does not vary periodically with atomic number. Neutron scattering arises from a combination of two sources, potential scattering which depends upon the number of nuclear particles and resonance scattering which depends upon the absorption of neutrons by the nucleus. The potential scattering varies periodically with atomic mass but the resonance scattering does not, sometimes it adds to the potential scattering and sometimes it is subtracted. There result characteristic neutron scattering lengths b, in units of 10^{-12} cm. Additionally, neutron scattering is essentially point scattering, independent of angle, since the nuclei are minuscule relative to the wavelength of the neutron while X-ray diffraction is strongly dependant on angle (intensities decrease rapidly with increasing angle) because the size of the electron cloud around an atom or ion is roughly the same as the wavelength of the diffracted X-rays.

No simple pattern to nuclear scattering can be seen from the following examples of coherent nuclear scattering lengths (b's in units of 10^{-12} cm), which were used in this work: O (b = 0.5805), S (b = 0.2847), Zr (b = 0.716), Nb (b = 0.7054), Hf (b = 0.777), and Ta (b = 0.691). These scattering lengths are for the elements with their natural abundances but the scattering length for a specific isotope can be substantially different. It is apparent that sulfur and oxygen should be distinguishable

through neutron diffraction while Ta, Nb, and Zr (and even Hf) will not be easily resolved.

SEM-EDS elemental analysis

Scanning electron microscopy with energy dispersive X-ray spectroscopy (SEM-EDS) was used in this research to investigate the compositions of specific phases in multi-phase samples. In particular, the κ-phases discovered in this work were analyzed to determine whether or not oxygen was required in their syntheses. The results were ambiguous in that oxygen was present but not determined to be necessary. The results pertaining to the heavy transition metal elements were more accurate than those pertaining to the light elements, sulfur and oxygen.

All samples were mounted in epoxy and hand-polished before data collection and analysis were performed by Warren Strazheim using a JEOL JSM-840 electron microscope and a Kevex EDX detector system with the accompanying software.

Magnetic susceptibility measurements

Magnetic susceptibility measurements were routinely performed on new compounds by Jerry Ostenson using a Quantum Designs superconducting quantum interference device (SQUID) with a 50 mm length of sample motion in order to detect superconductivity. In a typical experiment, magnetic flux exclusion (Meissner screening) was measured down to ~4K, the approximate b.p. of He, with an applied field of 50-100 Oe. Large (~100%) amounts of magnetic flux exclusion (uncorrected for demagnetization effects) indicated that the bulk of the samples became superconducting at the transition temperature, although uncorrected flux exclusions of up to 150% for pure, spherical superconducting samples are measured due to demagnetization effects. It is actually inappropriate to discuss flux expulsions that have not been corrected for demagnetization effects. Obviously, a sample can not expel more than all (100 %) of the magnetic flux present in the experiment. On the other hand, calculation of the demagnetization factors for irregularly shaped samples is difficult, if not impossible.

The magnetic susceptibility for selected samples was measured as a function of temperature (up to room temperature) and the results were core-corrected for diamagnetism.

3. NEW KAPPA PHASES

Introduction

New κ-phases were discovered in the Zr-Ta-S, Zr-Nb-S, Zr-V-S, Hf-Ta-S, Hf-Nb-S, and Hf-V-S systems and all but the Hf-Ta-S κ-phase were crystallographically characterized. Detailed accounts of the discovery and syntheses of these new compounds are given in the first section of this chapter. The X-ray single crystal investigations of these κ-phases are described in the next section. X-ray diffraction experiments reliably determined the metal site occupancies in these phases and it was found that statistical mixing of the metals primarily on one site occurred for the Ta and Nb compounds. The X-ray intensities also indicated that the octahedral nonmetal sites were not fully occupied by sulfur and the M-X distances to this site were substantially shorter than expected M-S distances. Previous investigations of other κ-phases had suggested that the presence of adventitious oxygen promoted the formation of these phases and that the oxygen (full or partial occupancy) was located on the octahedral sites. The simultaneous presence of sulfur, oxygen, and vacancies on these sites could not be determined solely through X-ray diffraction experiments but was entirely consistent with the M-X distances and electron intensities obtained through the X-ray single crystal work.

Combined neutron and X-ray powder refinements are described in the next section and prove with a high degree of reliability that the octahedral nonmetal sites are occupied by a mixture of sulfur, oxygen, and vacancies in the Zr-Nb-S and Zr-Ta-S κ-phases. These results are important and show that modern techniques of crystallography can answer the subtle and difficult questions of nonstoichiometry (both mixed occupancies and/or vacancies) common in solid state chemistry and materials science today. A discussion with a complete structural description and brief history of the κ-phases is given in the next section. Some of the important results from this work are also reiterated in this discussion section. A thorough study of the superconductivity found in the Zr-Nb-S κ-phase is described in the last section along with a brief description of the superconductivity found in the Hf-Nb-S κ-phase.

Synthesis and Characterization

A sample of Ta_4ZrS_2, prepared by mixing and pelletizing the appropriate quantities of previously synthesized Ta_2S and Zr metal, lost large quantities of sulfur upon arcmelting and exhibited a miscibility gap which was visually observed as two distinct regions while the sample was molten. The cooled pellet contained two well separated but poorly crystalline phases. Pieces of these two phases were pulverized and a Guinier X-ray powder pattern of the silver colored phase resembled that calculated for α-Ta_6S [35] while the Guinier powder pattern of the gold colored phase resembled those calculated for zirconium deficient monosulfides ($Zr_{1-x}S$) [20]. Further investigation of the Zr-Ta-S system revealed that Zr-rich samples cleanly reacted in the arcmelter without substantial loss of sulfur and appeared to be homogeneous.

A sample of $Zr_4Ta_{1.1}S_{1.6}$ was prepared by pelletizing the appropriate quantities of previously synthesized "Zr_3S", "Ta_3S", and Ta metal. This pellet was arcmelted for 30 secs. (at 10 V, 50 A), inverted and arcmelted again for 30 secs. (at 10 V, 75 A). The Guinier X-ray powder pattern of crushed pieces of this sample showed the patterns of two phases which resembled those calculated for Zr_2S [55] and Zr_3S_2 [89], although several of the observed reflection intensities were markedly different from those calculated for $Zr_4TaS_{2.5}$ with random metal occupancies in the Zr_2S structure. It seemed probable that Ta had ordered onto specific metal sites in the Zr_2S structure causing the differences between calculated and observed intensities. This "hypothetical" Ta ordering was of sufficient interest that an attempt was made to grow single crystals which would be suitable for crystallographic study. The sample was annealed in an induction furnace at 1300 °C for 15 hours with a residual pressure of $\leq 10^{-6}$ torr.

A Guinier X-ray powder pattern of a crushed piece of this annealed sample yielded interesting results. It no longer resembled that calculated for a mixture of Zr_3S_2 and Zr_2S, but instead appeared to be a mixture of Zr_3S_2 and an unknown phase. The unknown phase matched no calculated powder patterns for any of the known binary Ta or Zr sulfides and no ternary Ta-Zr sulfides were known to exist. This new

phase was indexed using the program TREOR [77]. In the final indexing, eighteen sharp intense lines (those identified as belonging to Zr_3S_2 were excluded) were indexed on a primitive hexagonal lattice with cell parameters a = 9.1000 (4) Å and c = 9.0245 (7) Å and a high figure of merit, M(18) = 44.

Small pieces of sample were mounted on glass fibers and examined with X-ray rotation photographic techniques in order to select single crystals. An irregular chunk was chosen for collection of an intensity data set using a rotating anode Rigaku AFC6R diffractometer with monochromatic Mo Kα X-radiation (λ = 0.71069 Å). The details of this data collection will not be fully discussed because another data set was collected for a different crystal, but the details of the initial structural solution will be discussed later. A structural solution (R = 3.2%, R_w = 3.5%) was obtained for this crystal in the space group $P6_3/mmc$ (#194) with lattice parameters obtained from the Rigaku AFC6R diffractometer, a = 9.069 (2) Å and c = 8.994 (3) Å, and an idealized stoichiometry of $Zr_9Ta_4S_4$.

The structure is that of a large group of ternary and quaternary compounds called κ-phases [39,40] which, in general, can be represented as $M_{9+x}M'_{4-x}XX'_3$. In this formula M and M′ can be a variety of early and middle transition metals, X and X′ can be a variety of nonmetals or vacancies, and X can also be 3d iron-group transition metals. This compound was the first Ta containing example of this structure type and it also exhibited the largest volume (by ~ 13%) and the largest amount of nonmetal (except carbon or oxygen) per formula unit of any known kappa phase. The refined stoichiometry, $Zr_{9.6}Ta_{3.4}S_{3.3}$, included mixed metal site occupancy of primarily one metal site and partial occupation of one of the two sulfur sites.

X-ray diffraction techniques depend primarily upon electron density and not on the specific type of element so that the electron density of a site partially occupied by sulfur would be nearly identical to that of a site which was occupied by the correct proportions of oxygen and sulfur, e.g. 2S ≈ 1S + 2O (in electron density). Also, the distances between the nearest metal sites and the partially occupied sulfur site fell between the expected M-O and M-S distances. Furthermore it has been suggested

that oxygen is required to stabilize kappa phases in some systems [42]. For these reasons, new samples with nominal stoichiometries $Zr_{9.60}Ta_{3.46}S_{2.63}O_{1.44}$ and $Zr_{9.8}Ta_{3.2}S_{3.6}$ were prepared in order to investigate the possibility of oxygen incorporation into the Zr-Ta-S kappa phase. These samples were prepared as before except that ZrO_2 (Johnson Matthey, Puratronic 99.9975%) was used for the source of additional oxygen. Pieces of these arcmelted and annealed samples were pulverized and photographed with the Guinier X-ray powder technique. The diffraction lines corresponding to the κ-phases in both samples were much more intense than any diffraction lines from the minor phases discussed below. This suggested that the κ-phases were the major phases (estimated > 80 wt.%). The first sample, which contained oxygen in the starting materials, had a volume of 595.2 (2) $Å^3$ calculated with the least squares program LATT99 [78] using the 2θ values for reflections obtained with the program GUIN [75], and the second sample, which did not initially contain oxygen, had a volume of 637.8 (2) $Å^3$ also calculated with LATT99. The difference in volumes appeared to be correlated with the different amounts of oxygen present in the samples, however the results obtained from electron microscopy discussed below are somewhat ambiguous.

Three phases, the major κ-phase (estimated at > 80 wt. %) and the minor Zr_2S and M(O) phases, were detected by the SEM-EDS technique. The symbol M(O) represents a Ta/Zr/O solid solution which is Ta rich, forms in a *bcc* structure like Ta metal, and contains a small amount of oxygen. A fourth phase , Zr_3S_2, was not detected in this SEM-EDS experiment but was observed to give diffraction lines in the Guinier X-ray powder patterns.

The κ-phase results from this SEM-EDS analysis are reported in Table 3.1. The detected values of elemental composition, these values scaled to a total of 13 metal atoms as in the κ-phase formula, $(MM')_{13}(XX')_4$, and the initial compositions before arcmelting are given in this table. The presence of Ti is discussed below.

The detection of titanium metal (4.4 - 9.4 atomic %) in these κ-phases was a complete surprise. It is possible that a Ti getter was inadvertently used instead of

Table 3.1 Bulk κ-phase stoichiometries from SEM-EDS

initial composition	detected value	scaled value
$Zr_{9.6}Ta_{3.46}S_{2.63}O_{1.44}$	$Zr_{47.2}Ta_{20.1}Ti_{9.4}S_{8.0}O_{15.4}$	$Zr_{8.00}Ta_{3.41}Ti_{1.59}S_{1.36}O_{2.61}$
	$Zr_{42.6}Ta_{18.3}Ti_{8.0}S_{7.8}O_{23.2}$	$Zr_{8.04}Ta_{3.45}Ti_{1.51}S_{1.47}O_{4.38}$
$Zr_{9.8}Ta_{3.2}S_{3.6}$	$Zr_{43.4}Ta_{16.8}Ti_{4.1}S_{12.8}O_{22.9}$	$Zr_{8.77}Ta_{3.40}Ti_{0.83}S_{2.59}O_{4.63}$
	$Zr_{49.2}Ta_{18.7}Ti_{4.4}S_{13.5}O_{14.1}$	$Zr_{8.85}Ta_{3.36}Ti_{0.79}S_{2.43}O_{2.53}$
$Zr_{9.6}Ta_{3.4}S_{4.0}$	$Zr_{60.8}Ta_{20.0}S_{16.6}O_{2.5}$	$Zr_{9.78}Ta_{3.22}S_{2.87}O_{0.40}$
$Zr_{9.5}Nb_{3.5}S_{3.5}$	$Zr_{60.2}Nb_{24.1}S_{8.0}O_{7.7}$	$Zr_{9.28}Nb_{3.72}S_{1.23}O_{1.19}$
$Hf_{11}Nb_2S_3$	$Hf_{51.1}Nb_{11.1}S_{15.1}O_{22.7}$	$Hf_{10.7}Nb_{2.32}S_{3.16}O_{4.74}$
	$Hf_{53.9}Nb_{9.2}S_{17.1}O_{19.9}$	$Hf_{11.1}Nb_{1.90}S_{3.52}O_{4.10}$
$Hf_{9.6}Nb_{3.4}S_{3.4}$	$Hf_{45.5}Nb_{17.3}S_{11.9}O_{25.4}$	$Hf_{9.41}Nb_{3.59}S_{2.47}O_{5.27}$
	$Hf_{50.1}Nb_{18.4}S_{15.1}O_{16.4}$	$Hf_{9.51}Nb_{3.49}S_{2.87}O_{3.11}$
$Zr_9Nb_4S_4$	$Zr_{54.3}Nb_{14.2}S_{9.3}O_{22.2}$	$Zr_{10.3}Nb_{2.70}S_{1.76}O_{4.21}$
	$Zr_{55.2}Nb_{14.4}S_{9.0}O_{21.4}$	$Zr_{10.3}Nb_{2.69}S_{1.68}O_{4.00}$

a Zr getter (Ti and Zr metals look similar) and the Ti was incorporated into the samples during arcmelting. It is more likely that the Zr metal used in synthesis of these samples (Johnson Matthey 99.9% –20+60 mesh) was from the same batch of Zr metal that was found to be contaminated with Ti [70]. Assuming that the Ti was a contaminant of the zirconium, the detected metal ratios (Zr,Ti)/Ta are quite similar

to the metal ratios of the initial samples. The detected amounts of sulfur are considerably less than the initial amounts, but are consistent within the same sample and reasonable since there were other sulfur-rich minor phases present and sulfur was lost upon arcmelting. The sample which was formulated with the most sulfur was analyzed to have the most sulfur.

The experimental values obtained for oxygen content in these samples are unrealistic and inconsistent within the same sample. The first sample, initially $Zr_{9.60}Ta_{3.46}S_{2.63}O_{1.44}$, was analyzed, in this experiment, to contain between two and three times as much oxygen as it contained sulfur. The second sample, initially $Zr_{9.8}Ta_{3.2}S_{3.6}$, was analyzed to contain between one and two times as much oxygen as it did sulfur. The large amount of oxygen found in these samples was not entirely unexpected since high temperature synthetic techniques are susceptible to adventitious oxygen contamination, however the total amount of sulfur and oxygen detected in these two samples was larger than possible in three out of four cases. If both nonmetal sites are fully occupied, the total amount of sulfur and oxygen cannot exceed four per formula unit in these κ-phases and it is unlikely that more than a few atomic % oxygen could be dissolved into the structure without disrupting it. In one sample, the analyzed sulfur and oxygen content summed to 7.22 per formula unit.

New binary zirconium sulfide materials, Zr_2S and "Zr_3S", were prepared from a different batch of Zr metal (Johnson Matthey, 99.9% -20+60 mesh) which had been obtained from the same supplier and analyzed using the ESCA technique which showed Zr to be the only metal present. All Zr subsequently used in this research was obtained from this "pure" batch or from a Zr crystal bar (Ames Lab). Samples of $Zr_{9.6}Ta_{3.4}S_{4.0}$ and $Zr_{9.6}Ta_{3.4}SO_{3.0}$ were prepared in the same general fashion as used previously. Pieces of the annealed, arcmelted pellets were pulverized and Guinier powder photographs were obtained. Comparison of the experimental powder patterns with calculated powder patterns of kappa phases and all known metal-rich binary Ta and Zr sulfides indicated that both samples had the kappa phase as the major component (estimated at > 80 wt.%). The sample with oxygen purposely added had

a much smaller volume (obtained from least squares calculations of the lattice parameters using the program LATT99) than the one without any added oxygen, 595.9 Å^3 vs. 647.2 Å^3.

The results of SEM-EDS analysis on $Zr_{9.6}Ta_{3.4}S_{4.0}$, given in Table 3.1, showed that no Ti was present. The detected level of oxygen in the $Zr_{9.6}Ta_{3.4}S_{4.0}$ sample was 0.4 oxygens per formula unit but the lowest possible detection sensitivity (under optimum conditions) for the technique of SEM-EDS is approximately 1 wt% for a light element such as oxygen in a heavy metal matrix [90] which is approximately 1 oxygen per formula unit in this system. The presence of oxygen in this sample was therefore not reliably determined with this technique and may or may not have been real. Thus, the question of oxygen occupancy and/or phase stabilization remained, in part, unanswered. It was apparent from the volume difference and phase identities in these samples that the kappa phase could form with varying sulfur and oxygen content in the Zr-Ta-S-O system but it was not known if oxygen was necessary. The detector had been serviced and cleaned shortly before this last analysis was performed and these particular results are felt to be more accurate than other SEM-EDS analyses discussed in this dissertation.

Samples with similar initial stoichiometries, $M_{9+x}M'_{4-x}S_{4-y}$ with $x \approx 0.6$ and $y \leq 1$, in the systems Zr-Nb-S, Hf-Nb-S, and Hf-Ta-S were investigated with M = Zr or Hf and M′ = Ta or Nb. The samples were prepared from previously synthesized binaries (Zr_2S, "Zr_3S", Hf_2S, "Hf_3S", Ta_2S, "Ta_3S", "Nb_2S", and/or "Nb_3S") and the metals (Zr, Hf, Ta, and/or Nb) and then arcmelted and annealed. New kappa phases were identified in all of these systems, however another new result was also found in the Hf-Ta-S system, the novel "stuffed" gamma brass, $Hf_{10.1}Ta_{2.9}S_3$ [45].

The results of SEM-EDS elemental analyses on κ-phase samples with the initial compositions $Zr_{9.5}Nb_{3.5}S_{3.5}$, $Hf_{11}Nb_2S_3$, $Hf_{9.6}Nb_{3.4}S_{3.4}$, and $Zr_9Nb_4S_4$ are also given in Table 3.1. Those samples which are grouped together were analyzed at the same time. Electron microscopy revealed that the Hf-Nb-S samples were nearly homogeneous single phase materials with minor amounts of M(O) present, the Zr-Ta-

S samples had κ as the major phase with minor amounts of Zr_2S and M(O) phases present, and the Zr-Nb-S samples had κ as the major phase with substantial amounts of Zr_3S_2, Zr_2S, and M(O) phases present. A different sample with initial composition $Zr_{9.3}Nb_{3.7}S_{3.7}$ was found to be nearly a single phase material and was used to investigate the superconductive properties of the Zr-Nb-S-O κ-phase [64]. ICP analysis for Zr, Nb, and S (but not oxygen) was performed on the $Zr_9Nb_4S_4$ sample and within ±4% relative error the stoichiometry was determined to be $Zr_{8.66}Nb_{4.34}S_{4.01}$ for the bulk material. Judging from this ICP analysis, the approximate phase identity of the sample, the initial composition, and the detected values listed in Table 3.1, SEM-EDS is not a quantitative technique for analysis of O or S in a heavy transition-metal matrix.

Further investigations suggested that the specific starting materials were not significant in the synthesis of the kappa phases discussed here as long as the overall stoichiometry was correct and the sulfur was available as a prereacted metal sulfide. Interestingly, the kappa phase $Hf_{9+x}Nb_{4-x}S_{4-y}$ was prepared as a nearly single phase material by arcmelting, but all attempts at annealing samples between 1200 °C and 1300 °C resulted in the disappearance of the κ-phase and formation of the binaries, Hf_3S_2 [93] and Hf_2S [54], and a metal solid solution, Nb(Hf), instead. Several attempts at synthesizing this kappa phase with oxygen purposely added, using HfO_2, resulted in formation directly from the arcmelt of the same binaries and metal solid solution that were formed by annealing as above. It is not known if this is an entropic effect (disproportionation of the Hf-Nb-S kappa phase at reduced temperatures) or is caused by the presence of adventitious oxygen. Other than the Hf-Nb-S kappa phase, temperature appeared to affect only the diffusional barriers in these systems. High annealing temperatures required less time of reaction to achieve sharply crystalline samples than did low annealing temperatures. Annealing did not change the phase identities of any of the other κ-phase samples.

It is interesting to note that the stoichiometries of the "stuffed" gamma brass and the κ-phase are similar, $M_{13}S_3$ vs. $M_{13}S_{4-y}$. In the Hf-Ta-S system the presence

of oxygen led to the stabilization of the κ-phase over the stuffed γ-brass phase. However, no single crystals of this kappa phase were obtained and thus no single crystal X-ray refinement was carried out. When the samples were carefully synthesized to exclude adventitious oxygen, the major phase obtained was the stuffed γ-brass phase and only weak lines could be identified as corresponding to the κ-phase. At the other extreme, when oxygen in the form of HfO_2 was used to synthesize a sample of initial composition $Hf_7Ta_6S_{2.6}O_{1.4}$, binary Hf_2S and the metals Hf and Ta were the only identifiable phases formed, much as in the Hf-Nb-S-O system. Somewhere between these extremes the kappa phase is stabilized. Trial and error experimentation suggested that the kappa phase formed most readily when the bulk composition, without considering the adventitious oxygen, was approximately $Hf_8Ta_5S_{4-x}O_x$ ($x \leq 0.5$). Two samples, $Hf_{8.3}Ta_{4.7}S_{3.5}O_{0.2}$ and $Hf_{8.3}Ta_{4.7}S_{3.5}O_{0.6}$, were arcmelted and annealed at 1300 °C for 15 hours in order to further investigate the role of oxygen in the formation of the Hf-Ta-S-O κ-phase. Both samples consisted of Hf_2S, Ta metal, and the κ-phase in approximately equal amounts after annealing. The Guinier diffraction lines were sharper (especially at high 2θ), indicating higher crystallinity, for the κ-phase in the $Hf_{8.3}Ta_{4.7}S_{3.5}O_{0.2}$ sample than in the $Hf_{8.3}Ta_{4.7}S_{3.5}O_{0.6}$ sample. This suggested that the optimum amount of added oxygen was less than 0.5 per formula unit, however the total oxygen content, including adventitious oxygen, was undetermined. The optimum hafnium, tantalum, and sulfur stoichiometry for this κ-phase is also indeterminate at present. The "stuffed" γ-brass and many κ-phases are known to exhibit mixed occupancies of at least one metal site. Phase widths associated with the mixed occupancies complicate study of the Hf-Ta-S-O system.

Kappa-phases in the Zr-V-S and Hf-V-S systems were discovered during a separate investigation. Zr_9S_2 [30], α-V_3S [29], and β-V_3S [29] are members of a class of compounds which contain doubly-centered polyhedra linked in different arrangements as discussed in the introduction. An obvious experimental avenue was to investigate the Zr-V-S mixed metal-rich system to see if any structures would form with new arrangements of these polyhedra. As before, the initial samples were

prepared from appropriate quantities of the binary sulfides (V_3S, Hf_2S, or Zr_2S) and the metals (V, Hf, or Zr). During these investigations, a sample with the composition Zr_2V_2S was arcmelted and annealed. A piece of this sample was crushed and a Guinier powder pattern of it was obtained. The powder pattern was identified as belonging to a kappa phase and further investigations resulted in finding that samples of the stoichiometric composition Zr_9V_4S were nearly homogeneous κ-phase materials. An arcmelted and annealed sample of Hf_9V_4S was also identified as a nearly homogeneous κ-phase material.

Kappa phase samples of the nominal stoichiometries $Zr_{10}Ta_3S_{3.4}$, $Zr_{9.6}Nb_{3.4}S_{3.4}$, and $Hf_{10}TaNb_2S_3$ were prepared in five gram quantities to be used for neutron data collections with the purpose of determining the sulfur/oxygen/vacancy populations and metal site occupancies in these phases. Two approximately 2.5 gram samples of each composition were formulated out of the binaries and metals, pelletized, and arcmelted. These samples were arcmelted a total of three times each, inverted between arcmeltings to promote homogenization, and then combined. The large sample size and the fact that they were supported on a water-cooled copper hearth allowed temperature gradients to form within the pellets upon cooling so that they were not totally homogeneous. The Zr-Ta-S kappa phase was annealed at 1220 °C for 18 hours, the Zr-Nb-S kappa phase was annealed at 1155 °C for 12 hours, and the Hf-Ta-Nb-S sample, which actually had two major phases ("stuffed" gamma brass and kappa) was not annealed since annealing had previously been observed to destroy the phase identity of arcmelted Hf-Nb-S samples.

All samples were crushed repeatedly until the particle size fell approximately in the range 0.1 - 0.5 mm in diameter which was suitable for neutron scattering experiments. A small quantity (~0.2 grams) of each sample was removed to be used in further X-ray powder diffraction experiments and the bulk samples were stored in a desiccator to protect them from the high atmospheric humidity found in Iowa during the summer. The approximately 0.2 gram portions of the bulk samples were ground with clean agate mortars and pestles until the largest particles were ≤ 0.05 mm long

on an edge and the majority of the particles were less than 0.005 mm in diameter (estimated from observations through an optical microscope).

Guinier X-ray powder patterns of the finely ground samples exhibited more diffuse diffraction lines than did Guinier powder patterns of less finely ground samples. There are two reasons for line broadening in these samples. The first reason is that the effect of particle size broadening begins to be observable when N (the number of unit cells in one direction within the crystal) is less than 3500 [91]. For these κ-phases, the body diagonals ≈ 18 Å, so that 3500 × 18 Å ≈ 6 μm for the approximate particle size at which line broadening begins to be observed. The majority of particles in these finely ground samples were estimated to be smaller than 5 μm in diameter and it is therefore likely that a significant number of particles contributed to the observed line broadening.

A second factor contributing to line broadening is sample degradation caused by reaction with atmospheric H_2O. The faint odor of H_2S gas was noticed upon grinding these samples in air which means that even though these metal-rich sulfides are not "air-sensitive", surface oxidation by atmospheric gases occurs. Fine grinding of these samples greatly increased their surface area and thus increased the amount of surface oxidation present in the finely ground samples relative to that found in the coarsely ground samples. Changing the average diameter of the particles from 0.1 mm to 0.005 mm increased the surface area by a factor of twenty.

Kappa phase samples from the five systems, Zr-Ta-S, Zr-Nb-S, Zr-V-S, Hf-Nb-S, and Hf-V-S were checked for superconductivity by measuring their magnetic flux exclusion at low temperatures with a Squid magnetometer. Only the Zr-Nb-S and Hf-Nb-S kappa phases exhibited significant flux exclusion during measurements to 2 K and these findings will be covered in the section on superconductivity.

X-ray Single Crystal Investigations

Single crystals of the previously mentioned kappa phases (except in the Hf-Ta-S and Hf-Nb-S systems) were obtained as small fragments from the corresponding arcmelted, annealed, and crushed samples. Single crystals were not obtained for the

Hf-Ta-S κ-phase and the single crystals from the Hf-Nb-S system were directly obtained from an arcmelted sample. Approximately 10 to 15 different fragments of each sample were examined with X-ray rotation photographic techniques in order to select the best "single" crystal of each. In all five systems of kappa phases for which crystals could be found, twinning appeared to be common, although it caused no insoluble problems. A more severe problem was that the suitable "single" crystals were generally of such a small size that an intense X-ray source was required for data collection. Out of the available diffractometers (Rigaku AFC6R, Enraf-Nonius CAD4, and a modified Hilger-Watts), only the rotating anode Rigaku AFC6R diffractometer was capable of collecting data sets with enough observed reflections to be useful for refinement. The data sets discussed here are recollections in all but the Hf-V-S system because the first data sets were not of the highest quality, due mostly to the small sizes of the mounted crystals. The data set for the Hf-V-S kappa phase was also not of the highest quality but was not recollected. The kappa phase X-ray single crystal refinements were performed on intensity data sets collected with a rotating anode Rigaku AFC6R diffractometer and monochromatic Mo Kα (λ = 0.71069 Å) X-radiation. The 2θ-ω scan technique was used in all five cases and the data collection temperature was consistently 23 °C (±1 °C). The kappa phase single crystal from the Hf-Nb-S system required using the program INDEX TWIN on the diffractometer to obtain a starting unit cell for the data collection, but the other four kappa phase single crystals were easily indexed using all unique reflections found by the SEARCH algorithm. The observed intensities were corrected for Lorentz polarization and absorption effects. In all cases PSI scan absorption corrections were performed, but in the Zr-Ta-S κ-phase system, an additional DIFABS [86] θ-dependent absorption correction was also applied in order to be able to anisotropically refine the sulfur thermal parameters. There was no decay observed in any of these data collections. Pertinent crystallographic details for the X-ray single crystal data collections and refinements of the five kappa phases are reported in Table 3.2 and include least squares lattice parameters calculated from powder patterns of the bulk

Table 3.2 Crystal data for kappa phases (space group $P6_3/mmc$, Z = 2)

Formula	$Zr_{9.7}Ta_{3.3}S_{3.1}$	$Hf_{10.0}Nb_{3.0}S_{3.0}$	$Hf_9V_4SO_{0.6}$	Zr_9V_4S	$Zr_{8.1}Nb_{4.9}S_{2.7}$
a, Å	9.122 (1)	9.080 (2)	8.578 (1)	8.626 (1)	9.119 (1)
c, Å	9.057 (2)	8.908 (4)	8.454 (1)	8.615 (3)	8.968 (1)
Volume, $Å^3$	652.7 (2)	636.0 (4)	538.7 (4)	555.2 (2)	645.8 (1)
d_{calc}, g/cm^3	8.10	11.27	11.47	6.32	6.59
Cryst. size, mm^3	0.11 × 0.03 × 0.02	0.09 × 0.05 × 0.01	0.04 ×0.04 × 0.02	0.06 × 0.03 × 0.01	0.12 × 0.05 × 0.03
Instrument	AFC6R	AFC6R	AFC6R	AFC6R	AFC6R
Orientation refl. #, 2θ	13, 13.9 - 16.4	13, 13.8 - 17.3	15, 14.6 - 18.2	15, 14.4 - 17.3	15, 13.8 - 32.1
Octants	hk±ℓ	hk±ℓ	±hk±ℓ	hk±ℓ	hk±ℓ
Maximum 2θ	65°	60°	55°	55°	60°
# refl.	956	1456	1812	574	1450
Unique (obs.)	466 (311)	421 (226)	268 (148)	277 (166)	386 (283)
# Parameters	27	28	19	20	25
μ (cm^{-1})	375	832	895	112	109
Secondary ext. coeff. (10^{-7})	3.93 (38)	0.60 (18)	-	-	-
Abs. corr.	DIFABS	Psi Scan	Psi Scan	Psi Scan	Psi Scan
Trans. factors, max., min.	1.0000, 0.7906	1.0000, 0.3428	1.0000, 0.3094	1.0000, 0.6878	1.0000, 0.7769
$R_{averaging}$	0.045	0.104	0.190	0.059	0.049
R^a	0.028	0.029	0.029	0.027	0.030
R_w^b	0.030	0.031	0.029	0.036	0.036
GOF[c]	0.96	1.04	0.90	1.11	1.43
pos. $e^-/Å^3$	2.06	2.83	3.00	1.47	1.76
neg. $e^-/Å^3$	-2.58	-2.60	-2.93	-1.91	-1.94

[a] $R = \Sigma \, | \, | F_o | - | F_c | \, | \, / \, \Sigma \, | F_o |$

[b] $R_w = [\Sigma w (| F_o | - | F_c |)^2 \, / \, \Sigma w \, | F_o |^2]^{1/2}$; $w = 1/\sigma^2(| F_o |)$

[c] $GOF = \Sigma((| F_o | - | F_c |) \, / \, \sigma_i) / (N_{obs} - N_{parameters})$

samples from which the single crystals were obtained using the program LATT99.

The initial kappa phase structural solution in these systems was found for the $Zr_4Ta_{1.1}S_{1.6}$ sample (which contained Ti) as mentioned previously. The structure was determined using the programs of TEXSAN [84]. The data were processed in the space group $P6_3/mmc$, even though three reflections, $00\bar{1}$, 001, and $11\bar{1}$, which should have been systematically absent had weak, but observable, intensities. These extraneous intensities could have originated from secondary diffraction off the (002), $(00\bar{2})$, and $(22\bar{2})$ planes. A psi scan absorption correction was applied and the equivalent reflections were averaged ($R_{averaging} = 0.08$) with good agreement. Direct methods supplied four strong peaks and three weaker peaks per asymmetric unit which were assigned as zirconium (strong peaks) and sulfur (weak peaks). Least squares full-matrix refinements of this trial structure converged and gave indications of how to proceed. One of the assigned sulfur positions had an extremely large isotropic thermal parameter which suggested that the electron density of that site was very low and indicated that the sulfur really wasn't there. Two of the zirconium positions had non-positive definite isotropic thermal parameters which indicated that the positions actually had more electron density than had been assigned to them and suggested that tantalum metal was occupying these sites rather than zirconium.

With these corrections, removing the sulfur and exchanging Ta for Zr on two of the metal sites, the residuals became $R = 0.042$, $R_w = 0.050$ for an isotropic refinement although the thermal parameters were irregular, some being large and others being small. To complete the structure, mixed Ta and Zr occupancies of the metal sites and partial occupancies of the sulfur sites were refined, followed by changing all of the isotropic thermal parameters to anisotropic. One of the metal sites refined with substantial mixing of Ta and Zr on that site and one of the sulfurs refined with a significant vacancy population. The fully occupied sulfur position would not refine anisotropically but all of the metal sites had well-behaved anisotropic thermal parameters. The residuals ($R = 0.032$, $R_w = 0.035$) were completely satisfactory at this point and did not change when the partially vacant sulfur site was fixed at full

occupancy and refined as a mixed sulfur-oxygen site.

The SEM-EDS results which showed that titanium was present in samples synthesized from the same zirconium sulfide starting materials as the sample from which this single crystal was obtained presented an insurmountable obstacle. While one can make an educated guess as to where the Ti was located (on the Zr positions), it is impossible to refine the mixing of three metals (Ta, Zr, and Ti) on any one metal site with X-rays alone. For this reason, new samples were synthesized and analyzed (SEM-EDS showed that Ta and Zr were the only metals present). New crystals were selected for examination on an X-ray rotation camera and intensity data were collected for the "best" single crystal on the Rigaku AFC6R diffractometer.

Later refinements of these kappa phase crystal structures used the atomic positions found in the Zr-Ta-Ti-S κ-phase as a starting point. In all cases, mixed metal occupancies, partial sulfur occupancies, anisotropic thermal parameters, and secondary extinction coefficients were included at some point in the least squares refinement cycles. Occupancies greater than 100% or less than 0% were not allowed. The large differences in the real part of the anomalous scattering for Zr and Nb when using Mo Kα radiation [18,92] allowed refinement of the mixed metal site occupancies in the Zr-Nb-S κ-phase. Atoms (only in the Hf-V-S system) which refined anisotropically to non-positive definite values were refined to positive isotropic values. Secondary extinction coefficients and occupancies were set equal to zero and not refined if their esd's were as large as their refined values. The positional, equivalent isotropic thermal, and occupancy parameters for the five different kappa phase X-ray single crystal refinements are listed in Tables 3.3, 3.4, and 3.5 respectively. The anisotropic thermal parameters for these refinements are given in Table 3.6 and structure factor tables, F_o and F_c (observed and calculated) are given in appendices A and D through G.

Data were collected for $Zr_{9.7}Ta_{3.3}S_{3.1}$ at a speed of 16.0 deg/min over a primitive hexagonal cell. All reflections in the hk±ℓ octants with $h \geq k$ were collected in a range out to 65° in 2θ and none of the systematically absent reflections were observed.

Table 3.3 **κ-phase positional parameters from X-ray single crystal refinements (M4 = 0,0,0; S1 = ⅓,⅔,¾; O = S2 = ½,0,0)**

		$Zr_{9.7}Ta_{3.3}S_{3.1}$	$Hf_{10.0}Nb_{3.0}S_{3.0}$	$Zr_{8.1}Nb_{4.9}S_{2.7}$	$Hf_9V_4SO_{0.6}$	Zr_9V_4S
M1 (x,2x,z)	x	0.19788 (8)	0.19752 (7)	0.19980 (6)	0.1973 (1)	0.1976 (1)
	z	0.5654 (1)	0.5678 (1)	0.5623 (1)	0.5521 (1)	0.5522 (2)
M2 (x,2x,¼)	x	0.4486 (1)	0.4450 (1)	0.4503 (2)	0.4565 (1)	0.4578 (2)
M3 (x,2x,¼)	x	0.1094 (6)	0.1127 (3)	0.11084 (8)	0.1076 (5)	0.1049 (2)

Table 3.4 **κ-phase B_{eq} parameters from X-ray single crystal refinements**

	$Zr_{9.7}Ta_{3.3}S_{3.1}$	$Hf_{10.1}Nb_{2.9}S_{3.1}$	$Zr_{8.1}Nb_{4.9}S_{2.7}$	$Hf_9V_4SO_{0.6}$	Zr_9V_4S
M1	0.94 (5)	0.84 (5)	1.08 (4)	0.77 (6)	0.89 (6)
M2	1.49 (9)	1.8 (1)	1.94 (8)	0.8 (1)	1.0 (1)
M3	0.58 (4)	0.8 (1)	0.65 (5)	0.5 (2)[a]	0.8 (2)
M4	0.55 (3)	0.4 (1)	0.45 (4)	0.7 (3)	1.1 (1)
S1	1.1 (2)	1.3 (4)	1.9 (2)	1.5 (4)[a]	1.7 (2)
S2	1.0 (3)	0.5 (5)	1.2 (3)	-	-
O	-	-	-	1.6 (2)[a]	-

[a] B_{iso} obtained for isotropically refined atoms

Table 3.5 κ-phase occupancies from X-ray single crystal refinements (%)

		$Zr_{9.7}Ta_{3.3}S_{3.1}$	$Hf_{10.0}Nb_{3.0}S_{3.0}$	$Zr_{8.1}Nb_{4.9}S_{2.7}$	$Hf_9V_4SO_{0.6}$	Zr_9V_4S
M1	Zr,Hf	98 (1)	98 (1)	100	100	100
	Ta,Nb,V	2	2	-	-	-
M2	Zr,Hf	100	100	68 (12)	100	100
	Ta,Nb,V	-	-	32	-	-
M3	Ta,Nb,V	76 (1)	64 (1)	100	98 (1)	100
	Zr,Hf	24	36	-	2	-
M4	Ta,Nb,V	100	96 (2)	100	100	100
	Zr,Hf	-	4	-	-	-
S1		100	100	100	100	100
S2		71 (2)	68 (3)	57 (2)	-	-
O		-	-	-	19 (7)	-

Table 3.6 Anisotropic thermal parameters ($\times 10^3$) for five different κ-phases from X-ray single crystal refinements ($U_{12} = \frac{1}{2}U_{22}$)

	U_{11}	U_{22}	U_{33}	U_{13}	U_{23}
$Zr_{9.7}Ta_{3.3}S_{3.1}$					
M1	13.7 (5)	9.8 (6)	10.8 (6)	−0.8 (2)	$2U_{13}$
M2	11.7 (6)	23 (1)	26 (1)	-	-
M3	7.6 (3)	7.2 (4)	7.0 (4)	-	-
M4	7.5 (4)	U_{11}	6.0 (6)	-	-
S1	18 (3)	U_{11}	6 (3)	-	-
S2	11 (2)	14 (3)	13 (3)	1 (1)	$2U_{13}$
$Hf_{10.0}Nb_{3.0}S_{3.0}$					
M1	11.0 (4)	10.2 (6)	10.6 (4)	−0.3 (2)	$2U_{13}$
M2	14.2 (8)	27 (1)	31 (1)	-	-
M3	9 (1)	10 (1)	10 (1)	-	-
M4	7 (2)	U_{11}	3 (3)	-	-
S1	23 (6)	U_{11}	6 (7)	-	-
S2	3 (4)	7 (6)	10 (6)	−4 (3)	$2U_{13}$
$Zr_{8.1}Nb_{4.9}S_{2.7}$					
M1	16.3 (4)	13.2 (5)	10.4 (4)	0.4 (2)	$2U_{13}$
M2	18.6 (6)	35 (1)	25.7 (9)	-	-
M3	9.1 (4)	8.3 (6)	7.0 (5)	-	-
M4	7.1 (6)	U_{11}	2.9 (7)	-	-
S1	34 (3)	U_{11}	4 (2)	-	-
S2	17 (3)	16 (3)	13 (3)	−1 (1)	$2U_{13}$

Table 3.6 continued

	U_{11}	U_{22}	U_{33}	U_{13}	U_{23}
$Hf_9V_4SO_{0.6}$					
M1	10.0 (5)	11.5 (8)	8.4 (5)	-0.2 (3)	$2U_{13}$
M2	8.4 (8)	14 (1)	9.8 (8)	-	-
M3[a] B_{iso} = 0.5 (2)					
M4	10 (4)	U_{11}	7 (6)	-	-
S1[a] B_{iso} = 1.5 (4)					
O[a] B_{iso} = 1.6 (2)					
Zr_9V_4S					
M1	12.6 (6)	13.8 (8)	7.7 (6)	-0.5 (3)	$2U_{13}$
M2	12.4 (7)	19 (1)	10 (1)	-	-
M3	13 (1)	12 (2)	4 (2)	-	-
M4	16 (2)	U_{11}	8 (3)	-	-
S1	26 (3)	U_{11}	13 (5)	-	-

[a] isotropically refined atoms

The final residuals including zeroes (all measured reflections which were not systematically absent) were R = 0.064 and R_w = 0.079 and there was one reflection, 100, which was not observed but had a fairly large calculated structure factor. $\Delta F/\sigma(F)$ for this reflection was -210.67/5.67 = -37.16 and it is not known why the reflection was unobserved. There is a possibility that the beam stop on the diffractometer was sufficiently off-center so that it shielded the detector from the 100 reflection at 5.24° in 2θ.

Data for $Hf_{10.0}Nb_{3.0}S_{3.0}$ were also collected at a speed of 16.0 deg/min over a

primitive hexagonal cell. In this collection, all reflections were measured in the hk±ℓ octants out to 60° in 2θ and two systematically absent reflections, $11\bar{1}$ and $44\bar{9}$ were observed with $I/\sigma(I) > 3$. The final residuals including the zeroes were R = 0.075 and R_w = 0.039 and no large $\Delta F/\sigma(F)$'s were found.

The data set for $Hf_9V_4SO_{0.6}$ was collected at a speed of 16.0 deg/min over the ±hk±ℓ octants of a primitive hexagonal unit cell. Reflections with h + k ≥ 0 in these four octants were collected out to 55° in 2θ and no systematically absent reflections were observed. No large $\Delta F/\sigma(F)$'s were found and the residuals including the zeroes were R = 0.089 and R_w = 0.044 for refinement of these data.

The data sets for Zr_9V_4S and $Zr_{8.1}Nb_{4.9}S_{2.7}$ were both collected at the slower speed of 8.0 deg/min over the hk±ℓ octants of primitive hexagonal cells. All reflections with h ≥ k in these two octants were collected out to 55° in 2θ for the Zr_9V_4S κ-phase and all reflections in these octants were collected out to 60° in 2θ for the $Zr_{8.1}Nb_{4.9}S_{2.7}$ κ-phase. The 001 and $00\bar{1}$ reflections in the Zr-V-S crystal and the 001 and 111 reflections in the Zr-Nb-S crystal were observed, $I/\sigma(I) > 3$, but should have been systematically absent. In the Zr-Nb-S refinement, the reflections $01\bar{2}$ and 220 had $\Delta F/\sigma(F)$'s of 6.00 and -5.27 respectively. The reflection 400 was found to have a $\Delta F/\sigma(F)$ of -5.63 in the Zr-V-S system. The residuals including zeroes were R = 0.047 and R_w = 0.038 for $Zr_{8.1}Nb_{4.9}S_{2.7}$ and R = 0.076 and R_w = 0.046 for Zr_9V_4S.

Examination of Table 3.2 reveals that the internal $R_{averaging}$ for the data sets collected in the Hf-Nb-S and Hf-V-S systems are much larger than in the other three systems. This result is related to the effects of crystal shape and absorption. These κ-phases contain more 5d metal, Hf in this case, than the others and have a larger linear absorption coefficient, μ, than the other κ-phases reported here. Furthermore, the difference between the maximum and the minimum transmission factors found in the PSI scans performed on the five crystals is much greater in the two Hf containing phases than in the others.

When refining occupancies, large correlations between the scale factors, secondary extinction coefficients, thermal parameters, and populations are commonly

found. This occurred in these refinements. Correlation, as used here, means that the absolute value of the calculated correlation coefficient was ≥ ½. In $Zr_{9.7}Ta_{3.3}S_{3.1}$, the scale factor correlated with the thermal parameters and the population of the mixed metal (Ta-Zr) sites, which also correlated with the thermal parameters of the nearest metal neighbors. The thermal parameters and population of the partially occupied sulfur site correlated with each other. In $Hf_{10.1}Nb_{2.9}S_{3.1}$, the scale factor correlated with the thermal parameters and population of the mixed metal sites, which correlated with the thermal parameters of the nearest metal neighbors as well. The thermal parameters and population of the mixed metal sites correlated with each other as did those of the partially vacant sulfur position. Similar correlations were found in $Zr_{8.1}Nb_{4.9}S_{2.7}$. In Zr_9V_4S, the scale factor correlated with the secondary extinction coefficient and with the zirconium thermal parameters. In $Hf_9V_4SO_{0.6}$, the esd's for the occupancy of the one mixed metal site were nearly as large as the occupancy refined for the lesser metal component. If this occupancy was not refined, there was only one correlation coefficient ≥ 0.5 and that was between the occupancy and thermal parameters of the oxygen. However, when the metal site was refined with mixed occupancy, the occupancy and thermal parameters of that site correlated with each other as did the occupancy and thermal parameters of the oxygen and the scale factor correlated with the thermal parameters of one Hf position.

The interatomic distances from these κ-phase refinements are given in Table 3.7 and were consistent with the refined occupancies. Distances involving M3 and M4 were, in general, shorter than those involving M1 and M2 which was in agreement with occupation of M1 and M2 by the group IV transition metals Hf or Zr and occupation of M3 and M4 by group V transition metals Ta, Nb, or V. The M1-S1 distances were substantially larger than the M1-S2 and M2-S2 distances which agreed with full sulfur occupation of S1 and partial sulfur occupation of S2 in the Ta and Nb κ-phases. The M1-S2 and M2-S2 distances in the V κ-phases were significantly smaller than in the Ta and Nb phases which agreed with oxygen occupancy (including partial or none) of the S2 site in the V κ-phase.

Table 3.7 **κ-phase interatomic distances < 3.6 Å (M-S, S-S < 3.3Å) obtained from X-ray single crystal refinements**

		$Zr_{9.7}Ta_{3.3}S_{3.1}$	$Hf_{10.1}Nb_{2.9}S_{3.1}$	$Zr_{8.1}Nb_{4.9}S_{2.7}$	$Hf_9V_4SO_{0.6}$	Zr_9V_4S
M1-M1	×2	3.344 (1)	3.333 (1)	3.348 (1)	3.060 (2)	3.086 (2)
M1-M1	×1	3.343 (2)	3.247 (2)	3.366 (2)	3.346 (3)	3.408 (3)
M1-M2	×2	3.446 (2)	3.451 (1)	3.428 (2)	3.203 (2)	3.229 (2)
M1-M2	×2	3.487 (1)	3.451 (2)	3.437 (1)	3.213 (2)	3.252 (2)
M1-M3	×1	3.181 (1)	3.130 (3)	3.134 (1)	2.880 (4)	2.942 (2)
M1-M3	×2	3.186 (1)	3.150 (1)	3.2142 (9)	3.043 (1)	3.074 (1)
M1-M4	×1	3.182 (1)	3.165 (1)	3.205 (1)	2.964 (2)	2.986 (2)
M1-S1	×2	2.716 (1)	2.683 (1)	2.698 (1)	2.624 (2)	2.649 (2)
M1-S2 (O)	×2	2.4960 (6)	2.4897 (7)	2.4776 (5)	2.3253 (6)	2.3380 (6)
M2-M2	×2	3.154 (4)	3.041 (3)	3.199 (5)	3.168 (4)	3.221 (4)
M2-M3	×2	3.0645 (9)	3.006 (5)	3.045 (1)	2.908 (7)	2.960 (8)
M2-S2 (O)	×2	2.4056 (9)	2.389 (1)	2.376 (1)	2.210 (1)	2.244 (1)
M3-M3	×2	2.994 (2)	3.068 (9)	3.032 (2)	2.77 (1)	2.715 (6)
M3-M4	×2	2.8486 (7)	2.845 (3)	2.8445 (8)	2.650 (5)	2.664 (2)

X-ray and Neutron Powder Investigations

X-ray powder diffraction data were collected for the finely ground samples, $Zr_{10}Ta_3S_{3.4}$, $Zr_{9.6}Nb_{3.4}S_{3.4}$, and $Hf_{10}TaNb_2S_3$. These samples were each loaded on a zero background holder and smoothed so that the tops of the samples were even with the top of the sample holder. The sample holder was placed into a Scintag XDS 2000 (45 kV, 30 mA) θ-θ powder diffractometer and data were collected with Cu Kα X-radiation over a range of 10 - 160° in 2θ as discussed in the experimental chapter.

Time-of-flight (TOF) neutron scattering data were collected for three 5 gram samples, $Zr_{10}Ta_3S_{3.4}$, $Zr_{9.6}Nb_{3.4}S_{3.4}$, and $Hf_{10}TaNb_2S_3$, on the High Intensity Powder Diffractometer (HIPD) at the Manual J. Lujan Neutron Scattering Center (LANSCE) at Los Alamos National Laboratory. One sample (Hf-Ta-Nb-S) was loaded into a fused silica sample container and the other two samples were loaded into vanadium sample containers. These sample containers (and others) were placed into a rotating sample changer and the whole apparatus was loaded into the HIPD.

Rietveld refinements were first performed separately on the X-ray and neutron data sets for these multi-phase systems using GSAS software and then the two types of data were combined in the final refinements. Data from the 153.4° TOF detectors were used in the refinements of the Zr-Nb-S and Hf-Ta-Nb-S samples while data from both the 90.0° and 153.4° TOF detectors were used for refinement of the Zr-Ta-S sample. The raw neutron data were limited in the refinements through RAWPLOT to include only areas containing visually resolvable Bragg peaks. Large background intensities at low 2θ angles in the X-ray data collected for $Zr_{10}Ta_3S_{3.4}$ and $Zr_{9.6}Nb_{3.4}S_{3.4}$ necessitated removal of portions of these data from the refinements.

Full X-ray and neutron refinements were separately converged for all three samples, including full metal site occupancy determinations of all major phases, before the two types of data were merged into the same refinements. All of the parameters which were refined using the X-ray powder data were fixed when the refinements were combined while the absorption, background, scale factor, and profile coefficient parameters were refined for the added neutron data. After convergence

of these neutron specific parameters was achieved, the other parameters were gradually added back into the least-squares refinements. The histogram scale factors for the X-ray data were always fixed at unity. Many trial and error attempts at refinement were required before the correct procedures leading to complete, undamped convergent refinements of the combined data were determined.

The initial refinements of the X-ray data included from seven to eight background parameters (terms of a cosine Fourier series), lattice parameters of the separate phases, and phase fractions (the number of unit cells for each phase that were present relative to the overall histogram scale factor which was set equal to unity). Starting models were based on the corresponding X-ray single crystal structure refinements. The positional and isotropic thermal parameters were refined next. After these least squares cycles had converged, the pseudo-Voigt profile coefficients *LY* (strain broadening) and *shift* were refined. Positional parameters refined to values which were consistent with those found in the X-ray single crystal work and the lattice parameters refined to values which were consistent with those calculated with LATT99 using Guinier X-ray powder films.

The vanadium "cans" were transparent to neutrons and contributed little to the overall neutron scattering of the Zr-Nb-S and Zr-Ta-S samples enclosed within them. Nine to ten terms of Fourier cosine series were used to model the backgrounds of these two data sets. The background for the first sample, Hf-Ta-Nb-S loaded into a thin-walled fused silica tube, was modeled both as a ten term Fourier cosine series and as the radial distribution function [93] of fused silica. Silica glass, although amorphous, exhibits short-range order and diffuse peaks corresponding in d-spacing to the interatomic distances; Si-Si, Si-O, O-O, etc. were detected in the background of the Hf-Ta-Nb-S sample. Refinement using the Fourier series background function resulted in lower residuals than did refinement using the radial distribution function. The refinement using the radial distribution function for background modeling will not be discussed further. Other parameters refined for the neutron data included absorption, the profile coefficients *difa*, *zero*, and *sig1*, and histogram scale factors.

The actual least squares refinements were not as simple as the above paragraphs suggest. They diverged when too many parameters were refined at the same time. In particular, multiple metal site fractional occupancies were not refined simultaneously with the phase fractions and thermal parameters except during the final cycles of the $Zr_{9.5}Ta_{3.5}S_{2.9}O_{0.6}$ κ-phase refinement. When attempts were made to do so, one or more parameters became negative while others became large in the positive sense. The particular parameters which became positive or negative varied from cycle to cycle. The phase fractions and thermal parameters were refined and then fixed while the fractional occupancies were refined. This was repeated until no change (within esd's) was observed for these parameters. The fractional occupancy of a single site could usually be refined along with the phase fractions and the thermal parameters of the other sites.

The largest problem in these refinements was caused by the presence of minor phases. The minor phases Zr_2S, Zr_3S_2, Hf_2S, Hf, Nb, and/or Ta had weak diffraction peaks and refinement of their positional, thermal, and fractional atomic parameters did not yield stable, realistic numbers. Even their lattice parameters did not refine well. Although these minor phases could not be completely refined, they were observable and contributed significantly to the overall diffraction pattern of the histograms. The approach used in this work was to input (and fix) the lattice parameters calculated from Guinier films using the program LATT99, and the atomic and thermal parameters from reported single crystal studies. The only parameters refined for the minor phases were phase fractions and profile coefficients. Weak diffraction peaks were observed, particularly in $Zr_{10}Ta_3S_3$ and $Zr_{9.6}Nb_{3.4}S_{3.4}$, which could not be identified with any known phase and thus were not modeled.

The refined phase fractions (as wt.%) and other total, X-ray, and neutron powder histogram statistics are given in Table 3.8 for these samples and details pertaining to the specific κ-phases are given in Table 3.9. The results reported for the combined X-ray and neutron refinement of the $Hf_{10}TaNb_2S_3$ sample and the $Hf_{9.2}Ta_{1.2}Nb_{2.6}S_{2.9}O_{0.6}$ κ-phase are felt not to be completely reliable. In particular, the

Table 3.8 Bulk powder results (Cu Kα X-ray and TOF neutron histograms)

total				
initial formula	$Hf_{10}TaNb_2S_3$	$Zr_{10.0}Ta_{3.0}S_{3.4}$		$Zr_{9.6}Nb_{3.4}S_{3.4}$
weight %	60 (2)% γ-brass	84.3 (4)% κ-phase		87 (2)% κ-phase
	32 (1)% κ-phase	13.2 (4)% Zr_2S		3.7 (2)% Zr_2S
	4.6 (2)% Hf	2.5 (1)% Ta		5.4 (1)% Nb
	2.6 (1)% Hf_2S	-		4.1 (1)% Zr_3S_2
# parameters	57	63		50
R_p	0.0446	0.0300		0.0343
R_{wp}	0.0726	0.0593		0.0786
reduced χ^2	2.960	2.886		3.274
expected R_{wp}	0.0422	0.0349		0.0434
D_{dw}	0.736	0.765		0.661
Cu Kα X-ray data				
2θ (deg)	22 - 160	24 - 160		20 - 160
# data points	6898	6798		6998
# reflections	1312	2301		1770
max # refl/data pt	824	688		776
R_p	0.0605	0.0672		0.0932
R_{wp}	0.0779	0.0882		0.1201
D_{wd}	0.654	0.595		0.556
TOF neutron data				
data bank (2θ)	+153.4°	+153.4°	+90.0°	+153.4°
TOF (msec)	3.27-15.9	3.12-16.3	2.24-11.75	2.40-15.5
# data points	3189	3334	3351	3770
# reflections	1103	2233	2233	4869
max # refl/data pt	334	361	378	942
R_p	0.0384	0.0302	0.0256	0.0292
R_{wp}	0.0585	0.0459	0.0354	0.0431
D_{wd}	1.074	1.293	1.068	1.087

Table 3.9 κ-phase powder results (Cu Kα X-ray and TOF neutron data)

κ-phase formula[a]	$Hf_{0.2}Ta_{1.2}Nb_{2.6}S_{2.9}O_{0.6}$	$Zr_{9.5}Ta_{3.5}S_{2.9}O_{0.6}$		$Zr_{9.6}Nb_{3.4}S_{2.9}O_{0.7}$
a (Å)	9.0925 (3)	9.1267 (1)		9.1391 (2)
c (Å)	8.9149 (5)	9.0584 (2)		8.9891 (3)
V (Å^3)	638.28 (4)	653.45 (2)		650.22 (5)
density (g/cm^3)[a]	11.463	8.122		6.615
Cu Kα X-ray data				
# reflections	588	598		597
$R(F_{obs}^2)$ (~R_{Bragg})	0.0892	0.0871		0.0591
$R(F_{obs})$	0.0428	0.0460		0.0283
TOF neutron data	+153.4°	+153.4°	+90.0°	+153.4°
# reflections	488	578	578	1214
$R(F_{obs}^2)$ (~R_{Bragg})	0.0939	0.0373	0.0310	0.0448
$R(F_{obs})$	0.0514	0.0214	0.0190	0.0247

[a] See text for discussion

sulfur/oxygen populations of the X′ site in the Hf-Ta-Nb-S κ-phase were indeterminate and the thermal parameters for this κ-phase had large esd's. The neutron and X-ray powder data for this sample did not mesh as well as did the data for the other samples resulting in elevated neutron residuals obtained for this sample through the combined refinement.

The most significant results obtained from these combined X-ray and neutron powder refinements were the determinations of the sulfur/oxygen/vacancy populations of the distorted octahedral X′ sites in the $Zr_{9.5}Ta_{3.5}S_{2.9}O_{0.6}$ and $Zr_{9.6}Nb_{3.4}S_{2.9}O_{0.7}$ κ-phases. The X′ site occupancies in these κ-phases refined from the combined X-ray and neutron powder data, and reported in Table 3.10, are consistent with both the electron densities and the interatomic distances obtained through Mo Kα X-ray single crystal experiments. The electron densities of the X′ sites in the Zr-Nb-S and Zr-Ta-S κ-phases determined through X-ray single crystal experiments corresponded to the partial sulfur occupancies reported in Table 3.5 but these electron densities could not be uniquely determined as resulting only from a mixture of sulfur and vacancies. As an example, the electron density of a site with 70% sulfur occupancy is equivalent to the electron density of the same site with a mixture of 60% sulfur and 20% oxygen occupancies. The M-X′ distances determined through X-ray single crystal experiments for the Zr-Nb-S and Zr-Ta-S κ-phases and reported in Table 3.7 were shorter than the expected Zr-S distances but longer than the expected Zr-O distances and are thus consistent with X′ being a mixture of sulfur, oxygen, and vacancies as determined in this work.

Table 3.10 κ-phase X′ (S2 or O) site occupancies (with calculated esd's)

$Zr_{9.6}Nb_{3.4}S_{2.9}O_{0.7}$	$Zr_{9.5}Ta_{3.5}S_{2.9}O_{0.6}$
22 (2) % O	19 (1) % O
64 (2) % S	62 (2) % S
14 (1) % vacancy	19 (1) % vacancy

Assuming neutral species and natural isotope abundances, sulfur scatters X-rays approximately twice as strongly as does oxygen. Assuming natural isotope abundances, the neutron scattering length for oxygen is (0.5805/0.2847) times that of sulfur. These two facts were used by the combined refinements of X-ray and neutron scattering data to arrive at models of sulfur/oxygen/vacancy populations on the distorted octahedral X′ sites of the $Zr_{9.6}Nb_{3.4}S_{2.9}O_{0.6}$ and $Zr_{9.5}Ta_{3.5}S_{2.9}O_{0.7}$ κ-phases. The X′ site occupancies for these κ-phases are reported in Table 3.10 with their calculated esd's. As mentioned previously, the sulfur/oxygen X′ site occupancy in the $Hf_{9.2}Ta_{1.2}Nb_{2.6}S_{2.9}O_{0.6}$ κ-phase did not refine to a physically possible result. Refinement of only the neutron data gave a total scattering length which was comparable to the neutron scattering lengths refined for the $Zr_{9.5}Ta_{3.5}S_{2.9}O_{0.6}$ and $Zr_{9.6}Nb_{3.4}S_{2.9}O_{0.7}$ κ-phases but addition of the X-ray data led to impossible results. It is probable that the much lower phase fraction (32 wt. %) of the κ-phase in the Hf-Ta-Nb-S system relative to the larger phase fractions (84-87 wt. %) of the κ-phases in the Zr-Ta-S and Zr-Nb-S systems caused the combined X-ray and neutron powder refinement to fail in the determination of the sulfur/oxygen X′ site occupancy in the Hf-Ta-Nb-S κ-phase.

The metal site occupancies refined using the combined powder data in the Zr-Ta-S-O κ-phase and reported in Table 3.11 were equivalent to those obtained through the corresponding X-ray single crystal refinement (Table 3.5). The metal site occupancies refined using the X-ray and neutron powder data in the Hf-Ta-Nb-S(O) κ-phase and reported in Table 3.11 were consistent with the trend obtained through inspection of the X-ray single crystal site occupancies reported in Table 3.5, i.e. Zr or Hf preferring to occupy the M1 and M2 positions and Ta, Nb, or V preferring to occupy the M3 and M4 positions with substantial mixing of the group IV and group V metals on M3. Because the neutron scattering lengths of Zr and Nb are approximately equal and the Cu Kα X-ray scattering factors are also approximately equal, the metal site occupancies could not be refined in the Zr-Nb-S-O κ-phase but were instead assigned according to the initial sample stoichiometry and the trend

Table 3.11 κ-phase metal site occupancies determined from Cu Kα X-ray and TOF neutron powder refinements (%)

		$Zr_{9.5}Ta_{3.5}S_{2.9}O_{0.6}$	$Hf_{9.2}Ta_{1.2}Nb_{2.6}S_{2.9}O_{0.6}$	$Zr_{9.6}Nb_{3.4}S_{2.9}O_{0.7}$
M1	Zr	100	-	100 [a]
	Hf	-	92 (2)	-
	Ta	-	-	-
	Nb	-	8 (2)	-
M2	Zr	94 (1)	-	100 [a]
	Hf	-	82 (2)	-
	Ta	6	8 (1)	-
	Nb	-	10 (1)	-
M3	Ta	76 (1)	30 (1)	80 [a]
	Nb	-	29 (2)	20 [a]
	Zr	24	-	-
	Hf	-	41 (2)	-
M4	Ta	100	8 (2)	100 [a]
	Nb	-	92 (2)	-
	Zr	-	-	-
	Hf	-	-	-

[a] metal site occupancies not refined, see text

discussed above. For the same reasons that Zr and Nb could not be differentiated in this combined refinement, the assigned metal site occupancies (if they were slightly incorrect) did not affect the results of the sulfur/oxygen X′ site occupancy determination in this κ-phase.

The refined formulas and densities in Table 3.9 refer to the stoichiometries of κ-phases used in the final cycles of the full refinements. The sulfur/oxygen contents of the X′ sites were refined ($Zr_{9.5}Ta_{3.5}S_{2.9}O_{0.6}$ and $Zr_{9.6}Nb_{3.4}S_{2.9}O_{0.7}$) and the metal contents were refined ($Zr_{9.5}Ta_{3.5}S_{2.9}O_{0.6}$ and $Hf_{9.2}Ta_{1.2}Nb_{2.6}S_{2.9}O_{0.6}$) or assigned according to the initial stoichiometry ($Zr_{9.6}Nb_{3.4}S_{2.9}O_{0.7}$). The sulfur/oxygen contents of the X′ site in $Hf_{9.2}Ta_{1.2}Nb_{2.6}S_{2.9}O_{0.6}$ did not refine to physically reasonable values so they were assigned according to the results obtained for $Zr_{9.5}Ta_{3.5}S_{2.9}O_{0.6}$.

The metal site occupancies (three different metals on the same sites) in $Hf_{9.2}Ta_{1.2}Nb_{2.6}S_{2.9}O_{0.6}$ could not be refined in one step. The Hf/Nb site occupancies were refined using only the X-ray data without attempting to differentiate between Hf and Ta. The Nb occupancies were fixed and the Hf partial occupancies were refined as mixed Hf/Ta occupancies using only the neutron data. The fractional occupancies of these three metals could be refined because the neutron scattering lengths of Ta and Nb are nearly equivalent but different from that of Hf while the X-ray scattering factors of Ta and Hf are nearly equivalent but different from that of Nb.

The overall residuals obtained for the bulk samples in these Rietveld refinements of X-ray data are not as low as those obtained in the X-ray single crystal investigations of the κ-phases. The Rietveld residuals were based on intensities ($I \sim F^2$) while the single-crystal residuals were based on F's. The residuals obtained from a refinement based on F's are expected to be approximately ½ as large as the residuals obtained from a refinement based on the corresponding F^2's. A better comparison is between the X-ray single crystal R and the X-ray or neutron powder R's (F_{obs}) of the κ-phases which are all based on structure factors calculated from observed intensities and have little correlation with background scattering. The powder residuals have magnitudes similar to the single crystal residuals in this

comparison. The residuals based on F_{obs} (derived from the Bragg peaks) for each individual phase in all three samples are given in Table 3.12 for refinement of both X-ray and neutron data. These residuals are consistently low, indicating that errors are not associated with any one phase.

It was suggested in the section on synthesis that particle size broadening might be a factor needing consideration in the X-ray diffraction investigations of these samples, yet the profile coefficient corresponding to this factor, LX, was not refined. Since the question of primary interest in these combined X-ray and neutron powder studies was related to determining the sulfur/oxygen/vacancy populations of the X' sites and the questions of particle size effects were of little or no interest, the approach of attaining the best empirical fit to the observed peak shapes was taken. If LX was refined instead of LY, the peak shapes did not fit as well. If both LX and LY were refined, the residuals became only slightly lower but the computation time increased and the two profile coefficients would not refine to stable numbers unless both were heavily damped. When LY was refined, without LX, the peak shapes were reasonable and the value of LY converged to a stable number.

All metal and nonmetal sites in the $Zr_{9.5}Ta_{3.5}S_{2.9}O_{0.6}$ κ-phase refined with reasonable isotropic thermal parameters. The Zr/Ta occupancies were refined and gave results equivalent to the X-ray single crystal work. All metal and nonmetal sites also refined in the $Zr_{9.6}Nb_{3.4}S_{2.9}O_{0.7}$ κ-phase with reasonable isotropic thermal parameters and the metal and nonmetal sites in the $Hf_{9.2}Ta_{1.2}Nb_{2.6}S_{2.9}O_{0.6}$ κ-phase refined with reasonable isotropic thermal parameters although their esd's were abnormally large. Table 3.13 lists the equivalent isotropic thermal parameters (U_{iso}'s) for these κ-phases, obtained from X-ray single crystal and combined X-ray and neutron powder refinements. Both techniques yielded similar results (the thermal parameters for M1 and M2 were consistently larger than those for M3 and M4).

Observed, calculated, and difference curves and reflection markers for a full multi-phase refinement of the Cu Kα X-ray powder data collected on the $Zr_{10.0}Ta_{3.0}S_{3.4}$ sample are shown in Figure 3.1. The fit obtained between observed and calculated

Table 3.12 Powder residuals based on $\Delta F/F_o$ for different phases

Hf-Ta-Nb-S	X-ray data		+153.4° neutron data	
phase	# reflections	R (F_o)	# reflections	R (F_o)
kappa	588	0.0428	488	0.0514
γ-brass	530	0.0361	457	0.0397
Hf	58	0.0425	46	0.0797
Hf_2S	136	0.0346	112	0.0679
Zr-Ta-S	X-ray data		+153.4° neutron data (+90.0° neutron data)	
phase	# reflections	R (F_o)	# reflections	R (F_o)
kappa	598	0.0460	578 (578)	0.0214 (0.0190)
Zr_2S	1687	0.0686	1640 (1640)	0.0324 (0.0259)
Ta	16	0.0463	15 (15)	0.0412 (0.0327)
Zr-Nb-S	X-ray data		+153.4° neutron data	
phase	# reflections	R (F_o)	# reflections	R (F_o)
kappa	597	0.0283	1214	0.0247
Zr_2S	1104	0.0308	3533	0.0362
Zr_3S_2	56	0.0412	94	0.0282
Nb	20	0.0187	28	0.0368

Table 3.13 κ-phase U_{iso}'s from different techniques

	X-ray single crystal [a]	Powder (X-ray and neutron)
	$Zr_{8.1}Nb_{4.9}S_{2.7}$	$Zr_{9.6}Nb_{3.4}S_{2.9}O_{0.7}$
M1	0.0133	0.0088 (3)
M2	0.0264	0.0190 (6)
M3	0.0081	0.0029 (4)
M4	0.0057	0.0051 (7)
S1	0.0240	0.017 (2)
S2 (O)	0.0154	0.006 (2)
	$Hf_{10.0}Nb_{3.0}S_{3.0}$	$Hf_{9.2}Ta_{1.2}Nb_{2.6}S_{2.9}O_{0.6}$
M1	0.0106	0.012 (1)
M2	0.0241	0.015 (2)
M3	0.0097	0.002 (1)
M4	0.0057	0.006 (3)
S1	0.0173	0.004 (9)
S2 (O)	0.0067	0.027 (7)
	$Zr_{9.7}Ta_{3.3}S_{3.1}$	$Zr_{9.5}Ta_{3.5}S_{2.9}O_{0.6}$
M1	0.0114	0.0087 (3)
M2	0.0202	0.0193 (5)
M3	0.0073	0.0042 (3)
M4	0.0070	0.0035 (5)
S1	0.0140	0.0087 (3)
S2 (O)	0.0127	0.005 (1)

[a] U_{iso}'s corresponding to refined U_{ij}'s or B_{eq}'s

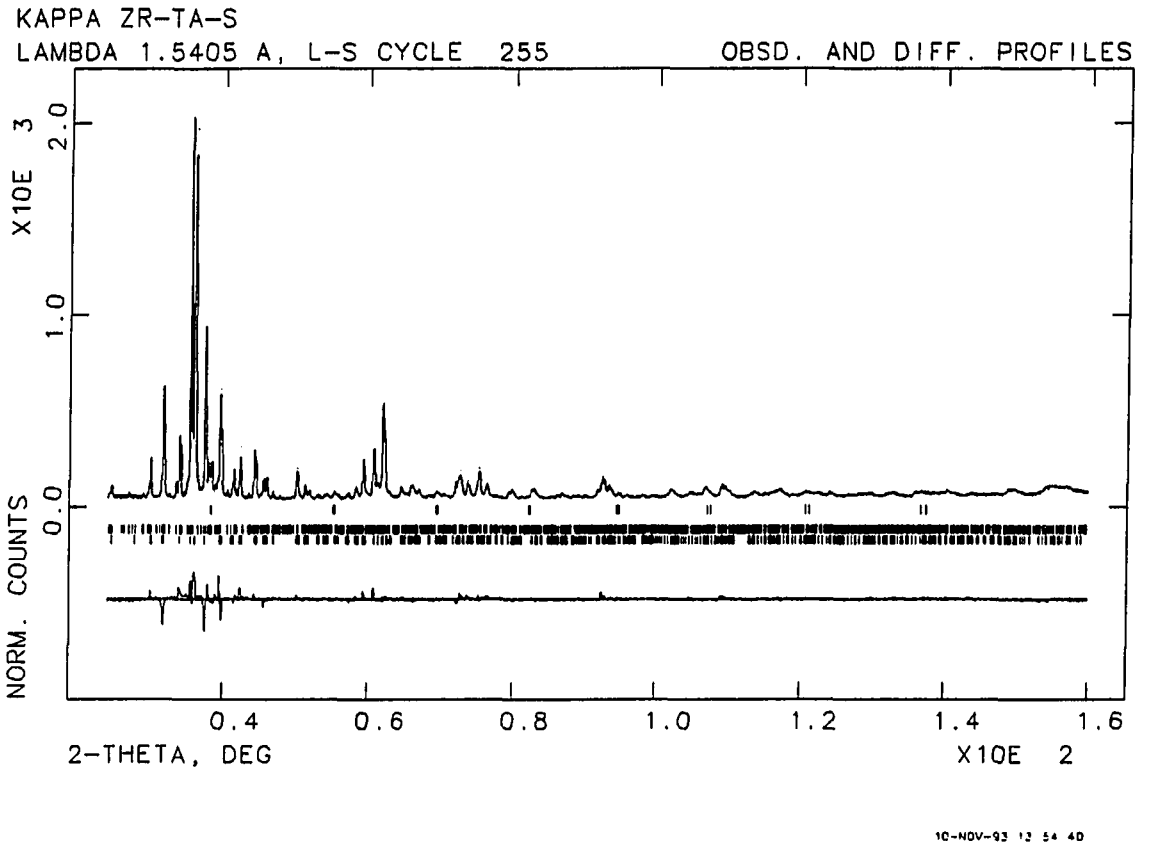

Figure 3.1 **Observed, calculated, and difference curves and reflection markers for $Zr_{10.0}Ta_{3.0}S_{3.4}$ Cu Kα X-ray powder data and refinement**

X-ray intensities was good for all three samples, $Zr_{10.0}Ta_{3.0}S_{3.4}$, $Zr_{9.6}Nb_{3.4}S_{3.4}$, and $Hf_{10}TaNb_2S_3$, but only the data for the $Zr_{10.0}Ta_{3.0}S_{3.4}$ histogram is shown here. A table of calculated and observed structure factors from the Cu Kα X-ray powder refinement of the $Zr_{9.5}Ta_{3.5}S_{2.9}O_{0.6}$ κ-phase in the $Zr_{10.0}Ta_{3.0}S_{3.4}$ sample is given in appendix B.

Observed, calculated, and difference curves and reflection markers for a full multi-phase refinement of the 90.0° TOF neutron powder data collected on the $Zr_{10.0}Ta_{3.0}S_{3.4}$ sample are shown in Figure 3.2. A good fit was obtained between observed and calculated neutron intensities for all three samples, $Zr_{10.0}Ta_{3.0}S_{3.4}$, $Zr_{9.6}Nb_{3.4}S_{3.4}$, and $Hf_{10}TaNb_2S_3$. A table of calculated and observed structure factors from the TOF neutron powder refinement of the $Zr_{9.5}Ta_{3.5}S_{2.9}O_{0.6}$ κ-phase in the $Zr_{10.0}Ta_{3.0}S_{3.4}$ sample is given in appendix C.

The calculated and observed Mo Kα X-ray single crystal, Cu Kα X-ray powder, and neutron powder structure factors for the Zr-Ta-S-O κ-phase are given in appendices A, B, and C to demonstrate for the interested reader the differences between Mo Kα X-ray diffraction, Cu Kα X-ray diffraction, and neutron scattering.

Discussion

The term kappa phase describes a large number of metal rich compounds that crystallize in the hexagonal spacegroup $P6_3/mmc$ with $a \approx c$. They were first discovered forty years ago by Rautala and Norton in the Co-W-C system [39]. They can be described as filled variants of the $Al_{10}Mn_3$ structure [94]. Most of the work on κ-phases has been done in the research groups of Härsta in Uppsala and Nowotny in Vienna but recent investigations in our laboratory have led to the discoveries of κ-phases in various new systems [42,95].

Kappa phases can be formulated (as stated previously in the section on synthesis) $M_{9+x}M'_{4-x}XX'_3$ where M and M′ may ($x > 0$ or $x < 0$) or may not ($x = 0$) share occupancy of some sites and the nonmetals, X and X′, occupy two different sites. These nonmetal sites may be occupied by the same (X = X′) or different (X ≠ X′) elements, or one of these positions may be vacant. A comprehensive list of the known κ-phases is given in Table 3.14 and the specific M and M′ metals are

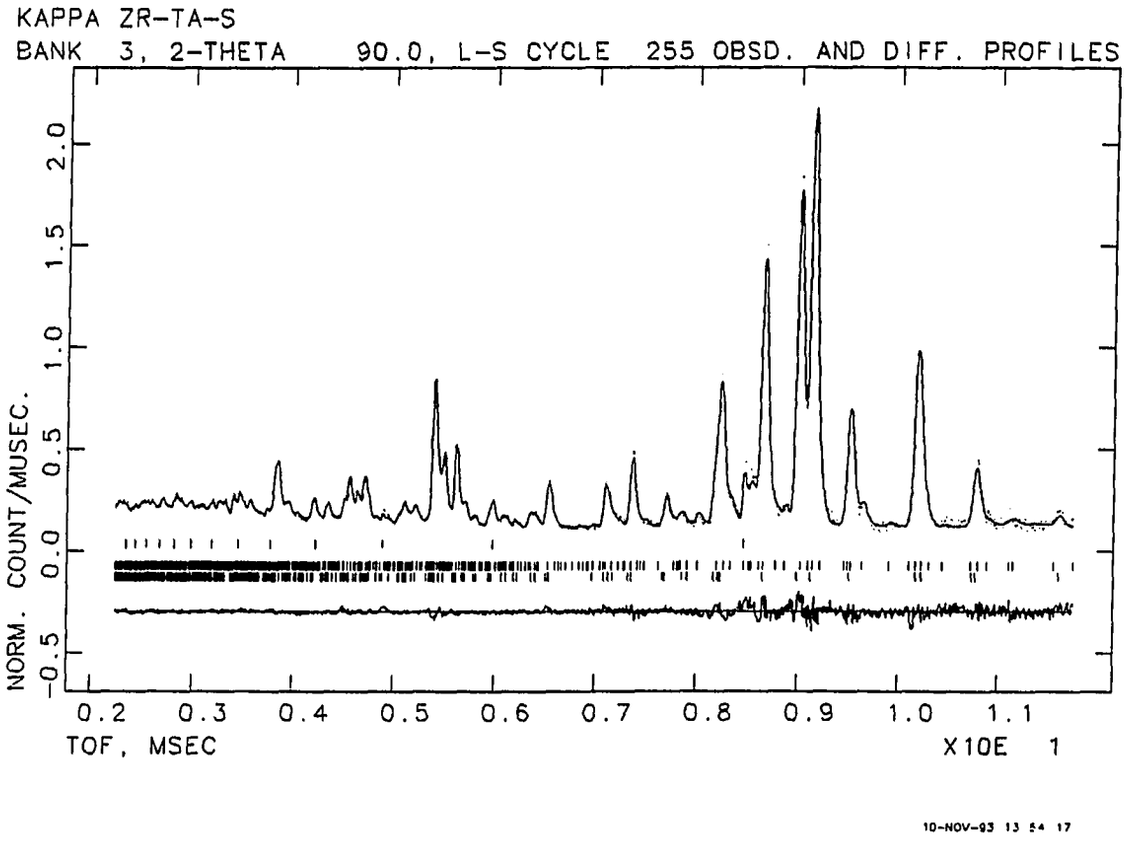

Figure 3.2 Observed, calculated, and difference curves and reflection markers from $Zr_{10.0}Ta_{3.0}S_{3.4}$ 90.0° TOF neutron powder data and refinement

Table 3.14 Known kappa phases M-M′-X, column headings represent M elements, row headings represent M′ elements[a], and the body of the table represents X and/or X′ elements

different metals on M′ sites	different metals on M sites: Hf	Zr	W	Mo	Ti
W	B,O,Si,P,S,Ge, As,Se,Fe,Co,Ni	B,O,Fe,Co,Ni,S	-	-	-
Mo	B,O,P,S,Ge,As, Se,Fe,Co,Ni	B,O,S,Ni-S	-	-	-
Re	B,O,Si,P,S,Ge, As,Se,Fe,Co,Ni	B,O	-	-	-
Os	B,O,Si,P,S,Ge, As,Se,Fe,Co,Ni	O	-	-	-
Ta	S[b],O[b] Se[c]	S[b],O[b]			
Nb	S[b],O[b]	S[b],O[b]			
V	S[b],O[b]	S[b]	-	-	-
Cr	-	-	C	-	-
Mn	-	-	C[d]	[d]	O
Fe	-	-	C[d]	[d]	O
Co	-	-	C	[d]	-
Ni	-	-	C	[d]	-
Cu	-	-	-	[d]	-

[a] substantial mixing of M and M′ elements on the same site is common

[b] this work

[c] under investigation

[d] phases reported as ternaries with Al distributed on the metal framework

indicated. M is usually Hf or Zr but can be W, Mo, and Ti. The M′ element is most commonly Mo, W, Re, or Os but can also be Cr, Mn, Fe, Co, Ni, or Cu, and now the phases with M′ = Ta, Nb, and V are known. Aluminum can substitute into the metal framework in various quaternary systems. The positions M1 and M2 are generally occupied by the M metal and the positions M3 and M4 are usually occupied by the M′ metal. In the work reported here, the M3 position (and the M2 position in the Zr-Nb-S system) exhibit mixed occupancy by both M and M′.

The nonmetal X′ element is found in a 6-fold site centering distorted metal octahedra. In the past this octahedral site has been reported as fully, and as partially, occupied by oxygen or carbon. It has been reported as 6-9% occupied by sulfur in a kappa phase of the Hf-Mo-S system, but this work on the new Ta and Nb containing κ-phases shows a much larger (> 50%) occupancy by sulfur. In addition to the chemically and structurally interesting mixed metal site occupancies and the nonstoichiometry of the nonmetal X′ position, the variability of the nonmetal X component found centering trigonal prismatic sites make the kappa phases exciting. As an example, consider the Hf-Mo-X systems. Kappa phases form for X = B, O, Si, P, S, Ge, As, Se, Fe, Co, and Ni. It is remarkable that the same structure forms for all of these different nonmetals and for third row iron group transition metals as well. If these compounds were found to have useful properties, their electronic structure could easily be tuned. Surprisingly, little is known about their physical properties. They appear to be hard, brittle, and metallic. The kappa phases discovered in the Hf-Nb-S and Zr-Nb-S systems are superconductors at low temperatures and will be discussed in the next section.

The κ-phase structure (for the idealized $Zr_9Nb_4S_4$ κ-phase) is shown in Figure 3.3 as a projection down the *c* axis. Centered columns of slightly distorted face-sharing icosahedra are located at the cell edges parallel to the *c* axis. The centering atoms are denoted as Nb2 (M4), the atoms which compose the shared faces are Nb1 (M3), and the atoms making up the waist of the icosahedra are Zr1 (M1). These columns are joined by distorted octahedra which are formed by four Zr1 (M1) atoms

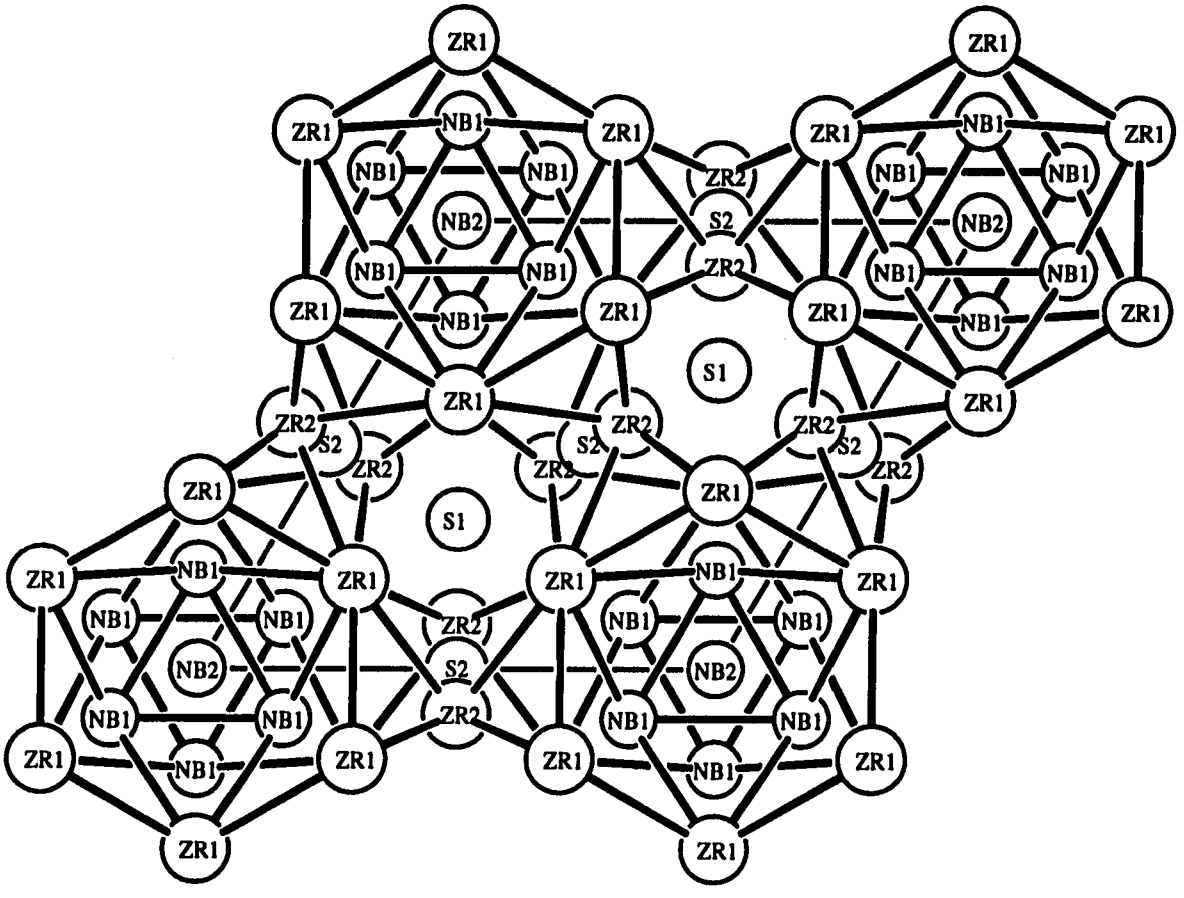

Figure 3.3 **Idealized $Zr_9Nb_4S_4$ kappa phase structure projected down the *c* axis, refined thermal parameters (Tables 3.4, 3.6, and 3.13) are not depicted**

in the *ab* plane and Zr2 (M2) atoms above and below the four Zr1 (M1) atoms. The octahedra are centered by the S2 position (corresponding to the X′ element), which contains a mixture of sulfur, oxygen, and vacancies in the Zr-Nb-S-O and Zr-Ta-S-O κ-phases.reported here. The S1 position (corresponding to X) is fully occupied by sulfur in all of the κ-phases reported here and centers a trigonal prism of Zr1 (M1) atoms. Figure 3.4 is an *ac* (or equivalent *bc*) facial slab of the κ-phase structure which shows clearly how the centered icosahedral columns are linked by columns of filled octahedra which share corners with each other and edges with the icosahedra.

A (110) section of this structure shows, in Figure 3.5, the trigonal prisms centered by S1, the distorted octahedra centered by S2, and also two other "interstitial" sites which have been reported as being occupied by hydrogen in other systems [96]. Empty distorted octahedral sites composed of three Zr1 (M1) and three Zr2 (M2) atoms share faces in the *ab* plane with three of the filled octahedral sites and share faces along the *c* axial direction with one empty octahedral site and one filled trigonal prismatic site. There are also smaller square pyramidal sites formed by Zr2 (M2) atoms capping each rectangular face of the trigonal prisms.

The X-ray single crystal refinements of the two vanadium κ-phases, $Hf_9V_4SO_{0.6}$ and Zr_9V_4S, suggest that these compounds are nearly stoichiometric with Hf (or Zr) on the M1 and M2 positions, V on the M3 and M4 positions, and S on the trigonal prismatic site. The refined oxygen population of the distorted octahedral site in $Hf_9V_4SO_{0.6}$ was small 19 (7)% but appeared to be real while the refined oxygen occupancy of the same position in Zr_9V_4S was zero (to within a large esd). Assuming oxygen occupation of the octahedral sites, the calculated M1-O (2.325 Å and 2.338 Å) and M2-O (2.210 Å and 2.244 Å) distances in these two compounds are acceptable Hf-O and Zr-O distances ($d_{Hf\text{-}O} \approx d_{Zr\text{-}O} \approx 2.21$ Å in CaF_2 type HfO_2 and ZrO_2) which suggests that oxygen occupancy of the octahedral site is possible in both phases.

Although the X-ray single crystal refinements showed that mixed metal site occupancies were unimportant in $Hf_9V_4SO_{1-x}$ and Zr_9V_4S, a sample with the initial composition $Zr_{6.5}V_{6.5}S$ contained a κ-phase with a larger volume than that of Zr_9V_4S.

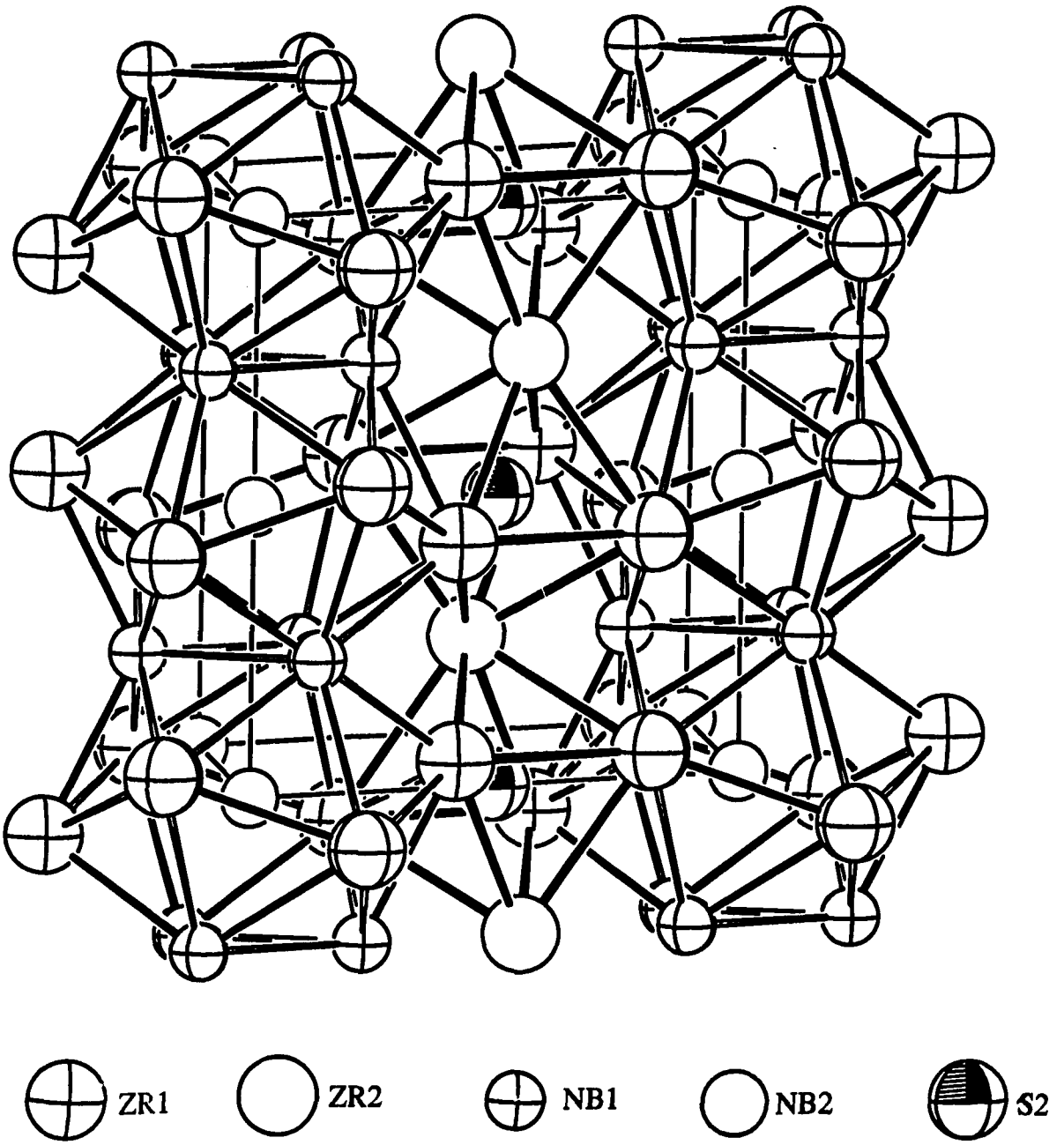

Figure 3.4 Idealized $Zr_9Nb_4S_4$ kappa phase *ac* facial slab showing centered metal icosahedral columns linked by filled distorted octahedra

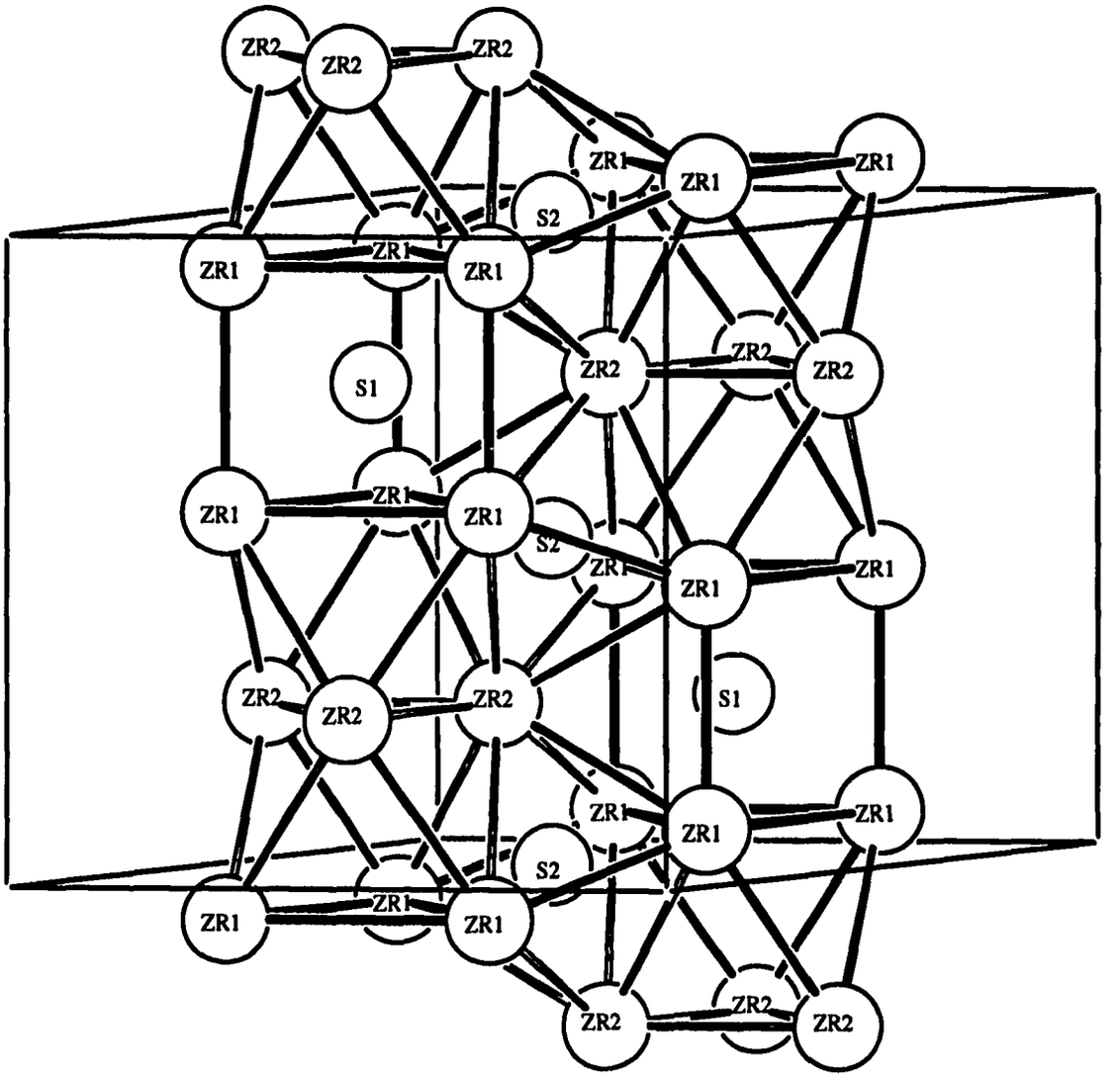

Figure 3.5 Idealized $Zr_9Nb_4S_4$ kappa phase (110) section showing trigonal prisms and octahedra

It is likely that Zr partially substituted onto the sites containing vanadium in Zr_9V_4S which led to a volume expansion. Table 3.15 lists the maximum and minimum lattice parameters calculated with LATT99 for all κ-phases investigated in this work.

The range in volumes determined for the Ta and Nb κ-phases, except for the κ-phase in the Hf-Ta-S-O system, was greater than that for the V κ-phases. The two Hf-Ta-S(O) samples listed In Table 3.15 had different initial stoichiometries but their κ-phases had nearly equivalent lattice parameters which suggests that this particular κ-phase does nothave a wide homogeneity range. The large variability in cell parameters of the three other Ta or Nb κ-phases is indicative of a large phase width which is primarily a function of S/O/vacancy content but is also a function of M/M′ content. This variability as a function of M/M′ content is demonstrated by the values listed in Table 3.15 for κ-phases in samples with the initial formulas; $Zr_8Nb_5S_4$, $Zr_9Nb_4S_4$, and $Zr_{10}Nb_3S_4$. These samples were identically prepared so that the sulfur content was assumed to be constant. The cell parameters showed a significant increase as the Zr content of the bulk samples was increased. Zr is larger than Nb, i.e. the Pauling radii $r_{Zr} = 1.454$ Å $> r_{Nb} = 1.342$ Å, and the increase in volume can be interpreted as an increase in the Zr/Nb ratio of the phase.

The variation in cell volumes listed in Table 3.15 of the Ta and Nb κ-phases as a function of S/O/vacancy content is extensive (except possibly for Hf-Ta-S-O) with the maximum ΔVol occuring in the Zr-Ta-S-O system where $\Delta Vol/Vol_{max} \approx 9\%$. In Table 3.15 the cell volumes of κ-phases prepared with oxygen purposely added to the sample are shown to be smaller than those where oxygen was not added and the only sources were adventitious.

In order to understand the κ-phase structure in general, and more particularly these new Ta and Nb κ-phases (and specifically, in order to investigate the superconducting properties of the $Zr_{9+x}Nb_{4-x}S_yO_z$ κ-phase), both the metal and nonmetal site occupancies must be known. The metal site occupancies were determined through the X-ray single crystal experiments previously discussed in this chapter however refinement of X-ray intensity data did not fully determine the X′ nonmetal site occupancy in the Ta and Nb κ-phases. Previous reports on Mo

Table 3.15 Least squares κ-phase lattice parameters

initial composition	a (Å)	c (Å)	Vol (Å^3)
$Zr_{10}Ta_3S_{3.4}$	9.122 (1)	9.057 (2)	652.7 (2)
$Zr_{9.6}Ta_{3.4}S_{2.6}O_{1.4}$	8.860 (1)	8.763 (1)	595.9 (1)
$Hf_{11}Nb_2S_3$	9.157 (1)	8.949 (1)	649.8 (1)
$Hf_{9.6}Nb_{3.4}S_{3.3}$	9.080 (2)	8.908 (4)	636.1 (4)
$Zr_{9.3}Nb_{3.7}S_4$	9.119 (1)	8.968 (1)	645.8 (2)
$Zr_{9.3}Nb_{3.7}S_{1.5}O_{1.5}$	8.933 (1)	8.776 (1)	606.5 (1)
$Hf_{8.3}Ta_{4.7}S_{3.5}O_{0.2}$	9.002 (1)	8.857 (3)	621.6 (3)
$Hf_9Ta_4S_4$	9.004 (1)	8.895 (1)	624.4 (1)
Zr_9V_4S	8.626 (1)	8.615 (3)	555.2 (2)
$Zr_{6.5}V_{6.5}S$	8.624 (1)	8.537 (1)	549.9 (1)
Hf_9V_4S	8.578 (1)	8.454 (5)	538.7 (4)
$Zr_8Nb_5S_4$	9.124 (1)	8.976 (2)	647.1 (2)
$Zr_9Nb_4S_4$	9.167 (1)	9.018 (3)	656.3 (3)
$Zr_{10}Nb_3S_4$	9.188 (2)	9.040 (8)	660.9 (7)

κ-phases suggested that oxygen may have helped in their formation and that the oxygen was located in the distorted octahedral X′ sites. The interatomic distances listed in Table 3.7 for M1-S2 (M1-O) and M2-S2 (M2-O) are between those expected for M-S and M-O (where M = Zr, Hf). These relatively short distances can be explained as M-S distances where S2 has a substantial vacancy population or as M-(S,O) distances where S and O share occupancy of the X′ site. The X-ray single crystal work performed on the Ta and Nb κ-phases showed that the electron densities of the distorted octahedral sites were consistent with less than full S occupancy (and greater than full oxygen occupancy) of the sites but X-ray diffraction alone could not be used to determine the S/O/vacancy populations of the X′ sites in the Ta and Nb κ-phases. This work has shown that X-ray diffraction combined with neutron scattering can be used to solve difficult and interesting problems such as the determination of the sulfur/oxygen/vacancy populations of the X′ sites in the $Zr_{9.6}Nb_{3.4}S_{2.9}O_{0.7}$ and $Zr_{9.5}Ta_{3.5}S_{2.9}O_{0.6}$ κ-phases.

Superconductivity

A sample with the initial composition $Zr_{3.7}Nb_{3.7}S_{3.7}$ was determined through electron microscopy to be the most homogeneous κ-phase material out of eight Zr-Nb-S samples with varying stoichiometries. The κ-phase volume fraction was estimated at > 90% for this sample from measurements of the κ-phase and total surface area in a low magnification SEM photograph using a spherical approximation where volume fraction ≈ (area fraction)$^{3/2}$.

The magnetic properties of this sample were investigated [64] over the reversible range in the field-temperature plane. The large volume % flux exclusion shown in Figure 3.6 was uncorrected for demagnetization effects but is indicative of full Meissner screening for the κ-phase in this sample. The T_c was determined to be approximately 10.35 Kelvin which is higher than that of Zr (0.61 ± 0.15 K) and Nb (9.25 ± 0.02 K) but is slightly lower than that of Nb_2Zr (10.8 K) or Nb_3Zr (10.8 K) [97]. A small amount of Nb/Zr alloy with a substantial oxygen content was observed in the sample through SEM. It was felt that this Nb/Zr alloy phase was not responsible for

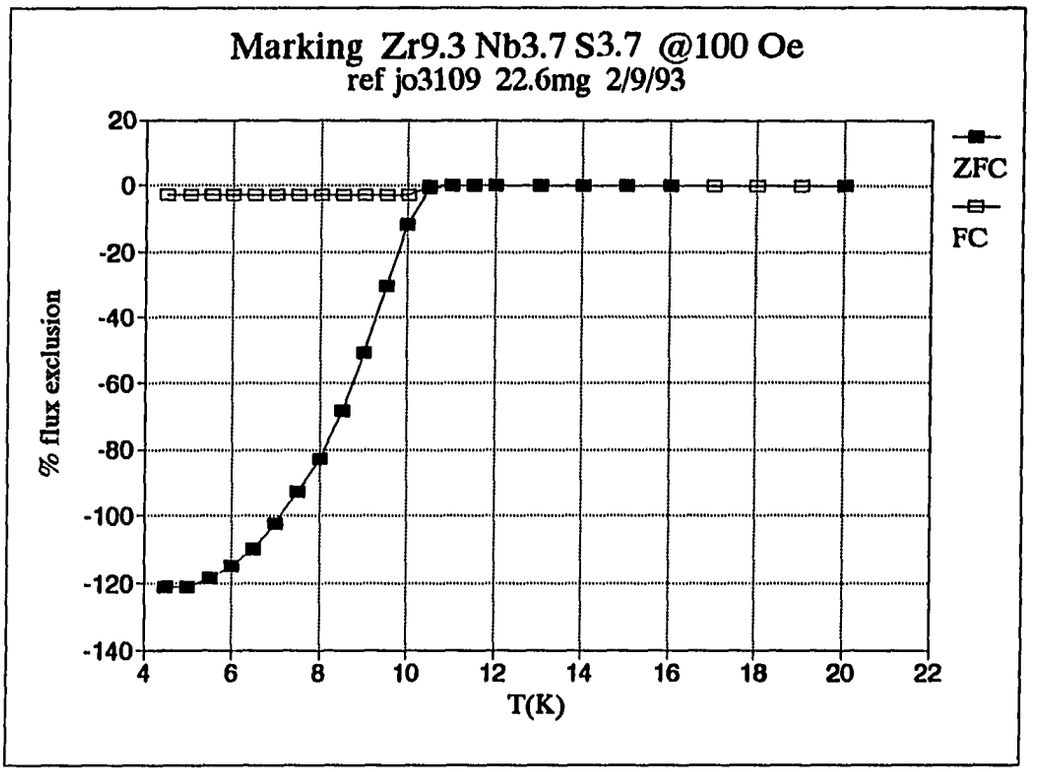

Figure 3.6 $Zr_{9.3}Nb_{3.7}S_{3.7}$ **volume % magnetic flux exclusion at 100 Oe (uncorrected for demagnetization)**

the superconductivity of the sample because oxygen is known to destroy superconductivity in the transition metals [98] and the large volume % flux expulsion (uncorrected for demagnetization) was consistent with the large κ-phase volume % phase fraction.

$Zr_{9.3}Nb_{3.7}S_{3.7}$ is an extreme type II superconductor and its upper critical field, H_{c2} (Intersection of the M vs. T curve with M = 0), is shown in Figure 3.7 as a function of temperature. The thermodynamic critical field, H_c, was estimated by integrating the area under the M vs. H curves shown in Figure 3.8 using the following formula

$$\int_0^{H_{c2}} - MdH = H_c^2/2$$

and H_c was extrapolated to the value $\mu_o H_c$ = 250 mT at 0 K. From these critical fields a Ginsburg-Landau κ (κ = H_{c2} /1.41 H_c) was calculated, ranging from 32 near T_c to 34 at 5K. This rather large κ is a similar to those of the high-T_c copper oxide superconductors but, in general, the above thermodynamic properties are more comparable to transition metal superconductors such as vanadium or niobium.

The Zr-Nb-S κ-phase is interesting for a number of reasons and is under continuing investigation. The structure is anisotropic with metallic columns of centered face-sharing icosahedra running parallel to the *c* axis and linked to each other through sulfur containing trigonal prisms and sulfur/oxygen containing distorted octahedra. It is probable that the superconductive properties are anisotropic as well but this cannot be determined until larger (~ 1 mm in length) single crystals are grown and used for measurements. The relative amounts of sulfur and oxygen contained in the octahedral sites can be varied and preliminary results show that the S2(O) site occupancy strongly affects T_c in this κ-phase. In Figure 3.9, the $Zr_{9.3}Nb_{3.7}S_{1.5}O_{1.5}$ κ-phase exhibited no superconducting behavior (at temperatures above 4 K). The T_c and small amount of flux exclusion was consistent with the presence of a small amount of oxygen-free Nb(Zr) metal in the bulk sample.

Introduction of oxygen onto the octahedral sites caused a contraction of the lattice relative to that of a sample with more sulfur on the octahedral site. This contraction of the lattice caused the energy bands to become wider and the increased

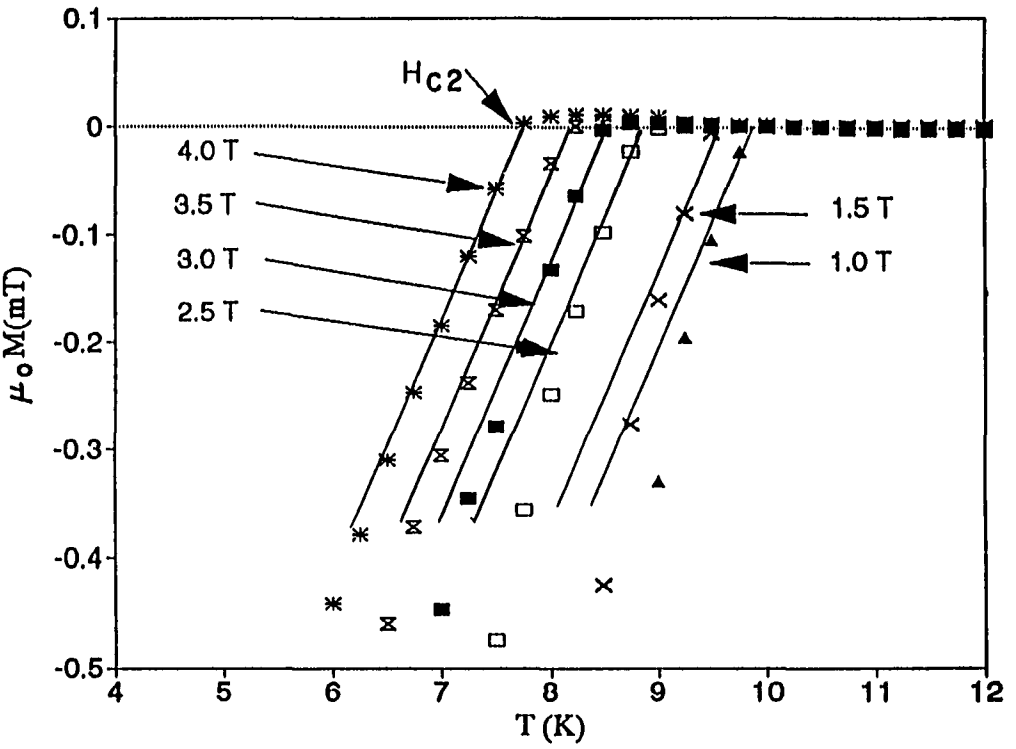

Figure 3.7 The upper critical field, H_{c2}, of $Zr_{9.3}Nb_{3.7}S_{3.7}$ at various temperatures

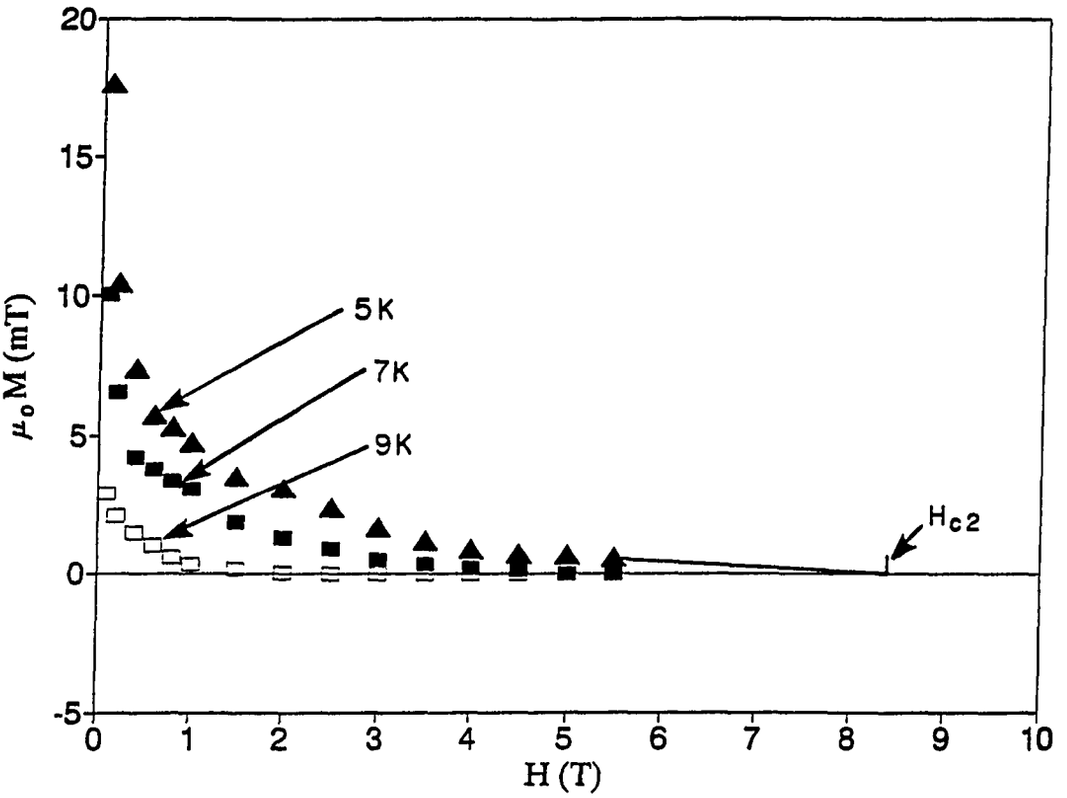

Figure 3.8 $Zr_{9.3}Nb_{3.7}S_{3.7}$ **M vs. H curves used for estimation of the thermodynamic critical field,** H_c

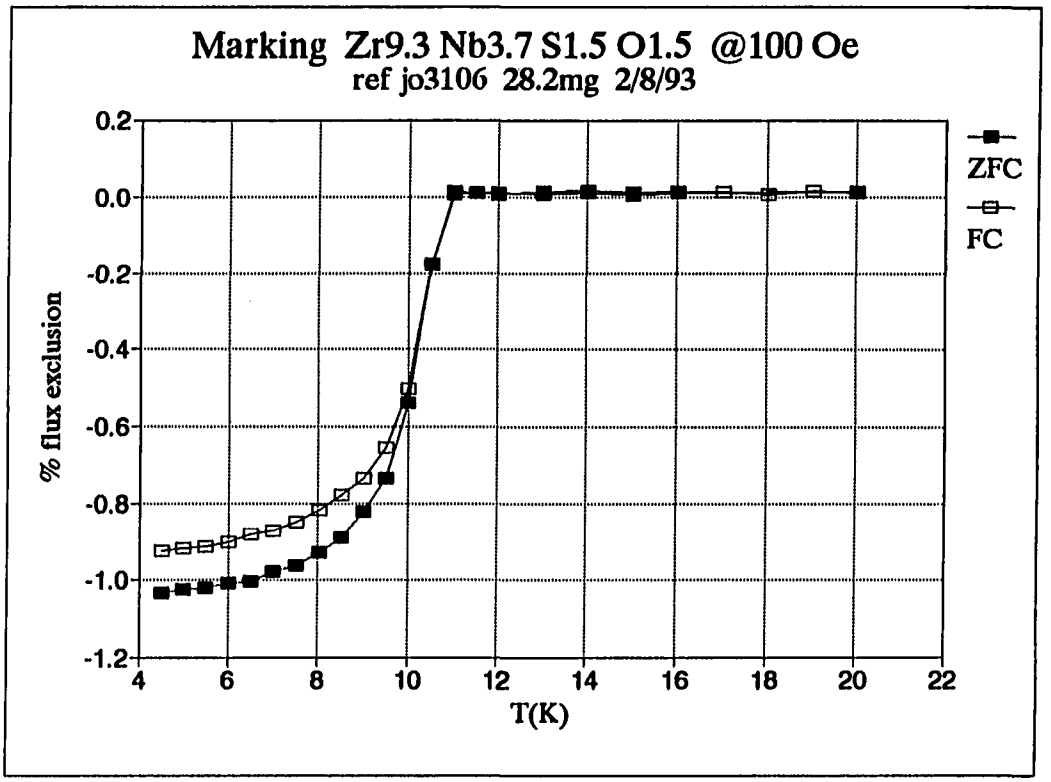

Figure 3.9 $Zr_{9.3}Nb_{3.7}S_{1.5}O_{1.5}$ **volume % magnetic flux exclusion at 100 Oe (uncorrected for demagnetization)**

orbital overlap diminished the ability to form Cooper pairs in the conduction band and destroyed the superconductivity. The exact mechanism for this destruction is unknown at present.

The Zr/Nb content is also variable and obviously plays an important role in the superconductivity of the κ-phase. $Zr_8Nb_5S_4$, $Zr_9Nb_4S_4$, and $Zr_{10}Nb_3S_4$ (phases mentioned earlier in discussion about variations of lattice parameters and mixed metal occupancies) were used to investigate the effects of Zr/Nb content. They showed variations in T_c and volume % flux exclusion with $Zr_8Nb_5S_4$ being slightly higher in both respects than $Zr_9Nb_4S_4$ while $Zr_{10}Nb_3S_4$ was substantially worse in both respects than either. The behaviors of $Zr_8Nb_5S_4$ and $Zr_9Nb_4S_4$ were approximately equivalent to that of $Zr_{9.3}Nb_{3.7}S_{3.7}$ shown in Figure 3.7 while the behavior of $Zr_{10}Nb_3S_4$ is shown in Figure 3.10. Because the total contents of M3 and M4 positions are 4 per formula unit, these results indicate that Nb substitution onto the Zr sites ($Zr_8Nb_5S_4$) does little to affect the superconductive properties of the phase while Zr substitution onto the Nb sites ($Zr_{10}Nb_3S_4$) dramatically reduces both T_c and volume % flux exclusion. In these last experiments, contraction of the lattice was associated with increased Nb content and improved superconducting properties in contrast to the previous lattice contraction associated with increased oxygen content and destruction of the superconducting properties.

A sample in the Hf-Nb-S system with an estimated κ-phase volume fraction ≥ 95% showed full Meissner screening at low temperatures and low magnetic fields consistent with the demagnetization factor of the sample. Hf-V-S, Zr-V-S, and Zr-Ta-S κ-phase samples showed no significant amounts of magnetic flux exclusion when measured to a temperature of 2 K at a field of 100 Oersted.

Figure 3.11 shows magnetic susceptibility data (uncorrected for demagnetization) for $Hf_{9.6}Nb_{3.4}S_{3.4}$ at 300 Oe. The T_c for the Hf-Nb-S κ-phase was between 6 and 7 Kelvin and a large portion of the sample was superconducting. The T_c measured for $Hf_{9.6}Nb_{3.4}S_{3.4}$ is lower than those of elemental Nb or Nb-rich Hf-Nb alloys, $Hf_{0-0.5}Nb_{1-0.5}$ (8.3 - 9.5 K) but is higher than those of Hf metal (0.128 K) or Hf-rich Hf_3Nb (> 4.2 K) [97].

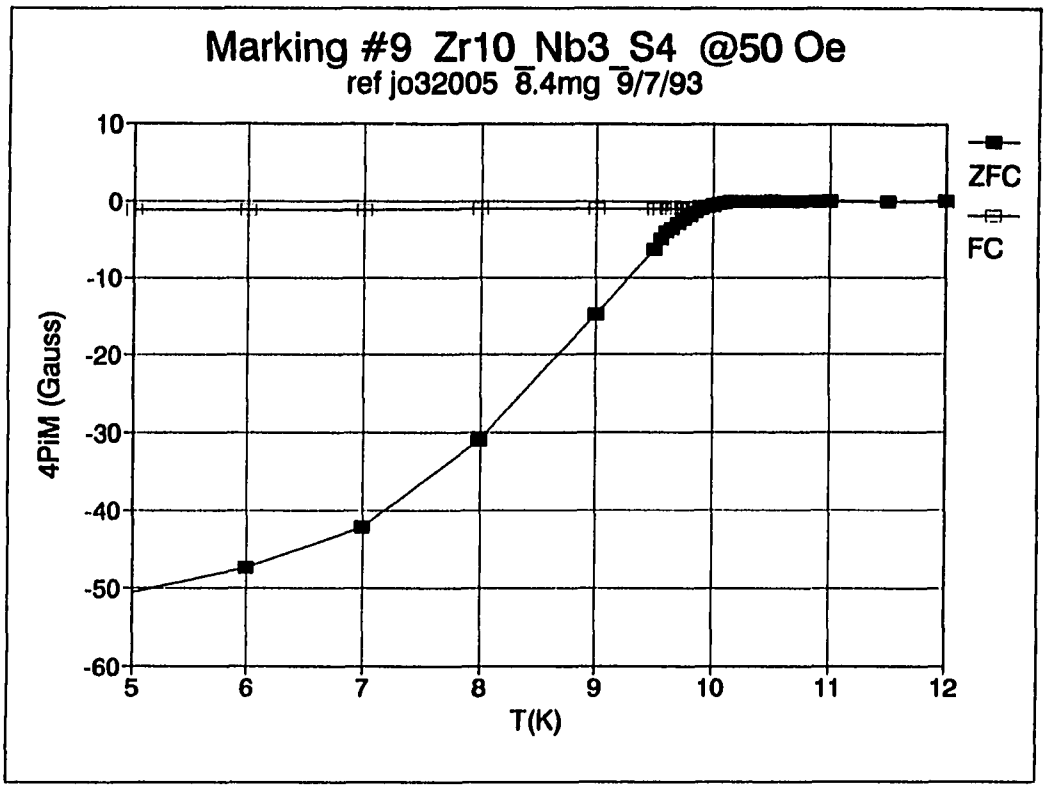

Figure 3.10 $Zr_{10}Nb_3S_4$ **volume % magnetic flux exclusion at 50 Oe (uncorrected for demagnetization)**

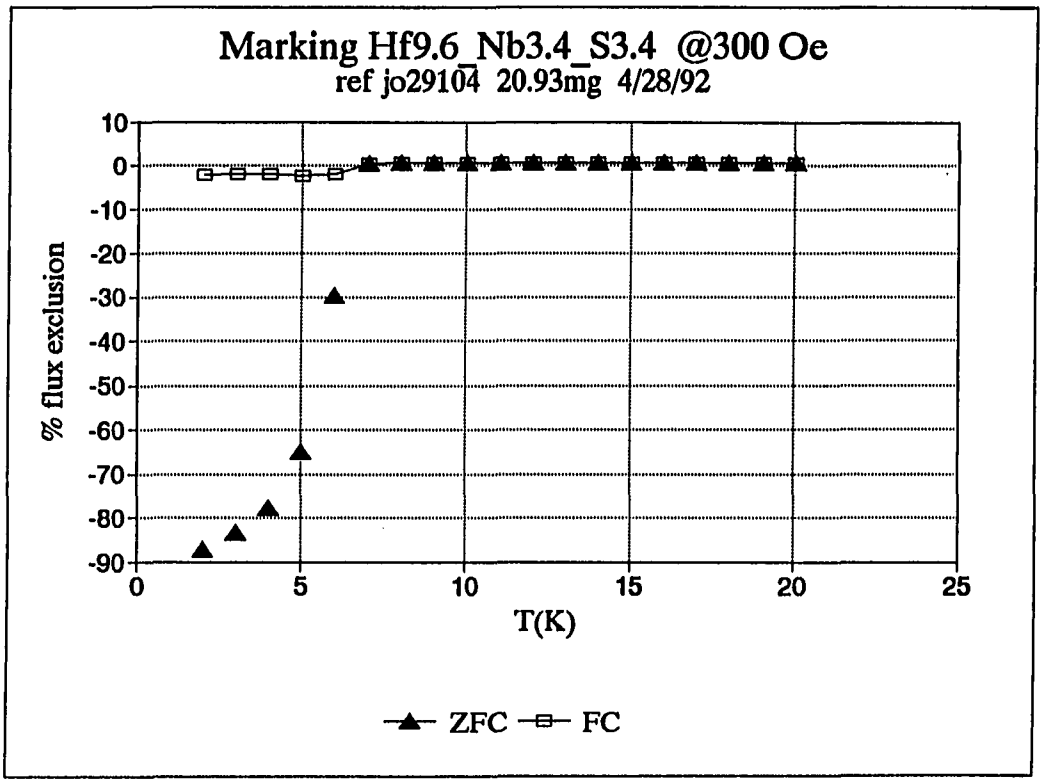

Figure 3.11 $Hf_{9.6}Nb_{3.4}S_{3.4}$ **volume % magnetic flux exclusion at 300 Oe (uncorrected for demagnetization)**

4. $Hf_{10}Ta_3S_3$, A NEW GAMMA BRASS STRUCTURE

Introduction

The novel "stuffed" γ-brass $Hf_{10}Ta_3S_3$ structure was discovered during this thesis research and is the subject of this chapter. This new structure is very similar to the famous γ-brass structure (Cu_5Zn_8) and has exciting theoretical implications in view of the Hume-Rothery rules which were, in part, developed for late-transition metal and main-group intermetallic gamma brass phases. A few of the known γ-brasses have one early-transition metal component (e.g. Al_8V_5) and many have one middle-transition metal component (e.g. Fe_3Zn_{10}) but none have previously been found with two early-transition metals. More importantly, this is the first time that sulfur has been found to play an integral role in the formation of a compound with this type of structure. $Hf_{10}Ta_3S_3$ appears to be the only known example of a "stuffed" γ-brass.

The next section describes the discovery of this new structure and the synthetic investigations which followed. The third section presents the X-ray single crystal experiments performed on this structure. Determination of the metal site occupancies was necessary to fully understand this structure and will be required for any future theoretical investigations. The rest of this chapter is primarily concerned with determination of the metal site occupancies in this structure through X-ray powder diffraction studies, neutron scattering experiments, and theoretical considerations. The final discussion section includes a description of the structure.

Synthesis and Characterization

The initial attempts to synthesize a $Hf_{9+x}Ta_{4-x}S_{4-y}$ κ-phase resulted, after arcmelting and annealing the samples, in the formation of the κ-phase and an unidentified phase. The 2θ values for diffraction lines corresponding to the unknown phase were obtained from a Guinier X-ray powder photograph of a $Hf_9Ta_4S_4$ sample using GUIN. Seventeen sharp, intense, and unidentified diffraction lines were indexed on a body-centered cubic lattice with a = 10.7896(7) Å using TREOR and resulted in a good figure of merit, M(17) = 25. A small single crystal was obtained

from this sample and intensity data were collected on a Rigaku AFC6R rotating anode diffractometer. Due to the size of the crystal, the collected data were extremely weak and a structural solution could not be obtained.

A different sample, with the nominal stoichiometry $Hf_9Nb_4S_4$ (Nb: Alfa, -60 mesh, 0.1 – 1% Ta, 99.8%), was arcmelted and then partially melted in the induction furnace at a temperature > 1400 °C resulting in a bulk mixture of Hf_3S_2, Hf_2S, and the metals. In addition to these bulk phases, single crystals (the presence of 0.1 - 1% Ta in the Nb is important to remember) also grew from the surface of the sample in a large enough quantity to obtain a weak, but observable, Guinier powder pattern after a four hour exposure to X-rays. This powder pattern matched that of the unknown *bcc* phase in the Hf-Ta-S system. Only one suitably sized single crystal was found in this sample. Analysis of rotation and zero and first layer Weissenberg photographs taken of this crystal corroborated the choice of unit cell derived from the powder photographs as body-centered cubic with $a \approx 10.8$ Å.

Data were collected for this single crystal using a Rigaku AFC6R rotating anode diffractometer and a structural solution was obtained in the space group I23, which is a subgroup of $I\bar{4}3m$, the space group found for Cu_5Zn_8 [99], an isotypical γ-brass. The metal positions were approximately equivalent to those found in the γ-brasses and sulfur was found "stuffed" into cavities along the face bisectors. This new structure will be discussed more completely in a later section.

The stoichiometry for this structure was determined to be $M_{13}S_3$ (the apparent stoichiometry of the crystal mentioned above was $Hf_{11.2}Nb_{1.8}S_3$, but the real stoichiometry was probably ~ $Hf_{10}Ta_{1.2}Nb_{1.8}S_3$). Trial and error syntheses showed that the "stuffed" γ-brass formed most readily in the Hf-Ta-S system near the composition $Hf_{10}Ta_3S_3$. Phase analyses performed on a variety of samples through Guinier powder film techniques suggested that there was a small Ta, Hf substitutional phase width centered around $Hf_{10}Ta_3S_3$. The maximum ΔVol/Vol for these various samples was approximately 0.5 % using unit cell volumes determined with LATT99. The stoichiometry, $Hf_{10}Ta_3S_3$, is used as representative of the structure throughout this

discussion except that the X-ray single crystal results refer to a sample with composition $Hf_{10.1}Ta_{2.9}S_3$ obtained through SEM-EDS.

Syntheses showed that samples with the "refined" formula $Hf_{11.2}Nb_{1.8}S_3$ formed in the κ-phase structure and not the "stuffed" γ-brass structure. However, the major phase in a $Hf_{10}TaNb_2S_3$ sample was found to be γ-brass which suggested that the single crystal mentioned above had a similar composition as well. Hf and Ta are nearly indistinguishable through Mo Kα X-radiation diffraction experiments and chemical separation of Ta and Nb is difficult because of their similarity. It is likely that a small amount of Ta was present in the Nb used to prepare the initial sample, was able to diffuse through the sample at high temperature and concentrate in the few crystals, and was refined as Hf in the structural solution.

The new compound $Hf_{10}Ta_3S_3$ was easily prepared with an approximately 90% wt. fraction by arc-melting (10V, 75A) pellets of the appropriate quantities of the metals and metal sulfides in an Argon atmosphere for 1 minute. These pellets could not be inverted and arcmelted again in order to prepare homogeneous samples because they violently shattered due to extreme brittleness. A typical reaction mixture follows:

$$7Hf + 3/2Hf_2S + 3/2Ta_2S = Hf_{10}Ta_3S_3.$$

The binary metal sulfides were prepared by direct combination of the elements in sealed evacuated quartz tubes which were heated at 400 °C until sulfur vapor could not be visually detected and then annealed at 800 °C for up to 1 week. Hf_2S was then pelletized and arc-melted to promote homogenization.

The sample that yielded the single crystal for which data were collected and the structure refined had a starting composition of $Hf_{10}Ta_3S_3$ with a weight loss < 1% observed upon arc-melting. SEM-EDS analysis of this arc-melted sample gave a stoichiometry of $Hf_{10.1}Ta_{2.9}S_{2.9}O_{0.1}$ for the major phase with an estimated error of < 0.5 wt.%. As discussed in the previous κ-phase chapter, the EDS results obtained shortly after the detector had been cleaned and serviced were the most realistic and that discussion applies to this analysis as well. The presence of oxygen was minimal

and therefore neglected. Guinier X-ray powder films showed diffraction lines corresponding to three phases, "stuffed" γ-brass, Hf metal, and Hf_2S, in the bulk $Hf_{10}Ta_3S_3$ sample. The SEM technique did not differentiate between Hf metal and the γ-brass, presumably because their electron densities were close. On the monitor they visually appeared to be the same phase. $Hf_{10}Ta_3S_3$ (~ 3.11 $e^-/Å^3$) is very similar in electron density to Hf metal (~ 3.17 $e^-/Å^3$) but is not as similar to Hf_2S (~ 2.75 $e^-/Å^3$). The least squares volumes used to arrive at the above electron densities were obtained from a Guinier film of the bulk sample using LATT99.

Nb and Zr containing "stuffed" γ-brass compounds were also easily prepared in the same fashion with bulk stoichiometries of $Hf_{10}TaNb_2S_3$ and $Hf_{8.25}Zr_{1.75}Ta_3S_3$ although the resulting phase fractions were not as high. Subsequent high-temperature annealing (> 1400 °C) had little effect on the parent compound but led to phase separation and/or disproportionation of the substituted compounds.

The $Hf_{8.25}Zr_{1.75}Ta_3S_3$ sample was prepared in a quantity ~ 1 gram and was used in an X-ray powder diffraction experiment. The $Hf_{10}TaNb_2S_3$ and $Hf_{10}Ta_3S_3$ samples were prepared in ~ 5 gram quantities and used for both X-ray powder diffraction experiments and neutron powder scattering experiments. The $Hf_{10}TaNb_2S_3$ sample was discussed in the previous κ-phase chapter. The major phase (~ 60 wt.%) in this sample was the "stuffed" γ-brass while the κ-phase (~ 32 wt.%) was a secondary phase. Pieces of all three samples were determined to be Pauli paramagnetic through magnetic susceptibility measurements. No indications of superconductivity in these samples were observed above 2 K.

Single Crystal X-ray Investigations

The structure was initially determined and refined for the "$Hf_{11}Nb_2S_3$" crystal using TEXSAN software in the space group $I\bar{4}3m$, which is the space group of many gamma brasses, until it became evident that sulfur and M4 had exceedingly large thermal parameters. Upon lowering the symmetry to a subgroup, I23, the S and M4 sites were changed significantly (as discussed later) and the refinement proceeded smoothly to completion. The anisotropic residuals decreased from R = 14.5% and

R_w = 16.5% to R = 4.5% and R_w = 4.9% after the correct space group was identified.

The beginning structural model was found using SHELXS-86 direct methods. Initially, a large electron density peak was found at the origin (which was reasonable considering that twenty-six atom Hf-Ta clusters are centered by the origin) and the structure was indeterminate. "Brute force" (increasing *np*, the number of subset phase permutations attempted, increasing *ns*, the number of subset reflections used for initial phase refinements, and increasing *nE*, the total number of refections used) applied to the direct methods increased the number of one-phase seminvariants found from 3 to 4 and led to two possible *E*-map solutions. The second solution was correct although it had a higher CFOM, combined figure of merit, than the first.

Suitable single crystals of the Hf-Ta-S "stuffed" γ-brass were difficult to find because the arc-melting technique of synthesis leads to twinning (common for the gamma brasses) and microcrystalline samples. A small irregularly shaped crystal was selected from the crushed sample of $Hf_{10}Ta_3S_3$ used in the SEM-EDS analysis and mounted on a glass fiber. An intensity data set for this crystal was collected at 16.0 deg/min (then recollected at a slower speed, 8.0 deg/min, in an attempt to lower the thermal parameter esd's) on a Rigaku AFC6R diffractometer using monochromatic Mo Kα X-radiation and the ω - 2θ scan technique out to 60° in 2θ over all reflections in the hkℓ octant which met the condition imposed by body-centering, h + k + ℓ = 2n.

The observed intensities were corrected for Lorentz polarization and absorption effects using TEXSAN. PROCESS determined that the space group was acentric (previously known) and the rather large $R_{averaging}$ = 18.7%, after a severe Psi scan absorption correction was applied, indicated that the absorption had not been perfectly modeled. Refinement of the recollected data resulted in significant improvement of the R-factors relative to those obtained from the 16.0 deg/min data but not of the thermal parameter esd's. Table 4.1 reports the crystal information pertaining to collection and refinement of the 8.0 deg/min data.

Inclusion of unobserved reflections into the full matrix least squares refinement did not change any of the refined parameters (within esd's). The residuals including

Table 4.1 Crystal data for "stuffed" gamma brass $Hf_{10}Ta_3S_3$

Formula	$Hf_{10.1}Ta_{2.9}S_3$
Space group	I23 (#197)
a Å	10.832 (1)
V Å^3	1270.9 (1)
Z	4
d_{calc}, g/cm^3	12.667
Crystal size, mm^3	0.13 × 0.06 × 0.04
μ (Mo Kα)	1063.5
Data collection instrument	RIGAKU AFC6R
Radiation (monochromated in incident beam)	Mo Kα (λ = 0.71069)
Orientation reflections, number, range (2θ)	13, 16.0 - 17.7
Scan method	2θ - ω
Octants measured	hkℓ
Data collection range, 2θ, deg	0 - 60
No. refl. measured	1063
No. unique data, total with $F_o^2 > 3\sigma(F_o^2)$	357, 195
No. parameters refined	23
Absorption correction	Psi scans
Trans. factors, max., min.	1.000, 0.2669
R[a], R_w[b], GOF[c]	0.034, 0.035, 0.84
Largest peak, e$^-$/Å^3	3.237
Largest negative peak, e$^-$/Å^3	-3.648

[a] $R = \Sigma \; | \; | F_o | - | F_c | \; | \; / \Sigma \; | F_o |$

[b] $R_w = [\Sigma w (| F_o | - | F_c |)^2 / \Sigma w | F_o |^2]^{1/2}$; $w = 1/\sigma^2 (| F_o |)$

[c] $GOF = \Sigma ((| F_o | - | F_c |) / \sigma_i) / (N_{obs} - N_{parameters})$

zeroes were R = 9.56% and R_w = 5.49%. The effects of anomalous dispersion allowed the selection of the proper enantiomer (R = 3.4%, R_w = 3.5% for the correct enantiomer vs. R = 3.5%, R_w = 3.7% for the incorrect enantiomer). No correlation coefficients > 0.5 were observed. One weak, low-angle averaged reflection, 110, had a large $\Delta F/\sigma(F)$, -7.08, which was probably due to its low intensity, the shape of the crystal, and strong absorption of X-rays by Hf and Ta. Removal of this reflection from the refinement slightly lowered the zero residuals but had no other effect.

The sulfur was not refined anisotropically due to its movement along the free parameter. This movement of the sulfur was evidenced by elongated thermal ellipsoids obtained for sulfur from DIFABS absorption corrected refinements. The esd's for the thermal parameters of the S and the two metal positions within bonding distance of the S (M3 and M4) were large which also suggested thermal motion for the sulfur. Tables 4.2 and 4.3 list the positional and anisotropic thermal parameters obtained for this crystal from refinement of the X-ray data. A Table of observed and calculated structure factors for this crystal is located in Appendix H.

The Laue class of space group I23 is $m\bar{3}$ which is a proper subgroup of the symmetry group of the lattice, $m\bar{3}m$, and therefore merohedral twinning of this crystal was a possibility. The large thermal parameter esd's for M3, M4, and S were also indications that twinning may have occurred although movement of the sulfur along its free positional parameter satisfactorily explained these esd's. For these reasons, the structure of $Hf_{10}Ta_3S_3$ was refined as a merohedral twin (and trill) using all possible unique twinning laws. A modification (SFLS, M. Eitel (1985) and H. Bärnighausen (1986), Universität Karlsruhe) of the program ORFLS [100] was used for refinement of an isotropic model which converged with a twin fraction of 2.47% for twinning across a diagonal mirror, e.g. σ_{x-y}, and the Hamilton R-factor test [101] showed that this result was significant to slightly greater than 95% probability. This small amount of possible merohedral twinning did not significantly alter the results reported here for $Hf_{10}Ta_3S_3$ as a single crystal.

A check for disordered twinning (small domain size) was also performed by

Table 4.2 Positional parameters for $Hf_{10}Ta_3S_3$

Atom	Site	*x*	*y*	*z*	B_{eq}
IT = M1	xxx	0.0971 (2)			0.2051 (7)
OT = M2	xxx	0.8399 (3)			0.180 (1)
OH = M3	x00	0.3368 (3)			0.4 (1)
CO = M4	xyz	0.2964 (2)	0.2816 (2)	0.0671 (2)	0.5 (1)
S	x½0	0.673 (2)			0.7 (2)

Table 4.3 Anisotropic thermal parameters (× 10^3) for $Hf_{10}Ta_3S_3$

site	U_{11}	U_{22}	U_{33}	U_{12}	U_{13}	U_{23}
M1	2.597 (9)	U_{11}	U_{11}	1.3 (7)	U_{12}	U_{12}
M2	2.28 (1)	U_{11}	U_{11}	0 (1)	U_{12}	U_{12}
M3	3 (2)	2 (1)	9 (2)	-	-	2 (1)
M4	6 (1)	5 (1)	10 (1)	0.2 (8)	-0.1 (9)	-0.6 (8)

splitting all atomic positions between possible sites and refining positions and occupancies. All twin occupancies either went to one and zero with the fully occupied position refining to that of the untwinned sites or else both partially occupied positions refined to the untwinned values, within esd's, and it was concluded that disordered twinning was not observed.

In the space group $I\bar{4}3m$ of the gamma brasses, any atom at x,1/2,0 also has symmetry equivalent positions at $\bar{x}$,1/2,0 and x+1/2,1/2,0 and $\bar{x}$+1/2,1/2,0. These four sites fall on the x,1/2,0 face bisector which is approximately 10.8 Å long in this unit cell. If these positions were equally spaced, they would be only 2.7 Å apart while the S-S van der Waals distance ≈ 3.6 Å. Due to sulfur-sulfur repulsion, the 24 fold site x,1/2,0 could only be 50% occupied by sulfur in this space group.

Upon lowering the symmetry to I23, the x,1/2,0 site is split into 2 twelve fold sites x,1/2,0 and x+1/2,1/2,0, either of which (but not both) could be fully occupied by sulfur, and the M4 site, x,x,z, loses symmetry to become an x,y,z site. The sulfur is found to order into one of the split x,1/2,0 sites and the M4 atoms rearrange slightly to accommodate the sulfur, maximizing M-S bonding without significant loss of M-M bonding.

X-ray Powder Investigations

X-ray powder diffraction experiments were performed to help determine the metal site occupancies in the "stuffed" γ-brass, $Hf_{10}Ta_3S_3$. The premise was that Zr in a $(Hf,Zr)_{10}Ta_3S_3$ sample would be found on the same sites as the Hf in the unsubstituted compound and that Nb in a $Hf_{10}(Ta,Nb)_3S_3$ sample would be found on the same sites as the Ta in the unsubstituted compound. It was found that the Nb dramatically preferred to occupy the M1 (IT) and M2 (OT) sites while Zr had a slight preference to occupy the M3 (OH) and M4 (CO) sites. These site preferences of Nb and Zr corroborate the results discussed and reported later in this chapter for the Ta and Hf site occupancies.

X-ray powder data for the finely ground bulk samples, $Hf_{8.25}Zr_{1.75}Ta_3S_3$, $Hf_{10}TaNb_2S_3$, and $Hf_{10}Ta_3S_3$, were collected on a Scintag XDS 2000 (45kV, 30 mA)

diffractometer using Cu Kα X-radiation with a Kevex Peltier detector (8.04 keV, 300 eV window) over a range of 10 - 160° in 2θ at a scan rate of 6 sec/step with a 0.02° step size. Each sample was loaded on a zero background holder and smoothed. Full profile Rietveld refinements were performed using GSAS software and a starting model based on the single crystal results.

In the previous κ-phase chapter, results of a combined X-ray and neutron powder refinement were reported for the $Hf_{10}TaNb_2S_3$ sample. These two types of data were combined in an attempt to refine the mixed sulfur/oxygen/vacancy population of the X′ site in the κ-phase after the metal site occupancies had been determined for both major phases (κ-phase and γ-brass) through separate X-ray powder and neutron powder Rietveld refinements. The two types of data were not combined for refinement of the γ-brass phase and the X-ray and neutron powder results are reported separately in this chapter.

The initial refinements of the X-ray data included up to six background parameters (terms of a cosine Fourier series), lattice parameters of the separate phases, phase fractions, positional, isotropic thermal parameters, and the pseudo-Voigt profile coefficients *LY* (strain broadening) and *shift*. Refinements of mixed metal occupancies and anisotropic thermal parameters were attempted in the final stages. For all three samples, the positional parameters refined to values consistent with those found in the X-ray single crystal work and the lattice parameters refined to values which were consistent with those calculated with LATT99 using Guinier X-ray powder films.

As in the κ-phase chapter, the largest problem in these refinements was caused by the presence of minor phases. Again, the approach was to input (and fix) the lattice parameters calculated from Guinier films using the program LATT99, and the atomic and thermal parameters from reported single crystal studies. The only parameters refined for the minor phases were phase fractions and profile coefficients.

The refined phase fractions (as wt.%) and overall X-ray powder histogram statistics are given in Table 4.4 for these samples. Details pertaining to the specific

Table 4.4 Bulk sample Cu Kα X-ray powder data and results (total histogram)

initial formula	$Hf_{10}TaNb_2S_3$	$Hf_{10}Ta_3S_3$	$Hf_{8.25}Zr_{1.75}Ta_3S_3$
weight %	60 (3)% γ-brass	90 (1)% γ-brass	89 (1)% γ-brass
	32 (2)% κ-phase	4 (1)% Hf_2S	3 (1)% Hf_2S
	5 (1)% Hf	6 (1)% Hf	8 (1)% Hf
	3 (1)% Hf_2S		
d-spacing (Å)	0.78 - 8.80	0.78 - 8.80	0.78 - 8.80
2θ (deg)	10.00 - 160.0	10.0 - 160.0	10.0 - 160.0
X-radiation	Cu Kα	Cu Kα	Cu Kα
# data points	7498	7498	7498
# reflections	1103	732	737
# parameters	32	23	30
max # refl/data pt	235	110	276
R_p	0.0621	0.0713	0.0711
R_{wp}	0.0799	0.0925	0.0932
reduced χ^2	3.624	5.052	5.056
expected R_{wp}	0.0432	0.0412	0.0414
D_{dw}	0.627	0.535	0.475

"stuffed" γ-brass phases are given in Table 4.5. The refined formulas and densities in Table 4.5 refer to the stoichiometries of the γ-brass-like phases used in the final cycles of the full refinements. The Zr content was refined on each metal site in $Hf_{8.3}Zr_{0.9}Ta_{3.8}S_3$ after Ta and Hf were placed in the idealized model, M1 = M2 = Ta and M3 = M4 = Hf. It was assumed that Hf and Ta were indistinguishable through X-ray diffraction. The γ-brass phase in $Hf_{10}Ta_3S_3$ was refined after assigning metal site occupancies derived from X-ray single crystal experiments and bond order calculations (discussed later), M1 = Ta, M2 = 45% Ta/ 55% Hf, M3 = M4 = Hf. The Nb occupancies in $Hf_{9.6}Ta_{1.3}Nb_{2.1}S_3$ were refined using X-ray data after the Hf and Ta site occupancies were determined using the neutron TOF data, as discussed later. The amount of Hf on M2 was held constant while Nb/Ta mixed occupancy was refined. Table 4.6 lists the refined Zr and Nb occupancies for the γ-brass phases in the $Hf_{8.25}Zr_{1.75}Ta_3S_3$ and $Hf_{10}TaNb_2S_3$ samples. Table 4.7 lists the residuals based on F_{obs} (derived from the Bragg peaks) for each individual phase in all three samples.

M3, M4, and S thermal parameters refined isotropically in the $Hf_{8.3}Zr_{0.9}Ta_{3.8}S_3$ "stuffed" γ-brass while the thermal parameters of M1 and M2 had to be fixed at positive values. All metal and sulfur thermal parameters in the $Hf_{10.1}Ta_{2.9}S_3$ γ-brass phase were fixed at positive values consistent with the X-ray single crystal results. In the $Hf_{9.6}Ta_{1.3}Nb_{2.1}S_3$ "stuffed" γ-brass, the thermal parameter for M1 was refined while all other metal and sulfur thermal parameters had to be fixed at positive isotropic values.

Figure 4.1 shows the observed, calculated, and difference curves and reflection markers for a full multi-phase refinement of the X-ray powder data collected on the $Hf_{10}Ta_3S_3$ sample. The fit obtained between observed and calculated intensities was very good for this sample as well as for $Hf_{10}TaNb_2S_3$ and $Hf_{8.25}Zr_{1.75}Ta_3S_3$.

Neutron Scattering Experiments

Neutron scattering experiments were performed in order to help determine the Ta and Hf site occupancies in the "stuffed" γ-brass, $Hf_{10}Ta_3S_3$. The premise was that the difference between the coherent neutron scattering lengths of Hf and Ta

Table 4.5 Cu Kα X-ray powder data and results (γ-brass)

γ-brass formula[a]	$Hf_{9.6}Ta_{1.3}Nb_{2.1}S_3$	$Hf_{10.1}Ta_{2.9}S_3$	$Hf_{8.3}Zr_{0.9}Ta_{3.8}S_3$
a (Å)	10.8365 (2)	10.8343 (1)	10.8530 (1)
V (Å^3)	1272.52 (5)	1271.75 (3)	1278.37 (4)
density (g/cm^3)[a]	11.69	12.66	12.18
# reflections	536	536	537
R(F_{obs}^2) (~R_{Bragg})	0.0758	0.0960	0.0750
R(F_{obs})	0.0427	0.0553	0.0450

[a] See text for discussion

Table 4.6 **Cu Kα X-ray Rietveld refinement results for $Hf_{8.25}Zr_{1.75}Ta_3S_3$ and $Hf_{9.6}Ta_{1.3}Nb_{2.1}S_3$**

γ-brass formula[a]	$Hf_{8.3}Zr_{0.9}Ta_{3.8}S_3$	$Hf_{9.6}Ta_{1.3}Nb_{2.1}S_3$
R_{wp}	0.0932	0.0799
R_p	0.0711	0.0621
phase fraction (wt. %)	89	60

site occupancies	% Zr	% Nb
M1	3 (1)	57 (1)
M2	6 (1)	48 (2)
M3	9 (1)	0[b]
M4	8 (1)	0[b]

[a] See text for discussion

[b] Negative occupancies set equal to zero

Table 4.7 X-ray powder residuals based on $\Delta F/F_o$ for different phases

Hf-Ta-Nb-S phase	# reflections	R (F_o)
kappa	596	0.0459
gamma brass	536	0.0427
Hf	136	0.0411
Hf_2S	58	0.0336
Hf-Ta-S phase	**# reflections**	**R (F_o)**
gamma brass	536	0.0553
Hf_2S	138	0.0720
Hf	58	0.0401
Hf-Zr-Ta-S phase	**# reflections**	**R (F_o)**
gamma brass	537	0.0450
Hf_2S	142	0.0733
Hf	58	0.0315

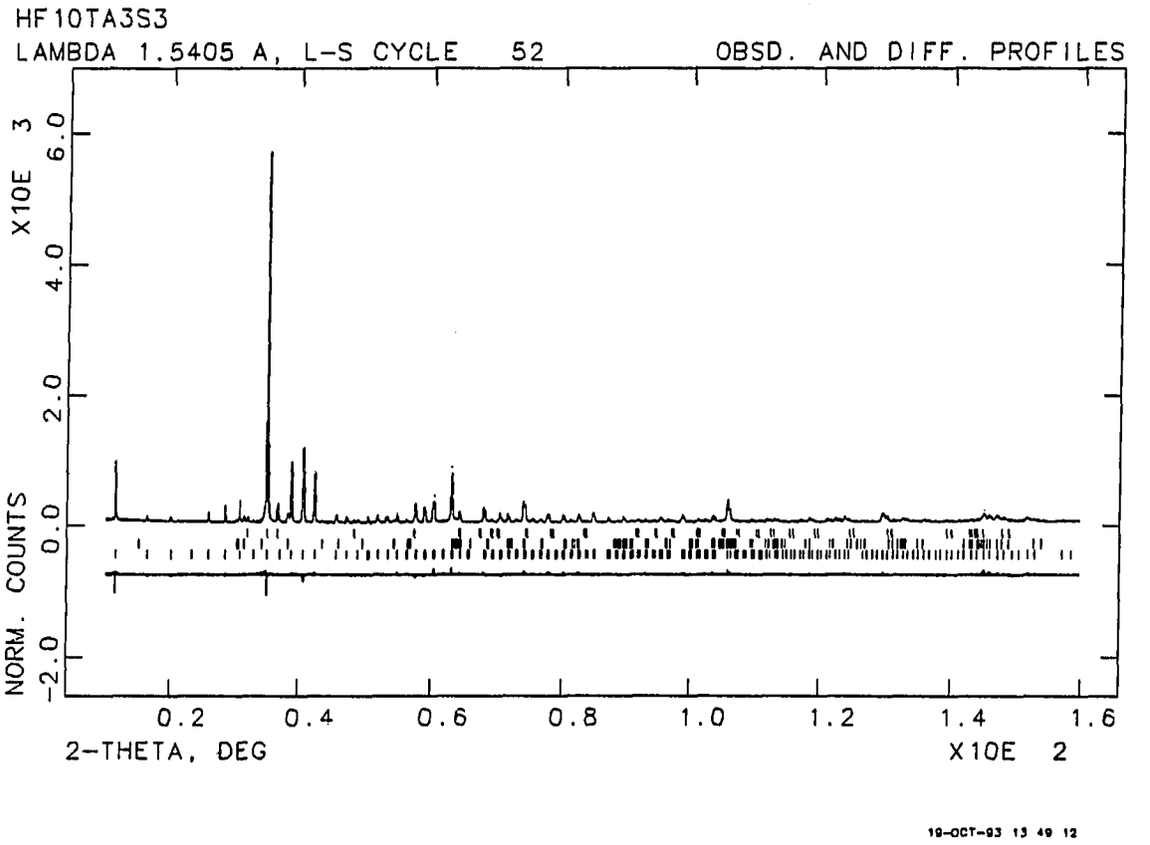

Figure 4.1 Observed, calculated, and difference curves and reflection markers for $Hf_{10}Ta_3S_3$ X-ray powder data and refinement

($b_{Hf} = 0.770 \times 10^{-12}$ cm, $b_{Ta} = 0.691 \times 10^{-12}$ cm, $b_{Nb} = 0.705 \times 10^{-12}$ cm) would be great enough to distinguish between Hf and Ta (or Nb) in a refinement of the neutron TOF data. The metal site occupancies determined through these experiments were not as precise as was anticipated but they invariably followed a trend which was consistent with the Ta and Hf site occupancies reported and discussed later in this chapter, i.e. Ta (Nb) occupation primarily of the M1 (IT) and M2 (OT) positions and Hf occupation primarily of the M3 (OH) and M4 (CO) positions. Furthermore, in agreement with the later discussion, the M3 (OH) position was found to show a trend toward substantial mixed Hf/Ta occupancy.

Time-of-flight (TOF) neutron scattering data were collected for two approximately 5 gram "stuffed" γ-brass samples, $Hf_{10}Ta_3S_3$, and $Hf_{10}TaNb_2S_3$, on the High Intensity Powder Diffractometer (HIPD) at the Manual J. Lujan Neutron Scattering Center (LANSCE) at Los Alamos National Laboratory. Data for $Hf_{10}Ta_3S_3$ were collected for 172,000 μA·hours and data for $Hf_{10}TaNb_2S_3$ were collected for 178,000 μA·hours. The latter sample (Hf-Ta-Nb-S) was previously discussed in the κ-phase chapter. Both samples were loaded into fused silica sample containers and placed into a sample changer and the whole apparatus was loaded into the HIPD.

Rietveld refinements using GSAS were carried out on the Neutron data sets from the ±153.4°, ±90.0°, and ±39.8° TOF detectors for these multi-phase systems. Full anisotropic refinements were attempted for both, including positional, thermal, occupancy, phase fraction, and lattice parameters and background and peak profile coefficients, *zero*, *difa*, and *sig1*. The neutron powder refinements were performed in the same general fashion as were the previously discussed X-ray powder refinements. The raw data were limited in the refinements through RAWPLOT to include only areas containing visually resolvable Bragg peaks. Because determinations of the metal site occupancies (the principle objective in this neutron scattering experiment) were ambiguous, refinement of the 153.4° data for the $Hf_{10}TaNb_2S_3$ sample is briefly discussed.

Positional parameters refined to values which were consistent with those found

in the X-ray single crystal work and the lattice parameters refined to values which were consistent with those calculated with LATT99 using Guinier X-ray powder films. The presence of minor phases affected the refinement results of the overall histogram. Their positional, thermal, and metal site occupancy parameters were fixed at values known from reported X-ray single crystal results just as in the X-ray powder refinements.

The backgrounds for both samples were modeled as twelve term Fourier cosine series and as twelve term radial distribution functions [95] of fused silica. The refinements using the Fourier series background functions resulted in lower residuals than did refinements using the radial distribution functions, so that the Fourier cosine series background functions were used in the refinements discussed here.

Table 4.8 lists the refined phase fractions (as wt.%) and overall neutron histogram statistics for the $Hf_{10}TaNb_2S_3$ and $Hf_{10}Ta_3S_3$ samples. Details of the specific "stuffed" γ-brass refinements are given in Table 4.9. The refined formulas and densities in Table 4.9 were calculated from results of the final least squares cycles which used the 153.4° TOF data banks. The formula and density of the $Hf_{9.6}Ta_{1.3}Nb_{2.1}S_3$ "stuffed" γ-brass corresponds to the fully determined metal site occupancies in this phase (discussed below). The residuals based on F_{obs} for individual phases in these two samples are given in Table 4.10 and only the minor Hf phase in the Hf-Ta-Nb-S sample has a large R (F_o).

As mentioned previously, X-ray diffraction of Mo (or Cu) Kα radiation can distinguish between Ta, Nb, and S but does not allow the differentiation of Hf and Ta. Neutron scattering, on the other hand, can distinguish between Hf, Ta and S but not between Ta and Nb due to the differences in their coherent scattering lengths which are: $b_{Hf} = 0.770 \times 10^{-12}$ cm, $b_{Ta} = 0.691 \times 10^{-12}$ cm, $b_{Nb} = 0.705 \times 10^{-12}$ cm, and $b_S = 0.285 \times 10^{-12}$ cm. The difference in neutron scattering length between Hf and Ta (or Hf and Nb) is not large and the resolution of neutron diffraction is inherently less than that of X-ray diffraction due to the neutron pulse width. For these reasons, the determination of site occupancies through interpretation of Reitveld refinements based

Table 4.8 Bulk sample TOF neutron powder data and results (total histogram)

initial formula	$Hf_{10}TaNb_2S_3$	$Hf_{10}Ta_3S_3$
weight %	64 (1)% γ-brass	93 (2)% γ-brass
	29 (1)% κ-phase	3 (1)% Hf_2S
	6 (1)% Hf	5 (1)% Hf
	1 (1)% Hf_2S	
d-spacing (Å)	0.65 - 3.165	0.48 - 4.78
TOF (msec)	3.27 - 15.90	2.40 - 24.00
data bank	+153.4 ° (2θ)	+153.4 ° (2θ)
# data points	3189	4646
# reflections	1103	1490
# parameters	33	37
max # refl/data pt	235	321
R_p	0.0350	0.0341
R_{wp}	0.0528	0.0508
reduced χ^2	1.498	1.621
expected R_{wp}	0.0432	0.0400
D_{dw}	1.318	1.166

Table 4.9 TOF neutron powder data and results (γ-brass)

γ-brass formula [a]	$Hf_{9.6}Ta_{1.3}Nb_{2.1}S_3$	$Hf_{10.2}Ta_{2.8}S_3$
a (Å)	10.8232 (2)	10.828 (2)
V (Å^3)	1267.86 (7)	1269.6 (6)
density (g/cm^3) [a]	11.73	12.68
# reflections	457	1126
R(F_{obs}^2) (~R_{Bragg})	0.0548	0.0734
R(F_{obs})	0.0315	0.0392

[a] See text for discussion

Table 4.10 TOF neutron powder residuals based on $\Delta F/F_o$ for different phases

Hf-Ta-Nb-S phase	# reflections	R (F_o)
kappa	487	0.0413
gamma brass	457	0.0317
Hf	47	0.1031
Hf_2S	112	0.0577
Hf-Ta-S phase	**# reflections**	**R (F_o)**
gamma brass	1126	0.0392
Hf_2S	256	0.0547
Hf	108	0.0464

upon this difference is difficult.

In the previous chapter, X-ray diffraction was used to determine the Nb vs. (Ta/Hf) site occupancies in the κ-phase and then neutron scattering was used to differentiate Hf and Ta with a reasonable degree of success. This approach did not yield reasonable results and was reversed for the Hf-Nb-Ta-S gamma brass-like phase. The Hf vs. (Ta/Nb) occupancies were determined first through neutron scattering and then Ta and Nb were differentiated through X-ray diffraction. Thedetermined metal site occupancies would have been somewhat quantitative if both approaches gave equivalent results.

When the fractional occupancies of all metal sites in these "stuffed" γ-brass compounds were simultaneously refined with all other parameters, the results were inconsistent with the known stoichiometries and, in fact, were physically impossible. However the trend was consistent with the metal site occupancies postulated previously. Ta (or Nb) preferentially occupied the IT and OT sites (to more than 100%) while Hf preferentially occupied the OH and CO sites (to more than 100%). When the metal site occupancies were refined cyclically one at a time until no changes to within esd's were observed, the results were still physically unrealistic (but to a lesser degree) and the trend for preferential occupancies was intact.

In the models used to obtain the results reported in Tables 4.8 to 4.10, the anisotropic thermal parameters from the X-ray single crystal refinement of $Hf_{10}Ta_3S_3$ were put into the least squares models of the γ-brass phases in the $Hf_{10}Ta_3S_3$ and $Hf_{10}TaNb_2S_3$ samples and the metal site occupancies were initially assigned as Ta on the IT and OT sites and Hf on the OH and CO sites. All parameters, other than metal site occupancies were refined to convergence. Subsequently, all parameters were fixed except Hf and Ta site occupancies, which were refined. Occupancies greater than 100% or less than zero were not allowed which resulted in refinement of substantial Hf and Ta partial occupancies of only the OT site in both systems. Because Ta and Nb have similar neutron scattering lengths but different X-ray scattering factors, the Hf content was fixed and the Ta/Nb occupancies were refined

in the refinement of the X-ray data for $Hf_{9.6}Ta_{1.3}Nb_{2.1}S_3$. Table 4.11 lists the metal site occupancies determined for these "stuffed" γ-brass systems. The metal site occupancy esd's were calculated by the refinements to be about 1% but it is felt that the real uncertainties in these site occupancies were much larger (> 5%).

Full refinements of combinations of neutron data and the X-ray single crystal data previously discussed were also attempted where the X-ray single crystal data were weighted in a one-to-one relationship with each TOF data bank used. All parameters, except site occupancies, were refined to convergence and then only the phase fractions were fixed when the occupancies were added to the refinement. The results were somewhat ambiguous in that the refined metal site occupancies depended upon which banks of TOF data were used. Table 4.12 lists refined % Ta site occupancies refined using various combinations of TOF data. It should be noted that for all but two of these combinations, negative (and physically impossible) occupancies were refined. These results are not quantitative but are meaningful none-the-less. In all cases, the largest amounts of Ta were found on the M1 (IT) and M2 (OT) sites while the smallest amounts of Ta were found on the M3 (OH) and M4 (CO) sites. Combined refinement of all six data banks simultaneously and of data banks 3 and 4 together gave physically possible occupancies, but the stoichiometries ($Hf_{8.7}Ta_{4.3}S_3$ and $Hf_{9.1}Ta_{3.9}S_3$ respectively) were unrealistic. Given the initial stoichiometry and the refined phase fractions and assuming that substantial amounts of Ta were not present in the minor phases, the composition of the "stuffed" γ-brass phase in the $Hf_{10}Ta_3S_3$ sample was ~ $Hf_{9.7}Ta_{3.3}S_3$. Table 4.13 lists overall histogram statistics for simultaneous refinement of all six TOF data banks which shows the differences in the qualities of the various data sets. The residuals obtained through GSAS for a refinement based on F_{obs} of only the X-ray single crystal data were R = 0.036 and R_w = 0.030 while refinement of all six powder histograms and the X-ray single crystal data resulted in higher single crystal residuals, R = 0.054 and R_w = 0.044.

Figure 4.2 shows the observed, calculated, and difference curves and reflection

Table 4.11 Metal site occupancies determined from neutron and x-ray powder refinements with fixed thermal parameters and no occupancies allowed > 100% or < 0%

	$Hf_{9.6}Ta_{1.3}Nb_{2.1}S_3$	$Hf_{10.2}Ta_{2.8}S_3$
M1 (IT)	38% Ta: 5% Hf: 57% Nb	100% Ta
M2 (OT)	29% Ta: 23% Hf: 48% Nb	39% Ta: 61% Hf
M3 (OH)	100% Hf	100% Hf
M4 (CO)	100% Hf	100% Hf
S	100% S	100% S

Table 4.12 %Ta site occupancies as a function of TOF data refined

Data banks	1,2	1,3	1,4	2,3	1,2,3,4,5,6
M1	108	78	48	104	66
M2	89	64	70	84	81
M3	-25	-20	-40	9	22
M4	-14	6	17	22	12
Data banks	2,4	3,4	1,2,3	2,3,4	1,2,3,4
M1	23	79	86	64	66
M2	43	52	68	63	72
M3	-61	24	-19	-20	-25
M4	-23	9	3	11	9

Data bank 1 = +153.4 °

Data bank 2 = -153.4 °

Data bank 3 = +90.0 °

Data bank 4 = -90.0 °

Data bank 5 = +39.8 °

Data bank 6 = -39.8 °

Table 4.13 Combined neutron powder histogram and X-ray single crystal refinement statistics

Data bank	Ndata	TOF range	R_{wp}	R_p	D_{dw}
+153.4 °	3483	2.85 - 16.0	0.0524	0.0354	1.094
-153.4 °	3353	2.85 - 15.0	0.0486	0.0331	1.234
+90.0 °	3691	1.72 - 10.6	0.0524	0.0410	0.559
-90.0 °	3332	2.04 - 10.6	0.0580	0.0456	0.559
+39.8 °	2805	1.6 - 6.35	0.0609	0.0459	0.593
-39.8 °	2680	1.7 - 6.35	0.0538	0.0420	0.606
total	20,560	-	0.0545	0.0410	0.701

	Nobs	$R(F_{obs})$	$R_w(F_{obs})$
single crystal plus powder	197	0.054	0.044
single crystal only	197	0.036	0.030

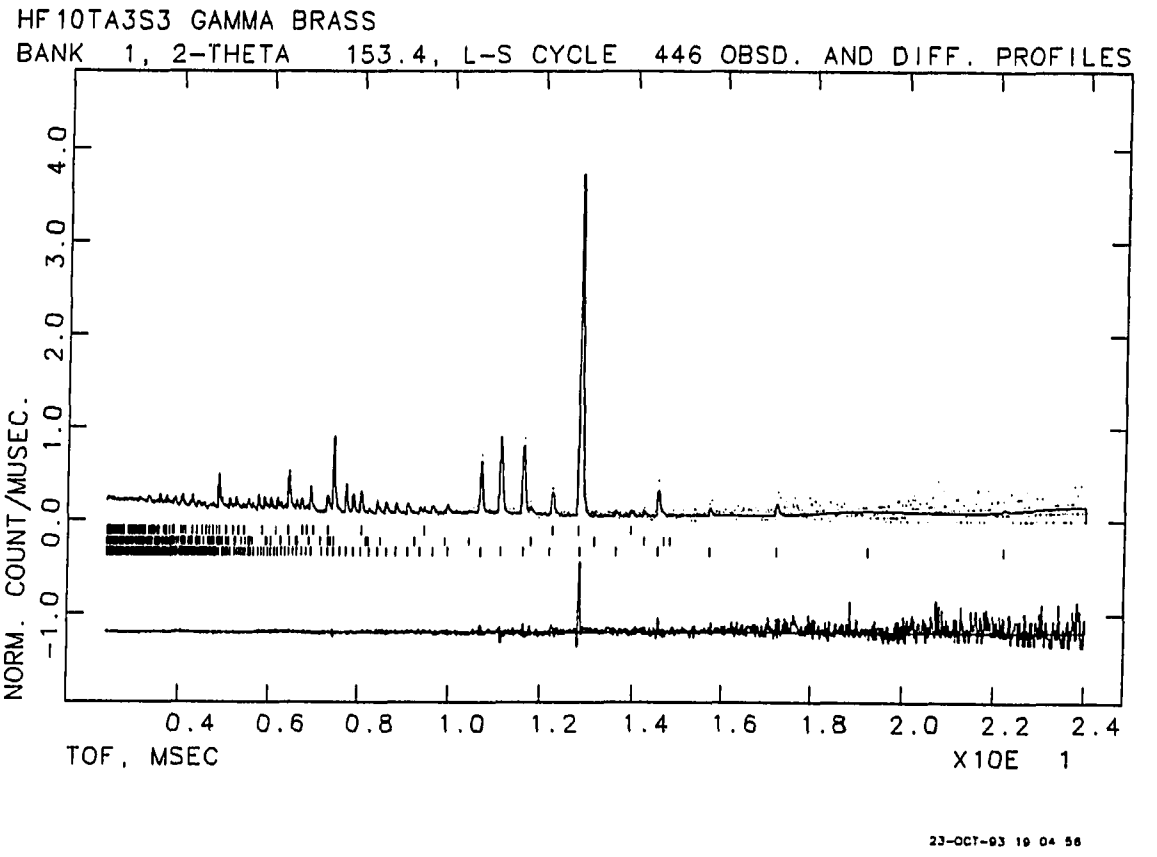

Figure 4.2 Observed, calculated, and difference curves and reflection markers from $Hf_{10}Ta_3S_3$ neutron powder 153.4° data bank and refinement

markers for a full multi-phase refinement of the +153.4° bank of neutron powder data collected for the $Hf_{10}Ta_3S_3$ sample. The fit obtained between observed and calculated intensities was very good. The fit between observed and calculated intensities was also quite good for the $Hf_{10}TaNb_2S_3$ sample.

Discussion

A number of complex, novel structures has been found in metal-rich systems. Among the most interesting are Hf_2S [54], Ta_6S [35,36], $Nb_{21}S_8$ [12], $Nb_{1.72}Ta_{3.28}S_2$ [49], and $Nb_{0.95}Ta_{1.05}S$ [50] (Ta_2Se type [51]), compounds that have led to a deeper understanding of chemical bonding in metal rich systems. Continued high-temperature investigations into ternary metal-rich sulfide systems have recently led to the novel "stuffed" gamma brass structure ($Hf_{10}Ta_3S_3$) reported here.

The structure of this new compound agrees with ideas about M-M and M-S bonding which grew out of previous metal-rich sulfide research and other ideas pertaining to binary alloy gamma brasses [99,102] (e.g. Cu_5Zn_8) are applicable as well. This new early transition metal sulfide forms in a modification of one of the structures for which the Hume-Rothery electron concentration rules [62] were developed in late transition and main group metal alloys and therefore has interesting theoretical implications.

The metal atoms in $Hf_{10}Ta_3S_3$ occupy the same positions as those in Cu_5Zn_8 with one small difference for the M4 site. The metal sites can be described as *bcc* packing of 26 atom units which are composed of the following polyhedra [103] (Figure 4.3): M1 forms a tetrahedron centered at the origin and denoted as the inner tetrahedron (IT), M2 caps the faces of the IT forming a larger tetrahedron denoted as the outer tetrahedron (OT), M3 caps the edges of the OT forming a large octahedron (OH) and M4 approximately caps the edges of the OH forming an enveloping cuboctahedron (CO) with the M3 atoms slightly protruding out of the centers of the rectangular faces.

Examination of Cu_5Zn_8 (Figure 4.4) reveals channel-like cavities along the face bisectors at positions x,1/2,0. These channels are too constricted to contain any

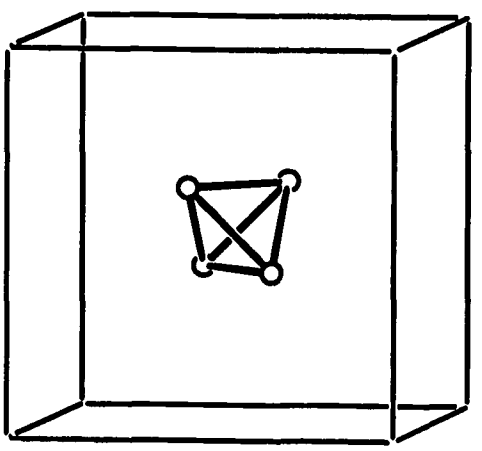

IT (M1)

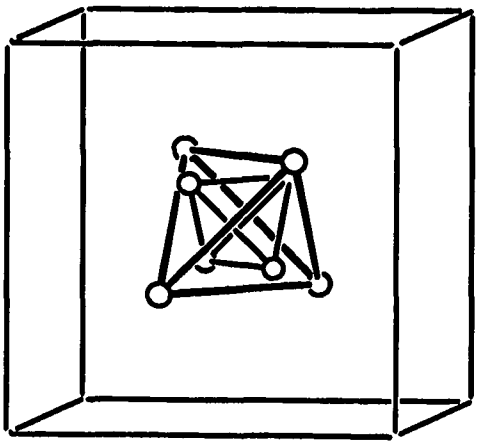

OT (M2)

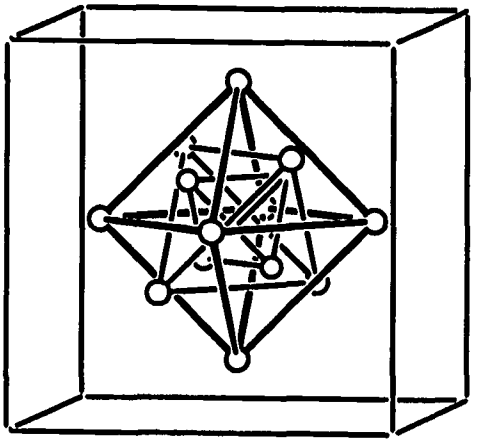

OH (M3)

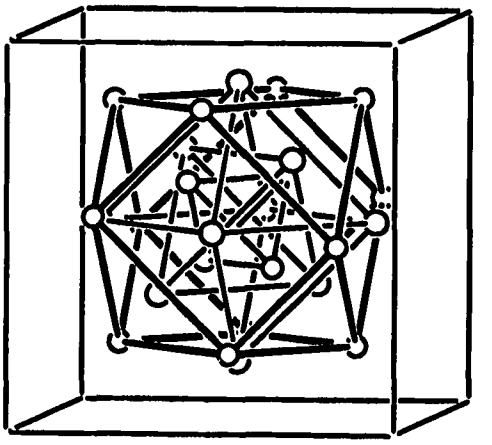

CO (M4)

Figure 4.3 Polyhedra composing the 26 atom units found in gamma brasses.

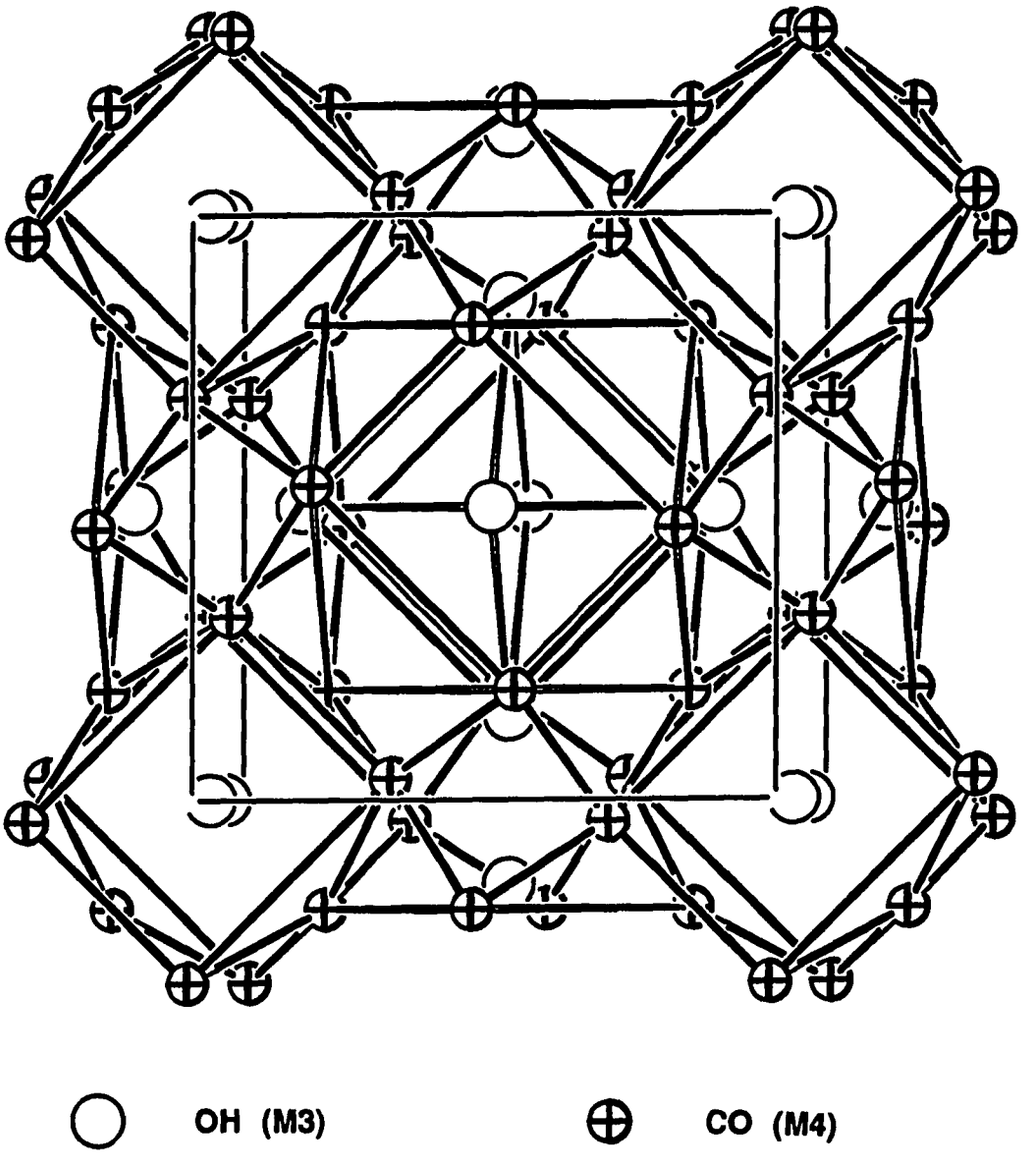

Figure 4.4 OH and CO metal framework showing channel-like voids of Cu_5Zn_8, refined thermal parameters are not depicted

elements except possibly hydrogen in Cu_5Zn_8, but in $Hf_{10}Ta_3S_3$ the unit cell is expanded (due mainly to the larger metal atoms Hf and Ta) so that sulfur can fit beautifully into the channels (Figure 4.5). These cavities are not perfect channels because M3 (OH) partially obstructs them.

Since Hf and Ta are nearly identical scatterers of Mo Kα X-radiation, the metal site occupancies could not be directly refined in $Hf_{10}Ta_3S_3$ through X-ray single crystal experiments. However, bonding ideas, interatomic distances, Rietveld refinements of X-ray data collected for the Zr and Nb substituted phases, Rietveld refinements of neutron data, bond-order calculations, and the stoichiometry provided insights into the probable site occupancies. The interatomic distances for $Hf_{10}Ta_3S_3$ are given in Table 4.14 and the refined metal occupancies are given in Tables 4.6 and 4.11 for the γ-brass-like phases, $Hf_{10}TaNb_2S_3$, $Hf_9ZrTa_3S_3$, and $Hf_{10}Ta_3S_3$.

Hafnium is more electropositive than tantalum forming stronger M-S bonds and Ta has an additional bonding electron relative to Hf and thus is favored in sites with only M–M bonds. Therefore, one expects Hf to be found in the M-S bonding sites (M3 and M4) and Ta to be found in M-M bonding sites (M1 and M2). Assuming that Zr substitutes for Hf and that Nb substitutes for Ta, the occupancies refined from the X-ray powder data for the substituted Zr and Nb compounds agreed with the expected site occupancies above. Nb showed a dramatic preference for the M1 and M2 (Ta) sites while Zr showed a much lesser preference for the M3 and M4 (Hf) sites. The metal site occupancies indicated through refinement of neutron scattering data also suggest that Ta is found primarily on the IT and OT (M1 and M2) while Hf is primarily found on the OH and CO (M3 and M4) sites. Accordingly, the following assignments were made: M1 = Ta, M2 = Ta, M3 = Hf, and M4 = Hf, leading to an idealized site assignment and stoichiometry of $Hf_9Ta_4S_3$ which was close to, but not the same as the experimentally known stoichiometry. This suggested that at least one of the four metal sites had mixed occupancy, a phenomenon that is common to ternary metal-rich sulfides [19,49,50]. Since Ta has a smaller Pauling radius [8] than Hf (r_{Ta} = 1.343 Å; r_{Hf} = 1.442 Å), it was expected that $d_{Ta\text{-}Ta} < d_{Ta\text{-}Hf} < d_{Hf\text{-}Hf}$, and

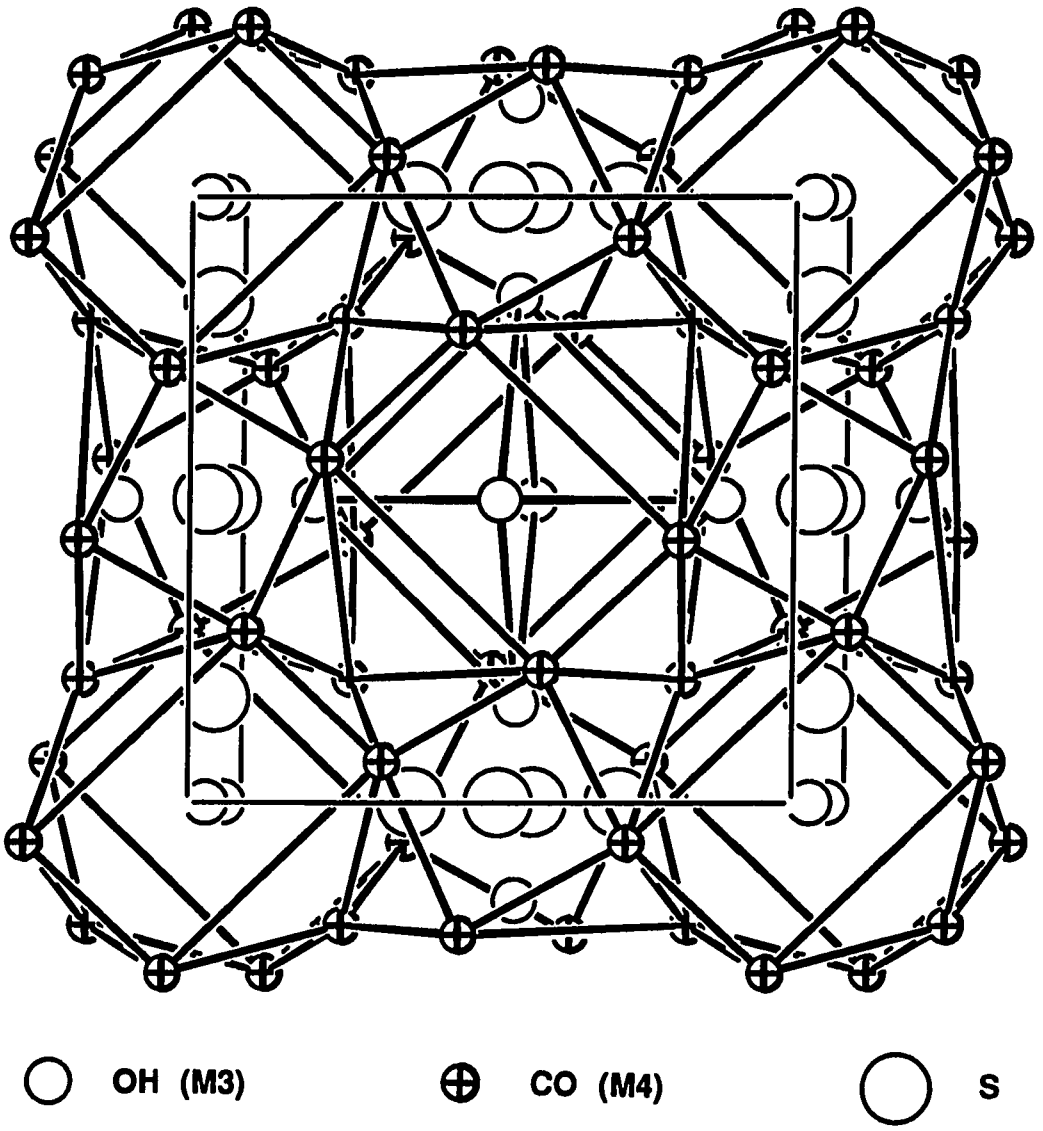

Figure 4.5 OH and CO framework showing sulfur positions in channels of $Hf_{10}Ta_3S_3$, sulfur on front and back faces is not shown, refined thermal parameters (Tables 4.2 and 4.3) are not depicted

Table 4.14 Interatomic distances < 3.8 Å for $Hf_{10}Ta_3S_3$

M1	-M2	x3	2.948 (5)	M4	-S		2.497 (3)
	-M4	x3	2.960 (4)		-S		2.604 (8)
	-M1	x3	2.974 (6)		-M1		2.9604 (8)
	-M3	x3	2.993 (3)		-M2		3.058 (6)
					-M2		3.157 (2)
M2	-M1	x3	2.948 (5)		-M3		3.166 (2)
	-M4	x3	3.058 (6)		-M3		3.346 (2)
	-M3	x3	3.111 (3)		-M3		3.398 (3)
	-M4	x3	3.157 (2)		-M4	x2	3.405 (4)
					-M4	x2	3.464 (2)
M3	-S	x2	2.58 (1)		-M4	x2	3.530 (2)
	-M1	x2	2.993 (3)				
	-M2	x2	3.111 (3)	S	-M4	x2	2.497 (3)
	-M4	x2	3.166 (2)		-M3	x2	2.58 (1)
	-M4	x2	3.346 (2)		-M4	x2	2.604 (8)
	-M4	x2	3.398 (3)		-S		3.75 (2)
	-M3		3.535 (6)				

comparison of the distances from M1 and M2 to M3 and M4 indicated that M2 had mixed Ta/Hf occupancy.

Bond-order calculations performed on the refined structure of $Hf_{10}Ta_3S_3$ using the Pauling bond-order equation [8], $D(1) = D(n) - 0.6 \log n$, and the Pauling single bond or metallic bond radii also suggested mixed metal occupancy occurred primarily on the M2 site. Assuming that the total bond orders for particular metal sites scale like the expected valences of those sites, and that pure Hf and pure Ta exhibit valences of 4 and 5 respectively, and that the radius for a particular site is directly proportional to its composition, the bond orders of the metal sites for differing models of occupancy (Table 4.15) can be calculated. The stoichiometric model resulted in a large discrepancy between the expected valence and the calculated bond order only for the M2 (OT) site. The total metal occupancies were then constrained to the stoichiometry determined through SEM-EDS and other models of occupancy were investigated. The model of statistical occupancy on all metal sites gave poor agreement and the proposed occupancy model gave the best agreement between expected and calculated values. In the investigation of $Zr_{6.45}Nb_{4.55}P_{4.0}$ [18] it was possible to refine metal site occupancies because of anomalous dispersion, and excellent agreement with occupancies based on bond-orders was obtained.

These metal site occupancies for $Hf_{10}Ta_3S_3$ cannot be inferred using long-standing arguments that would apply if this compound were strictly a binary alloy type of gamma brass. For gamma brasses, M_xN_y, the structure (I, F, or P) and the site occupancies have been shown to be determined by the following factors [104]: 1) avoiding contacts between the larger atoms when $R_M/R_N > 1.10$ and $x/y < 0.3$, 2) obtaining a relatively high packing fraction, and 3) maximizing the number of contacts between unlike atoms, M-N. The first factor, which dominates the choice of structure, had no relevance in this structure since R_{Hf} and R_{Ta} are < 10% different. With no size imposed restrictions the choice of structure was of the highest symmetry, body-centered cubic.

The second factor appears to be relevant to the packing within the Hf–Ta

Table 4.15 Calculated bond orders in different occupancy models for $Hf_{10}Ta_3S_3$

metal site	occupancy % Ta	expected valence	calculated bond order	
IT	100	5.00	4.98	
OT	100	5.00	3.73	stoichiometric
OH	-	4.00	4.28	model
CO	-	4.00	3.99	
IT	22.3	4.22	7.34	
OT	22.3	4.22	5.24	statistical
OH	22.3	4.22	4.29	model
CO	22.3	4.22	3.92	
IT	100	5.00	5.23	
OT	45	4.45	4.59	proposed
OH	-	4.00	4.41	model
CO	-	4.00	4.13	

clusters although the sulfur atoms isolate the 26-atom metal units so that the *bcc* packing is not condensed to the degree found in binary alloy gamma brasses. Comparison of the normalized Hf and Ta radii (R_{Hf} = 1.02, R_{Ta} = 0.94) In this new structure with the ideal calculated radii giving the highest packing fraction [104] (R_{IT} = 0.888(2), R_{OT} = 0.906(4), R_{OH} = 1.000(2), R_{CO} = 1.058(2)) generates the same idealized $Hf_9Ta_4S_3$ site assignments as discussed above: IT = Ta, OT = Ta, OH = Hf, and CO = Hf. The relative radii of Hf and Ta are nearly ideal for packing into 26-atom clusters which stabilize $Hf_{10}Ta_3S_3$ in a gamma brass type structure.

The third determining factor is not directly applicable to the "stuffed" gamma brass structure because the presence of 5d orbitals on the metals dramatically increases the metal-metal bonding capacity between metal atoms, and the presence of the sulfur atoms makes metal-sulfur bonding an important factor. In gamma brasses such as Cu_5Zn_8, the unlike metal-metal interactions may be viewed as the most bonding, but in the "stuffed" gamma brass this is no longer true. Ta-Ta and Hf-S bonding are as important as Hf-Ta bonding in this structure.

In the reported M_3N_{10} gamma brass, Pd_3Zn_{10} [102,104], there are 8M atoms on the OT sites and 4M atoms on the OH sites with 40N atoms occupying all remaining sites, maximizing the number of M-N contacts. In $Hf_{10}Ta_3S_3$, a $N_{10}M_3S_3$ "stuffed" gamma brass, there are 8M atoms on the IT sites and 4M atoms on the OT sites with the 40N atoms occupying all remaining sites, which effectively minimizes the number of unlike M-N contacts but maximizes d electron bonding as well as the packing fraction. Table 4.16 shows the reported site occupancies of $Hf_{10}Ta_3S_3$ and Pd_3Zn_{10} for comparative purposes.

The term "electron compound" has been used to describe compounds such as the β-brasses and the γ-brasses, the latter being of special interest and relevance to this dissertation. Hume-Rothery popularized this term as a description of phases with the same structure type which are found in differing systems (e.g. Cu-Al and Cu-Zn) with differing stoichiometries but with the same ratio of valence electrons to atoms. Electron counting rules, in particular the Hume-Rothery rules [62], have

Table 4.16 Reported site occupancies for $Hf_{10}Ta_3S_3$ and Pd_3Zn_{10}

site		$Hf_{10}TaS_3$	Pd_3Zn_{10}
IT	(M1)	Ta	Zn
OT	(M2)	45% Ta; 55% Hf	Pd
OH	(M3)	Hf	33% Pd; 67% Zn
CO	(M4)	Hf	Zn
S		S	-

played an important role in solid state chemistry, and materials science although they have not been well understood theoretically. Recently, the concept of second moment scaling has been shown to lead to the Hume-Rothery electron concentration rules for alloys [105] and the existence of the new γ-brass-like compound reported here presents a significant test for this approach. The unavailability of reliable Hückel parameters for Hf and Ta precluded a meaningful application of the theory at this time, however.

The gamma brasses were observed to form alloys with a ca. 20/13 to 22/13 ratio of s and p electrons to metal atoms and it is of interest to examine whether $Hf_{10}Ta_3S_3$, being a "stuffed" gamma brass, follows this rule as well. According to the ideas of Engel as modified by Brewer [63], the s and p electrons determine structure and Ta tends to have the configuration $d^{3.5}sp^{0.5}$ in alloys while Hf tends to have two possible configurations, $d^{2.5}sp^{0.5}$ for bcc structures and $d^{2.3}sp^{0.7}$ for hcp structures. The promotional energies required for the excited state configurations are compensated by bonding interactions. Zr also tends to have two possible configurations in alloys, bcc $d^{2.7}sp^{0.3}$ and hcp $d^{2.3}sp^{0.7}$. If the hcp configuration for Hf contributed substantially to the electronic structure of the "stuffed" gamma brass, Zr would readily substitute

for Hf because their hcp configurations are identical. That this is not observed suggests that the correct configuration for Hf is that corresponding to bcc. The configurations corresponding to bcc for Hf and Zr are different and thus the small amount of substitution of Zr for Hf observed in this structure can be understood in terms of the $d^{2.3}sp^{0.7}$ configuration of Hf. Furthermore, the bcc modification of Hf is found at high temperatures ($T \geq 1743°C$) and the "stuffed" gamma brass is synthesized at high temperatures by arc-melting. For these reasons the bcc electron configurations are used to count s and p electrons as 3×1.5 for Ta plus 10×1.5 for Hf for a total of 19.5 metal s-p electrons. An idea common to both the Hume-Rothery rules and the Brewer-Engel correlation is that the s and p conduction electrons, through Fermi surface interactions with the zone boundaries, determine the long range order of the crystal structure, and according to the Brewer-Engel ideas, the d-electron interactions are primarily short-range, i.e. to nearest neighbors. If these ideas are appropriate to the stuffed γ-brass, a proposal that suggests theoretical investigation, it is necessary that the $Hf_{10}Ta_3S_3$ formula unit provides approximately 20 to 22 electrons for the s-p conduction band and thus that approximately ½ to 2.5 s-p electrons are donated by the 3 sulfur atoms.

The fact that compounds with this structure did not form for $Hf_{10}Nb_3S_3$, $Zr_{10}Ta_3S_3$, or $Zr_{10}Nb_3S_3$ (which form in a κ-phase structure instead) is not surprising because the structures of the metal-rich binary sulfides [10] of the 5d transition metals (Ta_6S [35,36], Ta_2S [34], Ta_3S_2 [37], Hf_2S [54]) differ substantially from those of the 4d transition metals ($Nb_{21}S_8$ [12], $Nb_{14}S_5$ [13], Zr_9S_2 [30], Zr_2S2 [55]). This difference in the Hf-Zr case has been rationalized through the Brewer-Engel correlation [56,106], and it appears likely that interactions of the f shell with the outer electrons yielding significant differences in the excited-state energies are of importance in the formation of metal-rich structure by 5d metals.

Continuing with the Brewer-Engel analysis, and counting 1.3 s and p electrons for Zr and 1.0 for Nb, as suggested by Brewer (in the high-temperature *bcc* structure in the case of Zr) yields the electron counts given in Table 4.17. It therefore

Table 4.17 Electrons per metal atom for six different compounds using Brewer's high temperature *bcc* configurations

composition	e^-/a^a	
$Hf_{10}Ta_3S_3$	19.5	
$Hf_9ZrTa_3S_3$	19.3	form as γ-brass structures
$Hf_{10}TaNb_2S_3$	18.5	
$Hf_{10}Nb_3S_3$	18.0	
$Zr_{10}Ta_3S_3$	17.5	form as κ-phase structures
$Zr_{10}Nb_3S_3$	16.0	

[a] e^- per 13 metal atoms, sulfur electrons are not included

appears significant, within the context of the Hume-Rothery rules and the Brewer-Engel correlation, that $Hf_{10}Nb_3S_3$, $Zr_{10}Ta_3S_3$ and $Zr_{10}Nb_3S_3$ all crystallize in the κ-phase structure i.e. sufficient substitution to decrease the s-p electron count below a critical count destabilizes the γ-brass structure.

5. $Zr_{6.45}Nb_{4.55}P_{4.0}$, A NEW TERNARY STRUCTURE

Synthesis and Characterization

A sample of nominal composition $Zr_9Nb_4P_4$ was prepared from Zr and NbP and arc-melted (10 V, 75 A) for 45 seconds under an Ar atmosphere on a water cooled copper hearth. The NbP was prereacted for 1 month while slowly increasing the temperature up to 800°C as discussed in the experimental chapter. The pellet was subsequently inverted and arc-melted twice more to promote homogenization. Needle-like crystals grew from the surface of a partially melted sample of $Zr_9Nb_4P_4$ when it was inductively annealed at approximately 1700°C for 3 hours with a residual pressure of $< 1 \times 10^{-7}$ torr.

X-ray powder patterns of the annealed bulk $Zr_9Nb_4P_4$ sample showed that only two phases were present, the new $Zr_{6.45}Nb_{4.55}P_{4.0}$ compound and Zr metal. This phase information along with the substantial loss of sample, presumed to be mostly P, upon arc-melting makes the refined stoichiometry reasonable. A new sample of composition $Zr_{6.5}Nb_{4.5}P_{4.5}$ was arc-melted and annealed. Excess phosphorus was included in this sample to compensate for the presumed loss of P upon arc-melting. Guinier film techniques showed that the $(Zr,Nb)_{11}P_4$ phase reported here was the major phase.

An SEM-EDS analysis of the $Zr_9Nb_4P_4$ sample was inconclusive. The two phases, $M_{11}P_4$ and Zr, identified in the Guinier film of this sample appeared to be one homogeneous phase in this scanning electron microscopy experiment. It is likely that the Zr phase contained enough phosphorus and oxygen in solid solution to cause the electron density of the two phases to be nearly identical. In this case, differentiation would be impossible by observation of the SEM image on the monitor.

Single Crystal X-ray Investigation

A single crystal of dimensions $0.51 \times 0.11 \times 0.08$ mm^3 was selected from the partially melted $Zr_9Nb_4P_4$ sample and aligned along the needle direction (short axis of the unit cell) on a Weissenberg camera. Rotation, zero and first layer Weissenberg photographs showed the lattice to be body centered orthorhombic with cell

dimensions of approximately a = 3.6 Å, b = 9.7 Å, and c = 16 Å. An intensity data set was collected for this crystal on a Rigaku AFC6R rotating anode diffractometer with monochromatic Mo Kα X-radiation using the ω – 2θ scan technique out to 60°C in 2θ. Intensities were measured for reflections with h + k + ℓ = 2n over the ±hkℓ octants.

Data processing and structure refinement were performed using TEXSAN software. The observed intensities were corrected for Lorentz polarization and absorption effects and the internal $R_{averaging}$ = 2.3% after absorption corrections were applied was excellent. Least-squares lattice parameters were calculated using LATT99 from an X-ray powder pattern of the bulk sample. PROCESS suggested, incorrectly, that the crystal had an acentric spacegroup but the crystal was determined to have the space group *Immm* and the structure was found using direct methods for the initial model and refined anisotropically to the residual values R = 2.5%, R_w = 4.5%. Table 5.1 gives the crystal data for this new structure.

Initially, M2 was refined as Nb and M1, M3, M4, and M5 were refined as Zr. The refined thermal parameters were well-behaved and offered no information that appeared to be useful in determining the mixing of Zr and Nb on particular sites. It was anticipated that Zr and Nb occupancies would not be resolved using X-ray diffraction techniques since their electron densities are nearly the same. In order to determine the correct placement of the two metals in the structure, a Pauling bond order calculation was performed. This calculation was consistent with M1 occupation by Nb (as discussed later). With M2 = M3 = M4 = M5 = Zr and M1 = Nb, a dramatic improvement in the residual values to R = 2.0%, R_w = 2.8% was found.

Both Zr and Nb have absorption edges near the wavelength of Mo Kα X-radiation and the anomalous scattering corrections ($f = f_o + \Delta f' + i\Delta f''$) were important in this diffraction experiment. The atomic scattering factors for Zr and Nb drop off rapidly with (sinθ)/λ but the anomalous scattering corrections remain approximately constant, with the result that the difference between Nb and Zr scattering becomes increasingly resolvable as 2θ increases. Table 5.2 gives the real

Table 5.1 Crystal data for $Zr_{6.45}Nb_{4.55}P_{4.0}$

Formula	$Zr_{6.45}Nb_{4.55}P_{4.0}$
Space group	*Immm* (#71)
a Å	15.917 (1)
b Å	9.5684 (9)
c Å	3.5892 (3)
V Å^3	546.62 (13)
Z	2
d_{calc}, g/cm^3	6.895
Crystal size, mm^3	0.51 × 0.11 × 0.08
μ (Mo Kα), cm^{-1}	107.02
Data collection instrument	RIGAKU AFC6R
Radiation (monochromated in incident beam)	Mo Kα (λ = 0.71069)
Orientation reflections, number, range (2θ)	13, 13.1 - 17.2
Scan method	2θ - ω
Octants measured	±hkℓ
Data collection range, 2θ, deg	0 - 60
No. refl. measured	1183
No. unique data, total with $F_o^2 > 3\sigma(F_o^2)$	610, 536
No. parameters refined	31
Absorption correction	Psi scans
Trans. factors, max., min.	1.000, 0.8340
Secondary ext. coeff. (10^{-7})	4.507
R[a], R_w[b], GOF[c]	0.019, 0.027, 1.307
Largest peak, e$^-$/Å^3	1.847
Largest negative peak, e$^-$/Å^3	-1.586

[a] $R = \Sigma \, | \, | F_o | - | F_c | \, | \, / \Sigma \, | F_o |$

[b] $R_w = [\, \Sigma w (| F_o | - | F_c |)^2 / \Sigma w \, | F_o |^2 \,]^{1/2}$; $w = 1/\sigma^2 (| F_o |)$

[c] $GOF = \Sigma ((| F_o | - | F_c |) / \sigma_i) / (N_{obs} - N_{parameters})$

Table 5.2 Mo Kα X-ray centric anomalous dispersion corrections (in e^{-})

	$(\sin\theta)/\lambda = 0.0$ $2\theta = 0°$			$(\sin\theta)/\lambda = 0.9$ $2\theta = 80°$			$(\sin\theta)/\lambda = 1.3$ $2\theta = 135°$		
	f_o *	$\Delta f'$	f	f_o *	$\Delta f'$	f	f_o *	$\Delta f'$	f
Zr	40.00	-2.8	37.20	12.89	-2.8	10.09	9.03	-2.9	6.13
Nb	41.00	-2.1	38.90	13.31	-2.1	11.21	9.33	-2.2	7.13
Hf	72.00	-0.7	71.30	27.23	-1.0	26.23	19.62	-1.1	18.52
Ta	73.00	-0.8	72.20	27.70	-1.1	26.60	19.98	-1.2	18.78

* Thomas-Fermi-Dirac Statistical Model for atomic scattering factors

anomalous scattering corrections [92] for Zr, Nb, Hf, and Ta at various values of $(\sin\theta)/\lambda$ and equivalent 2θ's.

For all centrosymmetric structures, the imaginary component of the anomalous scattering correction exactly cancels and the real part remains. Both pairs of metal atoms shown in Table 5.2, Zr/Nb and Hf/Ta, differ by one electron but Zr and Nb have absorption edges near the energy of Mo Kα X-radiation while Hf and Ta do not. At $2\theta = 0°$, the ratios of the atomic scattering factors in electrons ($f_{Zr}/f_{Nb} = 37.20/38.90 \approx 0.9563$ and $f_{Hf}/f_{Ta} = 71.30/72.20 \approx 0.9875$) indicate that mixed occupancies are difficult to resolve by X-ray diffraction for either pair of metals but Zr/Nb determination is more probable than Hf/Ta. At $2\theta = 80°$, the ratios of the atomic scattering factors in electrons ($f_{Zr}/f_{Nb} \approx 0.9001$ and $f_{Hf}/f_{Ta} \approx 0.9861$) indicate that Zr/Nb occupancies can be correctly determined through Mo Kα X-radiation diffraction experiments, especially at large 2θ, while Hf/Ta occupancies can not be determined.

The metal site occupancies were refined for all metal sites, and indicated that M2 and M3 had mixed occupancy, while M1 = Nb and M4 = M5 = Zr. The resulting

decrease to the residual values R = 1.9%, R_w = 2.7% was found to be significant to greater than 99.5 % probability using the Hamilton R-factor test [101]. The residuals including zeroes, R = 0.025 and R_w = 0.044, were very low. Atomic positions and metal occupancies for this refined structure are listed in Table 5.3 and Table 5.4 lists the anisotropic thermal parameters. A Table of observed and calculated structure factors for this crystal is given in Appendix I.

As in most refinements involving occupancies, correlation coefficients > 0.5 were observed. The scale factor correlated with the secondary extinction coefficient and M1's (Nb) thermal parameters while the two metal sites with mixed occupancies showed correlation between their populations and thermal parameters. Three reflections had large $\Delta F/\sigma(F)$'s, two of which (200 and $2\bar{2}0$) were weak or unobserved. The third reflection (002) was very intense with F_{obs} = 512.83, F_{calc} = 605.11, $\sigma(F)$ = 7.73, and $\Delta F/\sigma(F)$ = -11.94 which are consistent with secondary extinction being the strongest along the short axis. It is plausible that the crystal grew more nearly perfect in this short axial direction than in the other axial directions leading to anisotropic secondary extinction. Removal of the 002 reflection from the least-squares refinements decreased the refined secondary extinction parameter to roughly ½ of its previous value and all other results were unchanged to within their esd's. The 002 reflection was not removed from the refinement discussed in this chapter which includes all of the collected intensity data.

Discussion

As mentioned in the introductory chapter, a number of early transition metal-rich binary phosphides, sulfides, and selenides including Ti_2S [52], Zr_2S [55], Ti_2Se [56], Zr_2Se [57], $Nb_{21}S_8$ [12], $Nb_{14}S_5$ [13], Ti_8S_3 [14], Ta_2P [11], Hf_2P [106], Nb_8P_5 [16], Nb_7P_4 [15], Nb_5P_3 [17], Zr_2P [107], and others have been found to form in structures which share the following characteristics: 1. a short axis, 3.3 Å – 3.6 Å, (dependant upon the specific metal constituents) perpendicular to mirror planes which contain all

Table 5.3 Positional parameters and occupancies for $Zr_{6.45}Nb_{4.55}P_{4.0}$

Atom	*x*	*y*	*z*	%Zr	%Nb
M1	0.29200 (2)	0.16228 (4)	0	-	100
M2	0	0	0	58 (8)	42
M3	0.90161 (4)	1/2	0	94 (6)	6
M4	0.34113 (4)	1/2	0	100	-
M5	0	0.72960 (6)	1/2	100	-
P	0.12147 (7)	0.2053 (1)	0	-	-

Table 5.4 Anisotropic thermal parameters ($\times 10^3$) for $Zr_{6.45}Nb_{4.55}P_{4.0}$

site	U_{11}	U_{22}	U_{33}	U_{12}	U_{13}	U_{23}
M1	5.1 (2)	6.0 (2)	7.5 (2)	-0.4 (1)	0	0
M2	4.8 (4)	5.3 (4)	8.1 (4)	0	0	0
M3	7.8 (3)	5.2 (3)	11.6 (3)	0	0	0
M4	6.9 (2)	4.9 (2)	6.8 (3)	0	0	0
M5	5.1 (3)	9.4 (3)	6.6 (2)	0	0	0
P	5.6 (4)	6.4 (4)	6.9 (4)	-0.4 (3)	0	0

atoms, 2. capped trigonal prismatic coordination of the nonmetals, and 3. metal coordinations related to *bcc*. Two ternary Nb-Ta sulfides ($M_{11}S_4$ and $M_{12}S_4$) were recently [47,48] found to form in structures of this general type with occupancy of the metal atom positions by long range averages of Nb and Ta. Since these two structures are unknown among the binaries it was concluded [19] that long-range averages of transition metals can have a different structural chemistry than do the corresponding binaries. In an effort to further explore this concept the ternary phosphide, $Zr_{6.45}Nb_{4.55}P_{4.0}$, reported here was synthesized and its structure was determined by single crystal X-ray diffraction.

This new ternary phosphide structure also has the above mentioned characteristics in common with many binary metal-rich sulfides, selenides, and phosphides. Examination of this new structure as depicted in Figure 5.1 shows these characteristics and reveals known coordinations [10] for all M and P sites. Because all atoms lie on the mirror planes perpendicular to the *c* axis (at $z = 0$ or $z = ½$), a view down the *c* axis, as in Figure 5.1, clearly shows all atoms.

The phosphorus coordination is a slightly distorted vertical trigonal prism of metal atoms tricapped with metal atoms. M1, M2, and M3 coordinations can be derived from bcc. M1 centers a cube-like unit of metal atoms with one edge substituted by phosphorus and capped by 1 P and 3 M atoms horizontally and two more M1 atoms vertically, M2 centers a distorted cube of metal atoms capped with four P atoms in the horizontal a-b plane and with two M1 atoms vertically, and M3 centers another cube-like unit of all metal atoms capped by 2 P and 2 M atoms horizontally and two M3 atoms vertically.

Both M4 and M5 center pentagonal prisms of metal atoms with two nonadjacent edges substituted by phosphorus. The pentagonal prism centered by M4 is capped by 4 M atoms horizontally and two M4 atoms vertically while the pentagonal prism centered by M5 is capped by 5 M atoms in the horizontal plane and two M5 atoms vertically. The M3-M4 distance is too large to consider M3 as capping the M4 centered pentagonal prism. Additionally, two of the bcc-like units centered by

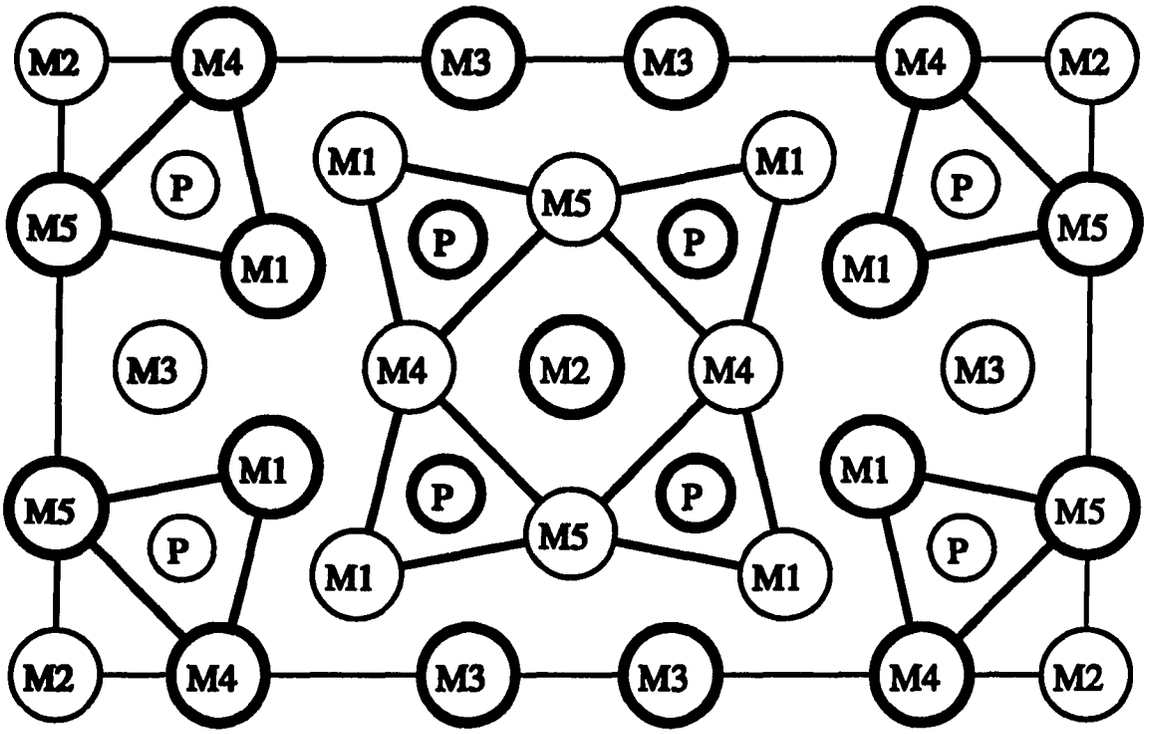

Figure 5.1 Projection down short *c* axis of unit cell for $Zr_{6.45}Nb_{4.55}P_{4.0}$ showing tricapped trigonal prismatic coordination of phosphorus, M2 positions are at 0,0,0 and ½, ½ ½, refined thermal parameters (Table 5.4) are not depicted

M1 share a face, as do two of the bcc-like units centered by M3, and significant lengthening of the M-M distances perpendicular to the short axis along these shared faces is observed.

One can also describe this structure through packing of one large cluster unit composed of 25 metal and 4 phosphorus atoms. This cluster has a bcc metal fragment centered by M2 and capped by 4 P which center 4 tricapped vertical trigonal prisms, each of which share one face with the central bcc fragment. By itself, this cluster has nearly tetragonal symmetry. Directly along the b axial direction four M3 capping atoms of the trigonal prisms in one cluster are shared by capping atoms of the adjacent clusters. Along the body diagonals, the cluster units are condensed so that four M1 capping atoms of trigonal prisms in one cluster are part of the trigonal prisms in the next cluster and vice versa. All clusters are directly stacked one upon another along the short axial c direction. The condensation of this cluster can further be viewed as cluster slabs in the bc plane stacked in a staggered shear structure along the a direction. This same unit, or a slight distortion of it, is found in the $Zr_{14}P_9$, Nb_2P, Nb_8P_5, Zr_2P, and Nb_7P_4 structure types although there are other units present in these structures as well. This ternary $Zr_{6.45}Nb_{4.55}P_{4.0}$ compound has the simplest and most symmetrical structure found in this structural class to date.

Bond order calculations (Kvexpol), making use of the Pauling bond order equation [8], D(n) = D(1) - 0.6 log n, and the Pauling metallic and single bond radii [8] (r_{Zr} = 1.454 Å, r_{Nb} = 1.342 Å, and r_P = 1.04 Å) were carried out on the refined atomic positions of this structure and helped to determine the metal site occupancies reported here. Initially, all metal sites were assigned the metallic radius of Zr. The total bond order for the M1 site was drastically larger than for any other metal site and this was taken to be an indication that M1 = Nb since Nb has an additional d electron relative to Zr and is therefore expected to participate in more bonding interactions than Zr. Nb is also smaller than Zr so that calculating the total bond order for a Nb site while using the metallic radius for Zr yielded an artificially large result. When it became apparent that anomalous scattering allowed differentiation

between Zr and Nb, all metal site occupancies were refined with the constraint that greater than 100% or less than 0% occupancies were not allowed. Table 5.3 lists these refined occupancy results along with their calculated esd's.

Mixed occupancies usually indicate that a compound has a substantial phase width associated with it and that proved to be true for this new ternary phosphide. Samples prepared with initial stoichiometries from $Zr_{6.45}Nb_{4.55}P_{4.08}$ to $Zr_{7.6}Nb_{3.4}P_{3.4}$ were determined through analysis of their Guinier photographs to contain the new $M_{11}P_4$ compound as the major phase. Unit cell volumes calculated with LATT99 ranged from 538.8 (2) $Å^3$ for the most Nb-rich sample to 547.9 (2) $Å^3$ for the most Zr-rich sample. The stoichiometry refined for the single crystal that is reported here falls at or near the Zr-rich phase boundary in this compound.

The results from bond order calculations for different metal site occupancy models are listed in Table 5.5. The following assumptions were made: 1) the total bond order scales like the expected valence of a particular site, 2) the expected valence of Zr is four and that of Nb is five, 3) the expected valence of a mixed metal site is linearly dependant upon the fractional occupancy, and 4) the radius for a particular site is linearly dependant upon the fractional occupancy of that site relative to the Pauling metallic radii. It is clear that the refined model (model C) gives the best agreement between observed and calculated values.

Interatomic distances for this structure calculated from the X-ray single crystal refinement are presented in Table 5.6. The shortest M-M distances fall in the order M1-M1 < M1-M3 < M2-M4 and the shortest M-P distances are M1-P < M5-P ~ M4-P ~ M2-P < M3-P. These distances are consistent with the assignments M1 = Nb and the other metal sites are primarily Zr, given the radii for Nb and Zr listed above. The metal site occupancies suggested from the bond order calculations corroborate the metal site occupancies refined using Mo Kα X-rays. Clearly, these techniques led to valuable results in the difficult situation presented by this new structure.

Table 5.5 Total bond orders calculated for different $M_{11}P_4$ Models

atom	A	B	C	D
M1	8.69 (4.0)	4.82 (5.0)	4.79 (5.0)	6.39 (4.41)
M2	5.49 (4.0)	5.49 (4.0)	4.56 (4.42)	4.10 (4.41)
M3	5.85 (4.0)	4.63 (4.0)	4.50 (4.06)	4.19 (4.41)
M4	5.13 (4.0)	4.50 (4.0)	4.34 (4.0)	3.88 (4.41)
M5	4.73 (4.0)	4.61 (4.0)	4.45 (4.0)	3.61 (4.41)

models (expected valence)

A M1 = M2 = M3 = M4 = M5 = Zr

B M1 = Nb M2 = M3 = M4 = M5 = Zr

C refined occupancies for $Zr_{6.45}Nb_{4.55}P_{4.0}$

M1 = Nb M2 = (42% Nb/58% Zr) M3 = (6% Nb/94% Zr) M4 = M5 = Zr

D stoichiometric random occupancies

M1 = M2 = M3 = M4 = M5 = (41% Nb/ 59% Zr)

Table 5.6 Interatomic distances < 4.0 Å for $Zr_{6.45}Nb_{4.55}P_{4.0}$

M1	-P	×2	2.5928 (8)	M4	-P	×4	2.7267 (8)
	-P	×1	2.745 (1)		-M2	×2	3.1008 (5)
	-M1	×2	2.7975 (6)		-M1	×4	3.1814 (5)
	-M3	×2	2.9455 (5)		-M1	×2	3.3247 (5)
	-M1	×1	3.1055 (8)		-M4	×2	3.5892 (3)
	-M4	×2	3.1814 (5)		-M5	×2	3.6178 (6)
	-M4	×1	3.3247 (5)		-M3	×1	3.8637 (9)
	-M5	×1	3.3729 (4)				
	-M1	×2	3.5892 (3)	M5	-P	×4	2.7104 (8)
					-M2	×2	3.1487 (5)
M2	-P	×4	2.756 (1)		-M3	×4	3.2403 (5)
	-M4	×4	3.1008 (5)		-M1	×2	3.3729 (4)
	-M5	×4	3.1487 (5)		-M5	×2	3.5892 (3)
	-M2	×2	3.5892 (3)		-M4	×2	3.6178 (6)
M3	-P	×2	2.843 (1)	P	-M1	×2	2.5928 (8)
	-M1	×4	2.9455 (5)		-M5	×2	2.7104 (8)
	-M3	×1	3.132 (1)		-M4	×2	2.7267 (8)
	-M5	×4	3.2403 (5)		-M1	×1	2.745 (1)
	-M3	×2	3.5892 (3)		-M2	×1	2.756 (1)
	-M4	×1	3.8637 (9)		-M3	×1	2.843 (1)
					-P	×2	3.5892 (3)
					-P	×1	3.867 (2)
					-P	×1	3.929 (2)

6. ZrNbP, A NEW Co_2Si TYPE PHASE

Synthesis and Characterization

A sample with the initial composition $Zr_4Nb_3P_3$ was prepared from Zr metal and previously synthesized NbP. This sample was pelletized at 10,000 psi and arcmelted (10 V, 70 A) twice for thirty seconds each time. The sample was inverted between arcmeltings to promote homogeneity. A Guinier X-ray powder photograph was obtained for a crushed piece of this arcmelted sample and the strongest diffraction lines on this film did not match any calculated powder patterns of known binary Zr and Nb phosphides. Weak lines corresponding to the recently discovered $(Zr,Nb)_{11}P_4$ [18] and Nb metal were identified.

Two-theta values for the strong lines in this Guinier film were obtained with GUIN and these values were indexed with TREOR. Seventeen sharp unknown lines were indexed on a primitive orthorhombic lattice with a = 8.337 (1) Å, b = 6.8861 (9) Å, and c = 3.5706 (4) Å and a high figure of merit M(17) = 95.

This sample was annealed two separate times in an induction furnace in order to sharpen the diffraction pattern and to obtain single crystals. The sample was placed on a thin piece of Nb foil which was inside of a tungsten crucible and heated at 1645 °C for two minutes followed by annealing at 1600 °C for thirty minutes and at 1555 °C for one more hour, but it did not show any signs of melting. Because partial melting of a sample is desirable for single crystal growth, the sample was placed back into the induction furnace and annealed again. The sample was heated at 1685 °C for two minutes followed by 1600 °C for two hours during this second annealing. This time, the sample was partially melted and small needle-shaped crystals had grown from its surface.

A Guinier powder pattern of this annealed sample revealed that the diffraction lines of the unknown phase had become sharper and more intense while the weak lines of the $(Zr,Nb)_{11}P_4$ and Nb metal phases had become barely discernible. A single crystal was selected from the bulk annealed sample and intensity data were collected for it on the Siemens P3 diffractometer. The unknown phase was determined to be

a Co_2Si type [25] structure with a stoichiometry of ZrNbP. Details of this data collection and subsequent structural refinement will follow in the next section.

A sample of the initial composition HfNbP was prepared out of Hf metal and NbP to see if a Hf-Nb-P phase would also form in the Co_2Si type structure. This new sample was pelletized and arcmelted (10 V, 50 A) for ten seconds, followed by inverting and arcmelting again (10 V, 65 A) for fifteen seconds, and followed once more by inverting and arcmelting (10 V, 70 A) for fifteen seconds. This sample lost a large amount of phosphorus (there was a yellowish residue over most of the inside of the arcmelter chamber). A piece of the sample was crushed and photographed using the Guinier powder technique. The resulting film had many sharp diffraction lines but because of the great number and overlap of the lines, no known phases could be positively identified when the film was compared to calculated binary Hf and Nb phosphide powder patterns.

This apparent multi-phase Hf-Nb-P sample was heated at 1685 °C for six minutes followed by annealing at 1600 °C for one hour. Although the sample did not melt, less than one half as many diffraction lines were observed in a Guinier film of this annealed sample as had been observed in the Guinier film of the arcmelted one. Furthermore, the Co_2Si type phase could be identified in the Guinier film through comparison with a hypothetical HfNbP powder pattern where the Hf was substituted for Zr in the known structure. A wt. fraction of 50% for this HfNbP phase was estimated following the observation that the intensity of the strongest diffraction line from this phase was approximately equal to that of the strongest diffraction line from the unidentified phase(s).

X-ray Single Crystal Study

The needles which had grown from the sample's surface were too small to be used in X-ray single crystal experiments. The bulk annealed sample was crushed and a wedge-shaped piece of dimensions $0.16 \times 0.08 \times 0.05$ mm^3 was mounted on a glass fiber and a rotation photograph (30 minute exposure) was taken using the

Siemens P3 diffractometer. This photograph showed the piece of sample to be a single crystal suitable for an intensity data collection.

The measured rotation photographic coordinates of fifteen reflections were input for indexing purposes and a primitive orthorhombic cell which had lattice parameters approximately equal to those calculated by TREOR was found. A high angle search found seventeen more reflections, which were added to the list and all 32 reflections were used to obtain the final orientation matrix. The Laue symmetry was determined to be *mmm*. Intensity data were collected using the Siemens P3 diffractometer (30 mA, 45 kV) with monochromatic Mo Kα X-radiation (λ = 0.71073Å) and the ω scan technique. All reflections in the octants h±k±l and also all reflections with h = -1 were collected out to 60° in 2θ. Four separate psi scans were performed for use in later absorption corrections.

The format of the intensity data set and the psi scan data set were converted by programs developed in Dr. Jacobson's group to a format which was usable by TEXSAN. The observed intensities were corrected for Lorentz polarization and an empirical Psi scan correction to the absorption was applied (using the averaged results from four different psi scans). No significant decay in the intensities of three standard reflections was noted. The automatic space group choice was undetermined but statistics indicated that the crystal was probably acentric.

When the space group of a structure is unknown, the normal procedure is to try one with high symmetry first and then work down to lower symmetry space groups if necessary. Careful inspection of the intensity data suggested that the first space group to try was *Pmnb* which is a nonstandard setting for one of the most common orthorhombic space groups, *Pnma*. The hkl data and unit cell were converted to the standard setting by matrix multiplication and equivalent reflections were averaged, resulting in a mediocre (0.128) internal $R_{averaging}$. The octants over which the intensities had been measured became ±hk±ℓ. Eight weak reflections (001, $\bar{3}$00, 100, 003, 320, 04$\bar{1}$, 005, and 010) which should have been systematically absent in this space group had, instead, $I > 3\sigma(I)$.

The direct methods approach to initial structural modeling found three peaks, two of which were strong and assigned as metal positions while the weaker peak was assigned as phosphorus. The positional and isotropic thermal parameters for this initial model converged quickly and the refinement continued with anisotropic thermal parameters, mixed metal occupancies, and the secondary extinction coefficient. The differences between the real parts of the Mo Kα X-radiation anomalous scattering for Nb and Zr allowed the refinement to distinguish between Zr and Nb on the metal sites just as had been done previously for $Zr_{6.45}Nb_{4.55}P_{4.0}$ [18]. The metal occupancies refined, within their esd's (e.g. 98 (6)% Zr), as fully occupied by Zr on one position and fully occupied by Nb on the other position so they were fixed in the least squares calculations.

The structure was solved in space group *Pnma* as Co_2Si type and excellent residuals, R = 0.022 and R_w = 0.029, were obtained from the finished refinement. The crystallographic details of this data collection and refinement are reported in Table 6.1, including least squares lattice parameters calculated by LATT99 from a Guinier powder pattern of the bulk annealed sample from which the single crystal was obtained. Occupancy, positional, and isotropic thermal parameters and anisotropic thermal parameters are reported in Tables 6.2 and 6.3 respectively. The table of observed and calculated structure factors is located in appendix J.

The residuals including unobserved reflections were R = 0.047 and R_w = 0.033 and two weak reflections ($53\bar{5}$ and $34\bar{5}$) had large $\Delta F/\sigma(F)$'s of -5.14 and -6.36 respectively. Correlation coefficients > 0.5 were observed between the scale factor, the secondary extinction coefficient, and the thermal parameters of both metals. The eight weak reflections which were observed but should have been systematically absent can be explained as either noise or secondary diffraction off strongly diffracting planes such as most of the (0,0,2n), (0,2n,0), and (2n,0,0) planes.

Later work showed the presence of a phase width for this compound indicating that the metal sites can be occupied by a mixture of both metals to a small degree. Samples with initial stoichiometries $Nb_3Zr_4P_3$ and $Nb_5Zr_2P_{3.1}$ were arcmelted and

Table 6.1 Crystal data for ZrNbP (Co_2Si type)

Formula	ZrNbP
Space group	Pnma (#62)
a Å	6.890 (1)
b Å	3.573 (1)
c Å	8.358 (1)
V Å^3	205.77 (7)
Z	4
d_{calc}, g/cm^3	6.94
Crystal size, mm^3	0.16 × 0.08 × 0.05
μ (Mo Kα)	106
Data collection instrument	Siemens P3
Radiation (monochromated in incident beam)	Mo Kα (λ = 0.71073)
Orientation reflections, number, range (2θ)	32, 16.3 - 29.2
Scan method	ω
Octants measured	±hk±ℓ
Data collection range, 2θ, deg	2 - 60
No. refl. measured	1568
No. unique data, total with $F_o^2 > 3\sigma(F_o^2)$	413, 282
No. parameters refined	20
Absorption correction	Psi scans
Trans. factors, max., min.	1.000, 0.7155
Secondary ext. coeff. (10^{-7})	20.7 (1.9)
R^a, R_w^b, GOF^c	0.022, 0.029, 1.360
Largest shift/esd, final cycle	0.001
Largest peak, e$^-$/Å^3	1.846
Largest negative peak, e$^-$/Å^3	-1.535

[a] $R = \Sigma \, | \, | F_o | - | F_c | \, | \, / \Sigma \, | F_o |$

[b] $R_w = [\Sigma w (| F_o | - | F_c |)^2 / \Sigma w | F_o |^2]^{1/2}$; $w = 1/\sigma^2 (| F_o |)$

[c] $GOF = \Sigma ((| F_o | - | F_c |) / \sigma_i) / (N_{obs} - N_{parameters})$

Table 6.2 Refined positional and isotropic thermal parameters for ZrNbP

atom	x	y	z	B(eq)
Nb	0.13994 (8)	1/4	0.93965 (7)	0.35 (2)
Zr	0.0332 (1)	1/4	0.33141 (8)	0.39 (3)
P	0.2622 (3)	1/4	0.6426 (2)	0.45 (6)

Table 6.3 Refined anisotropic thermal parameters for ZrNbP ($U_{12} = U_{23} = 0$)

atom	U_{11}	U_{22}	U_{33}	U_{13}
Nb	0.0051 (3)	0.0043 (3)	0.0041 (3)	0.0001 (2)
Zr	0.0051 (3)	0.0045 (4)	0.0052 (3)	0.0003 (2)
P	0.0046 (8)	0.0063 (8)	0.0063 (9)	0.0011 (7)

annealed, resulting in multiphase mixtures. Volumes for the Co_2Si type phase in these two samples were obtained from Guinier powder patterns using LATT99. The Nb-rich sample contained a Co_2Si type phase with a volume of 199.48 (5) $Å^3$ while the Zr-rich sample contained a Co_2Si type phase with a larger volume, 205.94 (8) $Å^3$. It is suggested, because Zr Is larger than Nb (as shown by the Pauling radii), that the range in volumes is caused by a range in composition of the metal sites.

Results and discussion

The structure of ZrNbP (Co_2Si type [25]) is shown in Figure 6.1 and emphasizes the trigonal prismatic coordination of phosphorus. All trigonal prisms are directly on top of one another along the *b* axial direction so that the structure can be described as zigzag sheets (approximately in the *ab* plane) of phosphorus centered edge-sharing trigonal prisms which are stacked along the *c* axis with every other sheet identical. Alternate sheets of zigzag prisms are staggered in the *b* axial direction so that each trigonal prism is tricapped by metal atoms which are parts of the neighboring sheets of trigonal prisms. Each Zr atom caps one prism and is a shared corner of four other prisms while each Nb atom caps two prisms and is a shared corner of two others.

The coordination environments of the two metals are polyhedra common to many metal-rich early transition metal phosphides and sulfides [10]. The Zr centers a pentagonal prism of metals with two nonadjacent edges substituted by phosphorus. All faces of this pentagonal prism are capped, but only one is capped by phosphorus. The Nb centers a distorted metal *bcc* fragment which has one edge substituted by phosphorus. Two phosphorus-centered trigonal prisms share the all-metal faces of the *bcc* fragment and metals cap the other four faces.

The lines drawn between atoms in Figure 6.1 do not represent strong bonding interactions, but are drawn instead for descriptive purposes. In fact ,the Zr-Zr distance within a trigonal prism is the longest interatomic distance < 3.8 Å in this structure. The shortest M-M distances in this structure, and presumably the strongest

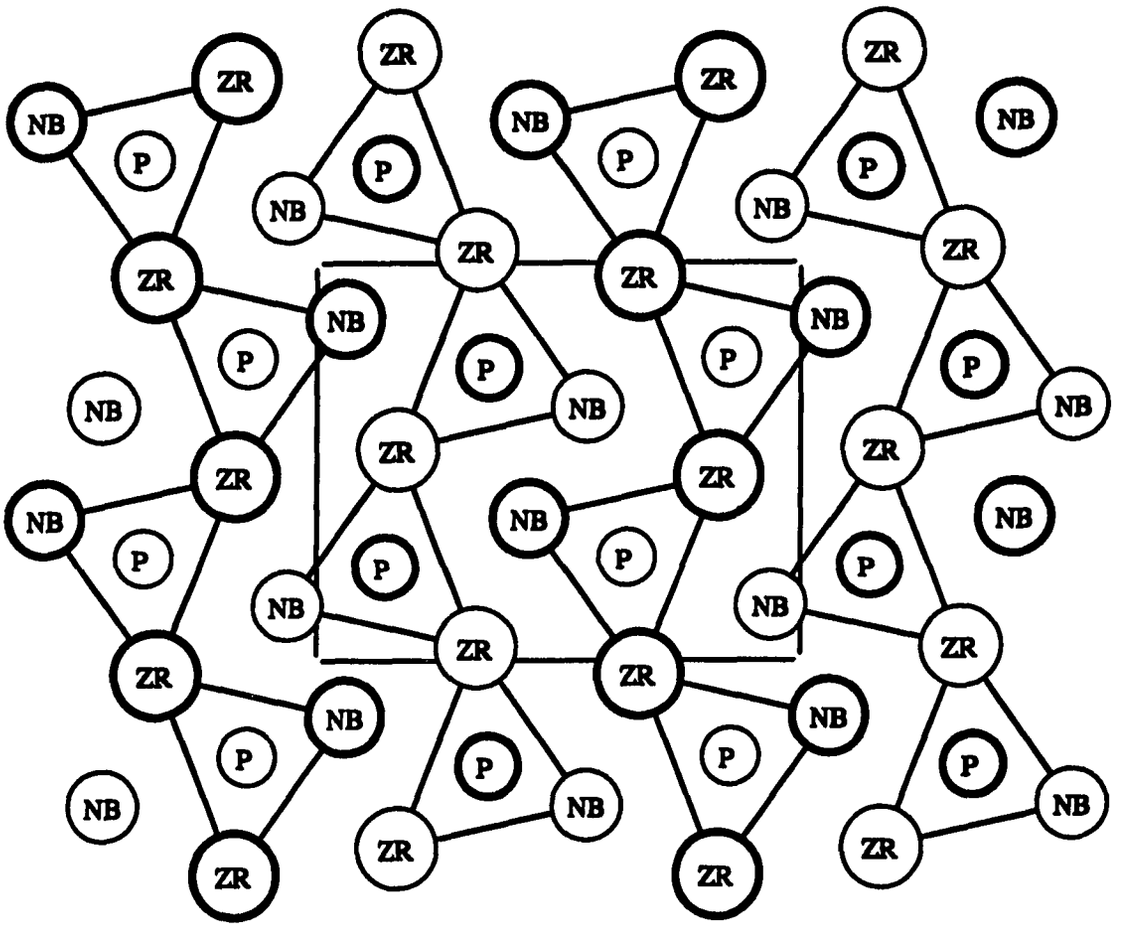

Figure 6.1 The Co_2Si type structure of ZrNbP projected down the short *b* axis, all atoms at y = ¼ are in bold and those at y = ¾ are not, refined thermal parameters (Tables 6.2 and 6.3) are not depicted

bonding interactions, are found between the capping atoms and the atoms which form the capped faces. The M-P distances between the centering phosphorus and all M atoms of that trigonal prism are short and presumably participate significantly in bonding. Table 6.4 gives a complete list of the interatomic distances < 3.8 Å obtained from the X-ray single crystal refinement for this structure.

The Co_2Si structure type is one of the most common found in solid materials. The geometrical arrangement and variability of the positional parameters are two factors which enable this structure to accommodate a wide range of compositions. There are close to 500 different compounds [20] which form with this structure. Many are metal-rich compounds such as isotypic Co_2Si, while others like ZrP_2 are nonmetal-rich, and still others such as Rh_2Ta are intermetallics. It is unlikely that all compounds which form in this structure do so for identical reasons.

The new structure $(Zr,Nb)_{11}P_4$ [18] formed in this ternary system at an M/P composition that was unknown in either of the binary phosphide systems. Zr_3P-Nb_3P (Ti_3P type [31]) and Zr_7P_4-Nb_7P_4 (Nb_7P_4 type [15]) solid solubilities were experimentally observed over a large range of Zr/Nb ratios. Zr_2P [107] and Nb_2P [108] form in complicated structures which are quite different from each other although they are similar in having one short axis perpendicular to mirror planes, trigonal prismatic coordination of phosphorus, and distorted metal *bcc* fragments. Given this history of solid solutions and complex structures for the Zr-Nb-P system, it is somewhat surprising that ZrNbP forms in such a simple structure as that of Co_2Si.

On the other hand, many ternary Nb-transition metal-phosphides and Zr-transition metal-phosphides were previously known to form in this structure and therefore it is not a complete surprise that ZrNbP is also a member of this group of compounds. These ternary Nb- and Zr-containing compounds which form in the Co_2Si type structure include NbCoP, ZrCoP, NbRuP, ZrRuP, NbRhP, ZrRhP, NbNiP, NbVP, ZrOsP, and ZrMnP.

Calculations of bond orders were performed for this structure in much the

Table 6.4 Interatomic distances < 3.8 Å for ZrNbP

Nb	-P	2.554 (1)	×2	Zr	-Nb	3.1220 (8)	×2
	-P	2.622 (2)	×1		-Nb	3.3171 (9)	×1
	-P	2.692 (2)	×1		-Nb	3.356 (1)	×1
	-Nb	2.8156 (9)	×2		-Zr	3.368 (1)	×2
	-Zr	3.0136 (8)	×2		-Zr	3.573 (2)	×2
	-Zr	3.1220 (8)	×2		-Zr	3.7040 (7)	×2
	-Zr	3.3171 (9)	×1				
	-Zr	3.356 (1)	×1	P	-Nb	2.554 (1)	×2
	-Nb	3.573 (1)	×2		-Nb	2.622 (2)	×1
					-Nb	2.692 (2)	×1
Zr	-P	2.717 (2)	×2		-Zr	2.717 (2)	×2
	-P	2.769 (2)	×2		-Zr	2.769 (2)	×2
	-Nb	3.0136 (8)	×2		-Zr	3.042 (2)	×1
	-P	3.042 (2)	×1		-P	3.573 (1)	×2

same way as has been discussed in previous chapters, using the Pauling bond order equation [8], d(n) = d(1) - 0.6 log n and Pauling radii [8] (r_{Zr} = 1.454 Å, r_{Nb} = 1.342 Å, and r_P = 1.10 Å). These calculations corroborated the results of the X-ray single crystal investigation which had used anomalous scattering effects to distinguish between Zr and Nb metals in the structural refinement. Results (metal sites only) are reported in Table 6.5 for bond order calculations performed on the refined structure, on a model of the structure with Zr as the only metal present, and on a model of the structure with both sites statistically occupied with a 50% Nb and 50% Zr mixture.

Interpreting these data requires one to make basic assumptions which have been discussed previously but bear repetition. One assumes that the total calculated bond order (Σn) for a particular atom scales like the actual amount of bonding present for that atom and that the actual bonding is close to the expected valence of that particular atom. The expected valence for Nb is five and that for Zr is four. In dealing with sites of mixed metal occupancy, one assumes that both the effective single bond radius, d(1), and the expected valence for a particular site can be calculated in a linear fashion from the known values for the two metals and their % composition on the site. The calculated bond order for phosphorus was not reported in Table 6.5 because, in general, nonmetal bond orders are unrealistically elevated.

The calculated bond orders for the refined model agree quite well with the expected valences of the metal sites. The calculated M-P bond orders are nearly equal for the two metal sites in the refined model which is reasonable since both metal sites make up the trigonal prisms which are centered by phosphorus. In the other models, the bond orders calculated for M1 are much larger than those calculated for M2. It is not reasonable that there could be such a large difference in bonding between two early transition metal sites in such a simple structure. This suggests, because the Pauling bond order depends on the radii of the atoms, that M1 has a smaller radius than was assumed in these two models leading to M1 = Nb and M2 = Zr as in the refined results.

The compound HfNbP was also synthesized and identified as forming in the

Table 6.5 Calculated bond orders for different models of ZrNbP

atom	expected valence	total bond order	M-M bond order	M-P bond order
refined model				
M1 = Nb	5.00	5.16	2.97	2.19
M2 = Zr	4.00	4.39	2.29	2.10
Zr only model				
M1 = Zr	4.00	8.98	5.62	3.36
M2 = Zr	4.00	5.30	3.20	2.10
statistical model				
M1 = 50% Zr 50% Nb	4.50	6.37	3.65	2.72
M2 = 50% Zr 50% Nb	4.50	3.78	2.08	1.70

Co_2Si type structure, but was not characterized through X-ray single crystal experiments. The unit cell for HfNbP is smaller than that for ZrNbP. Lattice parameters for both phases reported in Table 6.6 were calculated with the program LATT99 from their Guinier X-ray powder patterns. These values are reasonable given that Hf is smaller than Zr (shown by the Pauling radii [8], r_{Hf} = 1.442 Å and r_{Zr} = 1.454 Å). A contraction of the unit cell in the Hf phase relative to that in the Zr phase was expected.

The metal occupancies in the HfNbP phase were assigned without X-ray single crystal work being done. The Hf in HfNbP is expected to be on the same site as the Zr in ZrNbP because they are in the same group of the periodic table and have similar chemical behavior. Examination of a Guinier X-ray powder pattern from this

HfNbP sample shows that this idea is true. A line scanner, LS-20 (KEJ instruments, Täby, Sweden), was used to read data off of a Guinier pattern for the annealed HfNbP sample and the program SCANPI was used to obtain integrated intensities of various diffraction lines. The observed integrated intensities were then compared, as in Table 6.7, to calculated total intensities of the corresponding diffraction lines for different models of HfNbP. Only those observed lines which were well separated from the other lines, were indexed as belonging to the HfNbP phase, and were specifically identified were used in this comparison. The program PWDR was used to calculate for various models of metal occupancy the total intensities, corrected for absorption and anomalous dispersion, of all diffraction lines corresponding to the HfNbP phase, including the same specifically identified diffraction lines mentioned above.

The calculated intensities from the model with Hf on the Zr site matched the observed intensities much better than did the calculated intensities from the other models. A Rietveld refinement of powder data collected for this sample on a powder diffractometer would give a more quantitative answer to the question of metal site occupancy, but there is no doubt that the data reported here prove that the model for HfNbP, where Hf is located on the same site in HfNbP as Zr was found in ZrNbP, is substantially correct.

Table 6.6 Least squares lattice parameters for ZrNbP and HfNbP

compound	*a* Å	*b* Å	*c* Å	volume Å^3
ZrNbP	6.890 (1)	3.573 (1)	8.358 (1)	205.77 (7)
HfNbP	6.8504 (8)	3.5238 (4)	8.3007 (9)	200.4 (1)

Table 6.7 Observed integrated intensities for HfNbP and calculated intensities for different models of HfNbP in the ZrNbP (Co_2Si type) structure scaled to 100 % intensity for the 112 reflection

hkl	HfNbP observed	Hf on Zr site	Hf on Nb site	%Hf/ %Nb both sites
101	1.40	5.2	43.9	3.2
102	8.36	8.9	30.2	17.1
200	19.13	19.1	1.3	8.4
011	18.64	23.2	0.1	6.1
111	11.10	4.2	56.1	20.4
202	12.09	12.8	8.9	11.0
103	54.46	56	40.2	48.7
112	100	100	100	100
210	38.42	33.6	80.4	52.4
211	93.27	67.4	41.6	54.9

7. TERNARY SOLID-SOLUTION BINARY TYPE PHASES

Introduction

Opportunities to investigate metallic substitution into known binary metal-rich structures arose during high-temperature studies of ternary metal-rich early transition metal sulfide and phosphide systems. In the cases where large, well-shaped single crystals of these substituted binary structures were obtained from ternary samples, single crystal X-ray studies were performed.

The ternary phases with binary structures discussed here include the following mixed 4d-5d transition metal sulfide and phosphides: Hf-Zr-S (Ta_2P type [11]); Ta-Nb-P and Hf-Nb-P (Ti_3P type [31]) and; Zr-Nb-P and Zr-Ta-P (Nb_7P_4 type [15]). In all cases, the metal with the higher $\Delta H°_{atm}$ ($\Delta H°_{vap}$'s in units of cal/g-atom for Hf, Zr, Nb, and Ta = 148 (1), 145.5 (10), 172.4 (10), and 186.8 (6) respectively [60]) of the two metals is found preferentially on the sites which have the strongest M-M interactions.

Hf-Zr-S System with the Ta_2P Structure

Synthesis, Characterization, and X-ray Single Crystal Experiments

A sample with the initial composition $Zr_{4.02}Hf_{2.01}S_{2.01}$ was prepared by mixing the appropriate quantities of previously synthesized Zr_3S and Hf_3S powders. The sample was pelletized (~ 10,000 psi) and then arcmelted (10 V, 70 A) for thirty seconds, cooled, inverted and arcmelted again for the same amount of time. A substantial portion of the top of the arcmelted "button" consisted of needle-like crystals. A Guinier X-ray powder film of the bulk sample was indexed as a two phase mixture of metal and Zr_2S compounds and least squares lattice parameters for the latter phase were calculated with the program LATT99 from this film. Several of the needle-like crystals were examined on an oscillation camera to determine their quality and two of these were subsequently aligned along their long dimension and rotation photographs were obtained. Both appeared to be single crystals and the unit cell lattice parameter corresponding to the long dimension of the macroscopic crystals

(obtained through analysis of the rotation photographs) was approximately equal to the short *c* axis (~ 3.520 Å) reported for Zr_2S [55].

The larger crystal was selected for collection of an intensity data set on a rotating anode Rigaku AFC6R diffractometer (50 kV, 140 mA) using monochromatic X-radiation (λ = 0.71069 Å) and the 2θ-ω scan technique at a speed of 16.0°/minute. All reflections in the $hk\pm\ell$ octants were measured out to 60° in 2θ.

TEXSAN software was used to process the collected data and refine the crystal structure and an empirical absorption correction based on psi scans was applied. Two systematically absent reflections (500 and $00\bar{1}$) were observed to have $I > 3\sigma(I)$ and the internal $R_{averaging}$ was 0.09 after the absorption correction was applied. The initial atomic positions for all six metals and two of the three independent sulfurs were found using the direct methods technique. A full matrix least squares refinement of the metals (as Zr) and the two sulfurs followed by a difference Fourier calculation was used to position the final sulfur. Mixed Hf/Zr occupancies on each metal site were summed to full occupancy and manually adjusted until the isotropic thermal parameters for all metals and sulfurs refined to values which were similar to those reported for an X-ray single crystal refinement of Zr_2S [109]. The residual values R = 0.040 and R_w = 0.046 were obtained from the finished refinement.

In the final refinement, all atoms were refined anisotropically and all metal occupancies were allowed to vary which led to severe correlations between the scale factor, metal thermal parameters, and metal occupancies although the refinement converged. When the occupancies of the metal sites were fixed and all other parameters allowed to vary, no correlation coefficients with magnitude greater than 0.5 were obtained. The residuals including zeroes (all measured reflections which were not systematically absent) were R = 0.099 and R_w = 0.062 and there were four reflections with large $\Delta F/\sigma(F)$'s. The 200 and 13,2,0 reflections should have been observed but were not and had $\Delta F/\sigma(F)$'s of -10.64 and -5.76 respectively. The 020 and 910 reflections had $\Delta F/\sigma(F)$'s of -5.20 and 7.20 respectively. As a final check on

the validity of the refinement, all sulfur occupancies were refined and remained within ± 2 % of stoichiometric occupancy. Table 7.1 lists the crystal data for this mixed Hf-Zr solid solution Ta_2P type compound ($Zr_{4.4}Hf_{1.6}S_{3)}$.

Results and Discussion

The Ta_2P structure has been reported [20] for Ta and Hf phosphides and arsenides, Ti and Zr sulfides, and a Zr selenide. It was not surprising to find this ternary solid solution Hf-Zr-S compound with this structure. The positional, thermal, and occupancy parameters obtained for the $Zr_{4.4}Hf_{1.6}S_3$ crystal are reported in Tables 7.2 and 7.3 along with their estimated standard deviations and are in good agreement with those obtained previously for Zr_2S. Cell parameters are essentially the same for the two compounds which was expected since the radii of Zr and Hf are nearly identical (e.g. r_{Hf} = 1.442 Å and r_{Zr} = 1.454 Å according to Pauling [8]). The important difference between this structure and that previously reported for Zr_2S is that the metal sites are not equivalently occupied. Hf does not randomly substitute for Zr (in equal amounts on all metal sites) as can be seen by examining the refined occupancies in Table 7.2. Instead, Hf orders preferentially onto the metal sites.

It has been shown in metal-rich Ta-Nb-S systems that the 5d transition metal Ta is preferentially found on sites which have the most metal-metal bonding and the 4d transition metal Nb is found preferentially on sites which have less metal-metal bonding (but generally more metal-sulfur bonding) [47-50]. Extended Hückel band calculations [50] showed that Ta participates more strongly than Nb in both M-M and M-S bonding in $Ta_{1.05}Nb_{0.95}S$ but the gain in M-M bonding (Ta-Ta vs. Nb-Nb) obtained from the Ta/Nb occupancy pattern is greater than the loss in M-S bonding (Nb-S vs. Ta-S) obtained from the same occupancy. The preferential ordering of Ta onto the M-M bonding sites is energetically favored over both random Ta/Nb and preferential Nb occupancy of the metal-metal bonding sites.

The preference of 5d transition metals over 4d transition metals within the same group for the most metal-metal bonding sites is not unique to Ta-Nb-S metal-rich systems but is more general and occurs in metal-rich Ta-Nb-P and Hf-Zr-S

Table 7.1 Crystal data for Hf-Zr-S (Ta_2P type)

Formula	$Zr_{4.4}Hf_{1.6}S_3$
Space group	Pnnm (#58)
a Å	15.368 (3)
b Å	12.319 (1)
c Å	3.4781 (7)
V Å^3	658.5 (2)
Z	4
d_{calc}, g/cm^3	7.917
Crystal size, mm^3	0.25 × 0.02 × 0.01
μ (Mo Kα)	326
Data collection instrument	RIGAKU AFC6R
Radiation (monochromated in incident beam)	Mo Kα (λ = 0.71069)
Orientation reflections, number, range (2θ)	14, 13.3 - 17.2
Temperature, °C	23
Scan method	2θ - ω
Octants measured	hk±ℓ
Data collection range, 2θ, deg	0 - 60
No. refl. measured	2043
No. unique data, total with $F_o^2 > 3\sigma(F_o^2)$	1178, 647
No. parameters refined	61
Absorption correction	Psi scans
Trans. factors, max., min.	1.000, 0.6773
Secondary ext. coeff. (10^{-7})	not refined
R[a], R_w[b], GOF[c]	0.040, 0.046, 1.211
Largest peak, e$^-$/Å^3	2.558
Largest negative peak, e$^-$/Å^3	-3.321

[a] $R = \Sigma \, | \, | F_o | - | F_c | \, | \, / \Sigma \, | F_o |$

[b] $R_w = [\, \Sigma w (| F_o | - | F_c |)^2 / \Sigma w \, | F_o |^2 \,]^{1/2}$; $w = 1/\sigma^2 (| F_o |)$

[c] $GOF = \Sigma ((\, | F_o | - | F_c | \,) / \sigma_i \,) / (N_{obs} - N_{parameters})$

Table 7.2 Positional, thermal, and occupancy parameters for $Zr_{4.4}Hf_{1.6}S_3$

atom	occupancy (%)	x	y	z	B_{eq} (Å^2)
M1	Zr 50.2 (2.4) + Hf 49.8	0.4201 (1)	0.4163 (1)	0	0.61 (6)
M2	Zr 60.2 (2.1) + Hf 39.8	0.3923 (1)	0.0336 (1)	1/2	0.54 (6)
M3	Zr 75.0 (1.9) + Hf 25.0	0.5827 (1)	0.3726 (1)	1/2	0.56 (7)
M4	Zr 75.2 (2.0) + Hf 24.8	0.5264 (1)	0.1564 (1)	0	0.63 (7)
M5	Zr 85.8 (1.9) + Hf 14.2	0.2497 (1)	0.4272 (2)	1/2	0.49 (8)
M6	Zr 91.2 (1.7) + Hf 8.8	0.2975 (1)	0.2053 (2)	0	0.6 (1)
S1		0.4235 (4)	0.2538 (5)	1/2	0.6 (2)
S2		0.2111 (4)	0.0799 (5)	1/2	0.5 (2)
S3		0.3468 (4)	0.8210 (5)	1/2	0.6 (2)

Table 7.3 Anisotropic thermal parameters (Å^2) for $Zr_{4.4}Hf_{1.6}S_3$ (U13 = U23 = 0)

atom	U11	U22	U33	U12
M1	0.0072 (7)	0.0075 (7)	0.0085 (8)	0.0002 (5)
M2	0.0069 (8)	0.0057 (7)	0.008 (1)	-0.0004 (5)
M3	0.0068 (9)	0.0071 (9)	0.008 (1)	-0.0005 (6)
M4	0.0072 (9)	0.009 (1)	0.007 (1)	-0.0006 (6)
M5	0.006 (1)	0.007 (1)	0.006 (1)	0.0007 (7)
M6	0.008 (1)	0.007 (1)	0.007 (1)	0.0003 (8)
S1	0.010 (3)	0.006 (3)	0.006 (3)	-0.003 (2)
S2	0.007 (3)	0.011 (3)	0.000 (3)	-0.003 (2)
S3	0.007 (3)	0.006 (3)	0.009 (3)	0.001 (2)

systems as well [19]. Presently, the Hückel parameters for Hf are not reliably known and band calculations such as those used in the Ta-Nb-S systems cannot give meaningful results in Hf-Zr-S systems, however other simpler methods can be used to examine the relationship between M-M bonding and Hf/Zr site preferences in the Ta_2P type structure. Bond order calculations can be performed using the Pauling bond order equation [8], d(n) = d(1) - 0.6 log n where d(1) is Pauling's single bond length, n is the bond order, and d(n) is the observed bond distance, to get a rough (but meaningful none-the-less) idea of the relative amounts of M-M bonding associated with different metal sites and different Hf/Zr occupancies.

On a more primitive level, the structure of $Zr_{4.4}Hf_{1.6}S_3$ as shown in Figure 7.1 can be examined to get an idea of which sites are more and less M-M bonding. It is of interest to note that the Ta_2P type structure is one of a large group of structures (mentioned in the introduction) having a short (~ 3.5 Å) cell edge (*c* in this case) which is perpendicular to the mirror planes. All atoms in the unit cell fall on these mirror planes at either z = 0 or z = ½ and therefore a projection of the structure down the short axis shows the complete structure.

The metal positions in Figure 7.1 are numbered according to the amount of Hf which refined onto that particular site and the heavy lines represent short M-M interatomic distances (less than 3.22 Å). M1 has the largest %Hf occupancy and M6 has the least %Hf occupancy among these six metal positions. M1 and M2 participate in eight short M-M bonds, M3, M4, and M5 participate in four short M-M bonds and M6 participates in only three short M-M bonds. Qualitatively, the amount of Hf occupancy has a positive correlation with the amount of M-M bonding in this crystal structure.

Table 7.4 gives a list of the interatomic distances less than 3.6 Å in $Zr_{4.4}Hf_{1.6}S_3$. These distances (plus all distances out to 6.0 Å) were used by the program Kvexpol to calculate Pauling bond orders of the various atomic sites in this compound. The bond order calculations were interpreted with care. The calculated bond orders

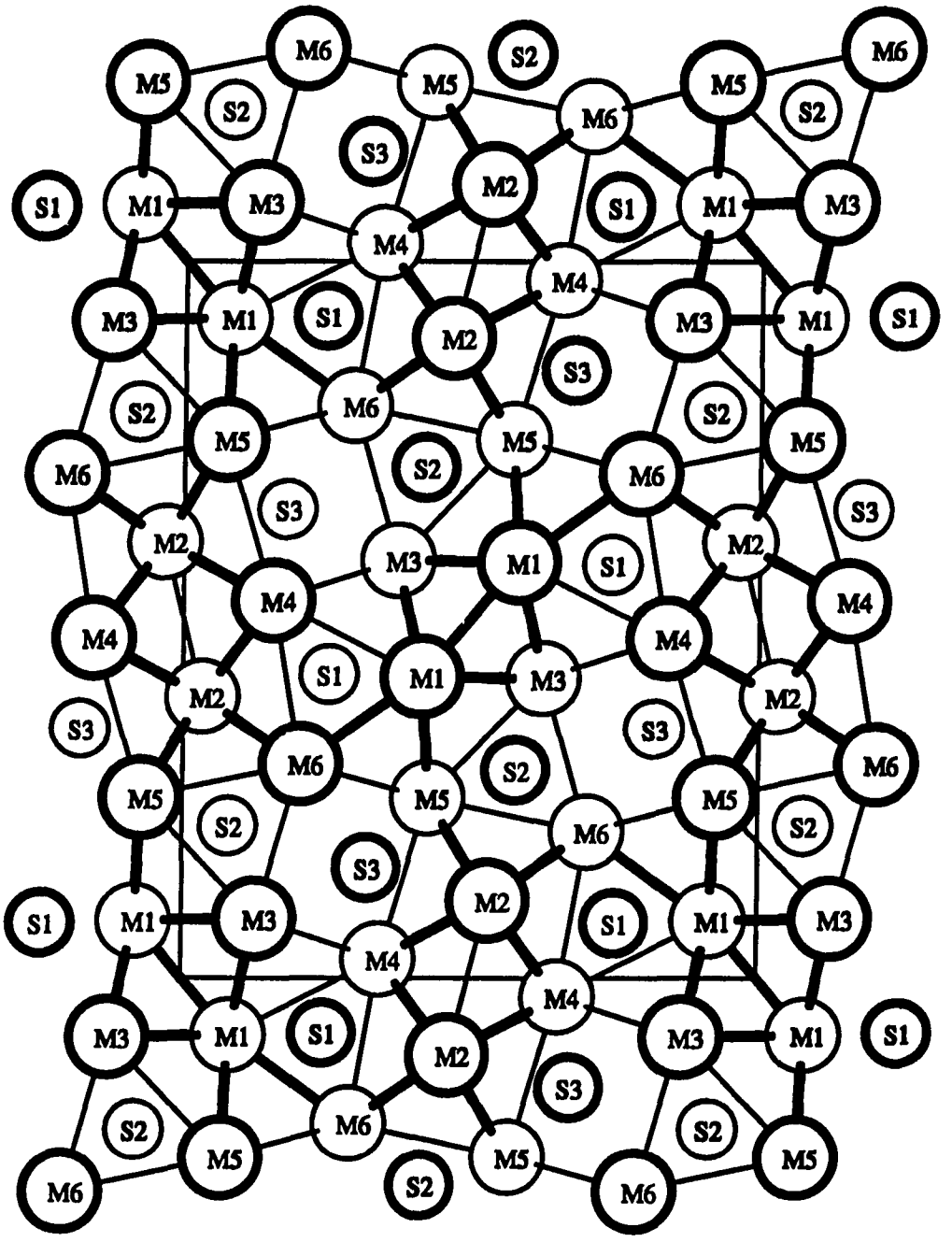

Figure 7.1 Projection of $Zr_{4.4}Hf_{1.6}S_3$ (Ta_2P type) down the short *c* axis, all atoms in bold are at the z = 0 level, all other atoms are at z = ½, and bold lines indicate M-M distances shorter than 3.22 Å, refined thermal parameters (Tables 7.2 and 7.3) are not depicted

Table 7.4 Interatomic distances < 3.6 Å in $Zr_{4.4}Hf_{1.6}S_3$

M1	-S1	2.653 (5)	×2	M3	-S3	2.621 (6)		M5	-S2	2.632 (5)	×2
	-S2	2.852 (6)			-S2	2.695 (5)	×2		-S3	2.633 (5)	×2
	-M3	3.091 (2)	×2		-S1	2.851 (6)			-M2	3.082 (2)	×2
	-M3	3.128 (2)	×2		-M1	3.091 (2)	×2		-M1	3.147 (2)	×2
	-M5	3.147 (2(	×2		-M1	3.128 (2)	×2		-M6	3.322 (2)	×2
	-M1	3.206 (3)			-M4	3.297 (2)	×2		-S1	3.420 (7)	
	-M6	3.211 (3)			-M6	3.438 (3)			-M5	3.4781 (7)	×2
	-M1	3.4781 (7)	×2		-M3	3.4781 (7)	×2		-M6	3.502 (3)	
	-M4	3.595 (2)			-M5	3.567 (3)			-M3	3.567 (3)	
									-M4	3.582 (3)	
M2	-S3	2.711 (6)		M4	-S3	2.627 (5)	×2				
	-S1	2.755 (6)			-S1	2.639 (5)	×2	M6	-S3	2.635 (6)	
	-S2	2.842 (6)			-M2	3.092 (2)	×2		-S1	2.670 (5)	×2
	-M5	3.082 (2)	×2		-M2	3.172 (2)	×2		-S2	2.678 (5)	×2
	-M4	3.092 (2)	×2		-M3	3.297 (2)	×2		-M2	3.102 (2)	×2
	-M6	3.102 (2)	×2		-M4	3.4781 (7)	×2		-M1	3.211 (3)	
	-M4	3.172 (2)	×2		-M6	3.570 (3)			-M5	3.332 (2)	×2
	-M2	3.413 (3)			-M5	3.582 (3)			-M3	3.438 (3)	
	-M2	3.4781 (7)	×2		-M1	3.595 (2)			-M6	3.4781 (7)	×2
									-M5	3.502 (3)	
S1	-M4	2.639 (5)	×2	S2	-M5	2.632 (5)	×2		-M4	3.570 (3)	
	-M1	2.653 (5)	×2		-M6	2.678 (5)	×2				
	-M6	2.670 (5)	×2		-M3	2.695 (5)	×2	S3	-M3	2.621 (6)	
	-M2	2.755 (6)			-M2	2.842 (6)			-M4	2.627 (5)	×2
	-M3	2.851 (6)			-M1	2.852 (6)			-M5	2.633 (5)	×2
	-M5	3.420 (7)			-S2	3.4781 (7)	×2		-M6	2.635 (6)	
	-S1	3.4781 (7)	×2						-M2	2.711 (6)	
									-S3	3.4781 (7)	×2

were by no means absolute, but instead scaled like the real amount of bonding present except in the case of sulfur. Calculated nonmetal bond orders were (in general) unrealistically high. When M1 has a larger calculated bond order than M2 within a binary structure, that is a good indication that M actually participates in more bonding than M2, especially if the difference is large. The idea of the bond order scaling like the real bonding is applicable to ternary systems as well. To a reasonable first order approximation, the single bond radius of a metal site with mixed occupancy is linearly proportional to the radii of the pure metals and their % composition on that site.

The results from bond order calculations performed on this compound are presented in Table 7.5 and show strong correlation between the amount of calculated M-M bond order and the refined %Hf occupancy of the various metal sites. M1 and M2 have the largest calculated metal-metal bond orders and the largest refined %Hf occupancies while M6 has the smallest calculated metal-metal bond order and the smallest refined %Hf occupancy. The trend that Hf prefers to occupy the sites with the greatest amounts of M-M bonding is clear, however there are minor discrepancies. M2 has the largest calculated M-M bond order but only the second largest refined %Hf occupancy. Also, M5 has a calculated bond order which is nearly equal to that of M3 and larger than that of M4 but has a smaller refined %Hf occupancy than either.

The discrepancy involving M2 can be explained in terms of its *bcc* coordination which is more consistent with Zr occupancy than with Hf. The known metal-rich binary hafnium sulfides, Hf_2S [54] and HfS [110], have only hexagonal coordinations of the metals whereas the *bcc* coordination of Zr is known in Zr_2S. The preference of Hf for hexagonal coordination in metal-rich compounds versus the preferences of Zr and Ti for *bcc*-like coordinations has previously been discussed [56,111] in terms of the Brewer-Engel correlation [63]. After extensive study, Brewer arrived at the conclusion that s- and p- conduction electrons determine the long-range order of alloy

Table 7.5 Calculated total and M-M bond orders for Zr_2S and $Zr_{4.4}Hf_{1.6}S_3$

	total bond order		M-M bond order		occupancy
	Zr_2S	$(Zr,Hf)_2S$	Zr_2S	$(Zr,Hf)_2S$	% Hf
M1	4.86	4.77	3.42	3.46	49.8
M2	4.85	4.99	3.81	3.94	39.8
M3	4.35	4.45	2.63	2.67	25.0
M4	4.56	4.89	2.42	2.56	24.8
M5	4.88	5.02	2.62	2.65	16.2
M6	4.72	4.75	2.17	2.18	8.9

phases. He found that ~2 s- and p-electrons in the conduction band of an alloy implied a *hcp* structure while ~1 s- and p-electron implied a *bcc* structure. He also found that gas phase promotion energies for metals correlated with their solid phase promotion energies. The energy required for promotion from the s^2d^2 ground state to the sd^3 excited state in the gas phase is more than twice as high for Hf as it is for Zr and Ti. In the pure metals, the α (*hcp*) to β (*bcc*) phase transition [9] occurs at 863°C for Zr and 1743°C for Hf which suggests that the *bcc* coordination requires less promotional energy for Zr than for Hf, the same conclusion reached using the Brewer-Engel correlation.

The minor discrepancy involving M5 cannot readily be explained but can, instead, be easily rationalized. The stoichiometry M_2S is not so metal-rich that M-S bonding can be ignored in the structure of $Zr_{4.4}Hf_{1.6}S_3$ and the trend that 5d transition metals prefer the most M-M bonding sites over 4d transition metals in the same group is best applied to cases where M-M bonding is dominant.Furthermore, minor discrepancies are allowed as long as the overall trend remains intact.

Ta-Nb-P and Hf-Nb-P Systems with the Ti_3P Structure

Synthesis, Characterization, and X-ray Single Crystal Experiments

A sample with initial composition $Nb_{1.2}Ta_{3.8}P_{2.05}$ was prepared from Ta, TaP, and NbP and pelletized. A different sample with the composition $Hf_8Nb_4P_4$ was prepared from Hf and NbP and also pelletized. The binary phosphides, TaP and NbP, were previously synthesized by direct combination of the elements as described in the experimental chapter.

The first sample (Ta-Nb-P) was arcmelted for 15 seconds at 10 V, 80 A, inverted, and arcmelted again to promote homogenization of the sample. The second sample (Hf-Nb-P) was arcmelted twice at 10 V, 60 A for 30 seconds each time and also inverted between arcmeltings.

Guinier X-ray powder patterns were obtained from crushed pieces of both shiny silver metallic samples and comparison of these Guinier patterns with calculated binary phosphide powder patterns indicated that the major phase was Ti_3P type [31] (space group $P4_2/n$) and the minor phase was *bcc* metal in both cases. The diffraction lines on both films were sharp and least squares lattice parameters were obtained from these films with the program LATT99. The $(Ta,Nb)_3P$ phase was found to have a = 10.1457 (5) Å, c = 5.0352 (7) Å and the $(Hf,Nb)_3P$ phase was found to have a = 10.4705 (3) Å, c = 5.2632 (1) Å.

Pieces of the arcmelted samples were examined with X-ray photographic oscillation techniques in order to select single crystals suitable for intensity data collection on a diffractometer. A plate-like crystal of dimensions 0.07 × 0.05 × 0.02 mm^3 from the Ta-Nb-P system was aligned along an axis. Interpretation of the rotation photo gave an approximately 10.3 Å cell edge which corresponded roughly to the a axis calculated for this Ti_3P type compound. The needle-like crystal of dimensions 0.18 × 0.04 × 0.03 mm^3 from the Hf-Nb-P system was only briefly examined with X-ray photographic techniques and determined to be a single crystal.

Intensity data for the $(Ta,Nb)_3P$ crystal were collected on a rotating anode Rigaku AFC6R diffractometer (50 kV, 140 mA) using monochromatic X-radiation (λ =

0.71069 Å) and the 2θ-ω scan technique at a speed of 16.0°/minute. Fifteen reflections were found using the SEARCH routine. Two of these reflections could not be indexed (the crystal was twinned) and two more reflections were redundant. A unit cell was indexed with the expected lattice parameters although the four-fold tetragonal Laue check failed. The strong absorption of X-rays by Ta coupled with the "platelike" crystal shape disrupted the four-fold symmetry of the scattering. All reflections in the hk±ℓ octants out to 69° in 2θ were collected. Four psi scans were performed at the end of the data collection which had an average minimum transmission equal to only 16% of the transmission maximum.

The intensity data were processed with TEXSAN software and corrected for Lorentz polarization and absorption effects using the averaged psi scan data. The direct methods approach to the initial structural model was used to locate all of the metal and phosphorus positions. These positions were approximately equivalent to those reported for Ta_3P [112] and an isotropic refinement including positional, occupancy, thermal, and secondary extinction parameters resulted in R = 0.080 and R_w = 0.101 for the residuals. A DIFABS absorption correction was applied to the data set and the residuals decreased to R = 0.046 and R_w = 0.052 for an isotropic refinement. There was little difference between the isotropic and final anisotropic residuals (R = 0.045 and R_w = 0.052), in part because a DIFABS correction tends to make atoms look spherical. Even with the DIFABS absorption correction, the phosphorus atom could not be refined anisotropically.

The internal $R_{averaging}$ after the data were corrected for absorption (DIFABS) was 0.163 and two weak reflections, 270 and 100, which should have been absent were observed with $I > 3\sigma(I)$. When the mixed metal occupancies were refined, the scale, secondary extinction, metal population, and metal thermal parameters were correlated, however when the metal occupancies were fixed, no correlation coefficients > 0.5 were found. The residuals, including zeroes, were R = 0.128 and R_w= 0.074 and no reflections had large differences between observed and calculated structure factors, $\Delta F/\sigma(F)$'s ≈ 0.

The intensity data for the $(Hf,Nb)_3P$ crystal were collected on an Enraf-Nonius CAD4 diffractometer (32kV, 55mA) using monochromatic Mo Kα X-radiation (λ = 0.71073 Å) and the omega scan technique. 21 reflections were found using the SEARCH routine, 16 of which were unique. The unit ceil was indexed as primitive tetragonal with close to the expected lattice parameters. Omega-theta plots showed that the ω-scan technique was the proper choice for data collection. Intensity data were collected in the $hk\pm\ell$ octants between 4° and 50° in 2θ. At the end of the data collection, four psi scans were collected, three of which were selected for use in correcting the measured intensities for absorption.

The program TEXSAN was used to correct the intensity data for Lorentz polarization and absorption. No decay of the standards was observed, the internal $R_{averaging}$ was 0.074, and no systematically absent reflections were observed. The atomic positions from the $Ta_{4.9}Nb_{1.1}P_2$ structural refinement were used as a starting model for this refinement. The complete anisotropic refinement including positional, thermal, metal occupancy, and secondary extinction parameters converged to values of R = 0.039 and R_w = 0.044 for the residuals. The phosphorus could not be refined with anisotropic thermal parameters. Correlations between the scale factor and the secondary extinction coefficient and metal thermal parameters were observed with fixed metal occupancies. The residuals, including zeroes, were R = 0.064 and R_w = 0.050 and no reflections with large differences between the calculated and observed structure factors were found.

Table 7.6 gives the crystallographic details of data collection and refinement for the two crystals, $Ta_{4.9}Nb_{1.1}P_2$ and $Hf_{4.2}Nb_{1.8}P_2$. Tables 7.7 and 7.8 list the positional, isotropic thermal, and occupancy parameters refined for the two crystals along with their esd's. Tables 7.9 and 7.10 list the refined anisotropic thermal parameters with esd's for the two crystals. Both refinements were completed using origin choice #1 (at $\bar{4}$) in the space group $P4_2/n$ while previous reports of Ti_3P type structures commonly use origin choice #2 (at $\bar{1}$) which is +(¼,¼,¼) from choice #1

Table 7.6 Crystal data for Ta-Nb-P and Hf-Nb-P (Tl_3P type)

Formula	$Ta_{4.9}Nb_{1.1}P_2$	$Hf_{4.1}Nb_{1.9}P_2$
Space group	$P4_2/n$ (#86)	$P4_2/n$ (#86)
a Å	10.1457 (5)	10.4705 (3)
c Å	5.0352 (7)	5.2632 (1)
V Å^3	518.30 (8)	577.01 (3)
Z	4	4
d_{calc}, g/cm^3	13.577	11.256
Crystal size, mm^3	0.07 × 0.06 × 0.02	0.20 × 0.03 × 0.02
μ (Mo Kα)	1064	782
Data collection instrument	RIGAKU AFC6R	Enraf-Nonius CAD4
Radiation (monochromated in incident beam)	Mo Kα (λ = 0.71069)	Mo Kα (λ = 0.71073)
Orientation reflections, number, range (2θ)	11, 15.1 - 17.2	16, 7.3 - 19.2
Temperature, °C	23	23
Scan method	2θ - ω	ω
Octants measured	hk±ℓ	hk±ℓ
Data collection range, 2θ, deg	0 - 69	4 - 50
No. refl. measured	2386	1144
No. unique data, total with $F_o^2 > 3\sigma(F_o^2)$	1204, 489	602, 383
No. parameters refined	36	36
Absorption correction	DIFABS	Psi scans
Trans. factors, max., min.	1.000, 0.1640	1.000, 0.5794
Secondary ext. coeff. (10^{-7})	2.98(42)E-07	3.07(32)E-07
R[a], R_w[b], GOF[c]	0.045, 0.052, 1.165	0.039, 0.044, 1.277
Largest shift/esd, final cycle	0.007	0.0002
Largest peak, e$^-$/Å^3	5.004	2.836
Largest negative peak, e$^-$/Å^3	-4.993	-2.716

[a] $R = \Sigma \, | \, | F_o | - | F_c | \, | \, / \Sigma \, | F_o |$

[b] $R_w = [\, \Sigma w (| F_o | - | F_c |)^2 / \Sigma w \, | F_o |^2 \,]^{1/2}$; $w = 1/\sigma^2 (| F_o |)$

[c] $GOF = \Sigma ((\, | F_o | - | F_c | \,) / \sigma_i \,) / (N_{obs} - N_{parameters})$

Table 7.7 Positional, thermal, and occupancy parameters for $Ta_{4.9}Nb_{1.1}P_2$

atom	occupancy (%)	x	y	z	B_{eq} (Å^2)
M1	Ta 91.4 (1.1) + Nb 8.6	0.3460 (1)	0.8393 (1)	0.2360 (3)	0.35 (3)
M2	Ta 70.1 (1.0) + Nb 29.9	0.2578 (1)	0.1049 (1)	0.9910 (4)	0.38 (4)
M3	Ta 88.1 (1.2) + Nb 11.9	0.0559 (1)	0.9582 (1)	0.2446 (3)	0.40 (3)
P		0.2657 (6)	0.0427 (5)	0.487 (2)	0.38 (8)

Table 7.8 Positional, thermal, and occupancy parameters for $Hf_{4.1}Nb_{1.9}P_2$

atom	occupancy (%)	x	y	z	B_{eq} (Å^2)
M1	Hf 78.0 (3.4) + Nb 22.0	0.3561 (1)	0.8359 (1)	0.2108 (2)	0.55 (6)
M2	Hf 83.7 (3.5) + Nb 16.3	0.2775 (1)	0.1090 (1)	0.9733 (2)	0.51 (5)
M3	Hf 47.8 (2.7) + Nb 52.2	0.0688 (1)	0.9647 (1)	0.2339 (3)	0.42 (6)
P		0.2892 (7)	0.0433 (7)	0.464 (1)	0.5 (1)

Table 7.9 Anisotropic thermal parameters ($Å^2$) for $Ta_{4.9}Nb_{1.1}P_2$

atom	U11	U22	U33	U12	U13	U23
M1	0.0043 (3)	0.0049 (3)	0.0042 (5)	0.0005 (3)	0.0006 (5)	-0.0003 (5)
M2	0.0044 (4)	0.0045 (4)	0.0055 (6)	0.0008 (4)	-0.0004 (6)	-0.0007 (5)
M3	0.0055 (3)	0.0055 (3)	0.0042 (5)	0.0006 (3)	-0.0001 (5)	0.0000 (5)
P*	0.005 (1)					

Table 7.10 Anisotropic thermal parameters ($Å^2$) for $Hf_{4.1}Nb_{1.9}P_2$

atom	U11	U22	U33	U12	U13	U23
M1	0.0045 (7)	0.0063 (7)	0.0102 (7)	0.0000 (5)	0.0003 (6)	0.0000 (6)
M2	0.0053 (7)	0.0064 (7)	0.0076 (6)	0.0008 (5)	-0.0005 (5)	-0.0001 (5)
M3	0.0039 (8)	0.0034 (8)	0.0085 (8)	0.0008 (6)	-0.0002 (6)	0.0008 (6)
P*	0.005 (1)					

in the unit cell. The atoms have been numbered the same as in previous reports for comparative purposes.

Results and Discussion

The Ti_3P structure is found [31] in group 4 and 5 transition metal phosphide, arsenide, silicide, and germanide systems and is structurally related to other phosphides, e.g. Fe_3P [113] (Ni_3P type [32]), and sulfides, e.g. Zr_9S_2 [30], α-V_3S [29], and β-V_3S [29]. This structure is also reported [20] with the compositions: $Fe_{12}Re_3B_5$, $Co_3Re_3B_2$, Y_3Sb, and Fe_9PB_2. The basic structural units in these compounds are twenty-two atom doubly centered Kasper polyhedra. Figure 7.2 is a view down the *c* axis of the Ti_3P structure showing a polyhedron which is centered by M1-M1 in the compound $Ta_{4.9}Nb_{1.1}P_2$. The four M1 atoms in the center of the picture (actually six M1 atoms because two more are directly beneath the two around the waist of the unit) demonstrate the 4_2 symmetry of the structure and point out some of the connectivity. Pairs of M1 atoms separated by a short metal-metal distance of 2.660 (2) Å center one polyhedron and are on the waist of another and vice versa. Figure 7.3 is another picture of the same unit which does not show the symmetry as clearly but shows all of the atoms in this polyhedron.

Questions of mixed metal occupancy and bonding in the $(Ta,Nb)_3P$ and $(Hf,Nb)_3P$ systems were of interest in this work. The refined metal occupancies were compared to calculated total and M-M Pauling bond orders to see if the trend previously observed, 5d metal preference over 4d metal for the most metal-metal bonding sites, held for these systems. The Pauling bond order equation [8], d(n) = d(1) -0.6 log n, was used to empirically relate bonding to interatomic distances. A complete list of interatomic distances derived from the single crystal X-ray studies of $Ta_{4.9}Nb_{1.1}P_2$ and $Hf_{4.2}Nb_{1.8}P_2$ are given in Table 7.11 along with their esd's. Table 7.12 lists those distances and comparable distances from other Ti_3P type compounds.

Examination of the interatomic distances in Tables 7.11 and 7.12 reveals differences between the group 4 and group 5 transition metal phosphides with the Ti_3P structure. Ta_3P, Nb_3P, and $Ta_{4.9}Nb_{1.1}P_2$ contain one M1-M1 distance, between

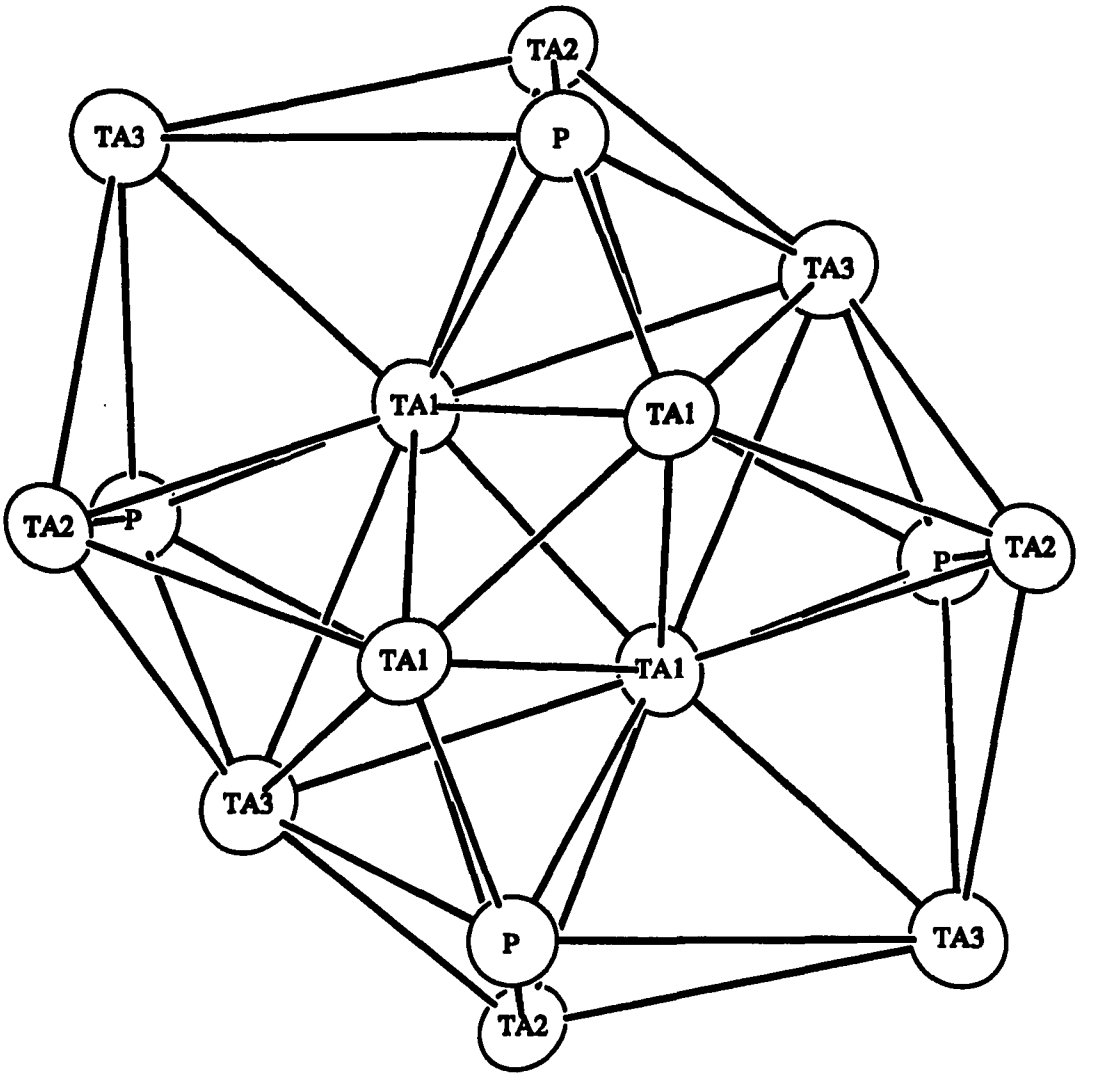

Figure 7.2 View down the 4_2 axis of $Ta_{4.9}Nb_{1.1}P_2$ showing a Kasper polyhedron which is doubly centered by M1 atoms, the % probability ellipsoids are exaggerated to accomodate the atom labels

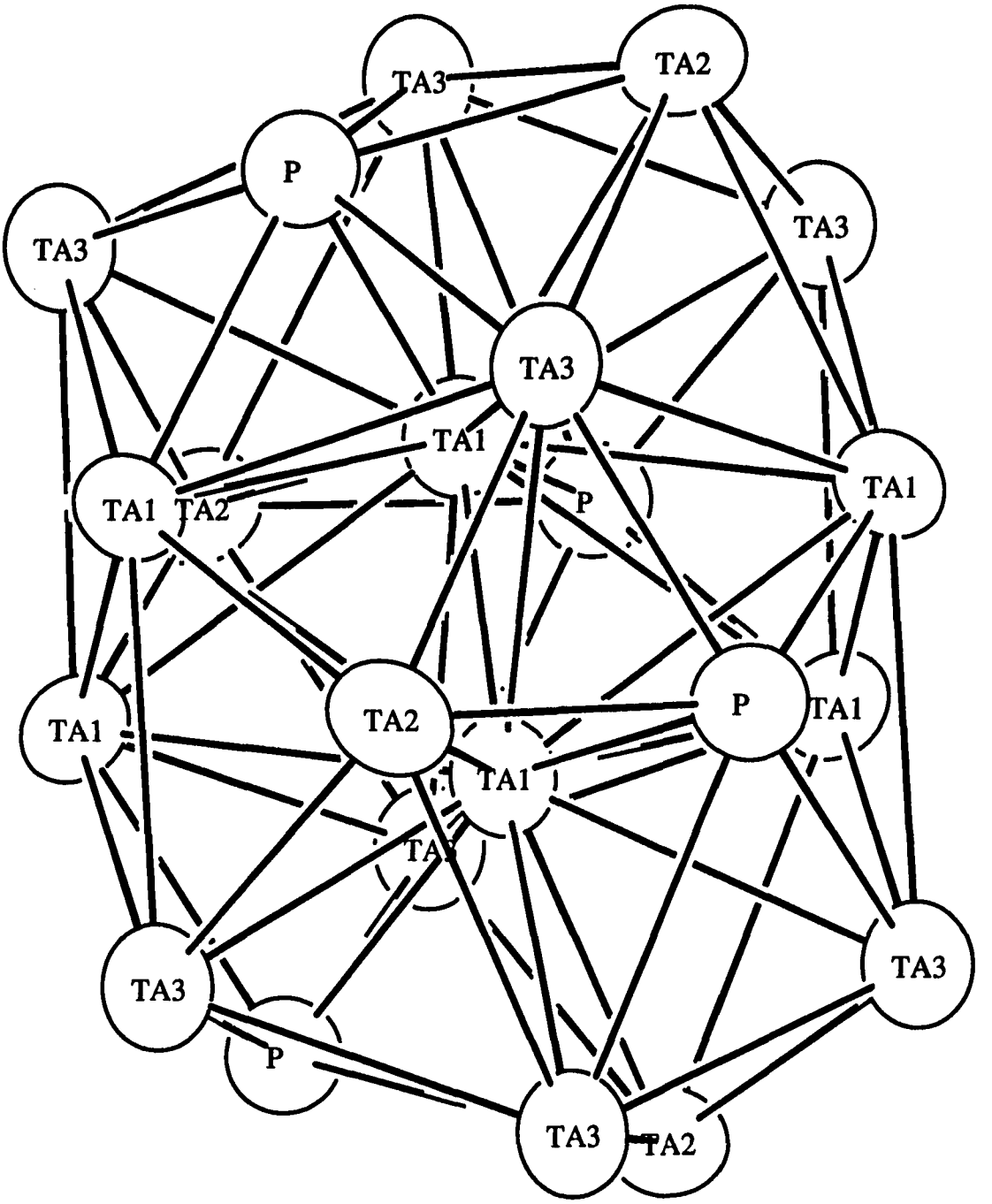

Figure 7.3 **A slightly rotated view of the same polyhedron depicted in Figure 7.2 more clearly shows all atoms, the % probability ellipsoids are exaggerated to accomodate the atom labels**

Table 7.11 Interatomic distances (< 3.6 Å for Ta-Nb-P) from X-ray single crystal structural refinements of $Ta_{4.9}Nb_{1.1}P_2$ and $Hf_{4.1}Nb_{1.9}P_2$

			$Ta_{4.9}Nb_{1.1}P_2$	$Hf_{4.1}Nb_{1.9}P_2$			$Ta_{4.9}Nb_{1.1}P_2$	$Hf_{4.1}Nb_{1.9}P_2$
M1	-P		2.554 (7)	2.643 (7)	M3	-P	2.548 (7)	2.601 (7)
	-P		2.586 (7)	2.691 (7)		-P	2.601 (7)	2.734 (7)
	-M1		2.660 (2)	2.859 (3)		-M2	2.836 (1)	2.990 (2)
	-M3		2.924 (2)	2.930 (2)		-M3	2.841 (3)	2.948 (3)
	-M3		2.964 (2)	3.091 (2)		-M2	2.886 (2)	2.983 (2)
	-M3		2.998 (2)	3.141 (2)		-M1	2.924 (2)	2.930 (2)
	-M2		3.085 (2)	3.214 (2)		-M3	2.936 (3)	3.236 (3)
	-M2		3.095 (2)	3.227 (2)		-M1	2.964 (2)	3.091 (2)
	-M1	×4	3.1427 (9)	3.319 (1)		-M1	2.998 (2)	3.141 (2)
	-M3		3.179 (1)	3.247 (2)		-P	3.038 (7)	2.793 (7)
	-M3		3.182 (1)	3.298 (2)		-M1	3.179 (1)	3.247 (2)
						-M1	3.182 (1)	3.298 (2)
M2	-P		2.549 (6)	2.694 (7)		-M2	3.213 (2)	3.137 (2)
	-P		2.58 (1)	2.677 (7)		-M2	3.456 (2)	3.864 (2)
	-P		2.602 (6)	2.681 (7)		-P	3.531 (7)	4.072 (7)
	-P		2.61 (1)	2.769 (7)				
	-M3		2.836 (2)	2.990 (2)	P	-M3	2.548 (7)	2.601 (7)
	-M3		2.886 (2)	2.983 (2)		-M2	2.549 (6)	2.694 (7)
	-M2		2.949 (2)	3.008 (3)		-M1	2.554 (7)	2.643 (7)
	-M1		3.085 (2)	3.214 (2)		-M2	2.58 (1)	2.677 (7)
	-M1		3.095 (2)	3.227 (2)		-M1	2.586 (7)	2.691 (7)
	-M2	×2	3.200 (3)	3.170 (2)		-M3	2.601 (7)	2.734 (7)
	-M3		3.213 (2)	3.137 (2)		-M2	2.602 (6)	2.681 (7)
	-M2	×2	3.339 (3)	3.607 (2)		-M2	2.61 (1)	2.769 (7)
	-M3		3.456 (2)	3.864 (2)		-M3	3.038 (7)	2.793 (7)
						-M3	3.531 (7)	4.072 (7)

Table 7.12 Selected interatomic distances (Å) for Ti_3P type compounds

	Ta_3P	$(Ta,Nb)_3P$	Nb_3P	$(Hf,Nb)_3P$	Hf_3P	Zr_3P
M1-M1 (×4)	3.135	3.143	3.154	3.319	3.359	3.400
-M1	2.664	2.660	2.636	2.859	2.926	2.965
-M2	3.085	3.085	3.096	3.214	3.256	3.317
-M2	3.093	3.096	3.102	3.227	3.341	3.376
-M3	2.933	2.924	2.931	2.930	2.977	2.982
-M3	3.180	3.181	3.188	3.298	3.379	3.406
-M3	2.966	2.998	3.061	3.141	3.146	3.201
-M3	2.964	2.964	2.966	3.091	3.139	3.193
-M3	3.178	3.179	3.183	3.246	3.299	3.339
-P	2.571	2.586	2.595	2.691	2.701	2.766
-P	2.550	2.554	2.565	2.643	2.697	2.734
M2-M2	2.949	2.949	2.947	3.008	3.004	3.023
-M2 (×2)	3.295	3.339	3.412	3.607	3.619	3.660
-M2 (×2)	3.227	3.200	3.169	3.170	3.177	3.202
-M3	3.274	3.213	3.139	3.137	3.165	3.214
-M3	2.845	2.836	2.836	2.990	3.058	3.087
-M3	3.395	3.456	3.527	3.864	3.958	4.016
-M3	2.874	2.886	2.900	2.983	3.050	3.104
-P	2.577	2.580	2.610	2.677	2.749	2.754
-P	2.595	2.602	2.619	2.681	2.693	2.739
-P	2.561	2.549	2.551	2.694	2.744	2.745
-P	2.597	2.610	2.640	2.769	2.751	2.809
M3-M3	2.854	2.842	2.825	2.948	3.012	3.052
-M3	2.899	2.936	2.993	3.236	3.228	3.293
-P	3.159	3.038	2.889	2.793	2.872	2.863
-P	3.414	3.531	3.665	4.072	4.105	4.217
-P	2.584	2.600	2.632	2.734	2.764	2.812
-P	2.552	2.548	2.537	2.601	2.645	2.678

the centering M1 pair of the polyhedra shown in Figures 7.2 and 7.3, that is much shorter (~2.66 Å vs. 2.84 Å) than any other M-M distance in the compounds. While this M1-M1 contact is still the shortest metal-metal distance in Hf_3P, Zr_3P, and $Hf_{4.2}Nb_{1.8}P_2$, the difference to the next shortest metal-metal contact is not as large (~2.86 Å vs. 2.93 Å in the ternary and even smaller in the other two). It can be seen that $Hf_{4.2}Nb_{1.8}P_2$ is more like the group 5 compounds than the group 4 ones in this respect, which is reasonable given its stoichiometry. More than one doubly centered polyhedron having strong interactions between its centering atoms can be described in these compounds. The M2-M2 and M2-M3 pairs also center polyhedra and these distances become smaller in some cases and larger in others upon moving from the group 4 to group 5 transition metal phosphides. The most striking difference between trimetal phosphides of these two groups is in the M3-P contacts. The group 4 compounds exhibit two short, one medium, and one long interatomic M3-P distance while the group 5 compounds exhibit three short and one long M3-P distance. The M3-P distance of 2.793 (7) Å in $Hf_{4.2}Nb_{1.8}P_2$ is shorter than the corresponding distance in any of the other compounds.

One expects to see identical interatomic distances in Nb_3P and Ta_3P because of their nearly identical size (as judged from their nearly identical Pauling and Slater [114] radii) and one also expects to see a fairly consistent increase in all of the interatomic distances when comparing Hf_3P to Ta_3P because Hf is larger than Ta (Pauling and Slater radii). This is not the case, there are complex anisotropic directional bonding interactions in these systems which vary from group to group and period to period. A complete investigation of these bonding interactions is beyond the scope of this discussion however an empirical look at the relationship between bonding and mixed metal occupancy is not.

The interpretation, assumptions required, and use of the Pauling bond order equation, $d(n) = d(1) - 0.6 \log n$, and Pauling's tabulated single bond radii have been discussed previously. The program Kvexpol was used to calculate the bond orders

reported in Table 7.13 for Ti_3P compounds, Ta_3P, Nb_3P, Zr_3P, Hf_3P, $Ta_{4.9}Nb_{1.1}P_2$, and $Hf_{4.2}Nb_{1.8}P_2$.

In looking at the Ta_3P, $Ta_{4.9}Nb_{1.1}P_2$, and Nb_3P series, one sees that in all cases the total bond orders for the metal sites are similar, M1 ≈ M3 ≥ M2 and the M-M bond orders are consistent with M1 ≥ M3 > M2. Ta has a higher $\Delta H°_{atm}$ than does Nb and can participate more strongly in bonding than Nb because of the larger radial distribution of its s and d orbitals. Because Ta is better at bonding than Nb and because M-M bonding is important in a metal-rich compound, the %Ta occupancy follows the same pattern as the amount of M-M bonding shown in Table 7.7, M1 (91% Ta) ≥ M3 (88% Ta) > M2 (70% Ta).

Examination of Table 7.13 shows that for the next series of compounds, Nb_3P, $Hf_{4.2}Nb_{1.8}P_2$, and Hf_3P, the total bond orders vary substantially and are inconsistent from compound to compound. Considering, again, that M-M bonding is of primary importance in metal-rich compounds, the focus will be upon the calculated M-M bonding. The magnitudes of calculated metal-metal bonding for Nb_3P fall in the order M1 > M3 > M2, for Hf_3P the order is M3 > M1 > M2, and for $Hf_{4.2}Nb_{1.8}P_2$ the order is M1 ≈ M3 > M2. The calculated M-M bonding for all three compounds is inconsistent except that M2 has the least M-M bonding in all cases. The Nb occupancies in $Hf_{4.2}Nb_{1.8}P_2$ read from Table 7.8 are M3 (52% Nb) > M1 (22% Nb) > M2 (16% Nb) which follow the same order as the amounts of M-M bonding in Hf_3P.

Recall that there are significantly different interatomic distances and bonding interactions in Nb_3P and Hf_3P and that $Hf_{4.2}Nb_{1.8}P_2$, being Hf rich, behaves more like Hf_3P than Nb_3P. When $Hf_{4.2}Nb_{1.8}P_2$ is viewed as being synthesized by introducing Nb onto the metal sites of Hf_3P (which is reasonable considering the Hf/Nb ratio) the trend that the stronger metal-metal bonding element, Nb, prefers to occupy the most M-M bonding sites in Hf_3P is followed. Nb has the stronger metal-metal bonding ability even though Hf is a 5d metal and Nb is a 4d metal. Niobium has five possible bonding electrons while hafnium has only four, and the $\Delta H°_{atm}$ for Nb is larger than that for Hf. It would be interesting to examine a ternary phase Nb_5HfP_2 with this

Table 7.13 Total and metal-metal bond orders for Ti_3P type compounds

	Ta_3P		$Ta_{4.9}Nb_{1.1}P_2$		Nb_3P	
	total	M-M	total	M-M	total	M-M
M1	4.89	3.61	4.80	3.57	4.71	3.53
M2	4.79	2.44	4.68	2.40	4.58	2.42
M3	4.88	3.54	4.81	3.48	4.72	3.36
P	4.96	-	4.86	-	4.72	-
	$Hf_{4.1}Nb_{1.9}P_2$		Hf_3P		Zr_3P	
	total	M-M	total	M-M	total	M-M
M1	4.79	3.65	4.82	3.72	4.49	3.55
M2	5.12	3.09	5.15	3.23	4.90	3.09
M3	5.00	3.64	5.46	4.08	5.16	3.86
P	4.54	-	4.41	-	4.06	-

structure to see if the trend for site occupancies followed the different direction (M1 > M3 > M2) suggested by substituting Hf into Nb_3P.

Zr-Nb-P and Zr-Ta-P Systems with the Nb_7P_4 Structure

Synthesis, Characterization, and X-ray Single Crystal Experiments

A sample with the initial stoichiometry Nb_5ZrP_4 was prepared from the appropriate quantities of Nb, Zr, and previously synthesized NbP, pelletized, and arcmelted twice for 30 seconds each time (10V, 80A) with inversion of the sample between arcmeltings. The sample was difficult to melt (probably because the NbP

starting material had an insulating polyphosphide coating on the surface of the particles) and lost a large quantity of phosphorus when it was melted. Another sample with the composition $Zr_7Ta_{4.1}P_{4.1}$ was prepared from Zr and TaP, pelletized, and arcmelted three times for 30 seconds each at 10V, 60A with sample inversion between arcmeltings. This sample melted easily. In both cases, large needle-like crystals with well-formed faces could be found in the top portions of the arcmelted samples.

Guinier X-ray powder films of the bulk samples resembled a calculated powder pattern of Nb_7P_4 in the Zr-Nb-P system but were weak and diffuse in the Zr-Ta-P system and did not match any calculated powder pattern. Needle shaped crystals from both samples were mounted on thin glass fibers and examined with X-ray single crystal photographic techniques.

A crystal from the Zr-Nb-P system was aligned parallel to its long dimension and the length of the corresponding unit cell parameter was calculated to be 3.44 Å from a rotation photograph. A zero layer Weissenberg photograph revealed the lengths of two other possible cell axes, 13.85 Å and 7.48 Å, as well as an angle of ~105° between them. Comparison of these values with those reported in the literature for binary Zr and Nb phosphides strongly suggested that the unit cell was of the Nb_7P_4 type (C2/m) with cell parameters a = 14.95 Å, b = 3.44 Å, c = 13.85 Å, and $\beta \approx 105°$. A *C*-centered cell aligned along the b axis would only give h,0,ℓ with h = 2n reflections in a zero layer Weissenberg photograph, which would look as if a was only ½ of its true value. The first layer Weissenberg photograph had different conditions for observation of reflections, h + k = 2n, and the correct a cell parameter was obtained from this photograph.

A crystal from the Zr-Ta-P system was investigated by X-ray single crystal photographic techniques in the same fashion as the Zr-Nb-P crystal. The resulting values for this crystal were a = 15.65 Å, b = 3.62 Å, c = 14.40 Å, and $\beta \approx 105°$ and it was also identified as a Nb_7P_4 type crystal.

Both crystals were large and diffracted strongly so that intensity data sets could be collected on a Hilger-Watts rotating anode diffractometer (modified by Dr. Jacobson's group). No information about these data collections and subsequent refinements will be noted except that a structural solution in the Nb_7P_4 type was obtained for the Zr-Ta-P crystal with residuals of $R = 0.047$ and $R_w = 0.054$ after a full anisotropic refinement using a DIFABS absorption correction, and the refinement for the Zr-Nb-P crystal "failed", without obtaining any values < 0.10 for the residuals. Second intensity data sets were collected for both crystals on the rotating anode Rigaku AFC6R diffractometer (50 kV, 140 mA) using monochromatic Mo Kα X-radiation ($\lambda = 0.71069$ Å).

The crystal from the Nb_5ZrP_4 sample was collected in automatic mode until the final high angle cell was determined. Initially, fifteen reflections were found by the SEARCH routine and indexed on a *C*-centered monoclinic cell. 25 new reflections were found in the 2θ range 26.4 - 34.4° and used to obtain the orientation matrix used in the data collection. *C*-centered reflections were collected from the hk±ℓ octants out to 60° in 2θ. After the data collection was finished, the automatic high angle POSTCELL routine failed. It appeared to have functioned correctly but psi scan intensities dropped to zero during the PSI procedure. When the orientation matrix used for the actual data collection was manually entered into the AFC6R.XTL file, psi scans were collected normally indicating that the final high angle cell had a poor orientation matrix associated with it.

The data collection for the crystal from the $Zr_7Ta_{4.1}P_{4.1}$ sample was also started in automatic mode. The automatic indexing arrived at a primitive triclinic unit cell and it was necessary to manually index the correct *C*-centered monoclinic unit cell using fourteen of the fifteen reflections found in the search. 25 new reflections were found in the 2θ range 25.4 - 29.6° with the high angle PRECELL routine and were used to obtain the orientation matrix used in the data collection. *C*-centered reflections were collected over the hk±ℓ octants out to 60° in 2θ and one psi scan was performed for later use in an absorption correction.

Both intensity data sets were corrected for Lorentz polarization and absorption effects using TEXSAN software and psi scan data. The automatic space group selection was correct (C2/m) in the $(Zr,Nb)_7P_4$ case but was undetermined for $(Zr,Ta)_7P_4$. The internal $R_{averaging}$'s were low, 0.012 for $(Zr,Nb)_7P_4$ and 0.024 for $(Zr,Ta)_7P_4$, but only 45 and 49 reflections were averaged respectively. The known positional parameters for Nb_7P_4 were used as a starting model and complete refinements including secondary extinction, positional, anisotropic thermal, and occupancy parameters were completed. Table 7.14 gives the details of both data collections and structural refinements.

The final residuals obtained for $Zr_{2.5}Nb_{4.5}P_4$ were R = 0.017 and R_w = 0.026 and no correlation coefficients > 0.5 were found. The difference between anomalous scattering of Mo Kα X-radiation by Zr and Nb was used to determine mixed metal occupancies. The residuals, including zeroes, were R = 0.024 and R_w = 0.028 and four weak reflections (200), (11,1,2), (2,0,13), and $(4,4,\overline{8})$ had $\Delta F/\sigma(F)$'s of 5.04, 7.38, 13.90, and -7.19 respectively.

The final residuals obtained for anisotropic refinement of $Zr_{6.1}Ta_{0.9}P_4$ were R = 0.027 and R_w = 0.037 and large correlations were observed between the scale, secondary extinction, metal occupancy, and metal thermal parameters. The residuals, including zeroes, were R = 0.049 and R_w = 0.043 and eight reflections, (001), (020), $(6,0,\overline{11})$, $(2,0,\overline{14})$, $(2,0,\overline{15})$, $(2,0,\overline{16})$, $(4,0,\overline{17})$, and $(2,0,\overline{17})$ were found to have $\Delta F/\sigma(F)$'s of 11.38, -9.10, 15.35, -12.31, 5.65, 5.83, 5.48, and -5.81respectively. The number of reflections in both refinements with differences between observed and calculated structure factors was somewhat large, but they were weak reflections and the two refinements are completely valid.

Refined positional, isotropic thermal, and occupancy parameters for $Zr_{2.5}Nb_{4.5}P_4$ and $Zr_{6.1}Ta_{0.9}P_4$ and their esd's are given in Tables 7.15 and 7.16 respectively while the anisotropic thermal parameters and esd's are reported in Tables 7.17 and 7.18.

Table 7.14 Crystal data for Zr-Nb-P and Zr-Ta-P (Nb_7P_4 type)

Formula	$Zr_{2.5}Nb_{4.5}P_4$	$Zr_{6.1}Ta_{0.9}P_4$
Space group	C2/m (#12)	C2/m (#12)
a Å	15.026 (8)	15.7006 (8)
b Å	3.490 (2)	3.6016 (1)
c Å	13.825 (7)	14.522 (2)
β	104.83 (4)°	104.74 (1)°
V Å^3	700.8 (6)	794.16 (9)
Z	4	4
d_{calc}, g/cm^3	7.297	7.059
Crystal size, mm^3	0.28 × 0.04 × 0.04	0.18 × 0.04 × 0.03
μ (Mo Kα)	111	206
Data collection instrument	RIGAKU AFC6R	RIGAKU AFC6R
Radiation (monochromated in incident beam)	Mo Kα (λ = 0.71069)	Mo Kα (λ = 0.71069)
Orientation reflections, number, range (2θ)	25, 26.4 - 34.4	25, 25.4 - 29.6
Scan method	2θ - ω	2θ - ω
Octants measured	hk±ℓ	hk±ℓ
Data collection range, 2θ, deg	0 - 60	0 - 60
No. refl. measured	1223	1366
No. unique data, total with $F_o^2 > 3\sigma(F_o^2)$	1178, 1025	1317, 1014
No. parameters refined	76	78
Absorption correction	Psi scans	Psi scans
Trans. factors, max., min.	1.000, 0.8567	1.000, 0.7818
Secondary ext. coeff. (10^{-7})	1.57(17)E-07	1.40(17)E-07
R[a], R_w[b], GOF[c]	0.017, 0.026, 1.14	0.027, 0.037, 1.29
Largest peak, e$^-$/Å^3	0.912	1.725
Largest negative peak, e$^-$/Å^3	-1.232	-2.838

[a] $R = \Sigma \; | \; | F_o | - | F_c | \; | \; / \Sigma \; | F_o |$

[b] $R_w = [\, \Sigma w (| F_o | - | F_c |)^2 / \Sigma w | F_o |^2 \,]^{1/2}$; $w = 1/\sigma^2 (| F_o |)$

[c] $GOF = \Sigma ((| F_o | - | F_c |) / \sigma_i) / (N_{obs} - N_{parameters})$

Results and Discussion

The structure of $Zr_{6.1}Ta_{0.9}P_4$ is shown in Figure 7.4 as a projection down the short *b* axis with all bold atoms at the y = 0 level and all other atoms at y = ½. This Nb_7P_4 [15] type structure has been reported [20] for a variety of early transition metal pnictides, e.g. Nb, Zr, and Hf arsenides, Ti, Nb, and Zr phosphides, $Ti_{31}CuP_{18}$, and has recently been found in the metal-rich Hf-Mo-P system [115]. It is similar to other early transition metal sulfide and phosphide structures in that the short axis is perpendicular to mirror planes upon which all atoms lie, the coordination of the nonmetal is trigonal prismatic, and the coordinations of some of the metals are distorted metal *bcc* fragments.

The M2 atom centers a distorted *bcc* fragment which shares faces horizontally with four vertical phosphorus centered trigonal prisms much like in the $M_{11}P_4$ structure. There is a difference in that the trigonal prisms centered by P2 and P3 in this structure are tricapped and bicapped respectively whereas all are tricapped in the $M_{11}P_4$ structure. M1 also centers a distorted *bcc* fragment which shares four horizontal faces with phosphorus centered trigonal prisms, however two of these are vertical tricapped trigonal prisms and two are horizontal monocapped trigonal prisms.

All atoms in the structure are part of one or the other of these two units. The two units alternate along the *c* direction with the two metal centers M1 and M2 also alternating in height (y = 0 or y = ½). They share capping atoms and parts of the trigonal prisms between them. Along the *a* direction, the units are the same. They are staggered relative to each other in the *b* direction (y = 0 or y = ½) and condensed so that atoms are shared between the units. Other common (to early transition metal phosphides, sulfides, etc.) metal coordinations can be described as well. M3, M6, and M8 center pentagonal prisms of metal atoms with two nonadjacent edges substituted by phosphorus. M4 centers a distorted *bcc* unit of metal atoms with one edge substituted by phosphorus.

It is apparent when looking at nearest neighbors in this picture, that M1, M2,

Table 7.15 Positional, thermal, and occupancy parameters for $Zr_{2.5}Nb_{4.5}P_4$

atom	occupancy	x	y	z	B_{eq} (Å^2)
M1	Nb 100	0	0	0	0.41 (2)
M2	Nb 100	0	1/2	1/2	0.39 (2)
M3	Zr 19.9 (6.0) + Nb 80.1	0.43047 (3)	0	0.82632 (4)	0.44 (2)
M4	Zr 51.0 (6.1) + Nb 49.0	0.19596 (3)	0	0.31079 (4)	0.32 (2)
M5	Zr 25.2 (6.1) + Nb 74.8	0.20936 (3)	0	0.79867 (4)	0.33 (2)
M6	Zr 51.9 (6.2) + Nb 48.1	0.33880 (4)	0	0.02868 (4)	0.44 (2)
M7	Zr 24.0 (6.2) + Nb 76.0	0.00277 (3)	0	0.66540 (4)	0.35 (2)
M8	Zr 77.7 (6.0) + Nb 22.3	0.17392 (4)	0	0.54140 (4)	0.40 (2)
P1	P 100	0.1747 (1)	0	0.1127 (1)	0.49 (4)
P2	P 100	0.3742 (1)	0	0.6038 (1)	0.54 (5)
P3	P 100	0.3707 (1)	0	0.3348 (1)	0.46 (5)
P4	P 100	0.0624 (1)	0	0.8484 (1)	0.51 (5)

Table 7.16 Positional, thermal, and occupancy parameters for $Zr_{6.1}Ta_{0.9}P_4$

atom	occupancy	x	y	z	B_{eq} (Å^2)
M1	Zr 67.8 (1.2) + Ta 32.2	0	0	0	0.65 (7)
M2	Zr 63.0 (1.2) + Ta 37.0	0	1/2	1/2	0.38 (4)
M3	Zr 97.4 (0.9) + Ta 2.6	0.43029 (7)	0	0.82577 (4)	0.54 (4)
M4	Zr 55.8 (1.1) + Ta 44.2	0.19782 (4)	0	0.31353 (4)	0.36 (3)
M5	Zr 97.8 (0.8) + Ta 2.2	0.20642 (7)	0	0.79591 (4)	0.35 (4)
M6	Zr 98.8 (0.8) + Ta 1.2	0.34119 (7)	0	0.02853 (4)	0.49 (4)
M7	Zr 95.2 (0.9) + Ta 4.8	0.00483 (7)	0	0.66465 (4)	0.45 (4)
M8	Zr 98.3 (0.8) + Ta 1.7	0.17563 (7)	0	0.54027 (4)	0.46 (4)
P1	P 100	0.1746 (2)	0	0.1134 (1)	0.5 (1)
P2	P 100	0.3753 (2)	0	0.6060 (1)	0.5 (1)
P3	P 100	0.3691 (2)	0	0.3414 (1)	0.4 (1)
P4	P 100	0.0620 (2)	0	0.8513 (1)	0.5 (1)

Table 7.17 Anisotropic thermal parameters ($Å^2$) for $Zr_{2.5}Nb_{4.5}P_4$ (U12 = U23 = 0)

atom	U11	U22	U33	U13
M1	0.0042 (3)	0.0070 (4)	0.0044 (3)	0.0009 (2)
M2	0.0039 (3)	0.0064 (3)	0.0044 (3)	0.0008 (2)
M3	0.0045 (3)	0.0055 (3)	0.0064 (3)	0.0011 (2)
M4	0.0029 (3)	0.0050 (3)	0.0041 (3)	0.0011 (2)
M5	0.0032 (3)	0.0046 (3)	0.0048 (3)	0.0011 (2)
M6	0.0059 (3)	0.0054 (3)	0.0049 (3)	0.0005 (2)
M7	0.0040 (3)	0.0048 (3)	0.0042 (3)	0.0007 (2)
M8	0.0052 (3)	0.0047 (3)	0.0051 (3)	0.0009 (2)
P1	0.0065 (6)	0.0067 (7)	0.0050 (6)	0.0006 (5)
P2	0.0061 (6)	0.0061 (7)	0.0087 (6)	0.0026 (5)
P3	0.0050 (6)	0.0066 (7)	0.0054 (6)	0.0005 (5)
P4	0.0064 (6)	0.0071 (7)	0.0063 (6)	0.0021 (5)

Table 7.18 Anisotropic thermal parameters ($Å^2$) for $Zr_{6.1}Ta_{0.9}P_4$ (U12 = U23 = 0)

atom	U11	U22	U33	U13
M1	0.0037 (5)	0.017 (2)	0.0044 (5)	0.0010 (4)
M2	0.0036 (5)	0.0054 (6)	0.0052 (5)	0.0007 (4)
M3	0.0047 (5)	0.0056 (6)	0.0103 (6)	0.0018 (4)
M4	0.0031 (3)	0.0054 (4)	0.0053 (4)	0.0013 (2)
M5	0.0029 (5)	0.0048 (6)	0.0054 (5)	0.0007 (4)
M6	0.0063 (6)	0.0051 (6)	0.0066 (6)	0.0005 (4)
M7	0.0036 (5)	0.0067 (6)	0.0064 (5)	0.0007 (4)
M8	0.0052 (5)	0.0059 (6)	0.0063 (6)	0.0011 (4)
P1	0.005 (1)	0.006 (2)	0.006 (1)	-0.002 (1)
P2	0.005 (1)	0.004 (1)	0.008 (1)	0.002 (1)
P3	0.003 (1)	0.005 (1)	0.008 (1)	0.001 (1)
P4	0.004 (1)	0.008 (1)	0.006 (1)	0.001 (1)

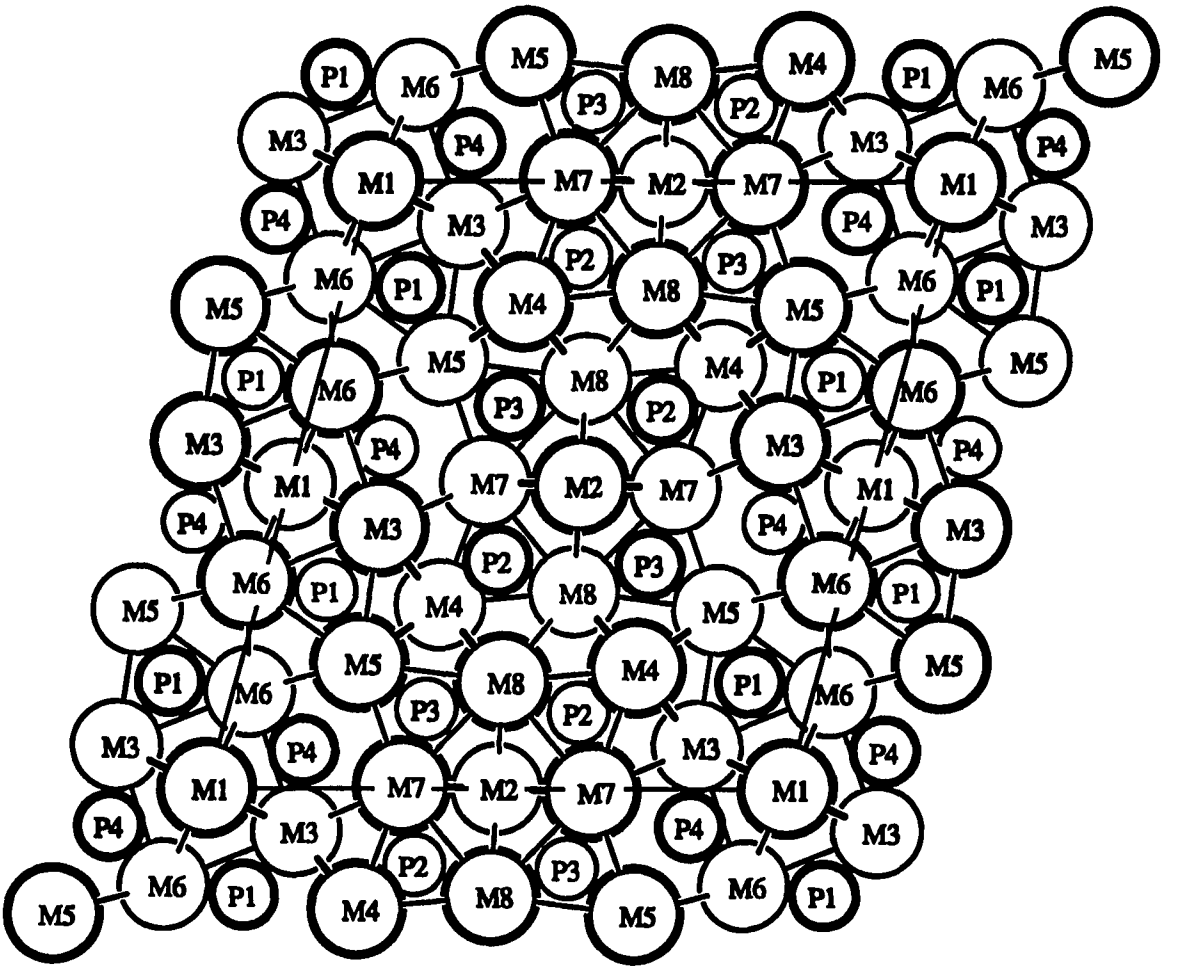

Figure 7.4 Projection of $Zr_{6.1}Ta_{0.9}P_4$ (Nb_7P_4 type) down the short, unique *b* axis, all atoms in bold are at the y = 0 level and all other atoms are at the y=½ level, refined thermal parameters (Tables 7.16 and 7.18) are not depicted

and M4 center *bcc*-like fragments and are the strongest metal-metal bonding sites. M3, M6, and M8 form the edges of these *bcc*-like fragments, center pentagonal prisms, and appear to be weaker metal-metal bonding sites. M5 and M7 also form edges of the *bcc*-like fragments but appear to be the least metal-metal bonding sites in the structure. The total and metal-metal bond orders for these different sites were calculated by the program Kvexpol from refined interatomic distances out to 6 Å using the Pauling bond order equation, d(n) = d(1) - 0.6 log n, and Pauling's tabulated single bond radii. The important distances in the refined structures of $Zr_{6.1}Ta_{0.9}P_4$ and $Zr_{2.5}Nb_{4.5}P_4$ are given in Table 7.19 and selected distances from $Zr_{2.5}Nb_{4.5}P_4$, $Zr_{6.1}Ta_{0.9}P_4$, Zr_7P_4, and Nb_7P_4 are given in Table 7.20. There appear to be no drastic differences in their interatomic distances, indicating no major changes in bonding such as those seen in the Ti_3P type compounds. There appears to be a relatively consistent and expected increase in the distances upon changing from the Nb rich Nb-Zr-P and Nb-P systems (r_{Nb} = 1.342 Å) to the Zr rich Zr-Ta-P and Zr-P (r_{Zr} = 1.454 Å) systems.

There are, of course, inconsistencies in this simplistic view which are again indicative of complicated anisotropic directional bonding just as in the Ti_3P type compounds. The M3-P2, M4-M5, M4-P1, M5-P3, and M7P4 distances in $Zr_{2.5}Nb_{4.5}P_4$ are slightly shorter than those distances in Nb_7P_4 even though Zr has a larger radius than NB and M3, M4, M5, and M7 exhibit substantial % Zr occupancies in $Zr_{2.5}Nb_{4.5}P_4$. Conversely, the M1-M3, M2-P2 distances in $Zr_{6.1}Ta_{0.9}P_4$ are slightly longer than those in Zr_7P_4 even though Ta has a smaller radius than Zr and substantial % Ta occupancies are found on M1 and M2.

Calculated total and metal-metal bond orders for Nb_7P_4, $Zr_{2.5}Nb_{4.5}P_4$, Zr_7P_4, and $Zr_{6.1}Ta_{0.8}P_4$ are given in Table 7.21. Since metal-metal interactions dominate bonding in metal-rich compounds, this discussion will concentrate on the calculated M-M bond orders. In the Zr-Ta-P system, the qualitative idea that M1, M2, and M4 are the most metal-metal bonding sites was corroborated by the bond order calculations. The refined Ta occupancies from Table 7.16 for the sites M1, M2, and M4 are an order

Table 7.19 Interatomic distances < 3.8Å in Nb_7P_4 type compounds

			$Zr_{2.5}Nb_{4.5}P_4$	$Zr_{6.1}Ta_{0.9}P_4$				$Zr_{2.5}Nb_{4.5}P_4$	$Zr_{6.1}Ta_{0.9}P_4$
M1	-P4	x2	2.506 (2)	2.586 (3)	M5	-P4	x1	2.475 (2)	2.591(3)
	-P1	x2	2.688 (2)	2.816 (3)		-P1	x2	2.547 (2)	2.686 (2)
	-M3	x4	2.936 (1)	3.071 (1)		-P3	x2	2.600 (2)	2.725 (2)
	-M6	x4	3.092 (1)	3.1870 (9)		-M4	x2	2.909 (1)	3.041 (1)
	-M1	x2	3.490 (2)	3.6016 (1)		-M7	x1	3.179 (2)	3.253 (2)
M2	-P3	x2	2.593 (2)	2.668 (3)		-M6	x2	3.186 (1)	3.357 (1)
	-P2	x2	2.650 (2)	2.782 (3)		-M3	x1	3.246 (2)	3.430 (2)
	-M7	x4	2.868 (1)	2.9788 (9)		-M6	x1	3.276 (2)	3.500 (2)
	-M8	x4	3.072 (1)	3.2200 (9)		-M8	x1	3.459 (2)	3.620 (2)
	-M2	x2	3.490 (2)	3.6016 (1)		-M5	x2	3.490 (2)	3.6016 (1)
M3	-P4	x2	2.600 (2)	2.696 (2)	M6	-P1	x2	2.589 (2)	2.701 (2)
	-P1	x2	2.633 (2)	2.734 (3)		-P4	x2	2.616 (2)	2.692 (2)
	-M4	x2	2.899 (1)	3.051 (1)		-P1	x1	2.983 (2)	3.163 (3)
	-M1	x2	2.936 (1)	3.071 (1)		-M1	x2	3.092 (1)	3.1870 (9)
	-P2	x1	2.975 (2)	3.087 (3)		-M6	x2	3.117 (2)	3.305 (2)
	-M7	x2	3.227 (1)	3.388 (1)		-M5	x2	3.186 (1)	3.357 (1)
	-M5	x1	3.246 (2)	3.430 (2)		-M5	x1	3.276 (2)	3.500 (2)
	-M6	x1	3.420 (2)	3.567 (2)		-M3	x1	3.420 (2)	3.567 (2)
	-M3	x2	3.490 (2)	3.6016 (1)		-M6	x2	3.490 (2)	3.6016 (1)
	-M6	x1	3.533 (2)	3.672 (2)		-M3	x1	3.533 (2)	3.672 (1)
M4	-P2	x2	2.487 (1)	2.570 (2)	M7	-P4	x1	2.459 (2)	2.629 (3)
	-P3	x1	2.561 (2)	2.616 (3)		-P2	x2	2.581 (2)	2.688 (2)
	-P1	x1	2.674 (2)	2.835 (3)		-P3	x2	2.581 (2)	2.694 (2)
	-M3	x2	2.899 (1)	3.051 (1)		-M2	x2	2.868 (1)	2.9788 (9)
	-M5	x2	2.909 (1)	3.041 (1)		-M4	x1	3.087 (2)	3.277 (1)
	-M8	x2	3.000 (1)	3.091 (1)		-M5	x1	3.179 (2)	3.253 (2)
	-M7	x1	3.087 (2)	3.277 (1)		-M3	x2	3.227 (1)	3.388 (1)
	-M8	x1	3.289 (2)	3.398 (1)		-M8	x1	3.367 (2)	3.549 (2)
	-M4	x2	3.490 (2)	3.6016 (1)		-M8	x1	3.436 (2)	3.594 (2)
						-M7	x2	3.490 (2)	3.6016 (1)

Table 7.19 Continued

			$Zr_{2.5}Nb_{4.5}P_4$	$Zr_{6.1}Ta_{0.9}P_4$				$Zr_{2.5}Nb_{4.5}P_4$	$Zr_{6.1}Ta_{0.9}P_4$
M8	-P2	×2	2.618 (2)	2.744 (2)	P2	-M4	×2	2.487 (1)	2.570 (2)
	-P3	×2	2.648 (2)	2.702 (3)		-M7	×2	2.581 (2)	2.668(2)
	-P2	×1	2.910 (2)	3.035 (3)		-M8	×2	2.618 (2)	2.744 (2)
	-M4	×2	3.000 (1)	3.091 (1)		-M2	×1	2.650 (1)	2.782 (3)
	-M2	×2	3.072 (1)	3.2200 (9)		-M8	×1	2.910 (2)	3.035 (3)
	-M4	×1	3.289 (2)	3.398 (1)		-M3	×1	2.975 (2)	3.087 (3)
	-M8	×2	3.305 (2)	3.385 (2)		-P2	×2	3.490 (2)	3.6016 (1)
	-M7	×1	3.367 (2)	3.549 (2)		-P3	×1	3.706 (3)	3.819 (5)
	-M7	×1	3.436 (2)	3.594 (2)		-P3	×1	3.708 (3)	3.890 (4)
	-M5	×1	3.459 (2)	3.620 (1)	P3	-M4	×1	2.561 (2)	2.616 (3)
	-M8	×2	3.490 (2)	3.6016 (1)		-M7	×2	2.581 (2)	2.694 (2)
P1	-M5	×2	2.547 (2)	2.686 (2)		-M2	×1	2.593 (2)	2.668 (3)
	-M6	×2	2.589 (2)	2.701 (2)		-M5	×2	2.600 (2)	2.725 (2)
	-M3	×2	2.633 (2)	2.734 (2)		-M8	×2	2.648 (2)	2.702 (3)
	-M4	×1	2.674 (2)	2.835 (3)		-P4	×2	3.431 (2)	3.712 (4)
	-M1	×1	2.688 (2)	2.816 (3)		-P3	×2	3.490 (2)	3.6016 (1)
	-M6	×1	2.983 (2)	3.163 (3)		-P1	×1	3.670 (2)	3.891 (4)
	-P1	×2	3.490 (2)	3.6016 (1)		-P2	×1	3.706 (3)	3.819 (4)
	-P4	×1	3.612 (2)	3.768 (5)		-P2	×1	3.708 (3)	3.890 (4)
	-P3	×1	3.670 (2)	3.891 (4)	P4	-M7	×1	2.459 (2)	2.629 (3)
	-P4	×1	3.737 (2)	3.878 (4)		-M5	×1	2.475 (2)	2.591 (3)
						-M1	×1	2.506 (2)	2.586 (3)
						-M3	×2	2.600 (2)	2.696 (2)
						-M6	×2	2.616 (2)	2.692 (2)
						-P3	×2	3.431 (2)	3.712 (4)
						-P4	×2	3.490 (2)	3.6016 (1)
						-P1	×1	3.612 (2)	3.768 (5)
						-P1	×1	3.737 (2)	3.878 (4)

Table 7.20 Selected interatomic distances for Nb_7P_4 type compounds

	Nb_7P_4	$(Nb,Zr)_7P_4$	Zr_7P_4	$(Zr,Ta)_7P_4$
M1-M3 (×4)	2.918	2.936	3.040	3.071
-P1 (×2)	2.670	2.688	2.856	2.816
-P4 (×2)	2.505	2.506	2.610	2.586
M2-M7 (×4)	2.855	2.868	3.048	2.979
-P2 (×2)	2.634	2.650	2.773	2.782
-P3 (×2)	2.592	2.593	2.702	2.668
M3-M4 (×2)	2.895	2.899	3.089	3.051
-P1 (×2)	2.612	2.633	2.761	2.734
-P2	3.007	2.975	3.264	3.087
-P4 (×2)	2.580	2.600	2.703	2.696
M4-M5 (×2)	2.917	2.909	3.083	3.041
-M8 (×2)	2.981	3.000	3.137	3.091
-P1	2.699	2.674	2.867	2.835
-P2 (×2)	2.460	2.487	2.627	2.570
-P3	2.542	2.561	2.666	2.616
M5-P1 (×2)	2.524	2.547	2.696	2.686
-P3 (×2)	2.603	2.600	2.744	2.725
-P4	2.447	2.474	2.582	2.591
M6-P1	2.969	2.983	3.128	3.163
-P1 (×2)	2.566	2.590	2.718	2.701
-P4 (×2)	2.600	2.616	2.695	2.692
M7-P2 (×2)	2.572	2.581	2.713	2.688
-P3 (×2)	2.567	2.581	2.716	2.694
-P4	2.475	2.459	2.643	2.629
M8-P2	2.873	2.910	3.043	3.035
-P2 (×2)	2.581	2.618	2.733	2.744
-P3 (×2)	2.632	2.648	2.730	2.702

of magnitude larger than the Ta occupancies of the other metal sites. Once again, the idea that the element (Ta vs. Zr in this case) able to participate in the strongest metal-metal bonding interactions preferentially occupies the most metal-metal bonding sites in a metal-rich compound is shown to be valid.

The metal site occupancy and bond order data for $Zr_{2.5}Nb_{4.5}P_4$ in Tables 7.15 and 7.21 suggest that the metal occupancies are not strongly correlated with the amount of M-M bonding in this case. The only obvious correlation is that Nb prefers to occupy the sites that center the all-metal distorted *bcc* fragments. The M4 sitewhich was strongly preferred by the group V metal, Ta, in $(Zr,Ta)_7P_4$ appears to be preferentially occupied by the group IV metal, Zr, in $(Zr,Nb)_7P_4$. Additionally, the M4-P2 interatomic distance is substantially shorter in $Zr_{2.5}Nb_{4.5}P_4$ than in $Zr_{6.1}Ta_{0.9}P_4$ even though the % Nb and Ta occupancies of M4 are similar. This observation, and the inconsistent interatomic distances cited above, suggest that the M_7P_4 stoichiometry is not sufficiently metal-rich that the M-P bonding can be disregarded, just as was suggested regarding the M-S bonding in $Zr_{4.4}Hf_{1.6}S_3$. Furthermore, although Nb has one more electron to use in bonding than Zr and has a larger $\Delta°H_{atm}$ than does Zr (which suggests that it forms stronger metal-metal bonds in the elemental form) it has a lower $\Delta°H_{atm}$ than Ta, does not form metal-metal bonds as strongly as Ta, and therefore does not preferentially occupy the metal-metal bonding sites in $(Zr,Nb)_7P_4$ as strongly as Ta prefers the metal-metal bonding sites in $(Zr,Ta)_7P_4$.

Table 7.21 Calculated bond orders for Nb_7P_4 type compounds

	Nb_7P_4		$(Zr,Nb)_7P_4$		Zr_7P_4		$(Zr,Ta)_7P_4$	
	total	M-M	total	M-M	total	M-M	total	M-M
M1	5.04	2.63	5.15	2.80	5.98	3.73	5.33	3.14
M2	5.22	3.13	5.55	3.52	5.60	3.60	5.50	3.68
M3	4.64	2.30	5.08	2.70	4.95	2.85	4.86	2.58
M4	5.74	2.81	7.38	3.99	5.82	3.35	5.66	3.17
M5	5.21	1.69	5.85	2.21	5.07	2.04	5.12	2.04
M6	4.02	1.56	4.80	1.94	4.12	1.78	4.15	1.75
M7	5.26	1.93	5.77	2.16	5.10	2.22	5.39	2.33
M8	4.07	1.74	5.57	2.65	4.27	2.09	4.37	2.13
P1	4.70	-	5.02	-	3.88	-	4.03	-
P2	5.07	-	5.65	-	4.27	-	4.34	-
P3	4.57	-	5.15	-	4.30	-	4.53	-
P4	4.97	-	5.30	-	4.74	-	4.71	-

8. IDEAS FOR FUTURE RESEARCH

The exploratory syntheses and structural characterizations discussed in this dissertation were quite successful and it appears likely that further research along similar lines will also yield interesting results. Much of the work presented here was centered around the stoichiometry $M_{9+x}M'_{4-x}X_{4-y}$ and in the Zr-Nb-S, Hf-Nb-S, and Hf-V-S systems, no other compositions were investigated. There is no apriori reason why other new phases can not be found in these systems.

The Hf-Zr-S system was more thoroughly investigated and the only indications of new phases were irreproducible. ESCA analysis indicated that small amounts of Cu were present in one series of samples and small amounts of Ca were present in a different series of samples which contained unknown phases. Investigation of the quaternary systems Hf-Zr-Ca-S and Hf-Zr-Cu-S may be worth pursuing.

The "stuffed" γ-brass $Hf_{10}Ta_3S_3$ is a very interesting structure and merits further investigation, both experimental and theoretical. The fact that this structure doesn't form in the Zr-Ta-S, Hf-Nb-S, and Zr-Nb-S systems is intriguing. A complete and rigorous explanation of this would be a "stiff" challenge to theoreticians. The explanation offered in this work was based on the difference in excited state electron configurations for Hf, Zr, Ta, and Nb as discussed in light of the empirical Brewer-Engel correlation. If the ideas of Brewer are correct, then this structure may also form for $Sc_{10}Ti_3S_3$, $Sc_{10}Ta_3S_3$, and $Hf_{10}Ti_3S_3$. According to Brewer, Sc and Ti (as well as Hf and Ta) have excited state *bcc* s- and p-electron configurations of $sp^{0.5}$ and according to Pauling, the single bond radii of Hf ≈ Sc ≈ 1.44 Å and Ta ≈ Ti ≈ 1.32-1.34 Å so that substitution of Sc for Hf and Ti for Ta may be possible. Perhaps a "stuffed" γ-brass, with W substituting for Ta, can be synthesized since W has the same electron configuration but a slightly smaller radius than Ta, ~ 1.30 Å.

The ratio of the metallic radii and the size of the face-bisecting "channels" were other factors which appeared to be significant in the formation of the new $Hf_{10}Ta_3S_3$ gamma brass-like phase. The radii of Ti and V are in the proper proportions and both have the s- and p- *bcc* $sp^{0.5}$ electron configuration according to Brewer. Sulfur may

fit into the "channels" in this hypothetical structure, so that a "stuffed" γ-brass might form with the composition $Ti_{10}V_3S_3$.

Investigations of ternary mixed-transition-metal-rich phosphide systems have recently been started in this research group. The potential for high-temperature syntheses of ternary metal-rich phosphides appears to be larger than for sulfides when one extrapolates from binary systems to ternary, i.e. there are more known binary metal-rich phosphides than sulfides.

Although two new phases were found in the Zr-Nb-P system, visual inspection of Guinier X-ray powder patterns indicated that more unidentified, and presumably new, phases were present in the Zr-Nb-P metal-rich system. Preliminary investigation of the Hf-Nb-P, Zr-Ta-P, and Hf-Ta-P systems also indicated that unidentified and presumably new phases were present in these metal-rich systems as well.

The Ta-Nb-P metal rich system was investigated in the regions Ta/Nb ≈ 1 and M/P ≈ 2 to 4 with Ta_3P and metal being the phases detected. Due to the richness of the Ta-Nb-S metal-rich system, a complete investigation is strongly suggested. The Hf-Zr-P system should also be investigated and all combinations of groups IV, V, and VI (and others) transition metal-rich phosphide systems are good candidates for exploratory synthesis.

Magnetic susceptibility measurements showed that the ZrNbP phase reported in this work was not superconducting above 2K. It is interesting to note that the related phases [28] (with the same structure type) ZrRuP, NbRhP, and TaRhP have T_c's ~ 4K while ZrRhP has a T_c ~ 1.5K and no T_c was observed for NbRuP or TaRuP above 1.1K. Can similar quaternary compounds such as $(Zr,Nb,Ru)_2P$ be synthesized with the same structure and if so, what are their superconducting properties?

The same M-M′-X systems investigated in this dissertation with X = S or P and others discussed above could easily be explored using X = Ge, Si, and C. No prereaction to form binaries would be required and preliminary studies could be performed in short order.

The idea of metals ordering onto various sites in order to increase bonding in the structure (metal-metal bonding in metal-rich systems) might be further explored. It would be interesting to see if Ta would prefer the most metal-nonmetal bonding sites in a Ta/Nb solid solution Se-rich compound like $(Ta,Nb)_3Se$ in the $TaSe_3$ [116] structure since Ta-Se bonds have a larger electronegativity difference than do Nb-Se bonds and should thus be stronger. Perhaps new mixed metal compounds will be stabilized in ternary nonmetal-rich systems just as they have been found to be in metal-rich systems.

The use of Mo Kα X-radiation anomalous dispersion to differentiate between Nb and Zr turned out to be a valuable tool. This idea could be further explored and perhaps quantified to a degree using Nb/Zr alloys. Elemental analysis and X-ray crystallography could be used in unison to determine the accuracy of this technique. Y and Sr also have large differences in their anomalous scattering of Mo Kα X-radiation which might be useful in structural investigations of new high T_c superconductors. It would be interesting to see if W Kα X-radiation could be used to distinguish between Hf and Ta through differences in anomalous scattering. The first row iron-group transition metals have large differences in their anomalous scattering of Cu Kα X-radiation which also might be useful for differentiating these elements if X-ray fluorescence was not an insurmountable problem.

REFERENCES CITED

(1) von Laue, M. *Sitz. math. phys. Klasse Bayer. Akad. Wiss.* **1912**, 303.

(2) Bragg, W.L. *Proc. Camb. Phil. Soc.* **1912**, *17*, 43.

(3) Kim, S.-J.; Nguyen, T.-H.; Franzen, H.F. *J. Solid State Chem.* **1987**, *70*, 88.

(4) McTaggert, F.K.; Wadsley, A.D. *Aust. J. Chem.* **1958**, *11*, 445.

(5) Nguyen, T.-H. Ph.D. Dissertation, Iowa State University, Ames, IA, 1980.

(6) a) Hägg, G. *Z. phys. Chem.* **1929**, *B6*, 221. b) Hägg, G. *Z. phys. Chem.* **1930**, *B7*, 339. c) Hägg, G. *Z. phys. Chem.* **1930**, *B8*, 455. d) Hägg, G. *Z. phys. Chem.* **1931**, *B12*, 33.

(7) Rundle, R.E. *Acta Cryst.* **1948**, *1*, 180.

(8) Pauling, L. *The Nature of the Chemical Bond, 3rd Ed.*; Cornell University Press: Ithica, NY, 1948.

(9) *Binary Alloy Phase Diagrams*, 2nd Ed.; T.B. Massalski Ed.; ASM International, Materials Park, Ohio, 1970.

(10) Franzen, H.F. *Prog. Solid St. Chem.* **1978**, *12*, 1.

(11) Nylund, A. *Acta. Chem. Scand.* **1966**, *20*, 2393.

(12) Franzen, H.F.; Beineke, T.A.; Conard, B.R. *Acta Crystallogr.* **1968**, *B24*, 412.

(13) Chen, H.-Y.; Tuenge, R.T.; Franzen, H.F. *Inorg. Chem.* **1973**, *12*, 552.

(14) Owens, J.P.; Conard, B.R.; Franzen, H.F. *Acta Crystallogr.* **1974**, *B30*, 427.

(15) Rundqvist, S. *Acta Chem. Scand.* **1966**, *20*, 2427.

(16) Anugul, S.; Pontchour, C.; Rundqvist, S. *Acta Chem. Scand.* **1973**, *27*, 26.

(17) Hassler, E. *Acta Chem. Scand.* **1971**, *25*, 129.

(18) Marking, G.A.; Franzen, H.F. *Chem. Mater.* **1993**, *5*, 678.

(19) Yao, X.; Marking, G.; Franzen, H.F. *Ber Bunsenges. Phys. Chem.* **1992**, *96*, 1552.

(20) *Pearson's Handbook of Crystallographic Data for Intermetallic Phases*, 2nd Ed.; P. Villars and L.D. Calvert, Eds.; ASM International, Materials Park, Ohio, 1991.

(21) Rundqvist, S. *Acta Chem. Scand.* **1962**, *16*, 287.

(22) Johnsson, T. *Acta Chem. Scand.* **1972**, *26*, 365.

(23) Rundqvist, S. *Acta Chem. Scand.* **1965**, *19*, 393.

(24) Rundqvist, S.; Jellinek, F. *Acta Chem. Scand.* **1959**, *13*, 425.

(25) Geller, S. *Acta Crystallogr.* **1955**, *8*, 83.

(26) Aronsson,B.; Bäckman, M.; Rundqvist, S. *Acta Chem. Scand.* **1960**, *14*, 1001.

(27) Snell, P.-O. *Acta Chem. Scand.* **1968**, *22*, 1942.

(28) Müller, R.; Shelton, R.N. *J. Less-Common Met.* **1983**, *92*, 177.

(29) Pedersen, B.; Grønwold, F. *Acta Cryst.* **1959**, *12*, 1022.

(30) Chen, H.-Y.; Franzen, H.F. *Acta Cryst.* **1972**, *B28*, 1399.

(31) Lundstrom, T.; Snell, P.-O. *Acta Chem. Scand.* **1967**, *21*, 1343.

(32) Rundqvist, S.; Hassler, E.; Lundvik, L. *Acta Chem. Scand.* **1962**, *16*, 242.

(33) Sellberg, B.; Rundqvist, S. *Acta Chem. Scand.* **1965**, *19*, 760.

(34) Franzen, H.F,; Smeggil, J.G. *Acta Cryst.* **1969**, *B25*, 1736.

(35) Franzen, H.F.; Smeggil, J.G. *Acta Cryst.* **1970**, *B26*, 125.

(36) Harbrecht, B. *J. Less-Common Met.* **1988**, *138*, 225.

(37) a) Hughbanks, T. *Prog. Solid State Chem.* **1989**, *19*, 329. b) Wada, H.; Onada, M. *Mater. Res. Bull.* **1989**, *24*, 191. c) Kim, S.-J.; Nanjundaswamy, K.S.; Hughbanks, T. *Inorg. Chem.* **1991**, *30*, 159.

(38) Harbrecht, B.; Franzen, H.F. *Z. Anorg. Allg. Chem.* **1987**, *551*, 74.

(39) Rautala, P.; Norton, J.T. *Trans AIME* **1952**, *194*, 1045.

(40) Hårsta, A.; Rundqvist, S. *J. Solid State Chem.* **1987**, *70*, 210.

(41) Mackay, R.; Franzen, H.F. *Chem. Mater.* **1993**, *5*, 857.

(42) Mackay, R.; Franzen, H.F. *Z. Anorg. Allg. Chem.* **1992**, *616*, 154.

(43) Harbrecht, B. *Z. Kristallogr.* **1988**, *182*, 118.

(44) Rogl, P.; Nowotny, H.; Benesovsky, F. *Monatsh. Chem.* **1973**, *104*, 182.

(45) Marking, G.A.; Franzen, H.F. *J. Am. Chem. Soc.* **1993**, *115*, 6126.

(46) Yao, X. Ph.D. Dissertation, Iowa State University, Ames, IA, 1991.

(47) Yao, X.; Franzen, H.F. *J. Solid State Chem.* **1990**, *86*, 88.

(48) Yao, X.; Franzen, H.F. *Z. Anorg. Allg. Chem.* **1991**, *598/599*, 353.

(49) Yao, X.; Franzen, H.F. *J. Amer. Chem. Soc.* **1991**, *113*, 1426.

(50) Yao, X.; Miller, G.J.; Franzen, H.F. *J. Alloys Comp.* **1992**, *183*, 7.

(51) Harbrecht, B. *Angew. Chem., Int. Ed. Engl.* **1989**, *28*, 1660.

(52) Owens, J.P.; Conard, B.R.; Franzen, H.F. *Acta Cryst.* **1967**, *23*, 77.

(53) Moody, G.J.; Thomas, J.D.R. *J. Chem. Soc.* **1964**, 1417.

(54) Franzen, H.F.; Graham, J. *Z. Kristallogr.* **1966** *123*, 133.

(55) Conard, B.R.; Franzen, H.F. *High Temp. Sci.* **1971**, *3*, 49.

(56) Franzen, H.F.; Smeggil, J.G.; Conard, B.R. *Mat. Res. Bull.* **1967**, *2*, 1087.

(57) Franzen, H.F.; Norrby, L.J. *Acta Cryst.* **1968**, *B24*, 601.

(58) Conard, B.R.; Norrby, L.J.; Franzen, H.F. *Acta Cryst.* **1969**, *B25*, 1729.

(59) Kapustinski, A.F. *Quart. Rev. Chem. Soc.* **1956**, *10*, 283.

(60) *Selected Values of the Thermodynamic Properties of the Elements*, prepared by Hultgren, R.; Desai, P.D.; Hawkins, D.T.; Gleiser, M.; Kelley, K.K.; Wagman, D.D., American Society for Metals, Metals Park, OH, 1973.

(61) Pecoraro, T.A.; Chianelli, R.R. *J. Catal.* **1981**, *67*, 430.

(62) Hume-Rothery, W.; Raynor, G.V. *The Structure of Metals and Alloys*; Institute of Metals, London, 1962.

(63) Brewer, L. In *Alloying*; Walter, J.L., Jackson, M.R., Sims, C.T., Eds.; ASM International: Metals Park, Ohio, 1988.

(64) Marking, G.A.; Franzen, H.F.; Ostenson, J.E.; Ling, M.M.; Finnemore, D.K. *Phys. Rev.* submitted.

(65) Franzen, H.F. *J. Solid State Chem.* **1986**, *64*, 283.

(66) Rundqvist, S. *Chem. Scr.* **1988**, *28*, 15.

(67) Schäfer, H.; Trenkel, M. *Z. Anorg. Allg. Chem.* **1972**, *391*, 11.

(68) McCullough, J.D.; Brewer, L.; Bromley, L.A. *Acta Crystallogr.* **1948**, *1*, 287.

(69) Reed, T.B. *Mat. Res. Bull.* **1967**, *2*, 349.

(70) Mackay, R.A. Ph.D. Dissertation, Iowa State University, 1993.

(71) Tipler, P.A. *Physics*, 2nd Ed.; Worth Publishers, Inc.: New York, 1982.

(72) Guinier, A. *X-ray Diffraction*; W.H. Freeman and Company: San Francisco, 1963.

(73) Clark, C.M.; Smith, D.K.; Johnson, G.J. "A Fortran IV Program for Calculating X-ray Powder Diffraction Pattern-Version 5," Department of Geosciences, Pennsylvania State University, University Park, 1973.

(74) Ziebarth, R.P., Ames Laboratory, Iowa State University, Ames, IA, unpublished research, 1984.

(75) Imoto, H. Ames Laboratory, Iowa State University, 1978, unpublished research.

(76) a) Werner, P.-E. "SCANPI Version 8 for IBM PC/AT," Arrhenius Laboratory, University of Stockholm, Sweden 1990. b) Malmos, G.; Werner, P.-E. *Acta Chem. Scand.* **1973**, *27*, 493. c) Johansson, K.E.; Palm, T.; Werner, P.-E. *J. Phys. E:Sci. Instrum.* **1980**, *13*, 1289.

(77) Werner, P.-E. TREORV4, Department of Structural Chemistry, Arrhenius Laboratory, University of Stockholm, Sweden, 1984.

(78) Takusagaw, F. Ames Laboratory, Iowa State University, 1981, unpublished research.

(79) a) Larson, A.C.; Von Dreele, R.B. *"Generalized Crystal Structure Analysis System"* LANSCE, MS-H805 Los Alamos National Laboratory, Los Alamos, NM 87545, 1986. b) Von Dreele, R.B.; Jorgensen, J.D.; Windsor, C.B. *J. Appl. Crystallogr.* **1982**, *15*, 581.

(80) Howard, S.A.; Preton, K.D. In *Reviews in Mineralogy, Vol. 20, Modern Powder Diffraction*; Bish, D.; Post, J., Eds.; Mineralogical Society of America, Washington D.C., 1989.

(81) Rietveld, H.M. *J. Appl. Crystallogr.* **1969**, *2*, 65.

(82) Johnson, C.K. "ORTEP-II, A Fortran Thermal-Ellipsoid Plot Program," Report ORNL-5138, Oak Ridge National Laboratory, Oak Ridge, 1976.

(83) Stout, G.H.; Jensen,L.H. *X-ray Structure Determination, 2nd Ed.*; John Wiley & Sons: New York, 1989.

(84) *TEXSAN: Single Crystal Structure Analysis Software, Version 5.0* Molecular Structure Corporation, The Woodlands, TX, 1989.

(85) Jacobson, R.A. and research group Ames Laboratory, Iowa State University, 1993, unpublished research.

(86) Walker, N.; Stuart, D. *Acta Cryst.* **1983**, *A39*, 158.

(87) Sheldrick, G.M. In *Crystallographic Computing 3*, G.M. Sheldrick; C. Krüger; R. Goddard, Eds.; Oxford University Press, 1985.

(88) Von Dreele, R.B. In *Reviews in Mineralogy, Vol. 20, Modern Powder Diffraction*; Bish, D.; Post, J., Eds.; Mineralogical Society of America, Washington D.C., 1989.

(89) Hahn, H.; Harder, B.; Mutschke, U.; Ness, P. *Z. Anorg. Allg. Chem.* **1957**, *292*, 82.

(90) Newbury, D.E.; Joy, D.C.; Echlin, P.; Fiori, C.E.; Goldstein, J.I. *Advanced Scanning Electron Microscopy and X-Ray Microanalysis*, pp. 245, Plenum Press, New York, 1986.

(91) He, L. Ames Laboratory, Iowa State University, 1993, unpublished research.

(92) *International Tables for X-ray Crystallography*, Vol. III, 2nd Ed., pp. 213-216, MacGillavry, C.H.; Rieck, G.D., Eds.; Kynoch Press, Birmingham, England, 1968.

(93) Klug, H.P.; Alexander, L.E. *X-ray Diffraction Procedures, 2nd Ed.*; John Wiley & Sons: New York, 1974.

(94) Taylor, M.A. *Acta Cryst.* **1959**, *12*, 393.

(95) Schewe-Miller, I. unpublished results, Ames Laboratory, Iowa State University, Ames, Iowa, 1993.

(96) a) Hårsta, A. *Acta Univ. Ups., Abstracts Uppsala Diss. Fac. Sci.*, **1985**, 767. b) Rupp, B.; Tuscher, E. *J. Less-Common Met.*, **1984**, *104*, L9.

(97) *CRC Handbook of Chemistry and Physics*, 65th Ed.; 1984, pp. E79-E88.

(98) a) Desorbo, W. *Phys. Rev.*, **1963** *132*, 107. b) Halbritter, J. *Appl. Phys. A*, **1987**, *43*, 1.

(99) a) Westgren, A.; Phragmén, G. *Phil. Mag.* **1925**, *50*, 311. b) Heidenstam, O.V.; Johansson, A.; Westman, S. *Acta Chem. Scand.* **1968**, *22*, 653.

(100) *ORFLS*: "*A Fortran Crystallographic Least Squares Program*" U.S. Atomic Energy Commission Report ORNL-TM-305, Oak Ridge National Laboratory, Oak Ridge, TN **1962**.

(101) *International Tables for X-ray Crystallography Tables*, Vol. IV, pp. 288-292, Ibers, J.A.; Hamilton, W.C., Eds.; Kynoch Press, Birmingham, England, 1974.

(102) Edström, V.-A.; Westman, S. *Acta Chem. Scand.* **1969**, *23*, 279.

(103) Bradley, A.J.; Jones, P. *J. Inst. Met.* **1933**, *51*, 131.

(104) Pearson, W.B.; Brandon, J.K.; Brizard, R.Y. *Z. Kristallogr.* **1976**, *143*, 417.

(105) Hoistad, L.M.; Lee, S. *J. Amer. Chem. Soc.* **1991**, *113*, 8216.

(106) Lundström, T.; Ersson, N.-O. *Acta Chem. Scand.* **1968**, *22*, 1801.

(107) Ahlzén, P.-J.; Rundqvist, S. *Z. Kristallogr.* **1989**, *189*, 117.

(108) Kuzma, Yu.B.; Orishchin, S.V.; Lomnitskaya, Ya.F.; Glov'jak, T. *Dopov. Akad. Nauk Ukr. RSR, Ser. B: Geo. Khim. Biol. Nauki* **1988**, *2*, 47.

(109) Yao, X.; Franzen, H.F. *J. Less-Common Met.* **1988**, *142*, L27.

(110) Franzen, H.F.; Graham, J. *J. Inorg. Nucl. Chem.* **1966**, *28*, 377.

(111) Smeggil, J.G. *Ph.D. Thesis*, Iowa State University, Ames, IA, **1969**.

(112) Rundqvist, S. *Nature* **1966**, *211*, 847.

(113) Rundqvist, S. *Acta Chem. Scand.* **1962**, *16*, 1.

(114) a)Slater, J.C. *J. Chem. Phys.* **1964**, *41*, 3199. b)Slater, J.C. *Quantum Theory of Molecules and Solids, Vol. 2*, McGraw-Hill Book Co., Inc., New York, 1963.

(115) Cheng, J. unpublished results, Ames Laboratory, Iowa State University, Ames, Iowa, 1993.

(116) Meerschaut, A.; Geumas, L.; Rouxel, J. *J. Solid State Chem.* **1981**, *36*, 118.

ACKNOWLEDGEMENTS

The author wishes to thank his major professor, Hugo F. Franzen for his friendship, guidance, trust, and patience. Past and present group members, in particular, and the solid state community at Iowa State University, in general, have made this work enjoyable and rewarding.

Dr. V. G. Young and Prof. R. A. Jacobson and his group members have provided valuable help with crystallography. J. E. Ostenson performed magnetic susceptibility measurements and Prof. D. K. Finnemore collaborated on the superconductivity study. Dr. W. E. Strazheim and F. Laabs conducted SEM-EDS analyses. J. W. Anderegg has been extremely helpful in many technological aspects related to this work and S. Standley has provided excellent secretarial help.

The author is most indebted to Margaret, Holly, and Christine for their love and understanding.

This work was performed at Ames Laboratory under contract no. W-7405-eng-82 with the U.S. Department of Energy. The United States government has assigned the DOE Report number IS-T 1646 to this thesis.

APPENDIX A: OBSERVED AND CALCULATED STRUCTURE FACTOR AMPLITUDES (×10) FOR $Zr_{9.7}Ta_{3.3}S_{3.1}$ FROM Mo Kα X-RAY SINGLE CRYSTAL DATA

k	l	Fo	Fc	sigF
^^^^^^^ h =	0	^^^^^^^		
0	2	1239	1083	85
0	4	5429	6066	0
0	6	4349	4499	0
0	8	2185	2119	99
0	10	2471	2396	68
0	12	2846	2864	66
^^^^^^^ h =	1	^^^^^^^		
0	-13	640	532	74
0	-8	1682	1692	38
0	-7	731	728	32
0	-4	2081	2100	65
0	-3	2229	2210	37
0	-2	228	193	95*
0	0	83	2190	57*
0	1	70	220	55*
0	5	451	452	26
0	6	0	33	0*
0	9	758	736	29
0	10	0	82	0*
0	11	326	345	0*
0	12	1133	1147	53
1	-10	582	671	59
1	-2	275	314	30
1	0	516	520	24
1	4	1236	1230	27
1	6	1112	1123	62
1	8	1245	1294	36
1	12	521	549	42
^^^^^^^ h =	2	^^^^^^^		
0	-11	352	154	75*
0	-10	1298	1279	43
0	-9	1685	1705	41
0	-8	1904	1940	0
0	-7	1645	1628	37
0	-5	324	334	35
0	-4	1880	1859	34
0	-3	3949	3938	61
0	-1	749	748	22
0	0	582	599	22
0	2	350	319	35
0	6	1954	1966	43
0	12	250	511	0*
0	13	1303	1311	40
1	-12	83	18	0*
1	-10	885	918	33
1	-9	429	387	41
1	-8	1261	1245	37
1	-7	405	369	80*
1	-2	3941	3833	61
1	0	1267	1260	30
1	1	311	280	73*
1	3	373	371	87*
1	4	564	563	52
1	5	360	339	36
1	6	1080	1032	32
1	11	385	325	50
1	13	260	333	0*
2	-12	845	910	63
2	-10	63	277	0*
2	-6	0	100	0*
2	-4	1473	1422	31
2	-2	2516	2498	41
2	0	3741	3738	60
2	8	140	101	0*
^^^^^^^ h =	3	^^^^^^^		
0	-13	769	722	41
0	-12	269	361	0*
0	-10	1869	1895	88
0	-8	442	257	40
0	-7	2285	2198	63
0	-5	4619	4668	72
0	-4	793	810	41
0	-3	1791	1779	77
0	-2	2124	2153	44
0	-1	5057	4997	0
0	0	2597	2585	44
0	6	3031	3062	51
0	9	1554	1478	42
0	11	2519	2506	52
1	-12	337	272	0*
1	-11	920	903	34
1	-10	926	894	32
1	-7	1168	1172	37
1	-6	1188	1195	53
1	-5	1412	1448	32
1	-4	850	853	48
1	-1	1729	1696	32
1	0	378	423	36
1	2	635	622	29
1	3	1435	1409	30
1	8	867	848	54
1	9	943	957	65
2	-12	814	880	59
2	-11	550	540	89
2	-9	938	945	77
2	-7	847	872	28
2	-6	644	723	0*
2	-5	758	729	26
2	-3	2469	2524	42
2	-2	774	726	0
2	0	539	546	29
2	1	181	101	0*
2	4	1682	1694	34
2	8	2061	2023	43
2	10	258	309	91*
3	-12	2002	2085	86
3	-10	1718	1791	44
3	-8	2304	2310	46
3	-6	2864	2849	90
3	0	5823	5896	92
3	2	2123	2113	38
3	4	4111	4092	66
^^^^^^^ h =	4	^^^^^^^		
0	-12	149	50	0*
0	-11	1006	1007	36
0	-10	1596	1562	45
0	-9	239	115	77*
0	-8	191	345	0*
0	-7	0	302	0*
0	-6	2380	2319	43
0	-5	1455	1498	33
0	-3	675	676	23
0	-2	2438	2460	40
0	0	177	171	67*
0	1	1075	1114	26
0	4	0	211	95*
1	-11	557	510	44
1	-10	472	521	46
1	-9	355	396	70*
1	-8	878	854	30
1	-7	59	230	0*
1	-5	885	868	68
1	-4	949	956	39
1	-3	1064	1092	71
1	-2	654	629	0*
1	0	787	823	41
1	1	509	504	21
1	6	757	762	62
1	12	478	499	51
2	-11	273	291	0*

k	l	Fo	Fc	sigF	k	l	Fo	Fc	sigF	k	l	Fo	Fc	sigF
2	-9	116	189	0*	1	-6	682	645	29	0	-11	1775	1743	49
2	-7	342	359	50	1	-5	416	450	38	0	-10	1579	1521	45
2	-5	577	585	29	1	-4	862	852	82	0	-8	261	148	89*
2	-4	2136	2128	40	1	-3	2069	2115	39	0	-7	1885	1879	42
2	-2	164	82	87*	1	-2	640	640	23	0	-6	2153	2099	45
2	-1	673	683	26	1	-1	960	957	31	0	-5	2987	3012	89
2	0	1794	1777	40	1	0	954	981	41	0	-4	68	288	0*
2	3	388	371	33	1	10	598	597	40	0	-3	1960	1993	38
2	6	470	495	0*	2	-10	663	678	36	0	0	371	311	43
2	8	1942	1967	43	2	-9	570	527	37	0	1	3192	3216	0
2	10	157	227	0*	2	-8	1295	1300	42	0	2	2636	2657	45
2	12	1111	1138	38	2	-7	309	262	0*	0	9	1476	1462	45
3	-10	540	566	0*	2	-6	1142	1112	39	1	-11	415	376	67
3	-8	590	528	66	2	-5	1240	1236	36	1	-10	1195	1229	43
3	-7	278	197	0*	2	-4	922	889	28	1	-9	500	477	60
3	-5	332	341	75*	2	-3	1314	1388	35	1	-8	0	221	0*
3	-1	339	386	78*	2	-1	718	719	25	1	-7	467	485	0*
3	0	3039	3098	55	2	0	207	137	83*	1	-6	1816	1788	41
3	2	692	667	24	2	2	0	86	0*	1	-5	452	456	47
3	3	221	226	0*	2	11	697	768	57	1	-4	112	177	0*
3	4	1599	1548	36	3	-8	1078	1187	0	1	-3	607	596	43
3	6	1089	1003	38	3	-7	1039	1076	33	1	-2	1364	1349	41
3	9	232	133	0*	3	-6	893	906	30	1	-1	499	506	29
3	11	265	158	79*	3	-5	199	106	0*	1	0	832	832	36
4	-10	587	637	0*	3	-3	2061	2107	87	2	-10	948	937	34
4	-8	1069	1140	83	3	-1	495	532	32	2	-8	523	536	87
4	-6	852	896	91	3	0	210	254	0*	2	-5	277	189	76*
4	-4	1098	1168	39	3	2	218	203	0*	2	-4	0	21	0*
4	-2	625	654	27	3	4	1033	975	31	2	-2	2664	2614	47
4	0	932	955	36	3	9	1080	1104	72	2	-1	234	158	80*
					3	10	686	676	49	2	0	848	881	38
^^^^^^^ h = 5 ^^^^^^^					4	-9	575	627	93	2	3	151	141	0*
					4	-8	235	21	0*	2	6	1112	1166	37
0	-12	385	107	69*	4	-7	440	513	48	2	7	76	204	0*
0	-11	0	208	0*	4	-6	1444	1517	96	2	9	0	194	0*
0	-10	567	509	40	4	-2	1311	1398	38	3	-9	1483	1521	76
0	-9	349	204	0*	4	-1	0	91	0*	3	-7	1615	1681	98
0	-8	1876	1820	42	4	0	678	592	36	3	-6	1672	1688	0
0	-7	262	164	74*	4	3	1165	1145	68	3	-5	1755	1774	41
0	-6	355	273	78*	4	4	0	234	0*	3	-3	2307	2330	45
0	-3	0	103	0*	4	5	0	303	0*	3	-2	1706	1637	68
0	-2	3809	3870	93	4	10	1028	1062	46	3	-1	2112	2150	42
0	0	2097	2127	41	5	-8	437	519	97*	3	0	830	855	40
0	1	238	93	57*	5	-6	578	559	38	3	4	435	486	89*
0	4	563	558	25	5	0	2173	2276	53	3	8	0	147	0*
0	5	112	145	0*	5	2	1472	1457	39	4	-9	396	485	0*
1	-11	183	316	0*	5	4	621	589	33	4	-8	402	461	56
1	-9	1076	1151	35						4	-7	627	649	36
1	-8	602	607	35	^^^^^^^ h = 6 ^^^^^^^					4	-6	1000	992	69
1	-7	1180	1207	35						4	-5	1362	1389	41

k	l	Fo	Fc	sigF
4	-2	1081	1053	38
4	-1	1268	1223	38
4	0	622	606	42
4	3	390	326	50
4	4	635	586	32
5	-7	447	450	0*
5	-6	0	22	0*
5	-5	0	81	0*
5	-4	878	890	42
5	-3	843	864	68
5	-1	414	336	0*
5	0	1080	1014	43
5	2	163	148	0*
6	-4	2508	2476	71
6	-2	1480	1461	49
6	0	2309	2252	59
6	6	742	730	36

^^^^^^^ h = 7 ^^^^^^^

k	l	Fo	Fc	sigF
0	-10	942	964	40
0	-9	306	310	73*
0	-8	885	862	59
0	-7	600	619	36
0	-6	1399	1387	40
0	-5	2107	2126	43
0	-4	503	470	31
0	-3	325	326	0*
0	-1	1699	1711	86
0	0	450	415	45
0	2	414	381	99*
1	-10	0	126	0*
1	-9	0	14	0*
1	-7	0	64	0*
1	-6	0	147	0*
1	-5	186	120	0*
1	-4	651	667	55
1	-3	0	10	0*
1	-2	1204	1189	37
1	0	1777	1755	46
1	1	202	108	0*
1	8	0	103	0*
2	-9	689	731	83
2	-5	980	988	37
2	-4	332	366	56*
2	0	1606	1579	50
2	1	1195	1097	45
2	2	1407	1419	47
2	3	963	1004	31
2	6	0	125	0*
2	7	818	866	42
2	8	368	393	97*
3	-8	391	422	0*
3	-7	253	273	0*
3	-6	1434	1481	44
3	-5	1298	1314	42
3	-4	206	18	0*
3	0	767	734	38
3	1	931	949	32
3	2	749	768	29
3	3	513	462	57
4	-7	0	93	0*
4	-6	659	680	37
4	-4	514	527	48
4	-3	0	43	0*
4	-2	410	308	0*
4	0	78	201	0*
4	1	265	150	79*
4	5	0	177	0*
5	-6	130	164	0*
5	-5	947	959	35
5	-1	704	668	54
5	0	692	676	47
5	2	481	544	0*
5	3	529	564	42
5	4	1148	1158	43
6	-1	0	76	0*
6	0	1516	1538	63
6	2	0	129	0*
6	3	146	121	0*

^^^^^^^ h = 8 ^^^^^^^

k	l	Fo	Fc	sigF
0	-9	633	672	43
0	-7	647	672	47
0	-6	811	778	30
0	-5	256	289	0*
0	-4	1330	1359	40
0	-3	1557	1556	39
0	-1	0	236	0*
0	0	756	759	38
0	2	0	51	0*
0	8	1652	1553	62
1	-8	1141	1161	37
1	-7	334	311	88*
1	-6	170	80	0*
1	-5	538	512	38
1	-2	124	206	0*
1	-1	561	551	34
1	0	986	1027	43

^^^^^^^ h = 9 ^^^^^^^

k	l	Fo	Fc	sigF
1	3	161	309	0*
1	4	1148	1185	42
1	9	41	194	0*
2	-8	1067	1085	37
2	-7	294	218	85*
2	-6	1005	1074	37
2	-5	707	722	32
2	-4	822	825	74
2	-3	873	840	51
2	0	261	223	0*
2	1	440	385	49
2	2	426	384	43
3	-7	0	80	0*
3	-6	841	774	49
3	-5	0	64	0*
3	-4	225	197	0*
3	-3	259	61	0*
3	-2	1524	1559	42
3	-1	0	65	0*
3	0	168	266	0*
4	-4	583	567	38
4	-1	871	841	55
4	0	1321	1359	58
4	2	1170	1151	38
4	3	706	676	35
4	5	757	794	42
5	-2	181	140	0*
5	-1	288	281	0*
5	0	0	142	0*
5	3	480	496	51

k	l	Fo	Fc	sigF
0	-8	2324	2298	51
0	-7	249	93	0*
0	-6	1260	1217	39
0	-5	566	568	39
0	-4	2673	2710	51
0	0	2542	2620	58
0	1	393	324	52
0	2	1919	1933	43
0	3	626	625	55
1	-7	307	37	0*
1	-6	217	115	0*
1	-5	723	698	34
1	-4	1216	1268	44
1	-1	474	498	41
1	0	1284	1180	53
1	2	383	328	0*
1	3	298	374	67*

k	l	Fo	Fc	sigF
2	-6	576	513	40
2	-4	618	594	38
2	-2	356	228	0*
2	-1	815	809	39
2	0	430	417	65
2	3	536	520	40
2	5	821	800	33
3	-1	1416	1498	46
3	0	415	382	74*
3	2	1696	1714	44
3	3	1559	1553	49
3	4	427	351	93*
3	5	1304	1280	64
4	0	223	222	0*
4	1	533	429	42
4	2	818	822	35

^^^^^^^ h = 10 ^^^^^^^

0	-4	1340	1286	45
0	-3	0	96	0*
0	-1	0	84	0*
0	0	2731	2674	62
0	2	892	878	53
0	5	155	66	0*
0	6	816	780	36
0	7	201	63	0*
1	-6	297	254	0*
1	-5	328	378	86*
1	-1	269	217	0*
1	0	684	676	51
1	2	432	354	48
1	3	441	357	97*
1	4	607	586	0*
2	-3	1166	1147	36
2	-2	970	929	59
2	-1	303	137	0*
2	0	517	439	59
2	4	356	64	0*

^^^^^^^ h = 11 ^^^^^^^

0	-3	853	821	35
0	0	826	770	48
0	1	461	460	0*
0	2	161	243	0*
0	4	620	612	65
1	-2	848	793	49
1	0	425	481	85*
1	1	138	236	0*

APPENDIX B: OBSERVED AND CALCULATED STRUCTURE FACTOR AMPLITUDES (×10) FOR $Zr_{9.5}Ta_{3.5}S_{2.9}O_{0.6}$ FROM Cu Kα X-RAY POWDER DATA

The column headings are

Column 1 - L

Column 2 - 10*(sign[sqrt(abs(Fo**2)/SCALE),Fo**2])
Fo**2 is the observed value corrected for absorption, etc.

Column 3 - 10*Fc computed to match Fo
The extinction correction, if used, is applied to Fc

H= 0 K= 0			H= 2 K= 1			H= 3 K= 2			H= 4 K= 2		
4	6521	7020	10	944	1033	8	2382	2364	9	295	296
6	5866	5956	11	220	242	9	1419	1487			
8	2013	2332				10	385	365	H= 4 K= 3		
10	2913	3012	H= 2 K= 2								
						H= 3 K= 3			0	3950	3702
H= 1 K= 0			0	4816	4560				1	671	623
			2	3271	3084	0	7561	7114	2	1098	1015
3	2605	2904	4	1383	1484	2	2823	2644	3	454	451
4	2097	2147	6	304	295	4	4865	4786	4	1380	1531
5	462	452	8	187	195	6	3703	3771	5	568	551
6	105	101	10	315	303	8	2527	2698	6	1409	1376
7	990	941							7	375	387
8	1632	1742	H= 3 K= 0			H= 4 K= 0			8	204	205
9	1102	1195							9	267	287
10	49	50	0	3736	3344	0	393	433			
11	460	439	1	6376	6107	1	1225	1142	H= 4 K= 4		
			2	2485	2412	2	2936	2876			
H= 1 K= 1			3	1765	1981	3	1173	1291	0	995	1114
			4	867	1034	4	134	132	2	828	845
2	0	187	5	5773	5775	5	1533	1694	4	1339	1356
4	1405	1387	6	3438	3798	6	2765	2824	6	1038	1116
6	1424	1331	7	2814	2853	7	147	156	8	1258	1289
8	1501	1503	8	236	256	8	412	409			
10	708	751	9	1680	1647	9	270	288	H= 5 K= 0		
			10	2145	2285	10	2010	1930			
H= 2 K= 0			11	3257	3386				0	3058	2830
						H= 4 K= 1			1	27	27
1	413	621	H= 3 K= 1						2	4672	4670
2	63	60				0	733	857	3	42	44
3	4485	4818	0	673	616	1	635	664	4	963	897
4	2205	2365	1	2164	1903	2	513	562	5	83	82
5	594	641	2	324	353	3	1432	1465	6	213	221
6	2197	2303	3	1515	1518	4	970	1088	7	108	125
7	1715	1746	4	1260	1197	5	1230	1137	8	2473	2570
8	2361	2571	5	1600	1640	6	764	848	9	170	164
9	2232	2232	6	1250	1163	7	221	227	10	511	532
10	1312	1364	7	1269	1276	8	1051	1001			
11	498	496	8	1132	1172	9	593	620	H= 5 K= 1		
			9	1004	1040	10	541	572			
H= 2 K= 1			10	795	792				0	1156	1210
						H= 4 K= 2			1	908	953
0	1658	1562	H= 3 K= 2						2	566	575
1	54	59				0	1670	1676	3	2705	2522
2	4514	4458	0	273	271	1	981	932	4	1070	1061
3	248	218	1	14	15	2	26	27	5	341	359
4	853	858	2	898	902	3	382	425	6	549	561
5	146	140	3	3444	3277	4	2476	2305	7	1301	1288
6	823	904	4	1811	1879	5	834	883	8	750	755
7	237	248	5	1040	980	6	896	862	9	1508	1456
8	1767	1714	6	1010	1041	7	486	484			
9	289	292	7	1039	1014	8	2250	2287			

H= 5 K= 2

0	338	336
1	994	921
2	243	222
3	2151	2048
4	1057	1072
5	1595	1649
6	1508	1441
7	312	322
8	1650	1644
9	894	913

H= 5 K= 3

0	33	37
1	494	526
2	336	320
3	2840	2744
4	1144	1144
5	201	199
6	1137	1165
7	1282	1214
8	1470	1526

H= 5 K= 4

0	802	798
1	254	265
2	1535	1485
3	1460	1439
4	257	282
5	673	693
6	1878	1793
7	445	466

H= 5 K= 5

0	2862	2967
2	1921	1999
4	443	442

H= 6 K= 0

0	321	346
1	3939	3952
2	3279	3244
3	2395	2283
4	374	419
5	4072	3765
6	2431	2502
7	2252	2400
8	333	344
9	1643	1710

H= 6 K= 1

0	1229	1172
1	331	331
2	1538	1481
3	503	532
4	287	268
5	245	278
6	2236	2169
7	388	408
8	294	274

H= 6 K= 2

0	1243	1181
1	145	159
2	3387	3133
3	28	27
4	103	100
5	240	236
6	1185	1219
7	153	152
8	735	751

H= 6 K= 3

0	1116	1201
1	2656	2590
2	1967	1830
3	3098	2942
4	592	628
5	2072	2114
6	2148	2104
7	2080	2157

H= 6 K= 4

0	776	812
1	1472	1497
2	999	1070
3	240	254
4	900	865
5	1814	1707

H= 6 K= 5

0	1400	1326
1	316	295
2	182	166
3	1116	1157

H= 7 K= 0

0	504	574
1	2081	2216
2	51	48
3	694	671
4	758	758
5	2816	2783
6	1580	1620
7	809	766
8	1280	1329

H= 7 K= 1

0	2168	2173
1	81	87
2	1463	1463
3	117	114
4	601	636
5	135	141
6	348	362
7	6	5

H= 7 K= 2

0	2371	2323
1	1181	1169
2	1802	1719
3	1045	1084
4	429	453
5	1100	1062
6	533	495

H= 7 K= 3

0	1111	1196
1	1137	1146
2	872	890
3	976	962
4	132	123
5	1621	1684

H= 7 K= 4

0	127	121
1	193	178
2	156	154
3	226	246

H= 8 K= 0

0	759	734
1	135	134
2	127	124
3	2056	2010
4	1672	1725
5	443	476
6	1183	1093
7	700	737

H= 8 K= 1

0	895	1062
1	637	662
2	183	190
3	343	347
4	1208	1291
5	685	653
6	144	149

H= 8 K= 2

0	222	238
1	521	539
2	316	316
3	1377	1320
4	1130	1128

H= 8 K= 3

0	368	385
1	53	55
2	1787	1903

H= 9 K= 0

0	2928	3063
1	472	491
2	2327	2494
3	1113	1098
4	3452	3288
5	856	912

H= 9 K= 1

0	1169	1107
1	782	730
2	404	369
3	532	552

H= 10 K= 0

0	3384	3621
1	246	252

APPENDIX C: OBSERVED AND CALCULATED STRUCTURE FACTOR AMPLITUDES ($\times 10^3$) FOR $Zr_{9.5}TA_{3.5}S_{2.9}O_{0.6}$ FROM NEUTRON POWDER DATA

The column headings are

Column 1 - L

Column 2 - 1000*(sign[sqrt(abs(Fo**2)/SCALE),Fo**2])
Fo**2 is the observed value corrected for absorption, etc.

Column 3 - 1000*Fc computed to match Fo
The extinction correction, if used, is applied to Fc

H= 0 K= 0

4	11116	10451
6	11145	10931
8	2473	2879
10	6527	6569
12	9928	9860
14	2169	2168

H= 1 K= 0

3	5237	5162
4	1366	1451
5	1352	1321
6	338	324
7	1885	1857
8	1620	1800
9	2961	2847
10	70	72
11	1555	1564
12	1575	1548
13	2469	2410
14	645	645

H= 1 K= 1

2	1170	1018
4	1636	1469
6	1620	1652
8	2555	2581
10	980	982
12	519	512
14	675	680

H= 2 K= 0

2	870	846
3	7991	8021
4	4896	4579
5	2724	2638
6	4385	4381
7	3066	2954
8	6337	6373
9	5071	4848
10	3150	3172
11	2418	2483
12	1936	1898
13	4480	4478
14	42	42

H= 2 K= 1

0	2601	2626
1	1016	982
2	6534	6268
3	679	639
4	2277	2143
5	768	752
6	157	132
7	401	399
8	4735	4751
9	131	128
10	1037	1069
11	105	107
12	28	28
13	281	286
14	4606	4567

H= 2 K= 2

0	8511	8485
2	5232	5531
4	2667	2802
6	1295	1282
8	862	846
10	416	427
12	3997	3793
14	4732	4740

H= 3 K= 0

0	6293	6306
1	9373	9315
2	1981	1929
3	1761	1589
4	2115	2066
5	10350	10401
6	6249	6188
7	4658	4816
8	731	715
9	2569	2505
10	4332	4344
11	8437	8479
12	2476	2387
13	1526	1608
14	652	648

H= 3 K= 1

0	146	298
1	2611	2398
2	1094	1043
3	1891	1806
4	1612	1685
5	2397	2400
6	1166	1095
7	1843	1951
8	2359	2289
9	1748	1739
10	835	859
11	2072	2128
12	479	452
13	1486	1569
14	166	167

H= 3 K= 2

0	2124	2115
1	468	442
2	1937	1901
3	6607	6690
4	1616	1633
5	2728	2700
6	2457	2551
7	2318	2246
8	4162	4069
9	3858	3885
10	1035	1061
11	2944	2890
12	727	713
13	3416	3386

H= 3 K= 3

0	11551	11625
2	4317	4598
4	7516	7502
6	8381	8435
8	4163	4159
10	6029	6105
12	6266	6443

H= 4 K= 0

0	442	421
1	1233	1138
2	4508	4459
3	4117	3907
4	747	741
5	2780	2771
6	5365	5458
7	671	677
8	1572	1504
9	1749	1779
10	4551	4561
11	2997	3050
12	510	492
13	1306	1331

H= 4 K= 1

0	598	549
1	1486	1478
2	177	192
3	3116	3144
4	1366	1261
5	2851	2776
6	688	806
7	516	515
8	1656	1621
9	1654	1698
10	579	596
11	2565	2521
12	757	741
13	1637	1636

H= 4 K= 2

0	1783	1794
1	1790	1697
2	925	939
3	642	621
4	3771	3644
5	1715	1841
6	3026	3052
7	1042	989
8	4688	4793
9	575	592
10	1997	2050
11	1451	1397
12	2767	2914
13	340	337

H= 4 K= 3

0	5904	5891
1	1172	1150
2	2668	2596
3	758	792
4	1001	1170
5	1145	1134
6	3634	3501
7	814	814
8	1765	1783
9	613	629
10	2069	2033

H= 4 K= 3

11	840	821
12	2930	2890

H= 4 K= 4

0	1963	2226
2	1710	1743
4	3062	3043
6	2788	2774
8	3341	3433
10	2443	2320
12	2330	2314

H= 5 K= 0

0	5522	5724
1	906	930
2	8022	8059
3	844	847
4	2506	2469
5	688	705
6	2602	2617
7	537	516
8	7480	7438
9	299	306
10	162	163
11	99	96
12	797	808
13	104	104

H= 5 K= 1

0	1715	1743
1	899	905
2	348	294
3	4757	4686
4	1612	1627
5	267	287
6	53	53
7	2416	2372
8	1302	1307
9	3267	3269
10	234	239
11	384	362
12	835	890
13	3022	3010

H= 5 K= 2

0	2075	2081
1	2302	2257
2	1837	1764
3	4838	4944
4	1424	1445
5	4383	4345
6	2817	2728
7	822	830
8	3569	3646
9	2672	2699
10	1539	1520
11	4091	4015
12	101	101

H= 5 K= 3

0	803	939
1	166	184
2	2233	2251
3	5945	5943
4	2104	2046
5	1619	1588
6	1872	1897
7	2456	2509
8	3609	3721
9	4002	3932
10	1181	1132
11	1502	1592
12	289	288

H= 5 K= 4

0	2513	2449
1	1681	1631
2	2007	1950
3	3028	2964
4	1140	1122
5	2814	2833
6	3277	3369
7	549	565
8	130	129
9	2001	1886
10	2555	2657
11	2258	2268

H= 5 K= 5

0	7309	7254
2	4279	4316
4	336	343
6	4321	4332
8	4472	4234
10	1879	1883

H= 6 K= 0

0	81	78
1	6920	6948
2	5822	5835
3	3262	3293
4	172	199
5	7440	7524
6	5155	4991
7	4716	4649
8	239	239
9	3228	3329
10	4573	4516
11	6258	6144
12	310	310

H= 6 K= 1

0	3153	3183
1	290	303
2	1455	1494
3	227	249
4	1019	1030
5	314	303
6	4027	3944
7	181	182
8	477	479
9	440	453
10	3070	2953
11	125	126
12	1316	1325

H= 6 K= 2

0	3355	3383
1	468	470
2	6652	6727
3	846	836
4	133	129
5	178	172
6	2270	2275
7	320	330
8	1880	1898
9	277	271
10	2997	2942
11	293	302
12	1410	1415

H= 6 K= 3

0	3262	3139
1	4976	4843
2	2630	2533
3	6138	6017
4	1727	1715
5	4067	4115
6	3895	3973
7	4677	4744
8	609	600
9	4951	4724
10	2913	3146
11	3143	3117

H= 6 K= 4

0	2299	2307
1	2925	2993
2	2177	2183
3	427	439
4	2505	2571
5	3857	3957
6	2622	2667
7	1473	1446
8	2655	2535
9	470	495
10	2513	2532

H= 6 K= 5

0	1809	1825
1	523	525
2	378	386
3	3036	3132
4	1247	1264
5	386	381
6	478	461
7	1453	1427
8	885	954
9	1984	1998

H= 6 K= 6

0	6032	6143
2	4199	4122
4	8072	7774
6	1361	1381
8	8374	8309

H= 7 K= 0

0	1865	2181
1	3822	4230
2	1626	1638
3	2997	2996

H= 7 K= 0

4	1305	1269
5	6416	6294
6	2903	2942
7	1039	1062
8	3234	3335
9	881	866
10	1973	1892
11	5507	5838
12	354	353

H= 7 K= 1

0	4770	4546
1	153	149
2	2508	2498
3	389	378
4	722	703
5	317	318
6	2249	2256
7	53	54
8	1826	1869
9	188	181
10	869	874
11	333	332

H= 7 K= 2

0	5604	5469
1	2036	1992
2	3207	3147
3	1860	1854
4	522	523
5	1938	1970
6	2813	2885
7	1783	1833
8	2883	2839
9	1772	1737
10	984	1029
11	1779	1772

H= 7 K= 3

0	3669	3680
1	2164	2173
2	616	624
3	3755	3802
4	669	673
5	3928	4051
6	4159	4260
7	209	204
8	1394	1366
9	1579	1682
10	3062	3036

H= 7 K= 4

0	633	635
1	386	394
2	690	708
3	857	873
4	1112	1141
5	801	791
6	1676	1614
7	115	113
8	2116	2233
9	431	428

H= 7 K= 5

0	1000	1004
1	2746	2722
2	2119	2091
3	3484	3427
4	2070	1977
5	4554	4470
6	1573	1610
7	24	24
8	3970	3945

H= 7 K= 6

0	4307	4200
1	286	281
2	860	840
3	924	935
4	1555	1680
5	42	41
6	2424	2412

H= 7 K= 7

0	4833	4768
2	2785	2785
4	526	524

H= 8 K= 0

0	466	453
1	36	35
2	322	315
3	5255	5106
4	3356	3381
5	1664	1716
6	3803	3823
7	1893	1899
8	5339	5266
9	3220	3104
10	2328	2496
11	1975	1958

H= 8 K= 1

0	669	656
1	1505	1498
2	547	550
3	656	660
4	1526	1531
5	1613	1618
6	415	420
7	954	940
8	2272	2154
9	605	614
10	14	14

H= 8 K= 2

0	318	322
1	1674	1677
2	517	528
3	3695	3735
4	2950	3029
5	3224	3259
6	4050	3981
7	695	662
8	4655	4657
9	2103	2097
10	2922	2913

H= 8 K= 3

0	781	803
1	496	512
2	3911	3977
3	245	251
4	1462	1463
5	448	440
6	891	848
7	165	167
8	2814	2803
9	25	24

H= 8 K= 4

0	6101	6021
1	1960	1932
2	4200	4150
3	1477	1422
4	2397	2278
5	2067	2028
6	403	435
7	1623	1623
8	374	374

H= 8 K= 5

0	1170	1145
1	1237	1208
2	1022	1012
3	2712	2757
4	1095	1160
5	2384	2371
6	1951	1935

H= 8 K= 6

0	2227	2214
1	1969	1966
2	1228	1230
3	688	683
4	2845	2836

H= 9 K= 0

0	5369	5405
1	1381	1394
2	6050	6112
3	3110	3181
4	6523	6569
5	2706	2752
6	3764	3821
7	571	551
8	6965	6800
9	1664	1747
10	3571	3546

H= 9 K= 1

0	939	947
1	1905	1912
2	942	964
3	1822	1879
4	1849	1874
5	2998	2962
6	126	121

H= 9 K= 1

7	184	181
8	2324	2504
9	869	875

H= 9 K= 2

0	30	30
1	2196	2244
2	865	886
3	647	641
4	1421	1403
5	2817	2662
6	1204	1177
7	1369	1465
8	2159	2171

H= 9 K= 3

0	2202	2135
1	4360	4214
2	5447	5245
3	4673	4428
4	1942	1899
5	3811	3880
6	131	135
7	3890	3874

H= 9 K= 4

0	1111	1116
1	496	502
2	1903	1937
3	778	837
4	774	779
5	463	467
6	2233	2228

H= 9 K= 5

0	2232	2236
1	1097	1104
2	1449	1445
3	2783	2766
4	808	814

H= 10 K= 0

0	9168	9327
1	557	562
2	4836	4890
3	521	533
4	3025	2987
5	538	517
6	3329	3256
7	446	465
8	1205	1203
9	411	413

H= 10 K= 1

0	1210	1187
1	824	812
2	467	459
3	1866	1804
4	1006	949
5	1618	1580
6	158	169
7	319	318
8	766	763

H= 10 K= 2

0	1769	1679
1	1397	1334
2	2361	2303
3	4409	4320
4	1022	1043
5	2807	2938
6	5553	5573
7	1194	1197

H= 10 K= 3

0	1553	1677
1	2849	3068
2	339	357
3	1034	1028
4	520	522
5	4271	4246

H= 10 K= 4

0	1395	1382
1	1165	1156
2	1348	1342
3	2357	2375

H= 11 K= 0

0	2293	2195
1	1027	973
2	408	387
3	3264	3201
4	1248	1256
5	236	253
6	560	559
7	1839	1829

H= 11 K= 1

0	2609	2620
1	258	261
2	1226	1248
3	450	484
4	787	792
5	580	584
6	3386	3378

H= 11 K= 2

0	2656	2620
1	126	125
2	1568	1568
3	427	427
4	625	623

H= 11 K= 3

0	357	359
1	1536	1549

H= 12 K= 0

0	2140	2210
1	2174	2211
2	2686	2650
3	7813	7821
4	568	563
5	302	304

H= 12 K= 1

0	2876	2855
1	1563	1554
2	2422	2414
3	2164	2182

APPENDIX D: OBSERVED AND CALCULATED STRUCTURE FACTOR AMPLITUDES (×10) FOR $Hf_{10.0}Nb_{3.0}S_{3.0}$ FROM Mo Kα X-RAY SINGLE CRYSTAL DATA

k	l	Fo	Fc	sigF	k	l	Fo	Fc	sigF	k	l	Fo	Fc	sigF
^^^^^^^	h =	0	^^^^^^^		8	0	710	938	0*	6	2	442	515	0*
					8	1	0	172	0*	6	4	513	472	0*
0	2	509	455	81	8	3	2946	2864	0	7	-2	1386	1396	45
0	4	5748	5706	91	8	8	1617	1674	0	7	4	360	239	0*
0	6	8008	8081	0	9	-7	400	169	0*	8	-4	605	516	0*
0	8	585	405	0*	9	2	2957	2807	65	8	-3	292	367	0*
0	10	3300	3348	87	9	3	1702	1646	50	8	-1	871	889	0*
0	12	3119	3201	88	9	4	2741	2639	0	8	2	0	300	0*
1	-8	769	666	0*	10	-5	409	444	0*	9	-4	375	377	0*
1	-2	480	324	71	10	-4	0	90	0*	9	0	198	114	0*
1	-1	417	393	47	10	0	3262	3227	0	9	1	1285	1244	78
1	0	122	130	0*	10	3	695	520	0*	10	-3	813	737	0
1	10	321	159	0*						10	2	0	210	0*
2	-10	980	902	88	^^^^^^^	h =	1	^^^^^^^						
2	-8	2936	3002	64						^^^^^^^	h =	2	^^^^^^^	
2	-5	2620	2616	53	0	-12	544	401	0*					
2	-4	2452	2443	50	0	-9	1634	1660	45	0	-11	1666	1651	48
2	-3	5861	5885	91	0	-7	1320	1233	38	0	-2	2341	2362	45
2	6	1886	1901	47	0	-4	412	498	73*	0	-1	969	977	33
2	9	2469	2464	76	0	-3	4396	4451	69	0	0	717	639	52
3	-11	3496	3504	72	0	5	895	947	37	0	7	1391	1362	39
3	-10	1771	1807	49	0	6	474	509	0*	0	12	370	131	0*
3	-9	511	531	0*	0	11	933	919	0	1	-10	0	171	0*
3	-8	654	678	0*	1	-10	150	511	0*	1	-6	636	730	62
3	-4	1420	1456	43	1	-6	1237	1241	49	1	-4	1443	1423	44
3	-3	348	401	0*	1	-2	725	772	0	1	-3	738	725	90
3	1	6991	6904	0	1	0	1095	1000	50	1	-2	4474	4497	71
4	-11	1057	1227	80	1	4	772	777	51	1	0	2473	2479	73
4	-10	1307	1246	0	1	8	1254	1345	70	1	12	573	255	0*
4	-8	126	309	0*	1	12	287	80	0*	2	-10	0	480	0*
4	1	312	274	0*	2	-8	2719	2685	66	2	-4	651	690	0*
5	-11	467	56	0*	2	-7	534	399	0*	2	0	5331	5378	91
5	-7	660	322	0*	2	-5	713	689	93	2	2	3152	3127	60
5	1	821	733	62	2	1	1037	1032	31	2	6	1981	1951	76
5	9	193	122	0*	2	9	299	153	0*	2	8	1560	1476	58
6	-10	1249	1197	65	2	11	0	140	0*	3	-5	1996	1957	50
6	-9	1031	993	0*	3	-11	604	623	0*	3	-4	762	756	96
6	-8	606	592	0*	3	-5	1052	1016	44	3	-1	318	393	0*
6	-7	1964	1956	52	3	0	411	586	0*	3	0	2218	2188	56
6	-6	1803	1792	74	4	-11	1178	1275	0	3	2	1307	1348	35
6	-5	4148	4024	0	4	-7	112	211	0*	4	-10	355	529	0*
6	-2	2658	2636	84	4	-6	565	544	92	4	-8	1502	1516	63
6	0	917	971	0*	4	-5	1990	1921	86	4	-7	862	640	0*
6	1	4209	4212	93	5	-9	1251	1351	0	4	-6	1182	1249	59
7	-7	0	41	0*	5	-8	548	646	0*	4	-5	1192	1238	68
7	-6	1024	1035	63	5	-6	359	257	0*	4	3	677	621	0*
7	-2	1787	1881	71	5	1	322	97	0*	5	-6	1601	1672	51
8	-7	869	784	0*	5	7	945	953	65	5	-5	2763	2777	84
8	-5	1117	1125	0	6	-9	311	63	0*	5	-4	654	558	0*
8	-2	286	457	0*	6	-3	364	301	0*	5	-2	1078	1108	72

k	l	Fo	Fc	sigF
5	1	1805	1741	50
6	-9	233	130	0*
6	-8	1378	1403	57
6	-5	416	158	0*
6	-3	488	520	0*
6	0	1611	1568	60
6	4	688	494	84
7	-8	1198	1251	0
7	-5	755	631	0*
7	-4	572	392	0*
8	-6	1435	1468	99
8	1	1159	1113	57
8	3	1835	1809	72
9	-1	803	774	0
9	3	0	40	0*
9	4	643	578	0*

^^^^^^^ h = 3 ^^^^^^^

k	l	Fo	Fc	sigF
0	-12	994	855	0*
0	-7	2307	2341	74
0	-6	3767	3827	67
0	-5	6717	6759	0
0	-2	1092	1143	37
0	0	5294	5212	86
1	-7	671	675	0*
1	-6	508	290	0*
1	-4	1498	1527	40
1	-3	676	649	50
1	1	1110	1131	33
1	2	1519	1553	39
1	8	1525	1468	46
1	9	444	484	0*
1	10	547	218	0*
2	-11	1580	1553	50
2	-10	404	593	0*
2	-8	2067	2044	52
2	-7	1213	1219	51
2	-6	1762	1785	48
2	-3	4926	4982	79
2	9	1918	2002	50
3	-10	2448	2240	0
3	-6	4509	4461	86
3	-2	2399	2490	62
3	0	7514	7495	0
3	4	3902	3951	76
3	8	1297	1231	98
4	-10	0	591	0*
4	-6	1727	1660	47
4	-3	845	786	78
4	-2	2256	2323	0
4	0	3180	3141	71
4	1	1050	1127	44
4	9	517	390	0*
5	-9	1661	1596	91
5	-8	1642	1731	0
5	-7	935	911	0*
5	-4	1070	1114	52
5	-1	0	469	0*
5	0	748	737	0*
5	2	1648	1635	45
6	-7	1738	1756	76
6	-6	1801	1735	48
6	-4	878	922	68
6	-1	2329	2388	59
6	0	1791	1885	78
6	3	2883	2922	66
6	8	0	156	0*
7	-4	0	156	0*
7	-2	240	139	0*
7	-1	406	495	0*
7	0	1911	1891	64
7	6	1710	1723	54
8	-5	0	237	0*
8	2	1545	1537	53
8	4	734	487	97
9	-2	2179	2192	57
9	1	1609	1615	55

^^^^^^^ h = 4 ^^^^^^^

k	l	Fo	Fc	sigF
0	-9	1369	1338	56
0	-7	826	757	0*
0	-6	2177	2157	53
0	-5	1395	1421	43
0	-3	3510	3543	70
0	-2	1782	1736	0
0	0	1183	1252	52
0	4	0	253	0*
1	-10	0	271	0*
1	-9	977	928	68
1	-4	451	511	0*
1	-2	0	55	0*
1	-1	1227	1202	35
1	0	0	52	0*
1	3	2323	2276	52
1	8	688	669	0*
2	-9	0	264	0*
2	-4	1079	1009	46
2	0	379	338	0*
2	1	1410	1422	37
2	2	207	112	0*
3	-8	1482	1567	54
3	-5	955	927	78
3	-4	370	142	0*
3	7	631	573	0
4	-8	1005	934	0*
4	-4	765	762	0*
4	-2	0	204	0*
4	0	0	215	0*
4	6	937	863	87
5	-8	0	42	0*
5	-6	1375	1420	53
5	-1	1136	1139	50
5	0	1345	1403	0
5	4	696	535	0*
6	-6	0	198	0*
6	-5	1425	1495	57
6	-4	1099	1072	58
6	-3	1020	915	60
6	-1	980	1044	61
7	-4	574	298	0*
7	0	740	646	0*
7	2	550	329	0*
8	0	2275	2380	79
8	3	534	410	0*

^^^^^^^ h = 5 ^^^^^^^

k	l	Fo	Fc	sigF
0	-10	459	474	0*
0	-8	3859	3932	0
0	-6	2356	2328	58
0	-5	651	455	0*
0	-4	1524	1441	58
0	-3	540	651	97*
0	-2	5328	5210	0
0	0	4703	4685	82
1	-10	0	62	0*
1	-5	676	689	91
1	-4	1058	1055	51
1	-3	2790	2749	81
1	0	1300	1263	50
1	2	624	587	99
2	-10	668	713	0*
2	-8	1713	1656	54
2	-3	3115	3079	62
2	0	1820	1879	57
2	7	326	247	0*
2	9	1487	1338	54
3	3	3131	3210	63

k	l	Fo	Fc	sigF
3	5	1505	1422	59
3	6	1057	987	57
4	-7	310	164	0*
4	-3	1532	1605	60
4	-2	777	789	77
4	5	1592	1674	51
5	-6	2390	2466	0
5	-2	2071	2123	0
5	0	4058	4158	0
5	4	0	166	0*
6	2	387	237	0*
6	4	0	292	0*
7	-1	1355	1475	60
7	4	465	623	0*

^^^^^^^ h = 6 ^^^^^^^

k	l	Fo	Fc	sigF
0	-4	961	954	55
0	-3	1635	1534	46
1	-10	967	992	0
1	-8	567	412	0*
1	-7	0	231	0*
1	-6	1872	1858	57
1	-5	375	562	0*
1	-1	719	681	65
1	0	2053	1998	66
2	-7	0	167	0*
2	-6	0	108	0*
2	1	514	363	0*
2	2	2862	2864	63
3	-2	1245	1187	49
3	5	1771	1746	49
4	-7	0	187	0*
4	-2	431	193	0*
4	0	866	1038	95
5	-6	0	152	0*
5	-5	0	286	0*
5	-1	153	192	0*
5	0	429	550	0*
5	3	1397	1512	61
6	-2	2100	2159	93
6	0	1839	1743	89
6	4	2182	2433	88

^^^^^^^ h = 7 ^^^^^^^

k	l	Fo	Fc	sigF
0	-9	1037	977	0
0	-8	2028	1943	56
0	-5	3073	2955	0
0	-4	1288	1229	72
0	-3	2775	2686	0
0	0	749	869	0
0	1	1916	1904	52
1	-9	0	103	0*
1	-8	1087	1037	70
1	-7	125	16	0*
1	-6	1368	1386	84
1	-5	437	181	0*
1	-3	411	158	0*
1	0	2692	2672	97
1	1	0	141	0*
2	-7	267	564	0*
2	-6	1899	1879	61
2	-3	644	628	0
2	-2	1373	1288	74
2	-1	598	718	0*
2	0	3343	3379	80
3	-5	1433	1464	58
3	3	2613	2750	64
3	7	194	582	0*
4	-6	740	752	0*
4	-3	530	408	0*
4	1	0	174	0*
4	5	258	281	0*
5	0	889	818	0
5	2	819	912	0
5	3	1494	1531	82

^^^^^^^ h = 8 ^^^^^^^

k	l	Fo	Fc	sigF
0	-6	1516	1433	52
0	-4	903	831	0
1	-7	267	408	0*
1	-5	694	830	0*
1	0	451	61	0*
1	6	0	272	0*
2	-5	1776	1805	68
2	-4	714	581	0*
2	-2	529	276	0*
2	0	1028	962	0*
3	-3	0	186	0*
3	0	428	686	0*
3	1	446	321	0*
4	1	339	690	0*
4	2	1199	1176	66

^^^^^^^ h = 9 ^^^^^^^

k	l	Fo	Fc	sigF
0	-6	1471	1313	0
0	-5	1381	1328	69
0	-1	827	762	96
0	0	2192	2186	0
1	-5	1736	1596	53
1	-3	912	781	0
1	2	0	138	0*
1	6	0	350	0*
2	-2	864	616	88
2	0	0	68	0*
3	0	879	1022	0*

^^^^^^^ h = 10 ^^^^^^^

k	l	Fo	Fc	sigF
0	1	0	557	0*
0	2	2493	2513	75
1	-1	855	582	0*
1	0	351	320	0*

^^^^^^^ h = 11 ^^^^^^^

k	l	Fo	Fc	sigF
0	0	1049	848	0
0	1	149	58	0*

APPENDIX E: OBSERVED AND CALCULATED STRUCTURE FACTOR AMPLITUDES (×10) FOR $Zr_{8.1}Nb_{4.9}S_{2.7}$ FROM Mo Kα X-RAY SINGLE CRYSTAL DATA

k	l	Fo	Fc	sigF	k	l	Fo	Fc	sigF	k	l	Fo	Fc	sigF
^^^^^^^	h =	0	^^^^^^^		7	-1	892	902	19	5	5	89	99	57*
					8	-7	662	646	17	5	8	431	451	13
0	2	385	386	11	8	-6	610	625	16	5	9	694	703	24
0	4	4385	4343	66	8	-5	476	484	26	6	-8	215	148	40*
0	6	3716	3666	57	8	-4	616	610	16	6	-6	947	962	24
0	8	657	666	22	8	0	0	13	82*	6	-5	99	104	68*
0	10	2207	2176	37	8	2	151	106	43*	6	0	672	690	28
0	12	1496	1585	31	8	8	971	989	35	6	1	89	79	64*
1	-10	85	92	66*	9	-5	476	486	14	6	2	558	562	15
1	-9	559	526	15	9	-3	455	446	14	7	-2	706	687	17
1	-3	2073	2036	32	9	0	1540	1517	30	7	1	0	16	67*
1	-2	126	31	16	10	-2	1058	980	24	7	8	252	254	55*
1	-1	107	109	16	10	0	1701	1674	33	8	-7	268	232	47*
1	0	652	643	12	11	0	380	318	55	8	-3	317	300	16
1	5	635	617	15						8	1	376	370	14
1	6	210	199	21	^^^^^^^	h =	1	^^^^^^^		8	4	510	525	14
1	8	740	710	17						9	-5	586	583	16
2	-8	1630	1611	26	0	-12	463	481	13	9	-4	553	538	30
2	-3	3149	3099	48	0	-4	788	753	14	9	-2	213	147	30
2	0	222	190	41*	0	7	781	733	16	9	0	523	496	18
2	2	659	690	13	0	11	373	383	14	9	3	354	338	36
2	10	849	837	22	1	-10	426	405	19	10	3	299	302	27
3	-12	200	180	44*	1	-6	632	622	26					
3	-9	901	894	19	1	0	142	109	27*	^^^^^^^	h =	2	^^^^^^^	
3	-6	2045	1972	32	1	2	133	170	28*					
3	0	2258	2468	63	1	4	611	556	39	0	-11	373	378	14
4	-11	564	563	18	1	8	829	808	57	0	-9	1039	1029	20
4	-9	225	191	43*	1	12	287	317	79*	0	-5	933	913	17
4	-3	1115	1104	19	2	-11	87	37	64*	0	-4	1401	1346	22
4	-2	1372	1355	26	2	-8	1329	1287	23	0	-1	117	132	38*
4	6	1297	1248	22	2	-6	299	258	11	0	6	1141	1081	19
5	-11	0	4	75*	2	-5	142	145	59*	0	7	1318	1268	22
5	-8	1824	1811	30	2	-1	275	295	17	0	12	412	435	21
5	-7	152	128	41*	2	12	63	158	70*	1	-10	229	191	35
5	0	1857	1932	30	3	-11	445	450	21	1	-7	115	72	60*
5	2	2882	2979	49	3	-8	716	692	18	1	-4	536	516	14
5	4	486	457	13	3	-5	709	701	21	1	0	1091	1170	19
6	-10	851	892	21	3	-4	622	566	19	1	2	2843	2823	43
6	-9	827	844	21	3	-1	822	868	15	1	3	213	227	39*
6	-8	72	24	70*	3	2	238	239	28	1	9	0	8	67*
6	-7	1041	1017	28	3	9	523	503	14	2	-10	58	242	85*
6	-4	230	245	37	4	-11	500	506	14	2	-8	160	184	58*
6	-3	947	970	19	4	-9	184	174	34*	2	-6	419	444	28
6	0	431	442	48	4	-7	243	213	29	2	-4	1109	1078	21
6	2	1418	1441	24	4	-4	497	472	14	2	-2	1605	1611	26
7	-9	111	15	70*	4	0	377	367	14	2	0	2781	3012	44
7	-7	0	7	71*	4	3	844	849	17	3	-11	549	549	15
7	-6	724	737	25	5	-7	838	848	19	3	-9	679	684	18
7	-5	1387	1399	24	5	0	572	557	19	3	-8	1210	1223	22
7	-4	261	256	16	5	4	568	566	15	3	-3	2259	2300	35

k	l	Fo	Fc	sigF
3	-1	38	29	55*
3	0	543	567	25
3	4	609	589	16
4	-10	223	296	41*
4	-9	126	182	53*
4	-8	1092	1081	21
4	-3	412	416	11
4	-1	462	481	12
4	0	624	620	21
5	-9	222	237	60*
5	-8	861	847	34
5	-7	253	280	19
5	-6	760	767	19
5	-3	1060	1076	24
5	4	299	285	32
5	10	526	542	16
6	-7	129	6	62*
6	-6	492	465	14
6	-5	76	84	69*
6	-4	0	79	68*
6	-3	106	76	53*
6	0	810	825	24
7	-8	385	372	61
7	-6	275	238	36
7	-4	268	263	29
7	-2	779	794	21
7	1	607	604	18
8	-1	528	513	14
8	0	110	200	89*
8	2	13	63	73*
9	-1	429	401	15
9	2	78	47	73*

^^^^^^^ h = 3 ^^^^^^^

k	l	Fo	Fc	sigF
0	-11	1822	1821	30
0	-10	1273	1266	26
0	-8	362	340	16
0	-7	1148	1118	20
0	-3	675	667	14
0	-2	904	907	16
0	-1	3540	3788	95
0	4	797	798	15
0	5	3788	3722	57
1	-10	449	461	23
1	-7	636	600	16
1	-6	551	520	14
1	-3	799	769	23
1	0	0	92	63*
2	-10	425	434	13
2	-7	937	904	19
2	-6	702	695	20
2	-5	867	854	18
2	2	616	658	15
3	-10	1430	1445	30
3	-6	2243	2224	37
3	-2	1196	1249	29
3	0	4105	4250	64
3	4	2513	2556	40
3	8	1028	1006	25
4	-10	419	438	15
4	-3	119	165	56*
4	-1	222	224	45*
4	0	1751	1763	30
5	-8	873	929	22
5	-7	806	832	21
5	-3	1614	1668	27
5	-2	619	636	16
5	0	0	85	93*
5	1	0	88	61*
5	4	597	600	23
5	5	501	500	14
6	0	801	765	33
6	1	1361	1344	24
6	2	800	789	24
6	4	395	408	21
7	-7	194	161	50*
7	-5	878	872	22
7	-3	703	733	18
7	-2	151	56	72*
7	0	630	609	23
7	1	495	460	22
7	6	765	787	30
8	1	94	87	68*
9	-2	989	980	25
9	-1	899	857	23

^^^^^^^ h = 4 ^^^^^^^

k	l	Fo	Fc	sigF
0	-10	886	868	20
0	-8	217	208	52*
0	-5	912	887	17
0	-4	91	112	56*
0	0	37	89	63*
0	1	389	399	17
0	7	276	279	23
1	-10	111	217	69*
1	-8	457	471	12
1	-6	301	294	13
1	-5	999	981	24
1	-2	186	150	58*
1	-1	565	612	16
2	-7	259	281	39
2	-6	479	471	14
2	-5	364	354	18
2	2	51	19	53*
2	4	985	986	19
3	-9	154	77	48*
3	-7	118	122	47*
3	-6	574	606	16
3	-5	222	180	40*
3	-4	563	570	25
3	-2	839	848	22
3	8	229	239	50*
4	-8	701	710	22
4	-4	494	529	19
4	0	180	175	44*
4	2	263	271	25
4	6	665	670	23
5	-6	731	805	36
5	-5	428	449	20
5	-2	791	785	28
6	-1	656	642	17
7	2	0	35	74*
7	3	137	37	77*
7	4	201	244	33
8	-2	743	701	19
8	-1	506	475	15
8	3	420	417	16

^^^^^^^ h = 5 ^^^^^^^

k	l	Fo	Fc	sigF
0	-10	212	191	30
0	-9	0	61	72*
0	-6	357	303	26
0	-5	260	216	24
0	-3	284	290	19
0	1	338	342	11
1	-10	244	241	38
1	-6	192	177	22
1	-3	1552	1578	25
1	1	382	395	16
1	2	0	56	61*
2	-2	299	271	34
2	-1	733	769	18
2	0	577	604	29
2	5	1248	1288	32
3	-9	670	686	17
3	-6	418	449	19
4	-8	0	101	77*

k	l	Fo	Fc	sigF
4	-7	261	305	37
4	-4	263	282	19
4	0	460	463	16
4	1	207	180	56*
4	3	711	707	37
5	-6	839	796	37
5	0	2015	1960	40
5	2	987	930	39
5	4	523	506	24
6	-4	369	382	18
6	0	329	318	23
7	-4	537	547	26
7	0	144	145	77*
7	1	504	499	27
7	2	492	462	15
7	3	506	458	23

^^^^^^^ h = 6 ^^^^^^^

k	l	Fo	Fc	sigF
0	-6	1295	1275	23
0	-1	2177	2215	34
0	5	2205	2209	35
1	-10	641	702	17
1	-9	147	125	59*
1	-7	25	100	69*
1	-4	215	211	20
1	-3	110	80	65*
2	-9	113	24	75*
2	-8	669	668	17
2	-2	1855	1846	30
2	1	139	131	62*
3	-8	76	59	75*
3	-7	945	984	22
3	-6	952	977	22
3	-5	1099	1127	22
3	3	1299	1315	24
4	-6	469	469	28
4	-5	854	881	34
4	0	382	369	32
4	2	440	433	15
4	3	229	173	27
4	4	360	385	16
4	7	176	151	43*
5	-6	0	71	82*
5	-5	0	123	70*
5	-2	0	3	81*
5	-1	176	162	45*
5	3	800	764	24
6	-2	945	905	30
6	0	1133	1202	42
6	4	1352	1349	73

^^^^^^^ h = 7 ^^^^^^^

k	l	Fo	Fc	sigF
0	-8	683	702	23
0	-3	753	750	19
0	-2	202	230	63*
0	0	467	488	24
1	-9	114	12	75*
1	-7	131	6	59*
1	-6	431	439	13
1	-5	80	14	62*
1	-4	472	475	13
1	0	1481	1437	28
1	3	70	18	54*
2	-7	421	460	15
2	-5	545	545	15
2	-3	553	547	18
2	0	1161	1131	26
3	-4	75	1	68*
4	-6	333	324	26
4	-5	0	43	84*
4	-1	115	45	74*
4	0	0	8	88*

^^^^^^^ h = 8 ^^^^^^^

k	l	Fo	Fc	sigF
0	-1	115	81	63*
0	3	1420	1422	44
1	-6	0	116	76*
1	-5	305	307	17
1	0	267	258	52*
1	2	280	256	29
2	-5	859	861	21
2	-4	351	361	16
2	-3	630	635	17
2	6	693	724	19
3	-5	157	32	55*
3	-4	204	185	90*
3	-2	1105	1072	23
3	0	389	361	24
3	3	128	94	65*
4	0	991	953	47

^^^^^^^ h = 9 ^^^^^^^

k	l	Fo	Fc	sigF
0	-7	0	127	77*
0	-6	822	817	22
0	-4	1483	1502	27
0	-1	266	264	26
0	2	1234	1205	24
1	-1	355	378	17
1	6	0	48	81*
2	-4	326	319	30
2	-3	351	373	18
2	0	254	174	37
3	0	314	302	46

^^^^^^^ h = 10 ^^^^^^^

k	l	Fo	Fc	sigF
0	-3	0	17	77*
0	-1	113	16	68*
0	4	524	539	14
0	5	0	15	95*
1	-2	217	178	44*
1	-1	293	270	43
1	0	181	152	75*

APPENDIX F: OBSERVED AND CALCULATED STRUCTURE FACTOR AMPLITUDES (×10) FOR $Hf_9V_4SO_{0.6}$ FROM Mo Kα X-RAY SINGLE CRYSTAL DATA

k	l	Fo	Fc	sigF	k	l	Fo	Fc	sigF	k	l	Fo	Fc	sigF
^^^^^^^	h =	0	^^^^^^^		-3	0	2724	2698	72	-6	6	660	674	0*
					-3	3	1336	1335	36	-6	8	863	765	86
0	2	1197	1248	58	-3	5	1371	1360	73	-6	9	0	522	0*
0	4	6568	6582	0	-2	-10	945	1015	0	-5	0	3179	3189	0
0	6	5516	5462	0	-2	-8	561	888	0*	-5	2	860	868	0
0	8	575	779	0*	-2	-6	854	830	0*	-5	8	943	991	95
0	10	5580	5622	0	-2	0	1447	1533	86	-5	9	637	641	0*
1	-2	758	851	0	-1	-7	2368	2373	50	-4	0	5257	5461	0
1	0	0	785	0*	-1	6	916	893	0	-4	2	2469	2350	59
2	-4	1690	1640	52	-1	8	448	126	0*	-4	4	2085	2071	66
2	2	4443	4435	72	-1	10	713	662	0*	-4	6	1654	1662	89
2	10	661	583	0*	0	-5	1591	1553	39	-3	1	1649	1646	59
3	-9	2325	2374	56	0	-1	0	195	0*	-3	4	0	45	0*
3	-6	2398	2408	68	0	3	3725	3682	62	-3	6	0	121	0*
3	-5	6382	6485	0	0	4	702	473	70	-3	10	955	1015	99
3	-3	0	130	0*	0	9	112	320	0*	-2	-9	0	302	0*
3	-2	366	57	0*	1	-2	676	811	0*	-2	-8	3161	3211	69
3	0	4708	4637	0	1	4	351	258	0*	-2	-5	3791	3821	66
4	-10	651	561	0*	2	-7	994	951	0	-2	0	166	499	0*
4	-8	505	587	0*	3	-7	406	71	0*	0	-7	3007	2918	64
4	-6	0	489	0*	3	8	1253	1213	52	0	-6	631	538	95
4	4	0	46	0*	4	-9	634	710	0*	0	-3	4728	4650	76
5	-4	628	94	0*	5	-6	755	876	0	0	-1	1094	1152	0
5	0	4195	4192	0	5	-5	1103	1212	0	1	-9	802	827	0
6	0	674	628	0*	6	-6	713	697	0*	1	-2	4439	4433	71
8	-6	1240	1246	0	6	-4	180	326	0*	1	8	2437	2448	51
9	-3	1370	1233	93	6	-3	488	29	0*	2	8	1283	1293	0
9	-1	799	829	0*	6	8	809	663	0*	2	10	2378	2276	65
					7	-6	1211	1174	0	3	-7	3444	3504	67
^^^^^^^	h =	1	^^^^^^^		7	3	557	362	0*	3	5	1724	1791	55
										4	7	0	275	0*
-9	1	1053	954	0	^^^^^^^	h =	2	^^^^^^^		5	-6	1255	1204	0
-9	3	434	583	0*						5	2	1078	960	0
-8	-2	974	873	0	-10	0	1394	1506	97	6	-7	1001	1045	79
-8	4	1352	1386	0	-9	2	1999	1938	64	6	-5	760	852	0*
-7	-7	404	17	0*	-9	3	539	497	0*	8	-2	250	447	0*
-7	1	0	279	0*	-9	4	896	815	95	8	-1	1612	1553	0
-7	2	0	505	0*	-8	-1	1158	1170	76					
-6	2	1086	1117	0	-7	-4	730	793	0*	^^^^^^^	h =	3	^^^^^^^	
-6	4	1355	1358	49	-7	0	2427	2475	69					
-6	7	1471	1461	94	-7	1	2023	2081	53	-10	-2	1635	1518	63
-5	-1	1632	1593	47	-7	3	1915	1926	58	-10	4	652	318	0*
-5	0	257	175	0*	-7	5	3841	3801	0	-8	1	554	538	0*
-5	2	447	302	0*	-7	7	1395	1290	0	-8	2	3020	3036	0
-5	3	1266	1315	87	-6	-2	889	564	0*	-8	3	2423	2415	64
-5	5	2817	2745	89	-6	0	1098	1134	0	-8	4	1431	1435	0
-5	7	798	840	0*	-6	1	1122	990	72	-8	5	2004	2026	72
-5	8	656	510	0*	-6	3	283	303	0*	-8	7	1747	1748	68
-4	3	0	89	0*	-6	4	435	200	0*	-7	-1	531	211	0*
-4	5	552	383	96*	-6	5	1046	1138	0	-7	0	2638	2730	0

k	l	Fo	Fc	sigF	k	l	Fo	Fc	sigF	k	l	Fo	Fc	sigF
-7	2	2777	2761	87	3	6	667	449	0*	0	-4	783	737	0
-7	3	630	339	0*	4	-6	702	614	0*	0	-2	1451	1491	90
-7	5	0	100	0*	5	0	1111	1304	0	0	1	2980	2934	68
-7	7	544	242	0*	5	4	707	733	0*	2	0	974	939	0
-6	-6	2809	2944	72						5	0	0	142	0*
-6	0	5753	5869	0	^^^^^^^ h =		5 ^^^^^^^							
-6	2	1027	1066	83						^^^^^^^ h =		7 ^^^^^^^		
-6	4	3645	3562	0	-10	0	4601	4718	0					
-6	8	938	822	0	-10	4	1929	2043	0	-10	3	1891	1899	98
-5	-6	1614	1569	43	-9	-5	1882	1975	0	-9	-1	458	555	0*
-5	-1	632	636	0*	-6	0	1526	1538	0	-9	0	2591	2750	74
-5	3	4956	5053	0	-6	3	2143	2071	70	-8	-1	0	97	0*
-5	4	1097	1129	80	-5	-6	521	285	0*	-8	0	2962	3032	79
-4	0	345	102	0*	-5	-5	1650	1695	70	-7	-3	3274	3098	0
-4	2	1322	1327	86	-5	-2	5854	5961	96	-7	-2	1169	1134	76
-4	6	226	67	0*	-5	-1	2027	2063	64	-7	1	0	599	0*
-4	9	356	105	0*	-5	3	1991	1917	99	-7	5	2520	2453	0
-4	10	0	312	0*	0	-9	1211	1161	70	-7	6	981	961	0*
-3	-10	2403	2442	57	0	-7	1382	1422	63	-7	7	2345	2228	0
-3	4	2089	2072	57	0	8	3937	3884	79	0	-4	426	551	0*
-3	8	439	526	0*	1	-8	993	1004	81	0	0	2123	2110	71
0	-7	0	91	0*	1	1	505	90	0*	1	5	0	59	0*
0	-1	5204	5197	0	2	-8	991	1019	0	2	5	0	496	0*
1	1	282	317	0*	3	-6	874	826	0*	3	-1	613	743	0*
1	4	523	634	0*	3	0	0	303	0*	3	0	554	675	0*
6	0	1572	1492	0	4	1	603	945	0*					
					5	-2	1540	1496	0	^^^^^^^ h =		8 ^^^^^^^		
^^^^^^^ h =		4 ^^^^^^^												
					^^^^^^^ h =		6 ^^^^^^^			-10	3	736	817	0*
-11	0	931	687	0						-9	-4	447	87	0*
-10	-1	0	323	0*	-11	-1	518	768	0*	-9	-2	0	60	0*
-10	0	0	328	0*	-10	2	632	233	0*	-8	-4	983	934	0
-10	4	576	153	0*	-10	3	1144	1138	68	-8	-1	1003	921	0
-9	2	579	429	0*	-9	-5	908	840	0	-8	2	445	263	0*
-9	3	1266	1289	0	-9	-1	1213	1336	0	-8	3	3355	3273	0
-9	6	1015	978	79	-9	2	447	472	0*	0	-5	766	497	0*
-8	-2	0	247	0*	-9	3	1906	1872	60	0	0	2301	2181	0
-8	0	968	672	0*	-9	4	685	869	0*	1	-5	1091	1004	0*
-8	4	529	319	0*	-9	6	1161	1089	0	1	0	432	382	0*
-7	-8	1722	1771	52	-8	2	2677	2621	60					
-7	4	375	511	0*	-8	3	1302	1378	89	^^^^^^^ h =		9 ^^^^^^^		
-5	6	322	250	0*	-8	4	0	353	0*					
-4	-7	2053	2022	52	-8	6	557	442	0*	-10	-1	0	379	0*
-4	-2	321	246	0*	-7	0	1127	1255	0	-9	0	991	996	0*
-4	-1	423	300	0*	-7	5	200	382	0*	0	2	1877	1862	66
0	-9	418	52	0*	-6	-7	863	692	0	1	0	566	67	0*
0	-5	1879	1906	56	-6	3	826	805	0					
0	-3	3043	2990	0	-6	5	3519	3478	0					
0	0	598	556	0*	0	-8	755	743	0*					
1	-4	920	195	0*	0	-6	866	941	0*					

APPENDIX G: OBSERVED AND CALCULATED STRUCTURE FACTOR AMPLITUDES (×10) FOR Zr_9V_4S FROM Mo Kα X-RAY SINGLE CRYSTAL DATA

k	l	Fo	Fc	sigF
^^^^^^^ h = 0 ^^^^^^^				
0	2	248	62	82*
0	4	3878	3829	59
0	6	2864	2845	46
0	8	183	130	94*
0	10	2745	2741	47
^^^^^^^ h = 1 ^^^^^^^				
0	-11	0	72	0*
0	-10	74	235	0*
0	-6	329	328	25
0	-5	828	780	26
0	-3	1660	1685	36
0	-2	282	327	73*
0	-1	0	5	65*
0	0	119	137	65*
0	4	95	201	83*
0	7	1002	1011	30
0	8	0	222	0*
0	9	95	96	0*
1	-4	97	181	63*
1	-2	330	343	15
1	0	355	363	16
1	6	389	399	47
1	8	570	583	33
1	10	462	451	27
^^^^^^^ h = 2 ^^^^^^^				
0	-10	396	379	30
0	-8	1419	1453	31
0	-7	1510	1514	66
0	-6	0	61	95*
0	-4	879	819	24
0	-3	2524	2505	51
0	-2	1811	1882	58
0	-1	165	191	0*
0	0	58	171	92*
0	5	1422	1454	43
0	9	69	63	93*
1	-10	288	263	42
1	-9	337	288	48
1	-8	1135	1127	31
1	-7	309	344	49
1	-6	428	337	0*
1	-5	474	505	17
1	-4	143	66	50*
1	-3	536	509	19
1	-2	2503	2495	39
1	0	1222	1238	26
1	1	630	657	22
2	-10	907	946	30
2	-8	331	448	0*
2	-4	1113	1080	48
2	-2	1153	1125	23
2	0	2738	2699	44
2	6	703	685	22
^^^^^^^ h = 3 ^^^^^^^				
0	-10	1204	1206	84
0	-7	173	271	99*
0	-6	1263	1270	91
0	-5	3169	3211	99
0	-4	961	896	25
0	-3	254	287	56*
0	-2	254	265	25
0	0	2062	2122	36
0	1	2770	2823	75
0	8	267	259	38
0	9	1197	1252	60
1	-10	362	333	66*
1	-9	171	237	97*
1	-8	451	478	52
1	-7	221	230	95*
1	-5	452	442	17
1	-4	198	212	48*
1	-2	201	231	89*
1	-1	490	498	17
1	0	0	130	95*
1	3	327	305	19
1	6	211	256	48*
2	-10	785	805	27
2	-9	336	276	33
2	-7	1490	1520	31
2	-6	697	709	51
2	-5	782	783	47
2	-4	328	288	21
2	-3	2240	2242	37
2	-1	325	291	18
2	0	1204	1191	29
2	2	341	345	19
2	8	578	581	23
3	-8	640	645	27
3	-6	1439	1435	29
3	-4	1931	1959	34
3	-2	653	651	30
3	0	3033	3054	50
^^^^^^^ h = 4 ^^^^^^^				
0	-10	412	390	81*
0	-9	0	105	0*
0	-8	248	217	50*
0	-7	718	703	85
0	-6	457	438	32
0	-4	131	5	93*
0	-3	1134	1101	63
0	-2	227	196	55*
0	-1	367	374	19
0	0	408	275	24
0	5	1004	1015	72
1	-9	163	257	94*
1	-8	362	328	30
1	-7	396	414	42
1	-6	139	171	94*
1	-5	1150	1133	33
1	-4	147	248	92*
1	-2	0	35	85*
1	-1	635	634	20
1	0	0	118	98*
1	3	628	647	22
2	-9	0	159	0*
2	-8	519	530	22
2	-7	0	90	0*
2	-5	445	403	19
2	-4	157	196	93*
2	0	0	171	0*
2	1	348	353	21
2	2	316	337	23
2	3	152	82	54*
2	6	268	208	31
3	-8	520	516	22
3	-7	29	175	94*
3	-5	166	135	99*
3	-4	503	508	20
3	-2	1042	1037	41
3	0	1458	1491	34
3	1	0	197	91*
3	3	233	243	45*
3	6	240	304	86*
4	-6	149	178	0*
4	-2	0	7	98*
4	0	0	61	0*
4	4	0	76	97*
^^^^^^^ h = 5 ^^^^^^^				

k	l	Fo	Fc	sigF
0	-9	474	511	36
0	-8	1634	1706	91
0	-7	640	632	23
0	-6	177	91	0*
0	-5	759	757	25
0	-4	161	6	98*
0	-3	882	867	36
0	0	1744	1809	36
0	1	934	941	27
0	2	2840	2889	72
1	-9	138	157	91*
1	-8	426	433	55
1	-7	872	788	30
1	-6	124	213	81*
1	-5	355	356	56
1	-4	596	585	20
1	-3	1121	1092	28
1	-1	233	167	40*
1	0	642	669	31
1	2	303	288	0*
2	-8	530	574	57
2	-7	556	557	22
2	-6	518	498	20
2	-5	1557	1576	43
2	-4	0	145	97*
2	-3	803	833	23
2	-2	377	411	39
2	0	791	836	40
2	1	860	858	29
3	-7	839	828	26
3	-5	796	767	28
3	-4	643	671	23
3	-3	1116	1119	78
3	-2	1199	1186	29
3	0	0	209	0*
3	1	77	123	96*
3	6	295	273	0*
4	-6	509	526	24
4	-4	290	289	0*
4	-3	603	611	36
4	-1	242	290	0*
4	0	494	516	29
4	2	343	335	0*
4	5	740	713	26
5	-2	697	687	34
5	0	1967	1952	44
5	4	898	863	30

^^^^^^^ h = 6 ^^^^^^^

k	l	Fo	Fc	sigF
0	-8	200	272	0*
0	-7	318	422	78*
0	-6	492	492	66
0	-5	1624	1649	60
0	-4	218	279	75*
0	-3	521	512	20
0	0	0	240	0*
0	1	1413	1445	69
0	2	726	731	36
1	-8	224	255	48*
1	-7	0	126	0*
1	-6	466	464	24
1	-5	140	8	81*
1	-4	0	150	0*
1	-3	209	168	53*
1	-2	61	7	0*
1	0	523	538	26
1	1	0	62	97*
2	-7	414	414	27
2	-6	319	305	81*
2	-5	378	363	27
2	-4	0	135	92*
2	-1	434	487	31
2	0	413	412	32
2	2	1255	1250	31
2	3	573	558	20
3	-6	527	523	23
3	-3	779	838	27
3	-2	239	285	41*
3	0	576	559	29
3	1	702	639	35
3	4	143	312	97*
3	5	433	446	0*
4	-3	329	307	36
4	-2	308	281	60*
4	0	329	209	41
4	1	324	298	32
4	4	182	136	0*
5	-2	415	377	66
5	-1	217	282	68*
5	0	129	29	0*

^^^^^^^ h = 7 ^^^^^^^

k	l	Fo	Fc	sigF
0	-7	756	741	27
0	-6	630	628	42
0	-5	1141	1202	73
0	-4	260	323	41
0	-2	0	193	0*
0	-1	431	462	34
0	0	947	979	44
0	3	1064	1079	32
1	-7	0	34	0*
1	-6	417	408	28
1	-5	0	84	0*
1	-3	141	67	84*
1	-2	509	457	22
1	0	1328	1324	39
1	1	0	37	0*
1	4	622	632	22
2	-6	214	156	0*
2	-4	323	259	0*
2	-1	438	391	24
2	0	1002	1035	46
2	2	949	961	34
2	3	370	360	30
2	5	426	349	46
3	-4	130	112	0*
3	-3	642	621	22
3	-1	483	443	24
3	0	289	286	52*
3	2	462	485	28
4	-1	111	30	85*
4	0	0	237	0*

^^^^^^^ h = 8 ^^^^^^^

k	l	Fo	Fc	sigF
0	-6	544	555	26
0	-5	148	212	0*
0	-4	312	323	57*
0	-3	1359	1368	34
0	-1	316	386	88*
0	0	796	828	36
0	2	188	50	0*
1	-4	0	68	0*
1	0	149	51	0*
1	1	207	337	0*
1	2	0	31	0*
1	3	0	196	0*
1	5	389	355	73*
2	-1	540	550	25
2	0	546	537	32
2	2	163	160	0*
2	3	400	399	31

^^^^^^^ h = 9 ^^^^^^^

k	l	Fo	Fc	sigF
0	-4	706	705	25
0	-3	457	462	28
0	-2	733	770	26
0	0	551	573	34
0	1	352	345	34
1	-2	269	256	0*
1	-1	0	100	0*
1	0	40	178	0*

APPENDIX H: OBSERVED AND CALCULATED STRUCTURE FACTOR AMPLITUDES (×10) FOR $Hf_{10.1}Ta_{2.9}S_3$ FROM Mo Kα X-RAY SINGLE CRYSTAL DATA

k	l	Fo	Fc	sigF
^^^^^^^ h = 0 ^^^^^^^				
0	10	5978	6135	0
1	15	4317	3796	0
2	10	4095	4162	0
2	14	2897	3137	0
3	5	2926	3005	0
3	11	2746	2545	0
5	1	4825	5022	0
5	5	10925	11406	0
6	8	4749	4705	0
9	5	3868	3790	0
10	6	4809	4874	0
12	6	7869	7757	0
13	7	4714	4668	0
^^^^^^^ h = 1 ^^^^^^^				
0	11	4979	5073	0
1	4	13532	13863	0
1	8	2899	2821	0
2	1	1274	786	0
2	3	2034	2050	0
2	5	2794	2484	0
3	2	3033	3156	98
3	6	5713	5630	0
5	2	3079	3168	0
5	8	5535	5499	0
6	5	4878	4757	0
6	9	2541	2558	0
7	8	2304	2236	0
7	10	3011	2862	0
11	10	3157	2733	0
^^^^^^^ h = 2 ^^^^^^^				
1	7	9637	9787	0
1	9	3842	3848	0
2	2	4156	4211	0
2	4	9165	9136	0
2	6	2746	2782	0
3	7	5230	4985	0
4	8	2863	2512	0
5	7	5361	5383	0
7	5	6395	6315	0
8	4	3077	3069	0
9	1	4874	4919	0
9	3	3204	3000	0
12	2	4883	4661	0

k	l	Fo	Fc	sigF
^^^^^^^ h = 3 ^^^^^^^				
0	1	2587	2586	0
0	3	15217	15703	0
0	9	3479	3541	0
2	3	9219	9158	0
2	7	5908	5872	0
2	13	4395	4343	0
3	6	8715	8774	0
3	8	8046	7787	0
3	12	6123	5817	0
4	1	5193	5254	0
4	7	4157	3976	0
5	8	3221	3202	0
6	5	3216	3136	0
7	6	3783	3759	0
7	8	3350	3358	0
8	5	3632	3688	0
10	7	2407	2144	0
11	8	2875	3171	0
12	5	2742	2935	0
13	2	3431	3451	0
14	5	2737	2484	0
^^^^^^^ h = 4 ^^^^^^^				
0	0	1629	2053	0
0	4	4835	4828	0
0	6	2905	3005	0
1	11	4374	4000	0
2	4	3165	3057	0
2	6	4027	4148	0
2	10	2669	2457	0
3	1	2342	2430	0
3	5	4002	3966	0
3	11	3385	3091	0
3	13	3138	3330	0
4	4	13168	12817	0
4	12	2294	2430	0
5	1	1878	2011	0
6	2	4999	4984	0
6	4	4583	4670	0
6	10	4850	4755	0
6	12	2881	2796	0
7	5	2955	2964	0
7	9	2471	2707	0
8	8	5151	5252	0
8	10	6081	6078	0
9	5	4828	5036	0
9	11	3033	2885	0

k	l	Fo	Fc	sigF
10	2	3932	3840	0
10	4	4356	4491	0
11	5	4475	4485	0
11	7	3305	3421	0
12	2	3143	3120	0
^^^^^^^ h = 5 ^^^^^^^				
0	1	5511	5895	0
1	10	8485	8534	0
2	3	1652	1663	0
2	5	4695	4567	0
2	13	2960	2761	0
3	2	2980	2813	0
4	1	4509	4450	0
4	5	6384	6225	0
4	13	4939	4685	0
5	8	4454	4596	0
6	3	2261	2425	0
7	4	3737	3824	0
9	2	2428	2264	0
10	1	7436	7278	0
11	4	2849	2727	0
14	1	3235	3373	0
^^^^^^^ h = 6 ^^^^^^^				
0	0	3599	3673	0
0	2	5127	5406	0
0	6	12450	12882	0
1	5	4901	4807	0
2	6	5548	5294	0
3	1	4939	4913	0
3	9	9111	9372	0
3	11	5318	5480	0
4	10	2543	2866	0
4	12	2572	3080	0
5	5	5149	5315	0
5	9	2903	2802	0
5	11	3858	3913	0
6	6	7814	7999	0
6	12	6273	6689	0
7	1	3356	3194	0
9	3	8781	8738	0
10	0	4287	4170	0
10	2	1980	1956	0
10	6	2778	2632	0
11	1	2490	2256	0
11	3	5712	5464	0
13	5	2096	1831	0

k	l	Fo	Fc	sigF
^^^^^^^ h = 7 ^^^^^^^				
0	11	3047	3198	0
1	0	3242	3445	0
1	2	8893	9005	0
1	4	2629	2435	0
2	7	3908	3755	0
2	13	4250	4411	0
6	5	3143	3160	0
7	4	7757	7957	0
7	6	1886	1747	0
8	5	3564	3579	0
8	7	4116	4285	0
8	9	3093	3103	0
9	6	2154	1799	0
10	7	6560	6733	0
^^^^^^^ h = 8 ^^^^^^^				
2	0	5668	5886	0
2	2	9588	9457	0
4	4	3352	3399	0
4	6	2496	2678	0
4	12	3825	4287	0
5	1	5995	5853	0
6	6	4504	4504	0
7	1	3922	3898	0
7	9	4471	4395	0
8	0	2564	2566	0
8	2	4280	4386	0
8	8	6278	6342	0
12	4	2963	3061	0
^^^^^^^ h = 9 ^^^^^^^				
0	1	2540	2754	0
0	3	3029	2907	0
0	5	5492	5025	0
0	7	4142	4327	0
0	9	11788	11734	0
1	4	4472	4608	0
3	8	3499	3577	0
4	1	3252	3357	0
4	5	5170	5029	0
6	1	3036	3232	0
6	9	3839	3887	0
7	2	2574	2110	0
7	6	2208	2289	0
8	3	4350	4447	0
10	1	3312	3211	0
^^^^^^^ h = 10 ^^^^^^^				
0	8	2421	2148	0
0	10	3503	3334	0
2	2	6686	6767	0
5	7	2106	2169	0
8	2	2707	2858	0
8	4	3072	3414	0
9	1	3504	3540	0
10	4	6797	6838	0
^^^^^^^ h = 11 ^^^^^^^				
0	5	4367	4511	0
1	2	6544	6394	0
1	4	2858	2706	0
2	1	5387	5407	0
2	5	4577	4759	0
5	2	2545	2423	0
^^^^^^^ h = 12 ^^^^^^^				
0	0	5650	5167	0
0	6	6605	6535	0
2	6	3823	3536	0
3	1	5086	5041	0
9	1	2428	2341	0
^^^^^^^ h = 13 ^^^^^^^				
2	7	4951	4760	0
4	1	3171	2858	0
4	5	4428	4425	0
^^^^^^^ h = 14 ^^^^^^^				
0	0	6324	6246	0
4	4	2748	2444	0

APPENDIX I: OBSERVED AND CALCULATED STRUCTURE FACTOR AMPLITUDES (×10) FOR $Zr_{6.45}Nb_{4.55}P_{4.0}$ FROM Mo Kα X-RAY SINGLE CRYSTAL DATA

k	l	Fo	Fc	sigF
^^^^^^^ h =	0	^^^^^^^		
0	2	5128	6051	77
0	4	3326	3524	51
2	0	116	95	6
3	1	5186	4938	78
3	3	3067	3101	47
3	5	1806	1814	30
4	0	2806	2683	42
4	2	2007	2031	31
4	4	1229	1227	22
5	1	544	554	11
5	3	453	434	13
5	5	309	297	14
6	0	3808	3610	58
6	2	2984	2914	46
6	4	1914	1884	31
7	1	1197	1199	20
7	3	835	856	17
8	0	1465	1441	24
8	2	1219	1205	21
8	4	834	790	18
9	1	1511	1479	25
9	3	1124	1118	21
10	0	903	905	17
10	2	778	772	16
11	1	1050	1077	19
11	3	859	824	18
12	0	1929	1996	31
12	2	1729	1765	29
13	1	278	296	14
14	0	1228	1245	23
^^^^^^^ h =	1	^^^^^^^		
-14	-1	404	424	14
-13	0	621	604	13
-12	-3	136	126	15
-12	-1	140	138	13
-11	-2	501	501	17
-10	-3	876	881	16
-10	-1	1154	1163	20
-9	-4	141	124	21
-9	0	142	155	10
-7	0	117	116	9
-6	-1	880	849	15
-4	-5	149	133	12
-3	-4	458	450	19
-3	-2	681	696	12
-2	-5	586	592	13
-2	-1	1778	1787	27
0	-5	168	169	11
0	-1	268	269	6
0	3	219	209	10
2	3	1011	1060	16
3	0	896	904	14
4	1	481	478	9
4	3	291	286	10
6	3	562	574	12
11	0	539	555	12
13	2	523	529	17
^^^^^^^ h =	2	^^^^^^^		
-14	0	374	378	12
-12	-2	594	603	13
-12	0	647	670	13
-11	-3	310	292	18
-11	-1	349	375	14
-10	-2	813	808	17
-9	-3	1608	1633	25
-8	0	1057	1068	17
-7	-3	771	779	14
-7	-1	1061	1063	17
-6	-4	1019	1026	22
-6	-2	1508	1516	23
-6	0	1854	1845	28
-5	-3	359	345	10
-5	-1	510	488	9
-4	-4	1227	1225	25
-4	-2	1921	1969	29
-3	-5	860	851	16
-3	-1	2216	2177	45
-2	0	434	339	11
-1	-1	253	268	7
0	-4	231	227	19
0	-2	339	351	13
1	3	152	148	8
2	2	227	223	8
2	4	136	114	19
3	3	1371	1395	22
4	0	2666	2576	53
5	5	222	217	13
8	2	895	906	15
8	4	614	611	14
9	1	2083	2105	32
10	0	913	926	16
^^^^^^^ h =	3	^^^^^^^		
-14	-1	216	217	13
-13	-2	147	137	14
-11	0	556	577	16
-9	0	1827	1862	53
-8	-3	314	322	19
-8	-1	421	420	10
-6	-1	2815	2792	43
-5	0	686	664	14
-3	-2	832	841	14
-2	-5	791	810	15
-2	-3	1302	1359	25
0	-5	545	538	26
0	-3	850	885	14
0	-1	1384	1457	21
1	0	421	427	7
1	2	288	294	22
1	4	157	157	10
2	1	2137	2142	32
3	0	1116	1107	17
3	4	526	532	12
4	1	745	719	12
4	3	470	482	10
4	5	294	288	11
5	2	538	549	16
5	4	408	372	12
6	3	1969	2010	30
7	0	1571	1588	24
7	2	1303	1334	21
7	4	886	891	16
9	2	1617	1627	25
9	4	1171	1149	20
11	2	484	506	17
12	1	1522	1531	24
13	0	163	158	12
^^^^^^^ h =	4	^^^^^^^		
-13	-1	1758	1771	28
-11	-3	559	551	13
-11	-1	719	725	16
-10	-2	1387	1388	22
-9	-3	654	653	13
-9	-1	883	876	15
-8	-2	169	172	9
-7	-3	1411	1411	32
-6	-2	475	479	14
-6	0	600	595	11
-5	-1	2014	1981	31
-4	-2	773	791	13
-4	0	1035	1028	16

k	l	Fo	Fc	sigF	k	l	Fo	Fc	sigF	k	l	Fo	Fc	sigF
-3	-5	390	376	13	6	3	1230	1220	20	-4	-1	2210	2173	37
-3	-1	1105	1105	17	7	0	1327	1334	21	-3	0	327	319	15
-2	-4	869	899	35	8	1	216	190	10	-2	-5	358	353	12
-2	0	2110	2065	32	9	2	1443	1452	32	-2	-3	620	603	12
-1	-5	962	952	17	10	1	263	249	14	-2	-1	907	892	18
-1	-1	2804	2722	42	13	0	160	173	13	-1	0	2932	2881	57
0	-4	248	243	8	13	2	186	170	12	0	1	835	839	13
0	-2	386	375	8						0	3	577	577	12
0	0	430	439	15	^^^^^^^	h =	6	^^^^^^^		0	5	351	364	11
1	3	1636	1662	25						1	2	2145	2214	38
2	2	1536	1534	27	-13	-1	587	572	14	1	4	1368	1382	22
3	3	679	706	12	-12	-2	364	350	11	3	2	279	268	10
4	4	471	479	25	-12	0	397	384	12	3	4	198	201	10
5	3	1309	1336	21	-10	0	170	149	18	4	3	1488	1522	23
5	5	790	798	19	-8	-2	723	722	13	5	2	1575	1594	24
6	4	315	289	9	-7	-1	175	175	8	6	1	1637	1619	25
7	1	1925	1930	36	-5	-3	522	501	11	6	3	1208	1214	20
8	0	207	218	18	-4	-4	753	753	27	7	0	2458	2447	37
10	0	1575	1593	25	-4	0	1350	1372	26	7	4	1433	1428	23
12	0	406	395	23	-2	-2	236	206	23	9	0	568	576	12
12	2	370	358	13	-2	0	296	289	7	10	3	650	617	15
14	0	571	581	14	-1	-3	307	308	11	11	0	1543	1570	25
					-1	-1	549	529	10					
^^^^^^^	h =	5	^^^^^^^		0	-2	1346	1357	21	^^^^^^^	h =	8	^^^^^^^	
					0	0	1774	1772	44					
-12	-1	1057	1057	18	0	4	867	872	16	-12	-2	465	453	27
-11	-2	1081	1082	18	3	1	82	62	11	-12	0	505	506	14
-11	0	1229	1239	20	4	2	1105	1112	18	-11	-3	283	287	19
-10	-3	235	228	9	5	1	753	747	13	-10	-2	908	902	16
-9	-4	1013	992	20	7	3	162	160	10	-10	0	1035	1027	17
-9	0	1689	1682	32	8	0	817	820	18	-9	-3	1262	1267	32
-7	-4	710	711	14	8	4	547	526	13	-9	-1	1623	1616	25
-7	-2	1115	1115	18	9	1	722	714	27	-8	0	615	634	27
-5	-2	144	124	19	9	3	538	532	13	-7	-1	1188	1183	19
-4	-3	381	390	25	10	2	163	143	11	-6	-4	498	499	13
-3	0	5352	4964	0	11	1	252	257	25	-6	-2	716	706	13
-2	-1	1682	1690	26	11	3	230	225	23	-6	0	816	824	21
-1	-2	347	351	9						-5	-1	1046	1031	18
0	-3	2903	3010	44	^^^^^^^	h =	7	^^^^^^^		-4	-4	1145	1157	31
0	-1	5016	4789	75						-4	-2	1756	1759	28
0	5	1748	1761	28	-13	0	957	959	17	-4	0	2193	2146	54
1	0	518	496	15	-12	-1	431	411	43	-3	-3	364	360	11
2	3	1128	1142	18	-11	-2	1395	1387	23	-3	-1	552	525	10
2	5	732	724	22	-10	-1	787	784	16	-2	-2	357	381	9
3	2	3774	3799	0	-9	-2	519	516	12	-2	0	459	452	9
3	4	2290	2359	57	-8	-3	983	995	17	-1	-3	124	119	11
4	1	617	604	11	-8	-1	1304	1303	31	-1	-1	190	159	7
4	5	202	194	10	-7	-2	2095	2085	32	0	-2	975	992	16
5	0	139	108	7	-5	-4	1055	1046	18	0	0	1267	1254	22
6	1	1745	1712	27	-5	0	1867	1933	37	0	4	649	626	13

k	l	Fo	Fc	sigF
2	4	265	263	9
5	3	770	768	14
7	3	890	899	16
8	2	556	548	12
8	4	377	380	14
11	1	369	364	13
^^^^^^^ h = 9 ^^^^^^^				
-13	0	1444	1434	24
-10	-1	2175	2148	34
-8	-3	821	812	15
-8	-1	1074	1069	18
-7	-4	774	759	23
-7	0	1330	1317	21
-6	-3	738	759	14
-6	-1	1056	1042	17
-5	-2	1091	1096	18
-5	0	1321	1325	33
-4	-1	1942	1937	38
-3	0	239	233	26
-2	-3	1957	1971	30
-2	-1	2927	2854	44
-1	-4	900	887	16
-1	-2	1412	1399	22
-1	0	1761	1767	52
0	-1	250	250	14
0	3	161	158	11
3	2	223	194	16
4	3	1389	1387	22
5	4	736	727	14
7	2	1173	1130	19
10	3	1690	1675	27
11	0	294	313	21
11	2	269	269	21
^^^^^^^ h = 10 ^^^^^^^				
-12	0	1042	1035	18
-10	0	427	426	12
-9	-1	273	261	10
-8	-2	284	255	13
-8	0	319	310	22
-7	-1	476	453	13
-6	-2	1084	1088	18
-6	0	1286	1284	30
-5	-3	1024	1023	17
-4	-4	173	166	26
-4	-2	309	308	16
-4	0	398	391	13
-3	-1	1598	1572	25
-2	-4	670	676	13
-2	-2	952	950	16
-1	-1	1313	1293	20
0	-4	1760	1738	28
0	-2	2729	2688	41
0	0	3469	3326	69
1	3	949	954	22
2	0	1117	1125	18
3	3	1120	1121	19
5	1	1299	1324	20
6	4	742	722	29
7	3	382	378	13
9	3	194	189	26
10	2	403	395	13
12	2	955	914	20
^^^^^^^ h = 11 ^^^^^^^				
-12	-1	933	935	29
-11	0	319	326	10
-10	-1	481	472	35
-9	-2	948	933	17
-9	0	1058	1067	35
-8	-3	401	411	22
-8	-1	561	559	12
-7	-4	475	451	13
-7	-2	604	612	19
-7	0	673	686	13
-6	-1	1658	1665	26
-5	-4	443	441	13
-5	0	813	811	14
-3	-2	111	115	13
-3	0	176	159	7
-1	-2	228	214	8
-1	0	285	274	9
0	-3	254	255	9
0	-1	408	403	16
2	1	1934	1917	53
2	3	1360	1377	22
5	2	684	684	13
6	3	1233	1254	25
10	3	377	356	12
11	2	296	300	10
^^^^^^^ h = 12 ^^^^^^^				
-12	0	187	180	13
-11	-1	906	915	19
-9	-3	786	763	16
-9	-1	948	942	17
-7	-3	1023	1027	18
-6	-2	647	657	13
-5	-3	825	827	26
-5	-1	1088	1094	18
-4	-4	1512	1517	24
-4	-2	2203	2214	34
-2	-4	1029	1031	20
-2	-2	1514	1547	28
0	-2	109	77	12
1	1	1437	1444	22
1	3	1060	1062	27
2	0	1815	1834	29
3	1	1131	1139	18
3	3	876	871	15
4	0	2620	2594	40
6	0	731	740	13
6	4	487	484	13
7	1	1314	1314	38
8	0	1950	1926	41
8	2	1700	1692	27
10	0	1187	1185	33
10	2	1051	1053	18
^^^^^^^ h = 13 ^^^^^^^				
-10	-1	640	635	27
-9	0	148	109	12
-8	-3	360	348	17
-8	-1	442	438	12
-7	0	1974	1997	31
-6	-3	301	320	10
-6	-1	411	403	14
-5	0	377	383	11
-4	-3	1054	1059	18
-4	-1	1382	1385	22
-2	-3	390	377	12
-1	-4	705	694	15
-1	-2	1035	1024	17
0	-3	883	877	16
0	1	1170	1170	19
1	0	1227	1210	21
2	1	488	494	11
3	0	1299	1333	28
3	2	1122	1142	18
3	4	785	771	15
5	2	332	329	13
5	4	256	229	17
7	2	1755	1753	28
11	0	1172	1178	28

k	l	Fo	Fc	sigF
^^^^^^^ h = 14 ^^^^^^^				
-11	-1	269	254	10
-10	0	822	831	16
-7	-3	721	721	15
-6	-2	573	573	22
-5	-3	986	983	17
-4	-4	136	109	17
-4	-2	182	181	10
-3	-3	494	518	25
-2	-2	963	969	16
-1	-3	1084	1057	18
-1	-1	1430	1415	42
0	-2	1606	1599	25
0	0	1857	1846	29
0	4	1146	1136	20
2	0	1129	1134	18
2	4	669	657	28
3	1	609	637	12
4	0	219	218	11
5	1	1275	1285	21
6	0	632	638	13
7	1	918	938	33
10	2	739	735	15
^^^^^^^ h = 15 ^^^^^^^				
-11	0	540	542	14
-10	-1	874	874	16
-6	-3	242	203	35
-4	-3	262	262	20
-3	-2	1343	1361	22
-2	-3	863	864	16
-2	-1	1080	1083	26
0	-3	962	958	17
0	-1	1265	1267	20
1	4	123	95	17
3	0	1530	1576	27
3	4	935	929	17
4	1	333	306	18
5	0	97	57	15
6	1	266	279	9
9	0	764	765	32
9	2	684	669	14
^^^^^^^ h = 16 ^^^^^^^				
-9	-1	2035	2038	32
-8	-2	355	375	11
-5	-3	1361	1365	22
-5	-1	1764	1774	28
-4	-2	281	266	10
-4	0	286	289	27
-3	-3	1113	1105	19
-3	-1	1424	1438	26
-1	-3	995	978	39
-1	-1	1303	1296	32
0	-4	229	205	34
0	-2	329	311	12
0	0	358	368	12
2	0	1460	1496	59
2	2	1295	1296	31
6	0	1547	1589	25
6	2	1371	1398	26
8	0	442	435	27
^^^^^^^ h = 17 ^^^^^^^				
-8	-1	523	526	13
-7	-2	956	968	17
-7	0	1057	1090	18
-6	-3	1328	1311	22
-6	-1	1624	1638	26
-5	0	807	845	15
-4	-1	767	791	21
-3	-2	819	812	15
-3	0	898	911	16
-1	-2	966	968	17
-1	0	1107	1110	33
0	-3	1026	999	25
0	-1	1276	1267	21
4	3	623	622	14
5	2	716	738	14
9	0	823	813	18
^^^^^^^ h = 18 ^^^^^^^				
-9	-1	358	360	21
-8	0	692	709	30
-7	-1	597	599	14
-6	-2	225	224	12
-6	0	257	255	22
-4	-2	1118	1101	32
-4	0	1231	1246	20
-3	-3	300	303	10
-1	-1	110	28	17
0	0	1423	1424	35
0	2	1275	1253	21
3	1	414	388	45
5	1	339	325	11
5	3	278	257	12
^^^^^^^ h = 19 ^^^^^^^				
-8	-1	232	213	18
-5	0	391	392	13
-4	-1	242	228	15
-3	0	1795	1827	28
-1	-2	217	211	27
-1	0	250	244	9
0	1	1663	1656	26
0	3	1360	1330	23
2	1	1211	1215	20
2	3	952	946	18
3	2	1630	1630	28
5	2	344	342	13
6	1	529	544	13
7	0	225	210	10
^^^^^^^ h = 20 ^^^^^^^				
-8	0	942	988	20
-6	0	984	1002	33
-2	-2	414	402	12
-2	0	465	472	27
0	0	1742	1730	27
0	2	1548	1529	25
3	1	880	888	23
4	0	855	839	44
4	2	761	735	15
5	1	201	198	11
^^^^^^^ h = 21 ^^^^^^^				
-7	0	601	621	14
-6	-1	1602	1632	28
-3	-2	585	577	22
-3	0	643	652	14
-1	-2	129	142	16
-1	0	177	172	12
0	1	764	769	15
2	1	1269	1274	35
5	0	678	664	14
^^^^^^^ h = 22 ^^^^^^^				
-3	-1	1218	1219	21
0	0	569	565	15
0	2	533	511	14

k	l	Fo	Fc	sigF
4	0	838	835	34
5	1	228	219	11
^^^^^^^ h = 23 ^^^^^^^				
-3	0	328	321	14
2	1	832	833	16
^^^^^^^ h = 24 ^^^^^^^				
0	0	1676	1687	27

APPENDIX J: OBSERVED AND CALCULATED STRUCTURE FACTOR AMPLITUDES (×10) FOR ZrNbP FROM Mo Kα X-RAY SINGLE CRYSTAL DATA

k	l	Fo	Fc	sigF
^^^^^^^	h = -5	^^^^^^^		
2	6	229	258	10
^^^^^^^	h = -4	^^^^^^^		
3	2	439	437	7
4	3	157	147	11
4	5	0	60	33*
^^^^^^^	h = -2	^^^^^^^		
2	0	335	330	7
2	4	110	81	7
4	4	0	59	30*
^^^^^^^	h = 0	^^^^^^^		
0	2	240	213	14
0	4	753	755	16
0	6	438	439	7
0	8	984	960	23
0	10	851	874	18
1	-11	145	156	21
1	-9	99	102	0*
1	-7	292	290	6
1	-5	1300	1317	24
1	-3	1235	1233	22
1	-1	224	222	4
2	-10	813	785	19
2	-8	864	851	19
2	-6	366	370	7
2	-4	604	597	14
2	-2	157	158	7
2	0	2390	2343	39
2	4	589	597	13
2	8	823	851	17
2	10	766	785	20
3	-9	16	72	56*
3	-7	202	219	10
3	-5	934	956	23
3	-3	821	823	22
3	-1	128	145	19
4	-6	243	245	15
4	-4	388	392	9
4	-2	134	108	7
4	0	1470	1447	34
^^^^^^^	h = 1	^^^^^^^		
-4	-3	671	697	18
-4	2	229	231	7
-3	-7	615	659	21
-3	6	336	343	8
0	1	227	226	4
0	2	453	456	8
0	3	1403	1397	24
0	4	837	804	14
0	5	698	699	13
0	6	778	763	14
0	7	753	735	14
0	8	61	17	35*
0	9	167	173	24
0	10	479	471	9
0	11	482	482	8
1	-11	96	119	24*
1	-10	691	695	11
1	-9	313	312	5
1	-8	578	575	10
1	-7	851	846	14
1	-6	459	448	7
1	-5	252	254	24
1	-4	179	197	26
1	-3	898	910	20
1	-2	1494	1491	24
1	-1	485	503	8
2	-10	429	424	8
2	-9	109	151	13
2	-8	77	13	42*
2	-7	630	640	20
2	-6	645	651	11
2	-5	575	575	10
2	-4	654	642	13
2	-3	1057	1072	29
2	-2	358	358	6
2	-1	162	156	9
2	10	273	424	0*
3	-9	266	259	12
3	-8	438	456	15
3	-7	652	659	15
3	-6	327	343	12
3	-5	193	186	7
3	-4	151	132	9
3	-3	636	615	12
3	-2	938	961	20
3	-1	317	321	6
4	-6	466	458	9
4	-5	402	396	13
4	-4	451	436	12
4	-3	701	697	24
4	1	48	104	0*
^^^^^^^	h = 2	^^^^^^^		
-4	-1	0	2	28*
-3	6	179	188	9
-2	-9	167	159	11
-2	1	0	10	92*
0	-9	206	177	7
0	0	394	415	8
0	1	57	15	34*
0	2	607	617	11
0	3	984	992	18
0	4	77	106	71*
0	5	1190	1214	22
0	6	664	647	13
0	7	21	91	22*
0	8	374	364	8
0	9	184	177	10
0	10	93	70	31*
0	11	286	286	12
1	-11	494	486	8
1	-10	516	506	8
1	-9	19	114	0*
1	-8	793	834	16
1	-7	626	633	10
1	-6	233	239	5
1	-5	763	766	13
1	-4	43	75	0*
1	-3	303	296	5
1	-2	577	588	10
1	-1	1251	1265	20
1	0	1571	1552	31
2	-10	0	60	0*
2	-9	14	159	44*
2	-8	316	319	12
2	-7	86	82	20*
2	-6	551	552	11
2	-5	1016	1015	28
2	-4	86	81	9
2	-3	801	781	16
2	-2	470	473	8
2	0	359	330	6
2	8	240	319	0*
3	-9	0	85	42*
3	-8	689	673	26
3	-7	497	496	9
3	-5	571	566	10
3	-4	0	52	17*
3	-3	167	208	0*

k	l	Fo	Fc	sigF	k	l	Fo	Fc	sigF	k	l	Fo	Fc	sigF
3	-2	398	396	7	3	-4	1005	1009	18	3	-5	416	413	8
3	-1	825	825	15	3	-3	322	311	6	3	-4	265	270	7
3	0	1012	1007	20	3	-1	285	283	6	3	-3	432	444	10
3	8	639	673	15	3	2	58	23	26*	3	-2	443	437	8
4	-6	388	397	11	3	8	229	233	23	3	-1	425	434	16
4	-5	686	714	13	4	-5	133	61	11	3	0	293	295	14
4	-4	53	59	44*	4	-4	0	71	26*	4	-5	75	60	37*
4	-3	505	526	9	4	-3	215	254	0*	4	-4	329	321	8
4	-2	123	307	0*	4	-2	648	650	11	4	-3	24	147	55*
4	-1	0	2	32*	4	-1	729	730	13	4	-2	600	596	11
4	0	196	205	11						4	-1	368	369	9
					^^^^^^^ h = 4 ^^^^^^^					4	0	0	4	33*
^^^^^^^ h = 3 ^^^^^^^														
					-3	6	555	563	11	^^^^^^^ h = 5 ^^^^^^^				
-4	5	5	61	23*	-1	3	581	588	11					
-2	4	121	116	7	-1	9	359	362	6	-3	-3	428	417	12
0	-11	12	39	46*	0	0	63	30	25*	-2	8	140	162	34*
0	1	1386	1397	33	0	1	635	660	13	-1	-7	60	115	22*
0	2	1220	1225	22	0	2	1001	1035	24	0	1	387	383	7
0	3	475	476	10	0	3	243	243	5	0	2	211	232	87*
0	4	144	140	4	0	4	548	545	10	0	3	185	183	6
0	5	42	110	87*	0	5	94	103	0*	0	4	1204	1187	21
0	6	136	112	8	0	6	1087	1064	19	0	5	136	135	12
0	7	279	279	6	0	7	566	542	11	0	6	278	285	6
0	8	498	503	13	0	8	482	493	12	0	7	146	137	10
0	9	987	991	18	0	9	86	153	88*	0	8	163	178	10
0	10	377	359	7	0	10	103	128	16	0	9	395	395	8
1	-10	35	91	0*	1	-10	68	31	0*	1	-9	937	944	16
1	-9	0	3	30*	1	-9	368	362	8	1	-8	253	256	8
1	-8	291	291	9	1	-8	92	21	0*	1	-7	114	115	13
1	-7	242	232	8	1	-7	664	672	11	1	-6	161	196	95*
1	-6	428	426	7	1	-6	693	714	12	1	-5	4	43	24*
1	-5	443	445	7	1	-5	536	526	9	1	-4	596	592	10
1	-4	1374	1363	23	1	-4	350	357	6	1	-3	566	551	12
1	-3	441	440	7	1	-3	591	588	13	1	-2	242	257	15
1	-2	56	24	54*	1	-2	609	596	11	1	-1	1230	1234	20
1	-1	392	403	6	1	-1	599	603	10	1	3	526	551	8
2	-10	305	327	17	1	0	404	413	10	2	-7	0	122	0*
2	-9	783	891	31	2	-9	110	137	0*	2	-6	233	258	63*
2	-8	436	445	9	2	-8	440	443	13	2	-5	25	118	34*
2	-7	206	249	0*	2	-7	484	481	11	2	-4	1033	1037	19
2	-6	108	98	20*	2	-6	929	934	22	2	-3	162	157	13
2	-5	91	92	16*	2	-5	10	87	21*	2	-2	65	203	0*
2	-3	385	385	7	2	-4	470	466	9	2	-1	340	325	5
2	-2	985	976	18	2	-3	212	204	7	3	-6	163	157	8
2	-1	1074	1096	19	2	-2	852	857	19	3	-5	85	33	10
3	-8	218	233	29	2	-1	542	538	10	3	-4	463	463	8
3	-7	172	193	28	2	0	24	27	29*	3	-3	412	417	8
3	-6	330	337	6	3	-7	541	540	10	3	-2	197	192	12
3	-5	332	337	11	3	-6	581	563	11	3	-1	947	939	16

k	l	Fo	Fc	sigF
3	6	144	157	39*
3	7	0	107	66*
4	-3	77	113	32*
4	-2	188	145	10
4	-1	234	234	11
4	2	163	145	21

^^^^^^^ h = 6 ^^^^^^^

k	l	Fo	Fc	sigF
-3	5	556	543	18
-1	1	199	228	0*
-1	8	100	141	52*
0	0	390	394	10
0	1	895	931	16
0	2	230	226	5
0	3	585	584	12
0	4	135	131	24*
0	5	99	57	11
0	6	149	154	7
0	7	710	702	20
0	8	496	495	8
0	9	94	93	29*
1	-7	4	1	19*
1	-6	803	808	13
1	-5	656	679	11
1	-4	201	211	63*
1	-3	256	252	13
1	-2	751	754	12
1	-1	237	228	13
1	0	93	82	14
2	-7	632	632	16
2	-6	147	137	18
2	-5	0	45	80*
2	-4	104	114	17
2	-3	528	516	9
2	-2	207	200	7
2	-1	814	812	15
2	0	340	346	9
3	-5	537	543	22
3	-4	172	171	17
3	-3	184	206	65*
3	-2	604	598	10
3	-1	144	172	0*
3	0	0	71	23*

^^^^^^^ h = 7 ^^^^^^^

k	l	Fo	Fc	sigF
0	1	520	516	9
0	2	662	670	11
0	3	424	445	9

k	l	Fo	Fc	sigF
0	4	631	674	14
0	5	192	207	0*
0	6	171	152	8
0	7	598	585	13
0	8	460	472	12
1	-7	0	11	0*
1	-6	515	504	8
1	-5	299	312	30
1	-4	608	600	10
1	-3	385	379	6
1	-2	388	385	6
1	-1	254	252	7
2	-6	13	135	0*
2	-5	191	188	12
2	-4	619	602	18
2	-3	403	397	7
2	-2	601	592	14
2	-1	464	464	10
2	4	590	602	10
3	-3	314	310	8
3	-2	309	318	10
3	-1	203	206	19

^^^^^^^ h = 8 ^^^^^^^

k	l	Fo	Fc	sigF
0	0	573	565	12
0	1	232	238	13
0	2	301	306	11
0	3	432	428	8
0	4	24	99	32*
0	5	661	657	20
0	6	196	207	13
1	-6	277	295	12
1	-5	178	182	0*
1	-4	233	304	0*
1	-3	447	450	11
1	-2	0	18	0*
1	-1	333	338	6
1	0	1091	1068	19
2	-4	71	86	46*
2	-3	394	387	11
2	-2	277	278	7
2	-1	202	214	9
2	0	510	506	13

^^^^^^^ h = 9 ^^^^^^^

k	l	Fo	Fc	sigF
0	1	0	117	88*
0	2	622	619	12
0	3	210	260	81*